STRESS RESPONSE BEHAVIOUR AND MECHANISM OF MANF

INVESTIGATING THE IMPACT OF THE STRESS RESPONSE ON *C. ELEGANS* BEHAVIOUR AND THE MECHANISMS BY WHICH MANF PROMOTES ORGANISMAL FITNESS AND HEALTH

SHANE K. B. TAYLOR, B.Sc.

A Thesis

Submitted to the School of Graduate Studies

In Partial Fulfillment of the Requirements for the Degree

Doctor of Philosophy

McMaster University

McMaster University

DOCTOR OF PHILOSOPHY (2024)

Hamilton, Ontario (Department of Biology)

TITLE: Investigating the impact of the stress response on *C. elegans* behaviour and the mechanisms by which MANF promotes organismal fitness and cellular health.

AUTHOR: Shane Kevin Brendan Taylor Hons. B.Sc. (University of the West Indies Cave Hill)

SUPERVISOR: Dr. Bhagwati P. Gupta

NUMBER OF PAGES: i-xvii, 1-250

Lay Abstract

Cellular perturbations or stress disrupt homeostasis, activating multiple stress responses. Activation of the stress response can determine the fate of an organism and is crucial to its health. Although the stress response pathways are generally understood, little is known about how the stress responses preserve animal behaviour or how they are regulated to promote organismal survival. My work has provided a basis for how stress responses affect behaviour positively and negatively in animals. I found that the stress response required mesencephalic astrocyte derived neurotrophic factor (MANF) to promote organismal survival. My thesis determined that MANF acts as more than a neurotrophic factor. MANF was found to not only be essential in neuronal health but also longevity and muscle health. Overall, this thesis demonstrated the impact of stress response on behaviour and the potential mechanism by which MANF is cytoprotective in whole organisms.

Abstract

Nothing is perfect, and this includes the ability to maintain homeostasis within the cell with age. Factors such as aging, chemicals, and gene dysfunction disrupt cellular homeostasis, leading to increased stress and compromising the ability of animals to maintain a healthy lifespan. Dysregulated homeostasis can be detrimental on an organismal level, impacting locomotion, and on a cellular level causing proteins to misfold and become aggregates, which are toxic to cells. Toxic protein aggregation and loss of locomotory function are key hallmarks of several age-related diseases. My Ph.D. work examined the collapse of homeostasis on electrotaxis, the age-associated increase in proteotoxicity, the decline in longevity, and neuronal and muscle health. On a behavioural level I demonstrated that loss of various components of the MT-UPR, ER-UPR, and HSR modulated the speed of animals. Additionally, I found that activation of stress responses due to chemicals and exercise reduced and increased the speed of animals respectively. On a cellular level I elucidated potential mechanisms by which Mesencephalic Astrocyte Derived Neurotrophic Factor (MANF) affects the stress response to maintain homeostasis and prevent protein aggregation. I observed the novel localization and role of MANF in lysosomes to potentially act as a critical regulator of the stress response to maintain proteostasis, neuronal health and longevity, thereby bringing balance to the cell. Furthermore, the broad tissue expression of MANF revealed its localization to muscles. This supports the ability of MANF to act as more than a neurotrophic factor as it was found to be required for muscular health in animals in an age-dependent manner. Overall, my Ph.D. research has provided new insights into the stress response and behaviour and the precise role of MANF in mediating stress response signaling to promote organismal and cellular fitness.

Dedicated to My Mummy

Aunty Michelle

and Uncle Robert

"Make sure you're happy with your choices."

Acknowledgements

These acknowledgements are a testament to my growth and those who saw it. I want to acknowledge those that I have lost and those that I have gained along the way. Thank you. This has been the most challenging and rewarding of experiences. I will never forget it.

I want to say a big thank you to my supervisor, Dr. Bhagwati Gupta. The day you took me on as a master's student I was elated with joy, and I could have never imagined the journey that we would embark on during my time at McMaster University. You have taught me so much, challenging my thinking and opening my mind to new and diverse ideas. Your guidance has led me to become the researcher that I always wanted to be. The biggest complement you gave me was at my exit seminar when you said how much you have seen me grow and how much my way of thinking has changed. I appreciate all the lab lunches and yearly invites to your house to celebrate various events and just to be outside and appreciate summer. Being in your lab has provided me with friends for life. I thank you so much for this journey. All good things must come to an end as they say.

To my committee members Dr. Ram Mishra, Dr. Ravi Selvaganapathy, and Dr. André Bedard, thank you so much for your guidance and wisdom these last 5 years. Dr. Mishra, I have appreciated your casual jokes and extensive knowledge throughout my journey. Dr. Selvaganapathy, your different perspectives on research have truly opened up my way of thinking. You have given many words of encouragement over the years. Dr. Bedard, the conversations that I have had with you have been very insightful and have greatly helped and guided my project. I sincerely appreciate everything that you have done and aided me with, because of your passion for science and research.

I would like to also thank my external, Dr. Stefan Taubert for agreeing to participate in my defense and also Dr. Ben Evans for agreeing to be my chair. Thank you for all the wise words you have given me throughout the years Ben, they have meant more to me than you realize.

I want to thank the graduate student community within biology. Being a part of this community was something that I did not foresee. The grad students within LSB have been an incredible joy to be around. You guys have been a sounding board and have solved so many of my problems. When I came to Mac I knew nothing, but the graduate students have taught me so much. Everyone has been open to me asking questions and learning. But most of all, this community let

me by myself, and I love that each one of you is unapologetically expressive of who you are as a person and scientist. Thank you for all the Fridays, and nights that we went out drinking together.

Thank you Dr. Shawn, for welcoming me to Mac, and always being ready to get Quik Chik and KFC with me. But most importantly, the single rum and coke we had on a Friday night together was welcoming and made me feel like I was back home in Barbados just liming. Thank you.

To the Gupta lab, thank you to the past and current members that have come and gone over the years who have supported me. Especially, the undergrads who listened to my endless rants about a variety of topics. Dear Dr. Avijit, you may never see this but I appreciated all the in lab conversations we had about our projects. I went from asking you questions 24/7 to challenging your ideas and questions. Being able to answer your hard questions was a pivotal moment for me, thank you for encouraging me so much. I will cherish our papers together and all the times we went for Quik Chik or KFC. Dear Dr. Nikita, from the day you came to the lab I had no idea we would become such great friends. We have been there for each other through thick and thin, supporting each other along the way. I could always trust you to take care of anything. Thank you for being an amazing friend as we would walk to gel doc and nanodrop so often together. Wouter, oh Wouter, I thank you for your insights on the most random things within a scientific context. The perspectives and answers you give to my questions always blows my mind and I thank you for encouraging me to be so open in my thinking. Thank you for always listening to me, being a friend, always being down for a drink and being incredible.

I would like to give a special thank you to Judy, Hannah, Ellie, Fiona and Dheepthi. Thank you for listening to me, being a pillar of support and thank you for being there. I had no idea the friends we would become. Thank you to Nicole for always being down for ice-cream and going on so many foodie adventures with me. Thank you to the boys, the lads, and lassies, for helping me get a PS4, I needed that outlet more than I realized. Thank you for the support. Thank you to my friends and family for being there as I took this journey. If I missed your name its cause I'm forgetful and but still grateful to you.

I found myself at Mac, I found family, And I found my wife, thank you Rachel. Thank you for always being there. Thank you for always listening. Thank you for always reading. Without you I couldn't have done it and become who I am today. I am a better person and scientist because of you, and I will forever be grateful and happy.

Table of Contents

List of Figures

List of Tables

List of Abbreviations

AD	Alzheimer's Disease
AMPK	5’ Adenosine Monophosphate-activated Protein Kinase
ARMET	Arginine Rich Mutated in Early Stage Tumor
ATF4	Activating Transcription Factor 4
ATF6	Activating Transcription Factor 6
ATFS-1	Activating Transcription Factor associated with Stress 1
Bax	Bcl-2-associated X protein
BiP	Immunoglobulin-binding protein
BDNF	Brain-Derived Neurotrophic Factor
CDNF	Cerebral Dopamine Neurotrophic Factor
CHOP	CCAAT-enhancer-binding protein Homologous Protein
DE	Differentially Expressed
DMSO	Dimethyl sulfoxide
DVE-1	Defective proVEntriculus 1
eIF2a	Eukaryotic Initiation Factor 2a
ERAD	ER-associated degradation
ER- UPR	Endoplasmic Reticulum Unfolded Protein Response
GDNF	Glial cell-Derived Neurotrophic Factor
GO	Gene Ontology
GRP78	Glucose Regulating Protein 78
HLH-30	Helix Loop Helix-30
HSR	Heat Shock Response
HSF-1	Heat Shock Factor 1
HSE	Heat Shock Element
HSP	Heat Shock Protein

HD	Huntington's Disease
IRE-1	Inositol-Requiring Enzyme 1
IIS	Insulin/Insulin growth factor-1 Signaling
KEGG	Kyoto Encyclopedia of Genes and Genomes
LSR	Lysosomal Stress Response
MANF	Mesencephalic Astrocyte derived Neurotrophic Factor
MTOR	Mammalian Target Of Rapamycin
MT-UPR	Mitochondrial Unfolded Protein Response
mtDNA	Mitochondrial DNA
NGF	Nerve Growth Factor
NGM	Nematode Growth Medium
NTFS	Neurotrophic factors
PD	Parkinson's Disease
PERK	PKR-like ER Kinase
polyQ	polyglutamine
PKR	Protein Kinase RNA
PQ	Paraquat
RAB	Ras-Associated Binding
RME	Receptor Mediated Endocytosis
SAP	SAF-A/B, Acinus and PIAS
Tuni	Tunicamycin
TP5	Truncated Peptide 5
TFEB	Transcription Factor EB (E-Box/Class E Basic)
UPR	Unfolded Protein Response
UBL-5	Ubiquitin-like protein
XBP-1	Xbox Binding Protein 1

Declaration of Academic Achievement

I, Shane Kevin Brendan Taylor declare that the work in this thesis is my own and the majority of the research was performed by me. I carried out the experimental design, figure creation, statistical analysis and data interpretation, analysis and curation. All initial manuscript drafts were completed by me followed by input from Dr. Gupta. The contributions of different authors are outlined below.

Chapter 2: **UPR and HSR pathways modulate electrotaxis behavior**:

There are two articles in this chapter listed in the **(Preface 2.1).**

Towards article **1)** I wrote the manuscript draft, analyzed the data, performed the statistical analysis, and curated and created all the figures for publication format. I and Hannan share co-author on this publication. I performed all QPCR experiments and mitochondrial muscle analysis. Hannan and Justin performed the electrotaxis behaviour analysis, Justin performed the GFP quantification experiments in Figure 1. I and Dr. Gupta responded to reviewer comments and reviewed and edited the final version for publication. Dr. Selvaganapathy and Dr. Mishra provided input and manuscript revision throughout the process.

Towards article **2)** I wrote the entire manuscript, analyzed the data, curated the data, made figures and responded to reviewer comments. Hannan performed experiments 1A and B. I performed the other experiments and provided images. Dr. Gupta reviewed and edited the publication for submission.

Chapter 3: **The neurotrophic factor MANF regulates autophagic flux and lysosome function to promote proteostasis in *C. elegans.***

There are two articles in this chapter listed in the **(Preface 3.1).**

Towards articles **1):** I wrote the manuscript draft and created all the figures and tables. Dr. Hartman provided RNA sequencing data and examined lifespan for supplemental Figure 5. I performed all other experiments and generated reagents. I, Dr. Hartman, and Dr. Gupta worked together to revise and edit the manuscript.

Towards articles **2)**: I wrote the manuscript draft, performed all the experiments, conducted the data analysis and designed the figures and tables. Dr. Gupta edited the manuscript.

Chapter 4: **The role of MANF in Muscle Maintenance in *C. elegans***

I wrote the manuscript draft, designed and performed the initial experiments, analyzed and interpreted the data, performed statistical analysis and created all figures. Gurtaaj performed burrowing, thrashing experiments. Me and Gurtaaj blind scored the muscle mitochondria morphology Dr. Hartman provided the RNA sequencing data. I revised the manuscript with feedback from Dr. Gupta.

1 Introduction

1.1 The Stress Response

Stress is a constant factor. It is an intrinsic part of life, and one that contributes to cell survival. The cell fights against toxic, harmful, and stressful environments that work to destroy it. Eukaryotic organisms have evolved unique mechanisms to protect against environmental, chemical, and genetic stressors. These are collectively known as stress responses, which are highly conserved signaling cascades that protect the cell against cellular damage and act to maintain homeostasis (Higuchi-Sanabria et al., 2018; R. C. Taylor & Hetz, 2020). These cellular stress responses detect imbalances within organisms, but as we age their functional capacity diminishes (Higuchi-Sanabria et al., 2018; R. C. Taylor & Dillin, 2011; R. C. Taylor & Hetz, 2020), a phenomenon supported by the damage or error theory of aging (Jin, 2010). More specifically the subcategory of wear and tear, where the essential components of the cell eventually wear out leading to aging (Jin, 2010). Similarly, the stress response eventually collapses and is a contributing factor towards aging. The decline of the stress response in function eventually leads to the accumulation of misfolded proteins, which are detrimental to the cell (Higuchi-Sanabria et al., 2018; R. C. Taylor & Dillin, 2011; R. C. Taylor & Hetz, 2020). These misfolded proteins activate the stress response, but due to their reduced function, they cause homeostatic imbalance and further sensitize organisms to stress. Furthermore, inactivation or dysfunction of these stress response networks can severely impact the health of an organism, reducing the longevity of animals and causing age-associated degeneration and neuronal damage (R. C. Taylor & Hetz, 2020). This dysfunctional stress response is observed in several age-related diseases, such as cancer, cardiovascular disease, Parkinson's Disease, and metabolic disorders, including diabetes (R. C. Taylor & Dillin, 2011). Maintenance and tightly controlled regulation of the stress response can potentially promote longevity and neuronal health by protecting against protein aggregation and other internal stressors (Higuchi-Sanabria et al., 2018; R. C. Taylor & Hetz, 2020).

Stress response at a cellular and molecular level

An accumulation of misfolded proteins due to age and homeostatic imbalances causes the cell's internal machinery to go haywire, activating distinct stress responses. One way in which the cell combats this is the use of organelle-specific stress responses (Higuchi-Sanabria et al., 2018). Well-known compartment-specific stress responses include the cytosolic heat shock response

(HSR), the mitochondrial unfolded protein response (UPR), and the endoplasmic reticulum UPR. Other organelles such as lysosomes may have their own specific signaling cascade for maintaining homeostasis (Higuchi-Sanabria et al., 2018; Lawrence & Zoncu, 2019; Saftig & Puertollano, 2021). In response to perturbed homeostasis, these organelle-specific stress responses work together in the cell to reduce protein translation, activate chaperones for correct protein folding, and activate multiple degradation pathways to clear protein aggregates. Altogether, this alleviates cellular stress and improves protein homeostasis (proteostasis) to prevent cell death. However, when proteostasis cannot be restored following activation of the stress response, the UPR pathways of different cellular compartments ultimately activate expression of genes that trigger cell death (Higuchi-Sanabria et al., 2018; R. C. Taylor & Dillin, 2011; R. C. Taylor & Hetz, 2020).

Proteostasis utilizes an adaptive stress response signaling to protect the proteome and maintain cellular function. Research has shown that manipulations of different organelle stress responses which maintain the cellular proteome can extend lifespan, protect neurons and rescue proteotoxicity in animals (Dutta et al., 2022; Higuchi-Sanabria et al., 2018). Uncovering the mechanisms which regulate and integrate organelle-specific stress responses can provide new tools to prevent dysregulation of cellular homeostasis. Additionally, dissection of the novel mechanisms used by regulators of the stress response will be paramount for improving and maintaining organismal health as we age (R. C. Taylor & Hetz, 2020), potentially enabling protection against an expansive suite of diseases. Overall, a better understanding of the function of the stress response in relation to aging will allow for the development of novel therapeutic targets which can prevent age-related decline of function in order to maintain organismal health.

My thesis provides an examination of how modulation of the various stress responses affects organismal survival in response to environmental changes. This thesis aims to examine novel mechanisms of stress response regulation by the neurotrophic factor MANF, which has been classically known as an ER-UPR regulator. I sought to elucidate the complexities of the role of MANF in cellular homeostasis to promote age-dependent health benefits. Advancing our understanding of MANF as a regulator on a cellular and tissue level will support its use as a novel therapeutic target in a multitude of diseases caused by dysregulated proteostasis.

1.2 Caenorhabditis elegans is an excellent model to study stress responses

The model invertebrate organism *Caenorhabditis elegans* has been used extensively to study the different stress response signaling cascades at the cellular and molecular level. This nematode has provided novel insights into stress response regulation and how restoring impaired proteostasis can protect against neurodegeneration and promote longevity.

C. elegans is a model organism of choice due to its ease of genetic manipulation, short life cycle of 3 days, and life span of roughly two weeks. It is easily cultivated within the lab and maintained under simple laboratory conditions(Corsi et al., 2015; Y. Xu & Park, 2018). Approximately 83% of its proteome is homologous with humans, and roughly 40% of *C. elegans* genes are related to human diseases, making it a great model for disease-specific studies (Corsi et al., 2015). *C. elegans* have a short lifespan, a relatively simple nervous system (302 neurons), and a conserved genome concerning stress-sensing signaling pathways. These factors make *C. elegans* a model organism well-suited to studying the requirements of the stress response and proteostasis network to maintain different aspects of health, such as longevity and neuron function (Higuchi-Sanabria et al., 2018; O'Brien & Van Oosten-Hawle, 2016). Using *C. elegans* provides an opportunity to study how genes affect whole organism health, tissue-specific signaling, and cell-cell communication. The manipulation of genes and proteins within *C. elegans* has been essential for advancing our understanding of different disease models, hallmarks of aging and age-related disorders (Caldwell et al., 2020; López-Otín et al., 2023; Wilson et al., 2023). However, the study of age-associated conditions can be complex in higher eukaryotes due to time restraints and ethics, whereas *C. elegans* provides an excellent opportunity to explore in-depth mechanisms for diseases of aging, impacting proteostasis. To this end, *C. elegans* has been extensively utilized as an invaluable model studying the cellular stress response to various stimuli that may impair the proteostasis network, a hallmark of aging (López-Otín et al., 2023; W. H. Zhang et al., 2022). As a model organism, *C. elegans* has provided a great deal to the field of stress signaling, but many fundamental questions remain including how the stress response is regulated and how it impacts the behaviour of animals.

1.3 Organelle specific stress responses

Cytosolic Heat Shock Response

Cells are equipped with multiple quality control mechanisms to maintain proper protein function within organelles. One of these is the cytosolic Heat Shock Response (HSR) which works to maintain balance within the cytosol. The HSR is activated in response to heat but can also be triggered by other cellular perturbations, including chemicals (e.g., paraquat or heavy metals) and genetic mutations (S. K. B. Taylor et al., 2021). The HSR is conserved across phyla and is regulated by Heat Shock Factor-1 (HSF1), the master transcriptional regulator of the cytosolic stress response, which upregulates genes that promote proper protein folding. Yeast, worms, and flies have a single HSF (HSF-1), whereas vertebrates and plants possess several. During periods of homeostasis, HSF-1 exists as a monomer bound by Heat Shock Proteins (HSP) 70 and 90 (Higuchi-Sanabria et al., 2018). When the cell experiences stress, HSF-1 trimerizes and enters the nucleus, acting as a transcription factor. HSF-1 causes the induction of several HSPs, including the cytosolic stress marker *hsp-16.2, hsp-70,* and *hsp-90* which act as chaperones **(Figure 1.1)**. These chaperones activated by HSF-1 allow the HSR to maintain protein homeostasis (proteostasis) within animals.

The HSR utilizes HSF-1 to maintain the protein folding capacity of the cell to reduce cellular stress. Due to HSF-1 being a component of the HSR, it has been implicated in metabolic disorders, neurodegeneration and cancer (Higuchi-Sanabria et al., 2018). Additionally, the role of HSF-1 in the HSR appears to be conserved in different species (including mice, worms, and flies) to maintain proteostasis. The loss of HSF-1 is highly detrimental and can result in shortened lifespan, neurodegeneration, and protein aggregation. Additionally, mutations in HSF-1 inhibits chaperone expression in response to heat stress (Hajdu-Cronin et al., 2004). Loss of chaperones regulated by HSF1 also reduces the survival of organisms (Higuchi-Sanabria et al., 2018). Inducing HSF-1 can prevent neurodegeneration in multiple animal models and has been found to extend lifespan in *C. elegans* (Higuchi-Sanabria et al., 2018). In *C. elegans* specifically, HSF-1 signals to other tissues from the neurons to mediate thermotolerance and longevity within these animals (Douglas et al., 2015). Activation of HSF-1 plays a role in other cellular responses that affect homeostasis, such as autophagy, lipid metabolism and innate immunity (Higuchi-Sanabria et al., 2018; Watterson et al., 2022). The complex regulation of HSF-1 demonstrates the importance of the HSR in maintaining appropriate cellular function within animals.

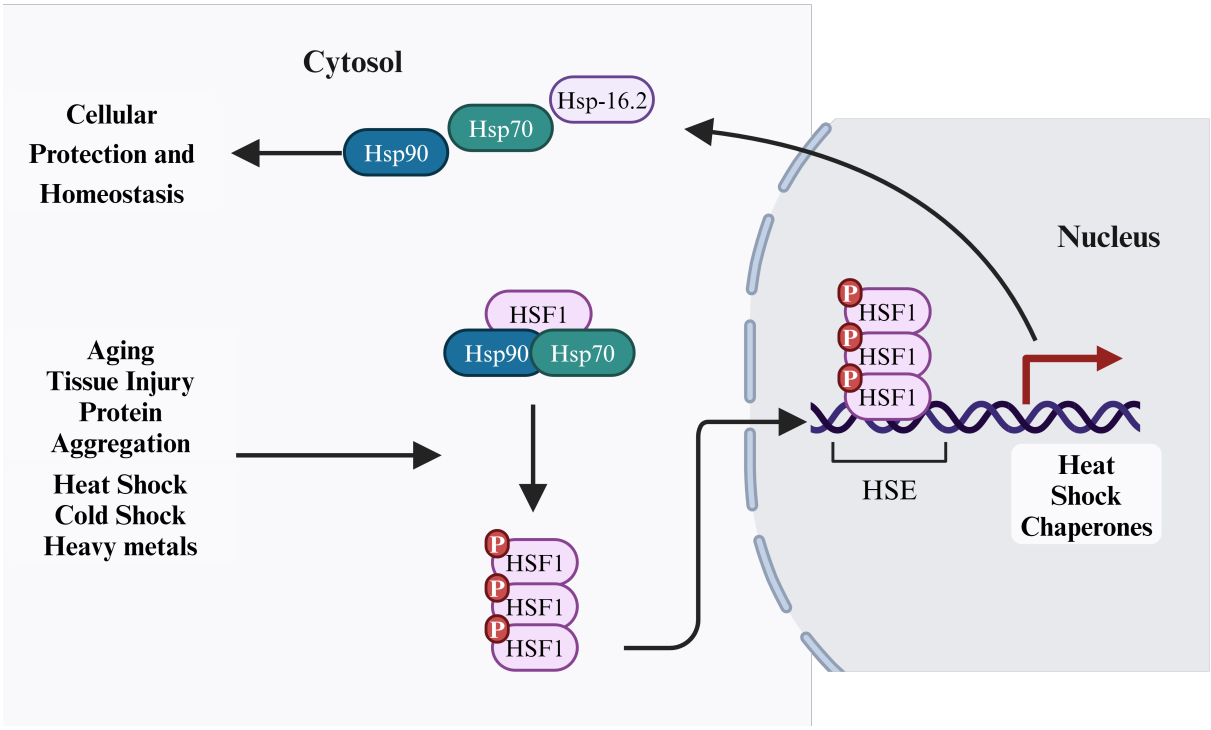

Figure 1.1. **The regulation of the cytosolic Heat Shock Response by HSF-1**. When homeostasis is maintained, HSF-1 is an inactive monomer bound in its inactivated state by HSP (HSP) 70 and 90 (Higuchi-Sanabria et al., 2018). When homeostasis is perturbed, HSF-1 is released by the HSPs. HSF-1 then trimerizes, gets phosphorylated, leaves the cytosol and enters the nucleus, where it acts as a transcription factor. HSF-1 binds to regions of DNA known as Heat Shock Elements (HSE). It activates several HSPs, and genes involved in protein maintenance, protein repair, autophagy and innate immunity in an attempt to regain homeostasis. Figure created using Biorender.com.

Mitochondrial – Unfolded Protein Response

Mitochondria are the powerhouse of the cell, and these organelles need to be tightly regulated to perform this crucial role. Due to their essential roles in cellular function, mitochondria possess protective capabilities to support their health, such as mitophagy and the mitochondrial unfolded protein response (MT-UPR). The MT-UPR is a quality control system involving a mitochondrial-to-nuclear signaling cascade. It is a transcriptional response program that works to recover the mitochondrial network from dysfunction and preserve mitochondrial proteostasis through chaperones and proteases (Jovaisaite et al., 2014; Nargund et al., 2015; Tran & Van Aken, 2020). The MT-UPR can be activated by an array of mitochondrial dysfunctions, including disruption of oxidative phosphorylation, mutations in mitochondrial DNA (mtDNA), mitochondrial and nuclear proteins imbalance, and the accumulation of misfolded proteins within

the mitochondria (Shpilka & Haynes, 2018). The MT-UPR was initially discovered in mammals, and since then, it has been found in models such as plants and yeasts, but has been well characterized in *C. elegans* (Tran & Van Aken, 2020).

Extensive studies in *C. elegans* have revealed that the Activating Transcription Factor associated with Stress (ATFS-1), an ATF5 homolog, regulates the MT-UPR by mediating the communication of mitochondrial stress to the nucleus (Fiorese et al., 2016; Jovaisaite et al., 2014). Under normal conditions, ATFS-1 is degraded by a protease once imported into the mitochondria (Higuchi-Sanabria et al., 2018; Nargund et al., 2015). During periods of mitochondrial stress, ATFS-1 cannot enter the mitochondria. Instead, it enters the nucleus where its transcriptional activity is regulated by the ubiquitin-like protein, UBL-5, and Defective proVEntriculus 1, DVE-1. Together, ATFS-1, UBL-5, and DVE-1 control the production of genes involved in maintaining mitochondrial proteostasis such as proteases, transporters, and chaperones (e.g., *hsp-6* and *hsp-60*) **(Figure 1.2)**. A very similar mechanism of action is also seen in other animal models (Tran & Van Aken, 2020). Additionally, the MT-UPR has been implicated in promoting the transcription of genes involved in processes such as development, aging, and metabolism (Tran & Van Aken, 2020). Dysregulation of the MT-UPR also results in diseases of aging such as cardiovascular and muscle dysfunction and neurodegenerative disorders(Higuchi-Sanabria et al., 2018; Nargund et al., 2015; Shpilka & Haynes, 2018; Tran & Van Aken, 2020). Maintaining the MT-UPR is vital for overall amimal health. Research in *C. elegans* shows that neuronal specific activation of the MT-UPR can lead to an extended lifespan (Durieux et al., 2011). However, constant activation of the MT-UPR can also lead to various detrimental effects, including cell death. This demonstrates the importance of tightly regulating defensive programs and how disease states can result from a loss of homeostasis. Genes involved in this regulation are exciting candidates for promoting organismal health, particularly with age.

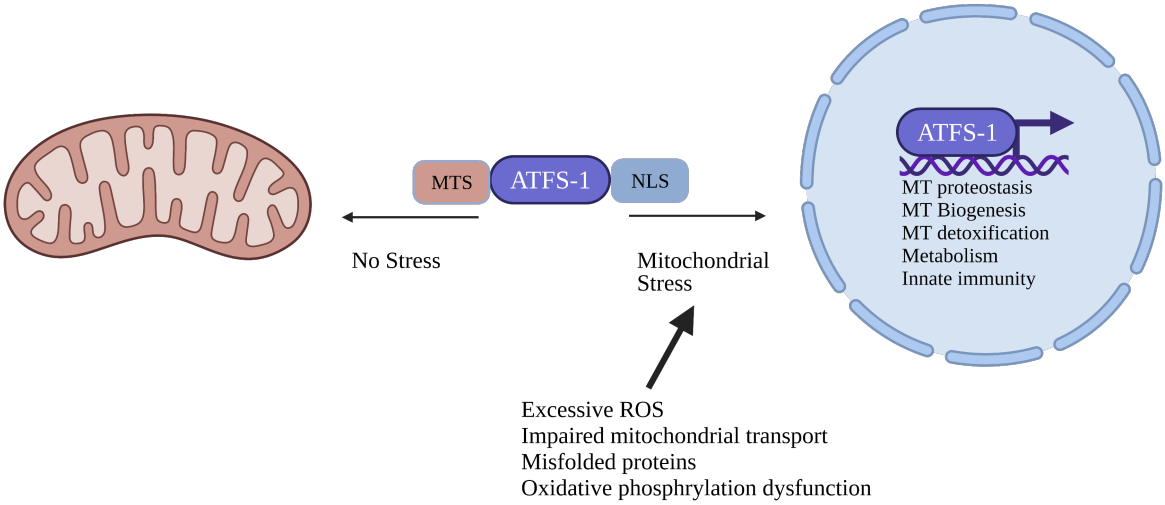

Figure 1.2. **Overview of the Mitochondrial Unfolded Protein Response in *C. elegans***. The transcription factor ATFS-1 regulates the MT-UPR (Nargund et al., 2015). ATFS-1 has a weak mitochondrial targeting sequence and nuclear localization sequence. Under basal conditions, ATFS-1 is imported into the mitochondria where it is degraded by the LON protease (Nargund et al., 2015; Shpilka & Haynes, 2018; Tran & Van Aken, 2020). However, during mitochondrial dysfunction, misfolded proteins enter the mitochondria where they are degraded by the mitochondrial protease ClpP into peptides. These peptides are transported out of the mitochondria to the cytoplasm via the mitochondrial transporter HAF-1. This leads to a reduction in the mitochondrial import efficiency and ATFS-1 cannot enter the mitochondria. Instead, it enters the nucleus with UBL-5 and DVE-1 to transcriptionally regulate overall mitochondrial homeostasis. An increase of mitochondrial chaperones such as HSP-6 and HSP-60 occurs in response to protein dysfunction of the mitochondria. The production of genes involved in maintaining mitochondrial proteostasis such as proteases, transporters, and chaperones are dependent on ATFS-1. Figure created using Biorender.com.

Endoplasmic Reticulum – Unfolded Protein Response

The endoplasmic reticulum is the site of significant protein synthesis and folding, necessitating a highly regulated response to misfolded or aggregated proteins. To combat protein misfolding, the endoplasmic reticulum unfolded protein response (ER-UPR) is at the center of this organelle-specific response. This quality control mechanism rectifies cellular stress by increasing chaperone production to correctly fold misfolded proteins, reduces translation, and activates cellular apoptosis when homeostasis cannot be achieved (Walter & Ron, 2011). The ER-UPR is

highly conserved between eukaryotes with three conserved transmembrane proteins that activate unique signaling pathways in response to stress. These three transmembrane proteins are inositol-requiring enzyme 1 (IRE1), protein kinase RNA (PKR)-like ER kinase (PERK) and activating transcription factor 6 (ATF6). These proteins each activate distinct signaling pathways with overlapping transcriptional activity.

IRE1 is the ancestral arm of the ER-UPR and performs a splicing mechanism of the intron encoding the transcription factor X-Box binding protein-1 (XBP1), the primary regulator of the ER-UPR. Collectively this is known as the IRE-1/XBP-1 signaling cascade of the ER-UPR, it leads to Spliced XBP1 activating transcription of chaperones such as the HSP-4 homolog, GRP78/BiP. The IRE-1/XBP-1 arm of the UPR also regulates the expression of genes involved in trafficking, lipid metabolism, lysosomes, and Endoplasmic Reticulum Associated Degradation (ERAD) (Hetz et al., 2020). The PERK arm inhibits translation through phosphorylation of Eukaryotic Initiation Factor 2α (eIF2α), which allows for the activation of the transcription factor ATF4, which regulates genes involved in autophagy, amino acid metabolism, apoptosis, ER chaperones, and un-spliced XBP1 (Hetz et al., 2020). The last arm of the ER-UPR pathway is mediated by ATF6, which, during stress, translocates to the Golgi body and is cleaved by proteases to create an ATF6 N-terminal fragment that enters the nucleus and activates UPR targets, including XBP-1, ERAD, and chaperone genes **(Figure 1.3)**. Overall, the ER-UPR is critical for maintaining appropriate cellular function and organismal health.

The ER-UPR, similar to the other organelle-specific stress responses, is also implicated in several disorders. Interestingly, the ER-UPR has been a focus of neurodegenerative disease research for therapeutic interventions due to its essential role in proteostasis (Cabral-Miranda & Hetz, 2017). Furthermore, research has demonstrated that the ER-UPR utilizes tissue-specific signaling to promote longevity and neuronal health and regulate lipid metabolism and lysosomal genes to maintain proteostasis (Imanikia, Özbey, et al., 2019; Imanikia, Sheng, et al., 2019; R. C. Taylor & Dillin, 2013; J. Xu & Taubert, 2021).

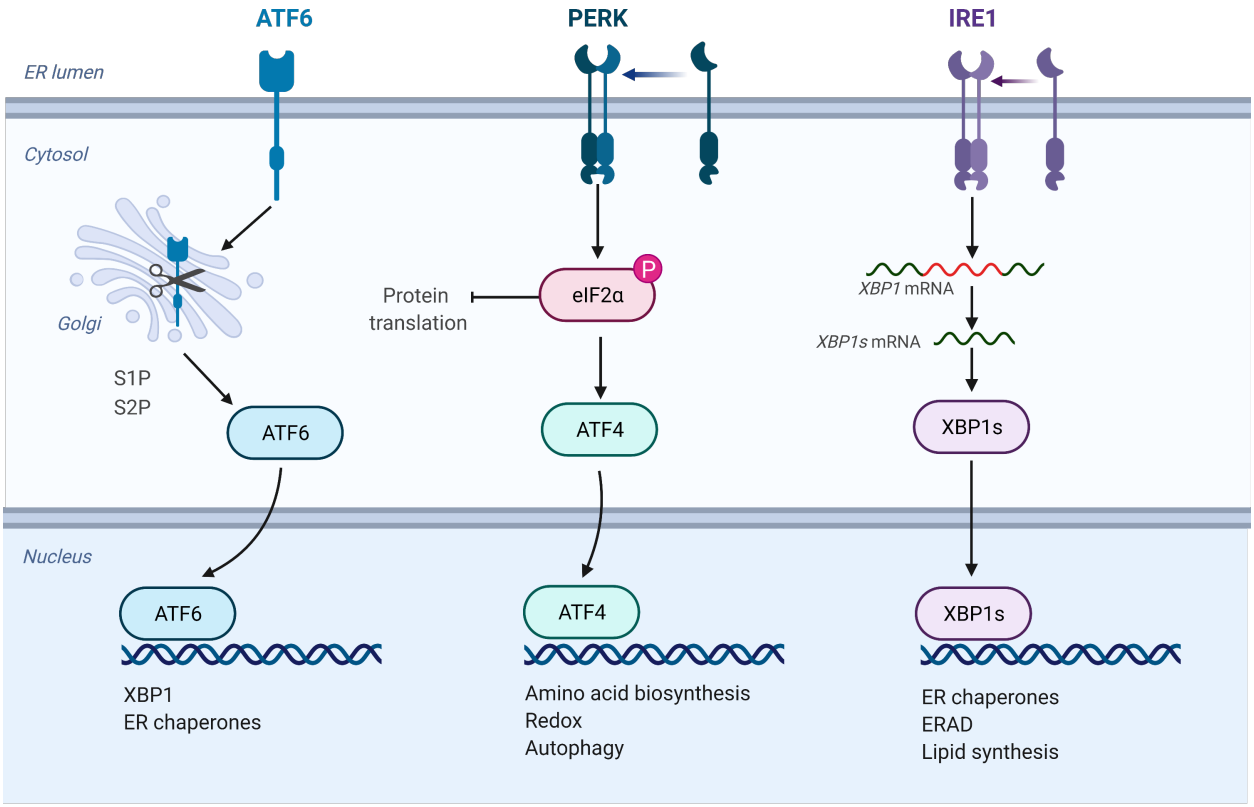

Figure 1.3. **Overview of the Endoplasmic Reticulum Unfolded Protein Response**. The three UPR transmembrane proteins IRE1, PERK and ATF6 work together to maintain cellular homeostasis. They each activate distinct downstream signaling pathways. When ER stress disrupts the natural homeostasis, the transmembrane proteins perform different roles. IRE1 exists as a monomer until stress is induced, upon stress it dimerizes and becomes phosphorylated. IRE-1 then acts as an endonuclease and cleaves 21bp from the intronic sequence of XBP1 mRNA. Spliced XBP1 goes into the nucleus and activates transcription of ERAD proteins, chaperones (HSP-4) and genes involved in immune signaling and lipid synthesis (Higuchi-Sanabria et al., 2018; R. C. Taylor & Hetz, 2020; Walter & Ron, 2011). PERK undergoes dimerization and phosphorylation in response to stress. PERK phosphorylates eukaryotic initiation factor 2α (eIF2α) which will inhibit protein translation. The eIF2α then induces ATF4 which enters the nucleus to drive the expression of genes such as un-spliced XBP1, ER chaperones and genes involved in apoptosis (e.g. CHOP). ATF6 responds to stress by translocating to the Golgi body where it is cleaved by site proteases (S1P and S2P) to create an ATF6 N-terminal fragment. This fragment goes to the nucleus with DNA- binding capability to activate UPR target genes, including XBP1 and ER chaperones. In summary, each arm of the ER-UPR is regulated by different signaling transduction mechanisms: ATF6 by proteolysis, PERK by translational control, and IRE1 by nonconventional mRNA splicing. Figure created using Biorender.com.

Lysosomal Stress Response

The above sections elucidate well characterized stress responses and the extensive work that has been done to understand their signaling cascades. In addition to these well-known and well-characterized stress responses, there is growing evidence that the lysosome could also be a site of stress response signaling. Lysosomes are acidic organelles that have been colloquially thought of as the garbage can of the cell. Lysosomes function to remove unwanted material within the cell through different mechanisms (Saftig & Puertollano, 2021). Autophagy, ERAD, and the ubiquitin-proteasome system all work together to send material to lysosomes for degradation or recycling (Lakpa et al., 2021; Saftig & Puertollano, 2021). In recent years, they have been established as centers for metabolic signaling and cell quality control of the cell (Lawrence & Zoncu, 2019; Saftig & Puertollano, 2021). Lysosomes respond to internal and external environmental changes such as calcium concentrations, inner lysosomal pH, autophagy, nutrient conditions, and protein misfolding (Lawrence & Zoncu, 2019; Saftig & Puertollano, 2021). The inability to react or sense these environmental changes can result in the accumulation of degradative material in lysosomes, leading to dysfunction or the activation of a signaling cascade. Additionally, the dysfunction of the lysosomes due to stressful conditions such as protein aggregation, lysosome de-acidification, mutations in degradative enzymes, or lysosomal fusion are implicated in lysosomal storage disorders, which lead to neurodegeneration (Lakpa et al., 2021). Overall, the multiple insults that the lysosome experiences have led to the emergence of a possible lysosomal stress response (LSR) (Lakpa et al., 2021; Saftig & Puertollano, 2021).

The existence of the LSR is a novel concept that is poorly studied. Recent papers suggest that lysosomes act as an active signaling platform to orchestrate different pathways to sense and respond to stress inducing conditions (Lakpa et al., 2021; Lawrence & Zoncu, 2019; Saftig & Puertollano, 2021). For instance, changes in nutrient availability, lysosomal calcium concentration and lysosomal dysfunction triggers dephosphorylation of the transcription factor TFEB, which then becomes localized to the nucleus (Lakpa et al., 2021; Lawrence & Zoncu, 2019; Napolitano & Ballabio, 2016; Saftig & Puertollano, 2021). Inside the nucleus, TFEB activates a suite of target genes involved in autophagy, lysosome biogenesis and function (Napolitano & Ballabio, 2016). This adaptive stress response restores lysosome function within the cell **(Figure 1.4)**. The transcriptional response of the lysosomes to stressful conditions is synonymous with how the other organelle-specific stress pathways operate. There is also the potential for one or more chaperones

to be activated in response to lysosomal stress to restore homeostasis within the cell. The lysosome could also work as a hub of cellular quality control, to support crosstalk between the different stress responses. This could be co-ordinated on the lysosomal surface by factors that are known to regulate cellular maintenance, such as AMPK and MTOR (Saftig & Puertollano, 2021).

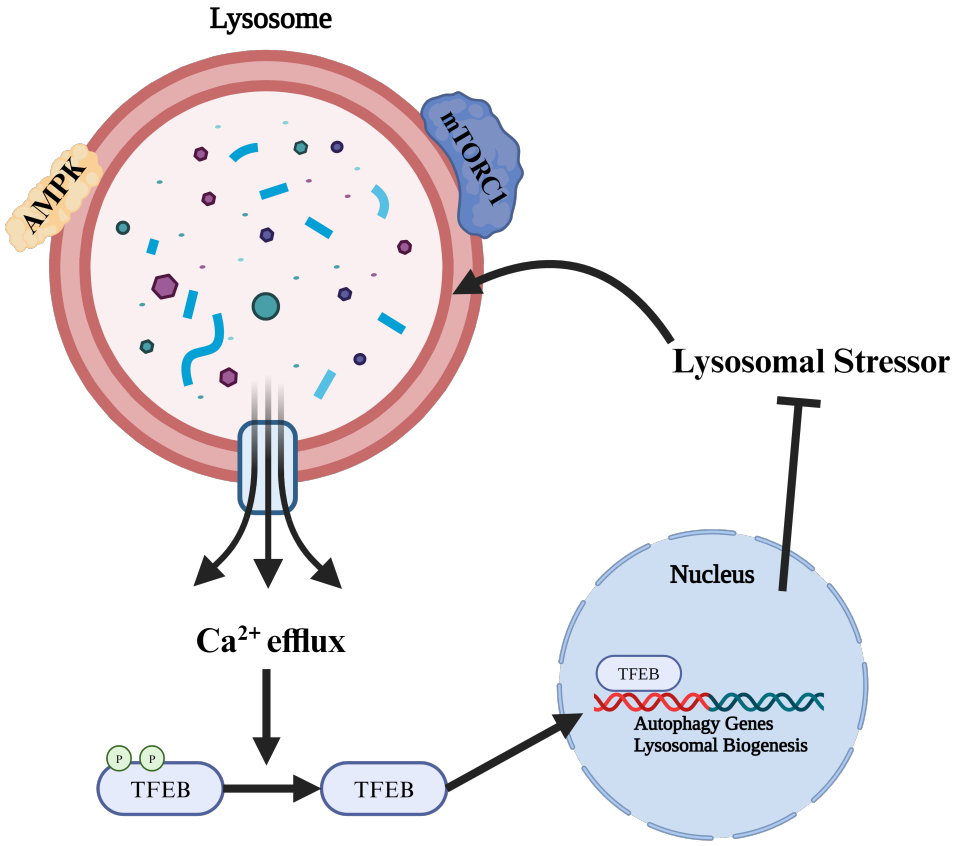

Figure 1.4. **Potential lysosomal stress response system**. Under conditions of lysosomal stress such as drugs which block lysosome function, nutrient availability, mutations in enzymes required for the breakdown of intracellular cargo, toxic protein aggregation, deacidification of intra-lysosomal pH, and calcium efflux into the cytoplasm, a transcriptional response is initiated. Lysosomal stress results in Calcium efflux which activates a signaling pathway that dephosphorylates the transcription factor TFEB. Following dephosphorylation TFEB enters the nucleus to transcribe genes involved in autophagy and lysosome biogenesis. This works to return the lysosome to a steady state balance and promotes the breakdown of intracellular material, returning the balance to the cell. Figure created using Biorender.com.

C. elegans as a model for Stress Research

Choosing a suitable model to investigate these wide cellular processes is instrumental to advancing our knowledge and understanding of stress response maintenance for the creation of targeted therapeutics. The different organelle-specific stress response pathways and the nutrient-sensing signaling cascades are well-conserved in *C. elegans.* A tremendous amount of work by several *C. elegans* labs has aptly demonstrated the complexities of different UPRs to maintain homeostasis within the nematode. For instance, loss of the main transcription factors of the MT-UPR (*atfs-1*), ER-UPR (*xbp-1*), and HSR (*hsf-1*) significantly alters the lifespan, development, thermotolerance of animals, and impairs proteostasis (Bennett et al., 2014; Hajdu-Cronin et al., 2004; Henis-Korenblit et al., 2010; Morley & Morimoto, 2004; Wu et al., 2018). Conversely, overexpression of these transcription factors causes beneficial effects such as lifespan extension and enhanced proteostasis.

The concept of the lysosomal stress response is yet to be fully discussed from the perspective of *C. elegans.* However, the *C. elegans* TFEB homolog, *hlh-30,* functions in a similar capacity as mammalian systems regulating lysosomal genes (Lapierre et al., 2013; O'Rourke & Ruvkun, 2013). It regulates the lifespan interventions of several long lived mutants in *C. elegans* (Lapierre et al., 2013; O'Rourke & Ruvkun, 2013), and is required for the lifespan extension observed following *xbp-1* overexpression (Imanikia, Özbey, et al., 2019).

Overexpression of transcription factors, like XBP-1 in the entire organism has been complicated concerning lifespan (Dutta et al., 2022). Hence, researchers have utilized tissue-specific reporters to understand the cell non-autonomous signaling of the stress response within *C. elegans.* Specifically, neuron-specific expression of the ER-UPR, MT-UPR and HSR signals to the intestine and promotes longevity, stress resilience, thermotolerance and proteostasis within *C. elegans* (Douglas et al., 2015; Durieux et al., 2011; Prahlad et al., 2008; R. C. Taylor & Dillin, 2013).

Work on the cell non-autonomous response of these pathways has recently elucidated glia's role in intestinal signaling in *C. elegans* (Frakes et al., 2020; Gildea et al., 2022). Glia, which promote neuronal maintenance, act as regulators of the ER-UPR and HSR in peripheral tissues to maintain longevity, proteostasis, and thermotolerance in animals (Dutta et al., 2022; Frakes et al., 2020; Gildea et al., 2022). This tissue-to-tissue signaling utilizes different neuronal subtypes, such as serotonergic and dopaminergic neurons, to utilize various neurotransmitters to activate a

transcriptional response in other tissues, thus promoting proteostasis (Dutta et al., 2022). The tissue-specific dissection of the different stress response pathways has advanced the field of aging and neurodegeneration, providing a greater understanding of the nuances surrounding the collapse of proteostasis with age. However, it remains to be explored how other signaling cascades can impact the stress response in animals and how they contribute to maintaining homeostasis. In response to conditions that are detrimental to cellular health, it remains to be determined how modulators of the stress response work to integrate and control the different stress response systems in a finely tuned network.

Signaling Pathways that modulate the stress response

Over the years, studies have identified signal transduction pathways within the cell that modulate different stress responses. These pathways are not organelle-specific but have a global response on the health of animals when activated. These signaling cascades respond to global stressors such as glucose, energy, and amino acid levels (J. Kim & Guan, 2019; Ottens et al., 2021; Salminen & Kaarniranta, 2012; R. C. Taylor & Dillin, 2011; van Heemst, 2010). Additionally, these signaling pathways can activate organelle-specific stress responses by regulating the respective transcription factors to maintain proteostasis and stress response within animals.

For starters, the insulin/insulin growth factor-1 signaling (IIS) pathway, as its name implies, is an insulin-regulated pathway, specifically a ligand and receptor pathway extensively characterized within the nematode *C. elegans* (R. C. Taylor & Dillin, 2011; Uno & Nishida, 2016). The work by Kenyon *et al.* describes the ortholog of the insulin/IGF-1 receptor, *daf-2*, whose loss of function mutations double the lifespan of animals (Kenyon et al., 1993). This is a result of the FOXO transcription factor, *daf-16,* being dephosphorylated, allowing it to localize to the nucleus and promote transcription of target genes. This extends lifespan due to the reduction of insulin activity (Kenyon et al., 1993). Studies on the IIS pathway have demonstrated that pathway function is well conserved across model organisms (R. C. Taylor & Dillin, 2011; van Heemst, 2010). Mutations in *daf-2* or reduced insulin levels governs the activity of HSF-1 and XBP-1, working in conjunction with DAF-16 to mediate lifespan extension and stress resistance (Henis-Korenblit et al., 2010; O'Reilly et al., 2014; R. C. Taylor & Dillin, 2011). This supports the involvement of other signaling cascades which activate the stress response and proteostasis.

Similarly, 5' adenosine monophosphate-activated protein kinase (AMPK) acts to maintain proteostasis and lifespan (Mair et al., 2011; Ottens et al., 2021; Uno & Nishida, 2016). AMPK is a well-conserved nutrient-sensing serine/threonine kinase activated when energy levels are low (Ottens et al., 2021; Salminen & Kaarniranta, 2012). Interestingly, loss of AMPK reduces lifespan in animals, whereas overexpression of AMPK extends lifespan (Mair et al., 2011; Martin-Montalvo et al., 2013; Uno & Nishida, 2016). Loss of AMPK also causes ER stress, activating different ER-UPR components (Y. Dong et al., 2010; Salminen & Kaarniranta, 2012), whereas overexpression suppresses ER stress (H. Kim et al., 2015). In contrast, inhibition of AMPK allows the HSR to become active to maintain the proteasome (Ottens et al., 2021). The interplay between the regulation of the different stress responses is complex.

Mammalian Target of Rapamycin (mTOR) signaling is another complex nutrient-sensing pathway that responds to energy changes within the cell, such as amino acid availability (J. Kim & Guan, 2019; Ottens et al., 2021; Papadopoli et al., 2019). It is aptly named, as the pharmacological drug rapamycin was found to extend the lifespan of animals as it inhibits TOR activity (J. Kim & Guan, 2019; Papadopoli et al., 2019). Since then, MTOR has been investigated as a regulator of hallmarks of aging, such as cellular senescence, energy homeostasis and proteostasis. The inhibition of TOR signaling has been linked to the clearance of aggregates in different diseases of aging or protein misfolding disorders (Ottens et al., 2021). Unsurprisingly, as MTOR appears to regulate proteostasis and aging, links to stress response pathways such as the ER-UPR and the MT-UPR have been uncovered recently (Appenzeller-Herzog & Hall, 2012; Statzer et al., 2022). For example, inhibiting TOR by rapamycin reduced the activity of ER-UPR targets (G. Dong et al., 2015). TOR activity has also been found to regulate the transcription factor ATF4, which is shared between the MT-UPR and ER-UPR (Dutta et al., 2022; Li et al., 2023; Naresh & Haynes, 2019; Quirós et al., 2017; Statzer et al., 2022). MTOR appears to coordinate with these different stress responses by inhibiting translation (Statzer et al., 2022).

Altogether, the pathways described above maintain cellular metabolism in response to energy, glucose and amino acid changes. Furthermore, these pathways are all interconnected such that AMPK inhibits TOR activity and stimulates IIS/FOXO transcription, whereas MTOR inhibits IIS (Ottens et al., 2021). Recently, these pathways have also been implicated in lysosomal signaling, as the lysosomal surface is a site for MTOR and AMPK to mediate their activity within the cell in a concerted manner. At the heart of these pathways, they work together to regulate

proteostasis and the stress response and prevent the collapse of homeostasis observed in many diseases, particularly those of aging. Neurodegenerative disorders have dysregulated stress response which inhibits their ability to restore proteostasis as discussed in the following section.

1.4 Neurodegenerative Disorders activate the stress response

The stress response pathways described above, which are known to decline in function with age, are dysregulated in neurodegenerative disorders. As people are living longer worldwide there is a concomitant increase in age-related neurological disorders (Martínez et al., 2017). Neurodegenerative diseases like Parkinson's Disease (PD), Alzheimer's Disease (AD), and Huntington's Disease (HD) are age-associated disorders which affect millions of people worldwide, the majority of whom are the elderly community. Currently, there is no known cure for these neurodegenerative disorders, and treatments are symptomatic at best. The therapeutics for these disorders either focus on slowing down or managing the symptoms associated with the diseases, but none can fully prevent it (Lamptey et al., 2022; Wilson et al., 2023). These diseases are characterized by loss of neuronal function, resulting in severe motor dysfunction and cognition impairment. Furthermore, these neurodegenerative disorders have distinct clinical hallmarks, i.e. severe motor dysfunction, bradykinesia and tremors in PD patients, memory loss and cognition impairment in AD patients, and uncoordinated involuntary body movements in HD (Hetz & Saxena, 2017; Scheckel & Aguzzi, 2018). These diseases all affect various neurons within the brain, such as the substantia nigra of the dopaminergic neurons, the hippocampal neurons, and the striatal neurons (Scheckel & Aguzzi, 2018).

Another hallmark shared between these diseases is mutations which result in the abnormal aggregation of misfolded proteins. Therefore, these neurodegenerative disorders are also classified as protein misfolding disorders (PMDs) (Hetz & Saxena, 2017). Mutations in the *SNCA, APP,* and *HTT* genes are pathological hallmarks observed in PD, AD, and HD, leading to the accumulation of α-Synuclein, β-amyloid, and PolyQ proteins respectively. These toxic proteins aggregate, creating a burden on neuronal cells. The protein aggregates disrupt the internal environment causing cellular stress (Hetz & Saxena, 2017; Wilson et al., 2023), which in turn activates the stress response. The chronic activation of the stress response eventually leads to cellular death as the UPR can no longer restore homeostasis within neuronal cells (Hetz & Saxena, 2017). Dysregulated proteostasis plays a significant role in neurodegenerative diseases. Current research involves looking at mechanisms to maintain proper stress response activity to promote neuronal

health by protecting against protein aggregation (Gomez-Pastor et al., 2018; Hetz et al., 2020; Shpilka & Haynes, 2018). These mechanisms can eventually be harnessed to sustain proteostasis or the stress response, particularly as animals age (R. C. Taylor & Hetz, 2020). Proteostasis is central to neurodegenerative diseases and many other disorders, activating the stress response and other cellular mechanisms such as ERAD, autophagy, and the ubiquitin lysosomal system (Hetz & Saxena, 2017).

C. elegans are heavily utilized to study the stress response and proteostasis when addressing mechanisms to combat these neurodegenerative diseases. Modulating the stress response to protect against these neurodegenerative disorders is well-studied to the *C. elegans* system due to its relatively simple nervous system. Harnessing the expansive body of research that exists on the stress response and the collapse of proteostasis, novel targets can be investigated with a broad view and quickly narrowed down with the widespread tools available at our disposal. Noteworthy targets for investigation are neurotrophic factors, which have been investigated for their neuroprotective capabilities.

1.5 Neurotrophic Factors: Overview

Neurotrophic factors (NTFs) are a class of small extracellular proteins that support the survival and differentiation of neuronal cells and the development of a mature nervous system. NTFs are also involved in maintaining neuron homeostasis and neuroregeneration via their anti-inflammatory and anti-apoptotic properties (Airavaara et al., 2009; Nasrolahi et al., 2018; Renko et al., 2018). Neurotrophic factors are of particular interest to the field of neurodegeneration, as they are being investigated as suitable therapeutic candidates in treating PD and other neurodegenerative diseases. Well-known NTFs include nerve growth factor (NGF), glial cell-derived neurotrophic factor (GDNF) and brain-derived neurotrophic factor (BDNF) (Jäntti & Harvey, 2020). These classical NTFs are secreted and bind to a receptor on the membrane surface, activating a signaling cascade to promote neuronal maintenance and survival following injury (Jäntti & Harvey, 2020). NGF, BDNF, and GDNF are reported to be protective of dopaminergic neurons but can also protect other neuronal types (Chmielarz & Saarma, 2020; Ducray et al., 2006; Popova et al., 2017). However, these NTFs have had limited success in clinical trials at mitigating the progression of PD without causing serious side effects (Chmielarz & Saarma, 2020). However, a novel NTF family known as the MANF/CDNF family (Jäntti & Harvey, 2020) shows promise, with success in intraputamenal delivery and drug tolerance being observed in human clinical trials

(Huttunen et al., 2023). Compared to other NTFs, the MANF/CDNF family is unconventional in both their structure and function.

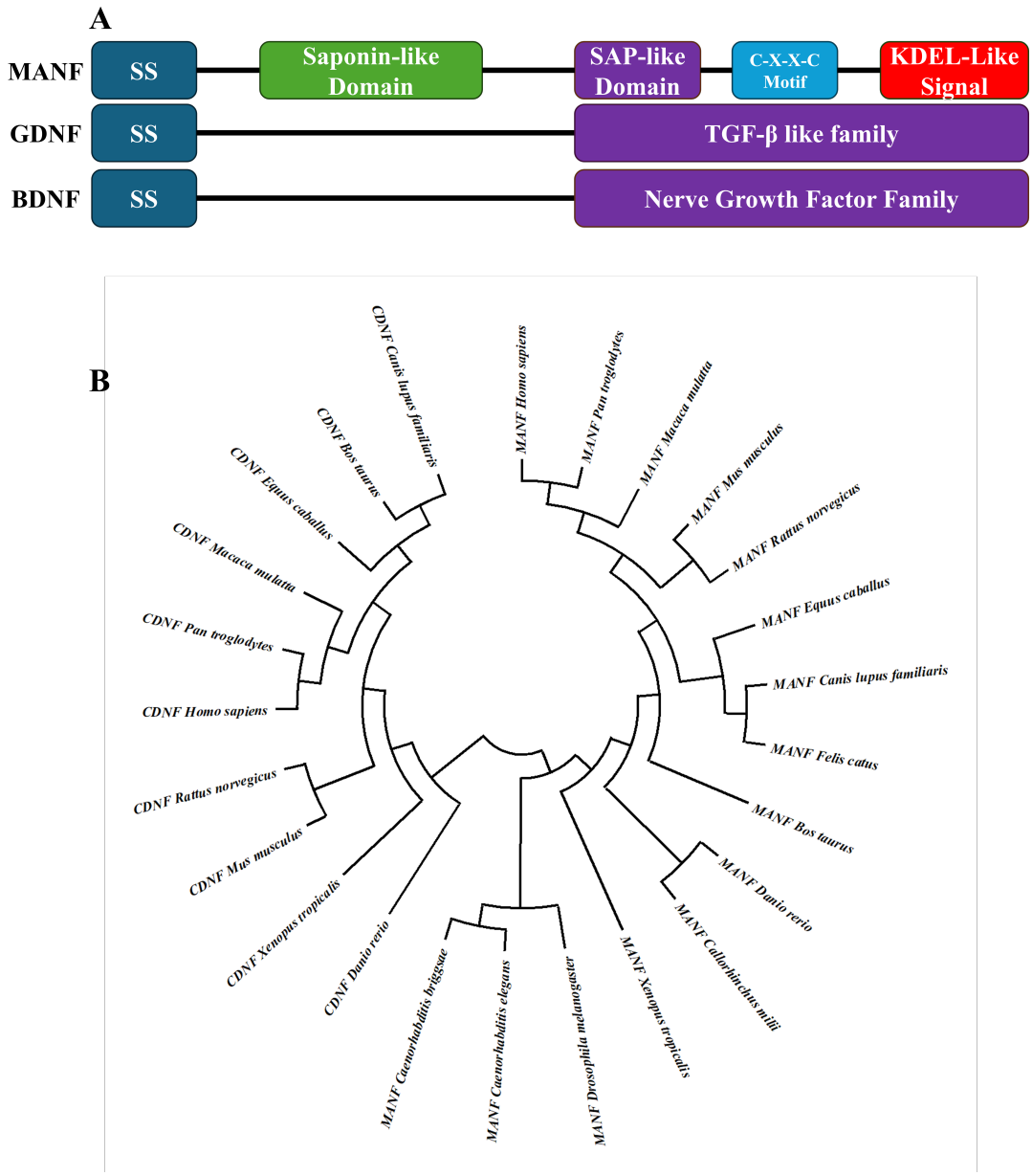

Figure 1.5. **The structure and homology of MANF. A)** MANF has a Saponin like domain, SAP domain and a KDEL like sequence. The Saponin family of proteins are reported to degrade lipids through membrane interaction. The SAP (SAF-A/B, Acinus and PIAS) domain is homologous to Ku70, a proapoptotic inhibitor of Bax (Bcl-2-associated X protein). The KDEL like sequence causes endoplasmic retention of MANF. BDNF and GDNF have homology to the TGFβ and NGF family respectively. Compared to BDNF and GDNF which have one major domain family, MANF has a two-domain architecture on the N- terminus and C- terminus. These domains are reported to

make MANF a bifunctional protein (Hellman et al., 2011). All three NTFs have a signal sequence. Families of MANF, GDNF, and BDNF were identified using InterPro and UniProt. GDNF and BDNF sequences have mature forms of their proteins that bind to receptors to facilitate their neurotrophic activity. **B)** Phylogenetic tree of MANF protein sequences generated using the maximum likelihood method performed with MEGA11 software. The phylogenetic tree was generated on MEGA11. Protein sequences of all 24 species were extracted from the NCBI ortholog list.

1.6 MANF/CDNF Family

Over the last 20 years, the evolutionarily conserved MANF/CDNF family of NTFS have become noteworthy targets for investigation as they possess neuroprotective capabilities in multiple animal models (Jäntti & Harvey, 2020; Pakarinen & Lindholm, 2023; Palgi et al., 2009; Richman et al., 2018; Voutilainen et al., 2009). Family members include **c**erebral **d**opamine **n**eurotrophic **f**actor (CDNF) and the **m**esencephalic **a**strocyte derived **n**eurotrophic **f**actor (MANF). This family of NTFs is structurally and mechanistically distinct from other classical NTFs (Lindahl et al., 2017). MANF/CDNF share no sequence homology with other NTFS (Parkash et al., 2009) and also have different domain families to those of classical NTFS, such as BDNF and GDNF (**Figure 1.5A**). Therefore, MANF/CDNF act through unknown mechanisms to have a cytoprotective function. Additionally, CDNF and MANF are paralogues, and both are present in vertebrates, but only MANF is present in invertebrates. MANF is highly conserved among many species, including humans, mouse, rats, *Drosophila,* and *C. elegans* (**Figure 1.5B**) (Nasrolahi et al., 2018; Richman et al., 2018). MANF is an 18-20 kDa protein that was initially derived from a cultured medium of rat type-1 astrocyte ventral mesencephalic cells (Petrova et al., 2003). It was previously known as arginine rich mutated in early-stage tumors (ARMET) due to the belief that the N-terminus was rich in arginine (Petrova et al., 2003; Voutilainen et al., 2015). However, subsequent studies found that it was not rich in arginine and it was subsequently renamed to reflect its neurotrophic properties (Mizobuchi et al., 2007; Petrova et al., 2003). MANF is crucial for the development and survival of the central nervous system, and MANF has been found to protect and restore the function of dopaminergic (DA) neurons in healthy animal models, as well as in various eukaryotic PD models (Jäntti & Harvey, 2020; Pakarinen & Lindholm, 2023; Palgi et al., 2009; Richman et al., 2018; Voutilainen et al., 2009). Initially, MANF was thought to be selectively protective of dopaminergic neurons, but subsequent studies determined that it has a broader role in multiple tissues (Jäntti & Harvey, 2020; Neves et al., 2016; Sousa-Victor et al., 2018, 2019; Sousa et al., 2023). MANF was found to be widely expressed in many tissues (i.e. the

pancreas, kidney, brain), but its expression declines with age, despite its role in maintaining homeostasis (Danilova et al., 2019; Jäntti & Harvey, 2020; Neves et al., 2016; Peled et al., 2021; Richman et al., 2018; Sousa-Victor et al., 2018, 2019; Sousa et al., 2023).

In the beginning, research on MANF was performed from the perspective of neurodegenerative disorders due to its discovery within dopaminergic neurons (Petrova et al., 2003). Consistent with this, research by many groups demonstrated that loss of MANF causes PD-like symptoms in several animal models (Apostolou et al., 2008; Palgi et al., 2009; Richman et al., 2018; Voutilainen et al., 2009). Loss of MANF in mouse models caused PD-like defects and resulted in severe diabetes from the loss of beta cells and increased the UPR activation in the pancreas islets cells (Lindahl et al., 2014, 2017; Petrova et al., 2003; Voutilainen et al., 2009). Knockdown of MANF in larval zebrafish impaired the development of dopaminergic neurons but could be rescued following exogenous MANF application (Chen et al., 2012). Deletion of MANF in *Drosophila melanogaster* causes axonal degeneration, dopamine reduction, loss of dopaminergic neurites, and larval lethality (Lindström et al., 2013; Palgi et al., 2009). Mutations in the *C. elegans* MANF/CDNF homolog, *manf-1,* also resulted in an age-dependent decline in dopaminergic neuronal health, α-Synuclein aggregation, and mobility (Richman et al., 2018). Work in *C. elegans* also reported that increased MANF-1 is neuroprotective in an α-Synuclein model, improving locomotion (Z. Zhang et al., 2018). Interestingly, loss of *manf-1* results in immunity to stress-inducing drugs and pathogens during the larval stages without growth inhibition (Hartman et al., 2019). However, the loss of *manf-1* in adults worms makes them susceptible to stress (S. K. B. Taylor et al., 2024).

Changes in MANF are associated with various diseases not limited to neurodegenerative disorders but also including inflammatory, metabolic, and skeletal disorders (Jäntti & Harvey, 2020; Pakarinen & Lindholm, 2023; Sousa-Victor et al., 2018; Sousa et al., 2023). In short, changes in MANF levels have been observed in PD, AD, stroke, type 1 and 2 diabetes, liver injury, and ischemia (Jäntti & Harvey, 2020; Pakarinen & Lindholm, 2023). Fortunately, MANF has been able to elicit protective benefits in these disorders via induction or exogenously applied MANF in different animal models (Jäntti & Harvey, 2020). The conserved property of MANF between species has been observed using human MANF, which can rescue the lethal effect observed in *D. melanogaster* MANF mutants (Palgi et al., 2009). Similarly, human MANF can be substituted in *C. elegans,* abrogating ER stress in these animals (Bai et al., 2018).

As discussed above MANF has a broad role within animals, and much of its function appears to be conserved between species. MANF can potentially regulate different processes within the cells due to its implication in many disorders. However, what mechanisms MANF may utilize to protect animals is not fully understood. Interestingly, research demonstrated that MANF expression also declines with age, suggesting a link between its function and age-related impairments on health of animals. *manf-1* mutants have reduced lifespan in *C. elegans,* strengthening this finding. Similarly, *MANF* RNAi also reduces lifespan in *D. melanogaster* (Smith et al., 2019; Sousa-Victor et al., 2019; S. K. B. Taylor et al., 2024). This phenomenon draws a parallel with not only age-dependent neurodegeneration but also with age-related disorders. MANF could contribute to hallmarks of aging, by affecting proteostasis and the stress response. Loss of MANF significantly dysregulates the ER-UPR in animals causing significant impact on organismal survival (Jäntti & Harvey, 2020; Richman et al., 2018).

1.7 More than a Neurotrophic factor MANF: a regulator of the UPR

A significant portion of my thesis focuses on elucidating the cellular and molecule roles of MANF in *C. elegans.* Previous work has suggested that MANF has the potential to protect against dysregulation of the stress response, a hallmark of neurodegenerative diseases (López-Otín et al., 2023; Pakarinen & Lindholm, 2023; Richman et al., 2018). MANF has an N-terminal signal sequence and an ER retention signal at its C-terminal, causing it to localize to the ER lumen (Lõhelaid et al., 2022; Richman et al., 2018). Additionally, MANF is critical in regulating the ER-UPR to maintain organismal health, making it distinct from classically secreted NTFs (Jäntti & Harvey, 2020; Lõhelaid et al., 2022; Richman et al., 2018; Sousa-Victor et al., 2019). Since identifying its ER retention signal and involvement in the UPR, MANF has been classified as a promoter of the UPR (Jäntti & Harvey, 2020; Lõhelaid et al., 2022). Loss of MANF in adulthood makes animals susceptible to ER Stress. Several studies have focused on understanding how MANF, a neurotrophic factor, is able to regulate the ER-UPR and its role within the ER (Jäntti & Harvey, 2020; Lõhelaid et al., 2022). Research on MANF has been primarily done in mouse and cell lines. However, only a handful of articles have been published using *Drosophila* and *C. elegans* models to date.

The research in different models has demonstrated multiple connections between the ER-UPR and MANF (Jäntti & Harvey, 2020). MANF overexpression reduces UPR activation in a cell line model of AD, and conversely, loss of MANF increases UPR activity (S. Xu et al., 2019). In

Drosophila, a transcriptomic study demonstrated that several changes in UPR, endosomal, and PD-related genes were altered and showed that MANF localizes partially to the ER and endosomal compartment (Palgi et al., 2012). Further research in *Drosophila* observed that ER stress-inducing chemicals (tunicamycin and thapsigargin) increase MANF expression (Lindström et al., 2016). The authors also elucidated a potential genetic interaction between ER-UPR components and MANF. They found that performing RNAi knockdown of XBP-1, GRP78, and PERK in MANF overexpression flies altered the wing shape in *Drosophila* and, in some cases, caused lethality (Lindström et al., 2016). This is supported by work in *C. elegans,* which shows that a mutation of *atf-6* or *pek-1* within *manf-1* mutants eliminates the larval resistance of *manf-1* mutants to tunicamycin (Hartman et al., 2019). Additionally, it was determined that a double mutant between *ire-1* and *manf-1* results in homozygous lethal worms, emphasizing the necessity of both genes for survival (Hartman et al., 2019). Other research investigating the IRE1/XBP1 arm of the ER-UPR demonstrates that XBP1s may be a transcriptional regulator of MANF, and inhibition of XBP1 or IRE1 attenuates the expression of MANF (D. Wang et al., 2018). Interestingly, MANF also regulates the expression of ER-UPR proteins, such as the chaperone GRP78/BiP (Richman et al., 2018).

MANF is reported to interact with GRP78/BiP and IRE-1 to regulate UPR activity (Eesmaa et al., 2021; Kovaleva et al., 2023). MANF can act as a cofactor with GRP78/BiP in UPR maintenance, but this is not required for the role of MANF in neuronal survival. Only the IRE-1 interaction is necessary for its protective capability on neurons (Eesmaa et al., 2021; Kovaleva et al., 2023). The role of MANF in heart disease and stroke may also depend on this ER-UPR arm, but it may be the precise interaction between XBP1 and MANF that is critical for regulating other stress response genes following a stroke (Lõhelaid et al., 2022).

1.8 More than a Neurotrophic factor: MANF is a regulator of proteostasis

Research over the years supports MANF being a UPR regulator working to maintain health in animals. Is the ER-UPR the only stress signaling pathway that MANF regulates? The broad pattern of MANF expression led to research on MANF's role beyond dopaminergic neurons. MANF is capable of modulating different processes to mediate cytoprotective capabilities (Jäntti & Harvey, 2020; Lõhelaid et al., 2022; Pakarinen & Lindholm, 2023; Palgi et al., 2009). MANF could potentially be involved in other pathways associated with neurodegeneration and metabolic disorders. The intricacies of the involvement of MANF with other UPRs such as (MT-UPR, HSR

and LSR) remain to be further explored. Recent work by Kim *et al.* (2023) demonstrated that MANF can restore mitochondrial homeostasis to treat kidney disease in mouse by activating p-AMPK, which stimulates mitophagy (Y. Kim et al., 2023). Additionally, within the context of alcohol-associated liver disease, the addition of recombinant MANF activates AMPK, ameliorating liver steatosis (H. Xu et al., 2023).

The ability of MANF to maintain neuronal and organismal health is complex with the addition of its role in different tissues. Unlike other NTFs, MANF is expressed broadly across tissues, where it is likely to have diverse functions. This complicates investigating its mechanism of action, making it difficult to elucidate how MANF may exert a cytoprotective function within animals. A universal receptor for MANF has not been identified, despite this being present in other NTF. Recently, a group demonstrated that in HeLa cells, Neuroplastin (NPTN) binds MANF to regulate immunity (Yagi et al., 2020). The same group also demonstrated that IRE1α facilitates the binding of MANF for neuroprotective properties in cell and rat models (Kovaleva et al., 2023). However, no *Drosophila* or *C. elegans* receptor for MANF has been identified. Additionally, an NCBI blast shows NPTN does not appear to share any sequence similarity with any *C. elegans* proteins, nor has it been identified in *C. elegans.* There may be a distant homolog of NPTN with low sequence similarity in *C. elegans,* or *C. elegans* MANF may be bound by a different, unknown receptor.

It remains to be seen if NPTN and IRE1α are also involved in MANF signaling in invertebrate models such as *Drosophila* and *C. elegans.* The binding of the IRE1α receptor is a possibility as this receptor is conserved in invertebrate models. If MANF binds to this receptor for UPR activity could MANF bind to other receptors to regulate the stress response? A proposed receptor for MANF activity are KDEL receptors which shuttle proteins that contain a KDEL like sequence to move between the ER and Golgi (Lõhelaid et al., 2022). These receptors are named after the canonical amino acid ER retention signal “KDEL”. Orthologs of MANF have variations in this sequence. For example, the human and mouse ER retention signal for MANF is “RTDL”, whereas in *D. melanogaster* and *C. elegans* it is “RSEL” and “KEEL” respectively(Henderson et al., 2013). The presence of the ER retention signal in MANF proteins supports the potential interaction between MANF and KDEL receptors for survival. A proposed mode of action for MANF could involve the retrograde cycling of MANF by KDEL receptors. Under normal conditions, MANF exists within the ER and is expected to shuttle back and forth between the Golgi

and ER. When cells experience stress or a calcium efflux occurs, MANF is secreted from the ER and is trafficked extracellularly, going to target cells to be cytoprotective (Lõhelaid et al., 2022; Pakarinen & Lindholm, 2023). Opposing papers argue whether the ER retention signal is necessary for MANF secretion in response to ER stress (Glembotski et al., 2012; Henderson et al., 2013). Research suggests that the MANF ER retention signals are relatively weak signals compared to the canonical "KDEL" signal (Glembotski et al., 2012). Changing the ER retention signal of MANF to KDEL reduces its secretion following ER stress (Glembotski et al., 2012).

As a secreted protein induced by stress, MANF could signal target tissues to elicit different responses including UPR activity. Once extracellular MANF is taken up, it could balance intracellular stress. Potentially, extracellular MANF could bind to ER- UPR sensors such as IRE1, activating the UPR in neuronal cells or tissues to prevent disease states (Jäntti & Harvey, 2020; Lõhelaid et al., 2022).

A substantial amount of work is required to understand the precise mechanism of MANF as a regulator of the stress response to mitigate neurodegeneration and promote proteostasis. Additionally, the role of MANF in maintaining organismal health as we age requires further investigation. MANF holds incredible potential to revolutionize our understanding of regulating different stress responses. Understanding the precise mechanism of action of MANF could facilitate therapeutic development for a broad spectrum of diseases with dysregulated stress responses. This would allow MANF to be employed as a potent therapeutic for age-related disorders and could lead to the development of novel genetic therapies for diseases with limited treatments(López-Otín et al., 2023; Sousa-Victor et al., 2019; W. H. Zhang et al., 2022). My work, described in subsequent chapters, demonstrates that MANF is at the intersection of proteostasis, neurodegeneration, longevity, and stress response maintenance and is well suited for addressing the effects of a dysfunctional stress response.

1.9 Thesis Objectives

Over the years, an in-depth analysis of the stress response and proteostasis has been done collaboratively in various model systems from mouse to *C. elegans.* The work described in this thesis aims to understand the contribution of maintaining the stress response to the promotion of healthy living in animals. The research objective that guided my Ph.D. thesis was to examine how changes in the stress response affect various aspects of health in animals such as behaviour and how stress response modulators like MANF prevent the collapse of proteostasis and promote organismal fitness. To this end I explored the following hypotheses:

1) The regulation of the stress response pathways mediates the behaviour of animals. I examined how environmental insults and genetic mutations in *C. elegans* affect the different stress response pathways to modulate electrotaxis behavior.
2) The stress regulating protein MANF modulates the UPR and proteostasis to promote neuronal health and survival. This thesis explored how the cytoprotective function of MANF acts as more than a neurotrophic factor. Additionally, I examined the role of MANF at the tissue and cellular level to understand its mechanism of action in modulating the stress response to promote organismal survival.

MANF has a broad expression pattern and is implicated in many disorders. The *C. elegans* systems present the opportunity to investigate the mechanisms of MANF from multiple viewpoints, including whole organism, tissue-specific, and organelle-specific perspectives. MANF can potentially be a central player in the maintenance of adaptive stress response signaling **(Figure 1.5)**. Understanding the function of MANF in *C. elegans* through its interaction with regulators of neurodegeneration and stress response signaling in a tissue and organelle-specific view will lay the mechanistic groundwork needed to effectively harness its therapeutic potential for treating age-associated disorders. This research addresses the gap in our understanding of genes which maintain the response to promote neuronal health and longevity and the multiple routes by which they accomplish this.

1.10 Chapter Overview

My thesis is organized into 5 chapters with an appendix. They are as follows: the introduction (Chapter 1). Chapters 2-4 describe research findings on the stress response and the investigation into the mechanism of MANF function. Chapter 2 is published; Chapter 3 is submitted for publication and currently under review. Chapter 4 is a written draft to be submitted to a peer-reviewed journal. Chapter 5 includes discussion and future directions which discusses the results and outlines potential areas for future investigations.

Chapter 2 demonstrates the requirements of the different organelle stress responses within the cell to modulate movement behavior in *C. elegans* using a novel microfluidic electrotaxis assay. This chapter also demonstrates that different chemical and environmental insults activate the stress response, impacting organismal health. Furthermore, it elucidates how transient stress can promote a better physiology in animals, but chronic stress is severely detrimental.

Chapter 3 elucidates the role of MANF in mediating proteostasis in *C. elegans.* This chapter presents for the first time the novel expression pattern of MANF to lysosomes which is dependent on the endosomal trafficking system. This chapter demonstrates that MANF overexpression extends lifespan, protects dopaminergic neurons, and reduces protein aggregation in *C. elegans*. The protective effect of MANF was dependent on the transcription factor TFEB/HLH-30 which regulates lysosomal genes and autophagy. This chapter shows that MANF utilizes the autophagy-lysosomal system to potentially clear protein aggregates.

Chapter 4 examines the novel role of MANF in maintaining age-dependent muscle health. This chapter shows that MANF regulates several genes related to muscle function. We show that Loss of MANF results in reduced muscle function and that MANF regulates mitochondrial health in animals.

Collectively, the work in these chapters emphasizes the broad role of the stress response in maintaining organismal health and the significant impact that regulators like MANF have on the cell, tissues, and physiology of the animal.

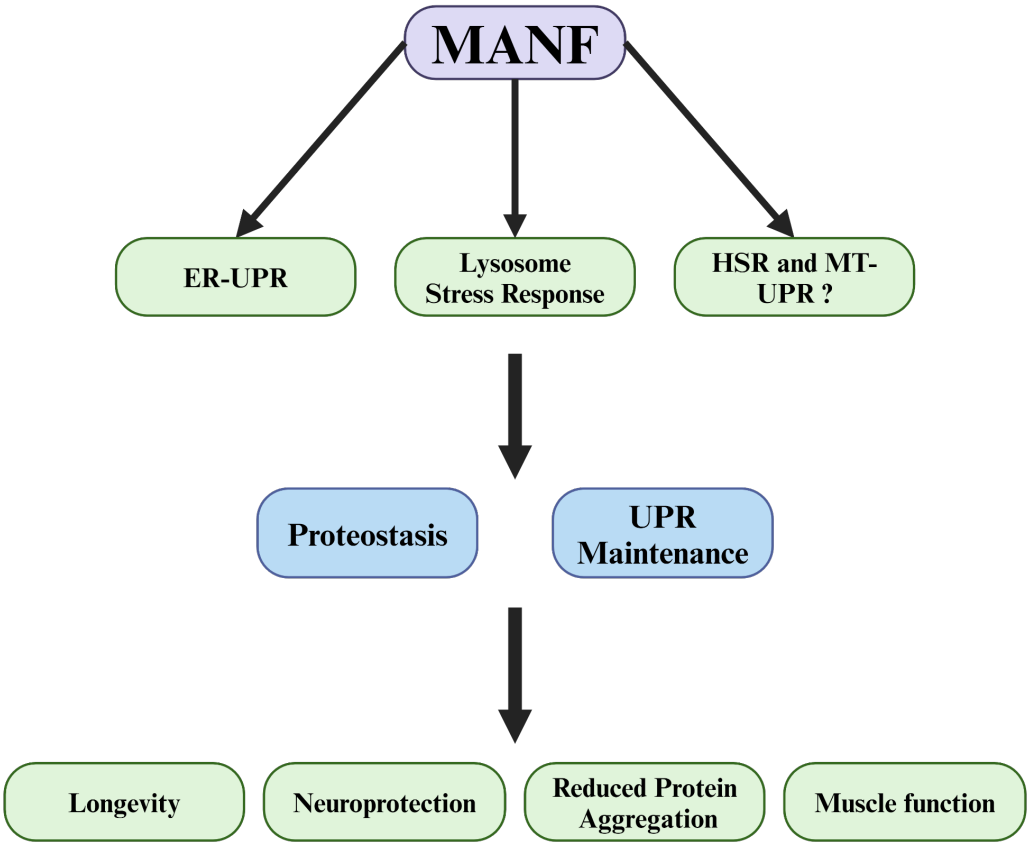

Figure 1.6. **MANF has the potential to be at the center of stress response signaling**. MANF has multiple functions unlike other known neurotrophic factors. MANF is able to regulate UPR maintenance and proteostasis within the cell, preserving homeostasis with age. The signaling of MANF to target tissues allows it to mediate longevity, neuroprotection, lysosome function and reduce protein aggregation in animals. Figure created using Biorender.com.

2 UPR and HSR pathways modulate electrotaxis behavior.

2.1 Preface

This chapter includes the following two articles in their originally published format:

1) *C. elegans* electrotaxis behavior is modulated by heat shock response and unfolded protein response signaling pathways by Shane K. B. Taylor[1], Muhammad H. Minhas[1], Justin Tong, P. Ravi Selvaganapathy, Ram K. Mishra & Bhagwati P. Gupta. Scientific Reports. **11**, 1–17 (2021). https://doi.org/10.1038/s41598-021-82466-z

2) Effect of starvation on electrotaxis response by Shane K. B. Taylor, Muhammad H. Minhas & Bhagwati P. Gupta. *microPublication Biolology.* (2023). DOI:10.17912/micropub.biology.000962

In this chapter we report on how the stress response plays a major role in mediating the movement of animals when stimulated by an electric current i.e. electrotaxis. The electrotaxis behavior is known to be affected by the neuronal health of animals. Therefore, we sought to examine the role of various stress inducing conditions, such as heat, starvation, chemical toxicity, exercise, and genetic mutations which are reported to affect the neuronal health of animals. This chapter mainly identified that the HSR and the UPR of the mitochondria and endoplasmic reticulum affect the locomotion of animals. Specifically, the major transcription factors of these stress response pathways *hsf-1, atfs-1* and *xbp-1* have a significantly reduced locomotory capability compared to control. These pathways all contribute in longevity, proteostasis and the neuronal health of animals. This work provides a further extension of how genes mediating the stress response are essential to maintaining the neuronal health of animals.

2.2 Taylor, S. K. B. *et al.* 2021. Scientific Reports

www.nature.com/scientificreports

scientific reports

Check for updates

OPEN

C. elegans electrotaxis behavior is modulated by heat shock response and unfolded protein response signaling pathways

Shane K. B. Taylor[1,4], Muhammad H. Minhas[1,4], Justin Tong[1], P. Ravi Selvaganapathy[2], Ram K. Mishra[3] & Bhagwati P. Gupta[1]✉

The nematode *C. elegans* is a leading model to investigate the mechanisms of stress-induced behavioral changes coupled with biochemical mechanisms. Our group has previously characterized *C. elegans* behavior using a microfluidic-based electrotaxis device, and showed that worms display directional motion in the presence of a mild electric field. In this study, we describe the effects of various forms of genetic and environmental stress on the electrotactic movement of animals. Using exposure to chemicals, such as paraquat and tunicamycin, as well as mitochondrial and endoplasmic reticulum (ER) unfolded protein response (UPR) mutants, we demonstrate that chronic stress causes abnormal movement. Additionally, we report that *pqe-1* (human RNA exonuclease 1 homolog) is necessary for the maintenance of multiple stress response signaling and electrotaxis behavior of animals. Further, exposure of *C. elegans* to several environmental stress-inducing conditions revealed that while chronic heat and dietary restriction caused electrotaxis speed deficits due to prolonged stress, daily exercise had a beneficial effect on the animals, likely due to improved muscle health and transient activation of UPR. Overall, these data demonstrate that the electrotaxis behavior of worms is susceptible to cytosolic, mitochondrial, and ER stress, and that multiple stress response pathways contribute to its preservation in the face of stressful stimuli.

Organisms have evolved intricate molecular machineries in order to respond to adverse or stressful stimuli as their survival depends on their ability to continuously monitor the environment and mount appropriate responses. Since the initial work of Hans Selye in 1936, who studied stress response in rats and termed it 'general adaptation syndrome'[1,2], the work in the field of stress biology has grown exponentially, leading to a better understanding of the connections between stress and diseases. Animals exposed to stressful conditions such as heat, toxins, starvation, and psychological stress activate signaling cascades leading to physiological changes. For instance, in the larvae of fruit fly *Drosophila melanogaster*, noxious stimuli induce a stereotyped escape response mediated by neuronal signaling that manifests as rolling and bending reactions[3]. Work in rats showed that when animals were separated from their mothers as pups they showed increased stress response to environmental conditions[4]. Studies in humans have shown that stress can induce intracellular signaling leading to changes in prefrontal cortex function, thereby impacting learning and memory[5]. In addition, there are numerous reports on the endocrine system responding to stress via signaling cascades mediated by hormones such as adrenaline and cortisol[6].

Detrimental stress in eukaryotes can often lead to an accumulation of misfolded proteins. The stress caused by this accumulation is mitigated by the molecular machinery consisting of several proteins that constitute the UPR signaling network[7]. The three well-known UPR pathways function in the cytosol, mitochondria, and ER, respectively[7]. The cytosolic heat shock response (HSR), UPR^{ER}, and UPR^{MT} regulate both the expression and function of multiple chaperons to maintain homeostasis. These chaperons are members of the heat shock protein family and are transcriptionally regulated by the heat shock factor (HSF), which is a major player in the HSR. Together, UPR^{MT}, UPR^{ER}, and HSR allay cellular stress by attenuating translation to maintain protein homeostasis within the cell, lowering reactive oxygen species (ROS), and inducing cell death[7].

[1]Department of Biology, McMaster University, Hamilton, ON, Canada. [2]Department of Mechanical Engineering, McMaster University, Hamilton, ON, Canada. [3]Department of Psychiatry and Behavioural Neurosciences, McMaster University, Hamilton, ON, Canada. [4]These authors contributed equally: Shane K. B. Taylor and Muhammad H. Minhas. ✉email: guptab@mcmaster.ca

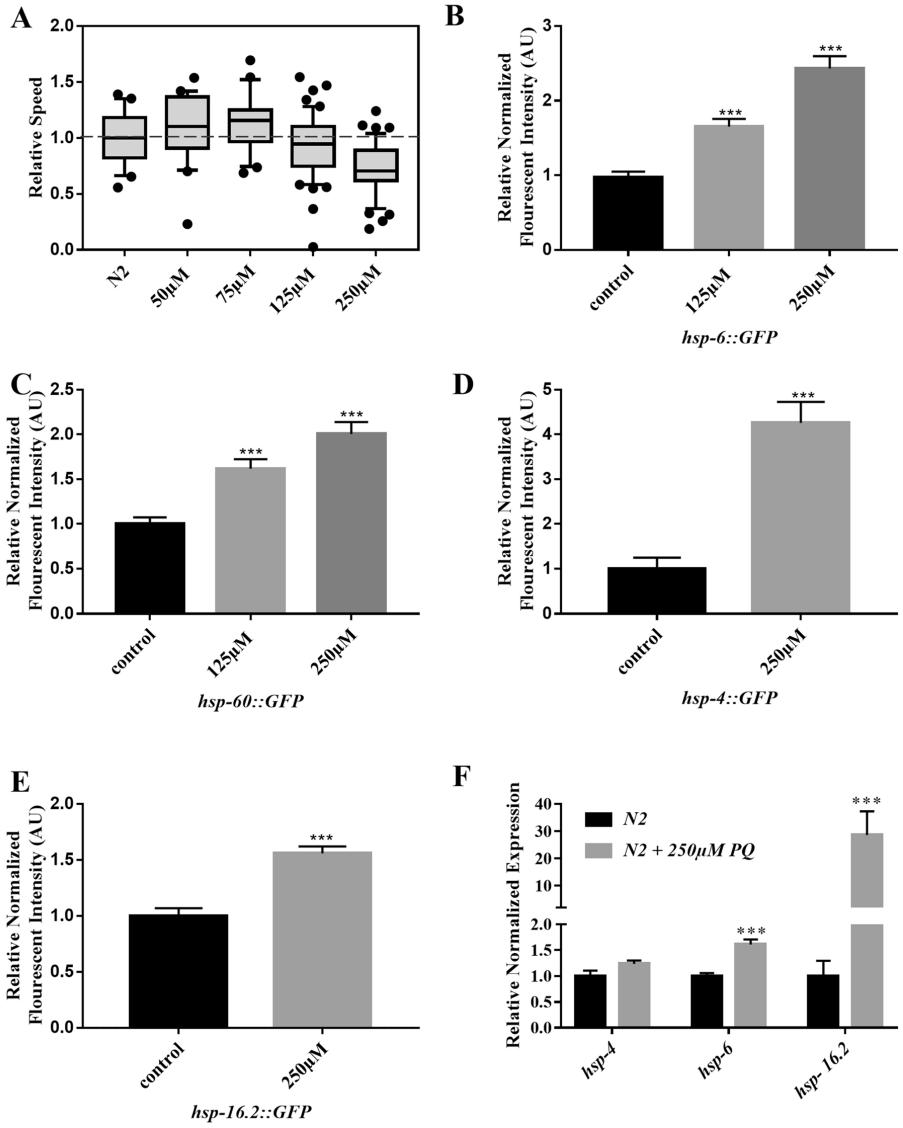
A
Relative Speed
2.0
1.5
1.0
0.5
0.0
N2
50µM
75µM
125µM
250µM
B
Relative Normalized Flourescent Intensity (AU)
3
2
1
0
***
***
control
125µM
250µM
hsp-6::GFP
C
Relative Normalized Flourescent Intensity (AU)
2.5
2.0
1.5
1.0
0.5
0.0
***
***
control
125µM
250µM
hsp-60::GFP
D
Relative Normalized Flourescent Intensity (AU)
5
4
3
2
1
0
***
control
250µM
hsp-4::GFP
E
Relative Normalized Flourescent Intensity (AU)
2.0
1.5
1.0
0.5
0.0
***
control
250µM
hsp-16.2::GFP
F
Relative Normalized Expression
40
30
20
10
2.0
1.5
1.0
0.5
0.0
N2
N2 + 250µM PQ
***
***
hsp-4
hsp-6
hsp-16.2

◂**Figure 1.** Effect of PQ treatments on electrotaxis and stress response markers. Boxes represent measurements from 25 to 75th percentiles, central horizontal lines represent medians, vertical lines extend to 10th and 90th percentiles, and dots represent outliers. (**A**) Wild-type (N2) animals treated with PQ. PQ did not induce speed abnormalities at 50 µM ($p = 0.128$), 75 µM ($p = 0.102$), or 125 µM ($p = 0.102$), but resulted in speed deficits at 250 µM ($p < 0.001$). (**B, C**) Fluorescence intensity in animals expressing *GFP* under mitochondrial *hsp-6* and *hsp-60* promoters following PQ treatments. GFP fluorescence corresponding to both *hsp-6::GFP* and *hsp-60::GFP* reporters showed increased fluorescence following treatments with 125 µM ($p < 0.001$ in both cases) and 250 µM ($p < 0.001$ and $p = 0.003$ respectively) PQ. (**D, E**) Fluorescence intensity of PQ-treated *hsp-4::GFP* and *hsp-16.2::GFP* animals. Fluorescence was increased following treatment with 250 µM PQ ($p < 0.001$ in both cases). (**F**) Quantitative reverse transcription-polymerase chain reaction (RT-qPCR) analysis showed an increase in *hsp-6* ($p < 0.0001$) and *hsp-16.2* ($p = 0.0007$) but not *hsp-4* ($p = 0.1125$) transcripts in N2 day-1 adults following exposure to 250 µM PQ. Number of animals were (**A**) N2 untreated: n = 80, N2 + 50 µM PQ: n = 20, N2 + 75 µM PQ: n = 20, N2 + 125 µM PQ: n = 50, N2 + 250 µM PQ: n = 45. (**B**) *hsp-6::GFP* untreated: n = 40, *hsp-6::GFP* + 125 µM PQ: n = 32, *hsp-6::GFP* + 250 µM PQ: n = 31, (**C**) *hsp-60::GFP* untreated: n = 33, *hsp-60::GFP* + 125 µM PQ: n = 34, *hsp-60::GFP* + 250 µM PQ: n = 35. (**D**) *hsp-4::GFP* untreated: n = 27, *hsp-4::GFP* + 250 µM PQ: n = 29, (**E**) *hsp-16.2::GFP* untreated: n = 31, *hsp-16.2::GFP* + 250 µM PQ: n = 20. (**F**) N2 untreated: n = 2 batches, N2 + 250 µM PQ: n = 2 batches. Statistical analyses for panels A-E were done using one-way ANOVA with Dunnett's post hoc test. qPCR results in F were generated by BioRad's CFX Maestro software (version 3.1, https://www.bio-rad.com/en-ca/category/qpcr-analysis-software) and data was analyzed using one-way ANOVA with Tukey's post hoc test. AU: Arbitrary Unit.

UPR^{MT} is activated following mitochondrial dysfunction induced by misfolded protein accumulation within the mitochondria, and disrupts oxidative phosphorylation[8]. The response is similar across eukaryotes, although the regulation in mammals appears to be more complex[8]. Experiments in the nematode *Caenorhabditis elegans* have revealed that ATFS-1 (activating transcription factor associated with stress-1), an ATF5 homolog and bZip transcription factor family member, acts as a sensor protein[9]. ATFS-1 is normally degraded inside healthy mitochondria, but upon mitochondrial dysfunction is transported to the nucleus to regulate gene expression[8]. Failure to reduce mitochondrial stress can result in dysfunctional mitochondria which, if not cleared by the protective mechanism of mitophagy[8,10], can lead to several deleterious conditions, including premature aging, sarcopenia, and cardiovascular disease[10].

Similar to mitochondrial stress, ER stress is triggered by the accumulation of misfolded proteins in the ER. The UPR^{ER} response is facilitated by three different transmembrane proteins: inositol-requiring enzyme 1 (IRE1), protein kinase RNA (PKR)-like ER kinase (PERK), and activating transcription factor 6 (ATF6), which then activate distinct signaling pathways. There are significant redundancies between the pathways, with overlapping transcriptional activity. All three pathways regulate the expression of chaperones, including GRP78/BiP[11]. A key transcription factor that modulates UPR^{ER} signaling is the X-Box binding protein-1 (XBP1). While IRE1 is the main regulator of XBP1 activity, ATF6 and PERK also participate in IRE1-XBP1 signaling[11,12]. Failure to regulate ER stress can lead to diseases such as neurodegeneration, metabolic disorders, and cancer[13,14].

Much of our knowledge of how stress affects behavior and the underlying signaling mechanisms have emerged from studies using a small set of model organisms, including *C. elegans*. This model nematode (worm) is a particularly attractive system due to its genetic tractability, ease of culture, and short life cycle, all of which serve to greatly expedite the rate of discovery[15]. Despite its relative simplicity, approximately half of *C. elegans* genes have homologs in humans and utilize many of the same processes[16]. Cellular stress can affect diverse processes in worms. Manipulations that increase mitochondrial and ER stress affect lifespan, fertility, susceptibility to diseases, and many behavioral processes[17–19]. The small size of the worm greatly facilitates experimentation using microfluidic devices[20]. Our lab has been investigating electrotaxis in *C. elegans* and how it is impacted by stress caused by genetic and environmental factors. In an earlier study, we demonstrated that a mild DC electric field in a microfluidic channel stimulates *C. elegans* to move towards the cathode in a directed manner, a response that is robust, highly repeatable, sensitive, and instantaneous[21]. Electrotactic movement serves as a powerful noninvasive response to evaluate the functional output of the nematode's locomotory circuit following manipulation[22]. To understand whether the response is affected by treatments that increase stress, we exposed animals to different environmental conditions as well as investigated the impact of genetic mutations. Our findings show that chronic stress compromises electrotaxis speed whereas some forms of transient stress augments it. We found that worms exposed to chemicals that induce ER and mitochondrial stress exhibit reduced speed. A similar phenotype was also observed in mutant strains with disrupted mitochondrial and ER function. The essential role of HSR and UPR^{MT} is further supported by our data showing that animals having defects in both *atfs-1* and *hsf-1* function have a significantly slower movement response. Our analysis of the UPR^{ER} genes reveals that *ire-1/xbp-1* and *pek-1* pathways play essential roles in regulating the electrotaxis of *C. elegans*. We also report that a polyglutamine enhancer-1 protein, PQE-1, maybe involved in the maintenance of HSR and mitochondrial and ER stress, likely due to its role in regulating the global protein synthesis[23,24]. To examine the sensitivity of electrotaxis speed to stress-inducing conditions, we exposed worms to chemical stressors, heat, different bacterial diets, and dietary restriction as well as daily exercise. The results showed that while chronic heat and reduced diet caused a decreased electrotactic movement, exercise had an increased response. Overall, our findings demonstrate that the electrotactic response of *C. elegans* is sensitive to cytosolic, mitochondrial, and ER stress. The results form the basis of future investigations of HSR, UPR^{MT}, and UPR^{ER} signaling utilizing microfluidic electrotaxis as a functional output of nematode locomotor circuits.

Results

Paraquat-induced oxidative stress reduces the electrotaxis speed of *C. elegans*. Oxidative stress is known to affect the behavioral responses of *C. elegans*[17,18,25]. To investigate whether this form of stress can also alter electrotaxis in animals, we used paraquat (PQ), a herbicide that disrupts mitochondrial function by inducing the generation of superoxides[26,27]. High concentrations of PQ have a detrimental effect on the lifespan of worms and cause damage to dopaminergic (DA) and other neurons by increasing ROS levels[17,18,26–28]. We examined the effect of PQ-induced stress on electrotaxis by exposing animals to different doses of the chemical. While exposures to low or moderate concentrations ranging from 50 to 125 µM had no effect on the movement of day-1 adults, 250 µM of PQ caused a significant defect, resulting in a slower speed in the microfluidic channel (Fig. 1A). In addition to electrotaxis, PQ-exposed animals showed increased expression of mitochondrial chaperones. Specifically, the mitochondrial stress response reporters *hsp-6::GFP* (HSP70 family) and *hsp-60::GFP* (HSP60 family) were significantly upregulated (Fig. 1B,C).

To determine whether PQ affects other processes, we examined the expression of two other chaperones for ER and cytosolic stress, namely HSP-4 (BiP/GRP78 family member, ER stress) and HSP-16.2 (HSP16 family, cytosolic stress) following PQ treatment. Although the GFP reporters for both these chaperons showed a statistically significant increase in fluorescence, the fold change of the ER GFP reporter was much higher than that of mitochondrial reporters (Fig. 1D,E). Similar to changes in fluorescence reporters, the transcript analysis also showed higher levels of *hsp-6* and *hsp-16.2* following PQ exposure (Fig. 1F). We did not see a significant increase in *hsp-4* transcript. These results are consistent with the previously reported finding that PQ induces both mitochondrial and ER stress in different animal models[29–31]. Overall, PQ causes multiple stresses in *C. elegans* that contribute to a decrease in electrotaxis speed.

Mutations in genes regulating mitochondrial function affect electrotaxis. To further investigate whether the electrotactic response is perturbed by mitochondrial dysfunction, we conducted a survey of mutants affecting mitochondrial processes and UPR^{MT}. The set of genes consisted of an ortholog of ubiquinol-cytochrome C reductase (*isp-1*, Rieske iron sulfur protein subunit of mitochondrial complex III), a subunit of mitochondrial complex I (*gas-1*), a subunit of mitochondrial complex II (*mev-1*, cytochrome b), PTEN-induced kinase 1 (*pink-1*), mitochondrial uncoupling protein (UCP) ortholog (*ucp-4*), two mitochondrial superoxide dismutase orthologs (*sod-2* and *sod-3*), coenzyme Q7 ortholog (*clk-1*), and *atfs-1*. Some of these genes are reported to affect motility of *C. elegans* on solid media and thrashing in liquid environment[32–35].

Analysis of the electrotactic response showed that most of the mutant animals, including *mev-1(kn1)*, *pink-1(ok3538)*, *ucp-4(ok195)*, *clk-1(e2519)*, *sod-2(gk257)*, *sod-3(tm760)*, and *sod-2(gk257); sod-3(tm760)* double, had no obvious defects; however, two particular mutants, *isp-1(qm150)* and *gas-1(fc21)*, showed a significantly reduced electrotaxis speed (Fig. 2A). Although both genes encode components of the electron transport chain, *isp-1(qm150)* is long-lived with resistance to oxidative damage[36], while *gas-1(fc21)* is short-lived with increased ROS and sensitivity to oxidative damage[37], suggesting that neither lifespan differences nor ROS toxicity correlate with electrotaxis phenotypes. This notion is supported by the other mutant data, indicating that *mev-1(kn1)* has increased ROS and oxidative damage with short lifespan, *clk-1(e2519)* shows decreased oxidative damage and long lifespan, and *sod* mutants show increased oxidative damage with normal or extended lifespans, yet all exhibit similar electrotaxis speeds (Fig. 2A)[38,39].

We chose a subset of mitochondrial genes for further investigation. Specifically, we explored the possibility that mutant animals may not exhibit an electrotaxis phenotype on their own, but may do so when subjected to further stress. Consistent with this, *mev-1(kn1)* and *pink-1(ok3538)*, which show sensitivity to PQ[18,38], displayed electrotaxis defects at exposure concentrations that do not alter the speed of control animals. Specifically, *mev-1(kn1)* animals exhibited speed deficits when cultured under chronic exposures to either 50 µM or 75 µM PQ (Fig. 2B). Similarly, *pink-1(ok3538)* animals were also affected, displaying significantly reduced electrotaxis speed at 125 µM PQ (Fig. 2C). Interestingly, *ucp-4(ok195)* adults displayed increased sensitivity to PQ under our chronic exposure paradigm, exhibiting slow electrotaxis at 75 µM (Fig. 2D). Thus, PQ-induced stress and mitochondrial defects perturb *C. elegans* electrotaxis speed.

To further investigate the effect of perturbations in UPR^{MT} on electrotaxis, we examined the phenotypes of two different *atfs-1* alleles, a genetic null *atfs-1(gk3094)* and a gain-of-function *atfs-1(et15)*. While the *gk3094* mutation prevents the UPR^{MT} response, an opposite phenotype is caused by *et15*[40–42]. Additionally, the HSR is activated in *gk3094* animals[41]. Both *atfs-1* mutants displayed significantly slower speeds than wild-type controls, although the null allele phenotype was most severe (Fig. 2E). We also knocked down *atfs-1* in *isp-1* and *gas-1* mutant strains and found that while the electrotaxis speed of *isp-1(qm150)* was reduced, there was no change in *gas-1(fc21)* animals (Fig. 2F). Collectively, these data demonstrate that electrotaxis speed is sensitive to disruptions in mitochondrial function, UPR^{MT}, and HSR.

Impairment of UPR^{ER} causes electrotaxis speed deficits. Our finding that PQ induces the expression of ER chaperone *hsp-4::GFP* (Fig. 1C) led us to investigate the impact of ER stress on electrotaxis using tunicamycin, a chemical that promotes protein misfolding by inhibiting protein glycosylation[43,44]. As shown in Fig. 3A, chronic exposure to tunicamycin at concentrations of 5 µg/mL or greater significantly reduced electrotaxis speed. These results are supported by the analysis of *hsp-4::GFP* reporter expression and *hsp-4* transcript (Fig. 3B,C), suggesting the detrimental effect of tunicamycin exposure[40]. As expected, *hsp-6* level was unchanged (Fig. 3C). We did not test electrotactic responses of animals at concentrations higher than 10 µg/mL due to significant toxicity, as judged by the highly pronounced larval lethality and slow growth of escapers at this concentration (data not shown).

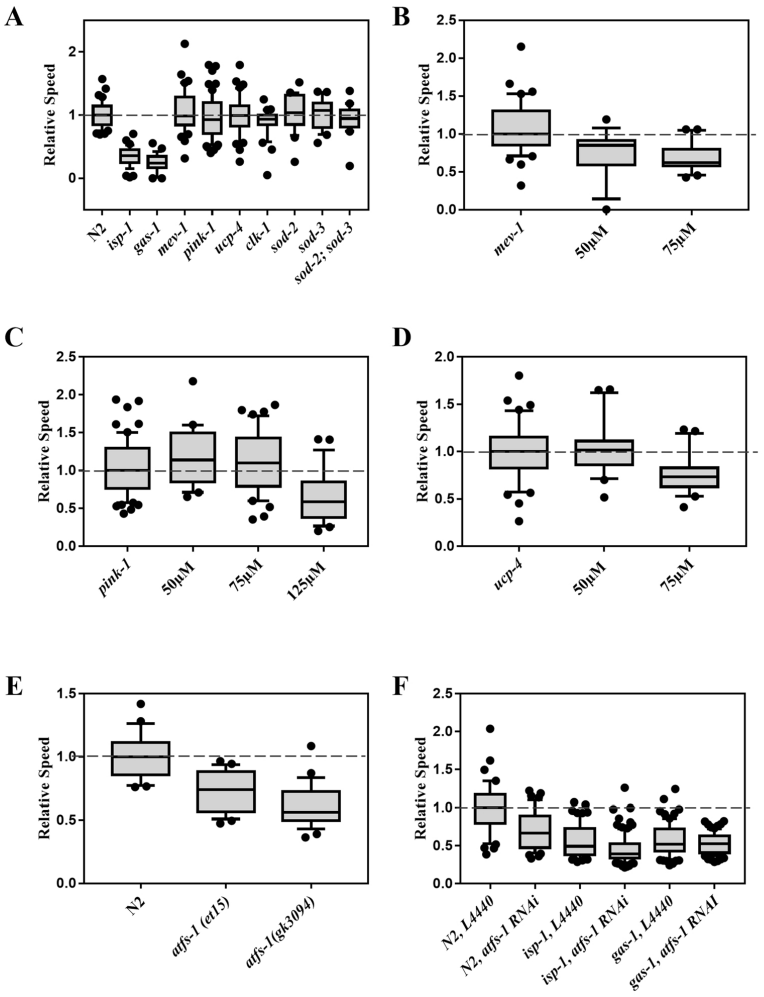

Figure 2. Electrotaxis of mitochondrial mutants. Refer to Fig. 1 for a description of box plot. (**A**) *isp-1(qm150)* ($p < 0.001$) and *gas-1(fc21)* ($p < 0.001$) animals exhibit speed defects. In contrast, *mev-1(kn1)* ($p = 0.567$), *pink-1(ok3538)* ($p = 0.239$), *ucp-4(ok195)* ($p = 0.942$), *clk-1(e2519)* ($p = 0.065$), *sod-2(gk257)* ($p = 0.509$), *sod-3(tm760)* ($p = 0.578$), and *sod-2(gk257); sod-3(tm760)* double ($p = 0.485$) mutants are comparable to the wild-type (N2) control. (**B**) *mev-1(kn1)* animals exhibited significant slowness following treatment with 50 μM ($p = 0.003$) or 75 μM ($p < 0.001$) PQ. (**C**) *pink-1(ok3538)* animals showed no obvious defect following treatment with 50 μM ($p = 0.394$) or 75 μM ($p = 0.694$) PQ, but were significantly slower following treatment with 125 μM PQ ($p < 0.001$). (**D**) *ucp-4(ok195)* animals were normal following treatment with 50 μM ($p = 0.946$), but showed significant slowness when treated with 75 μM PQ ($p = 0.002$). (**E**) *atfs-1(et15)* and *atfs-1(gk3094)* animals showed defective electrotaxis phenotype ($p < 0.001$ and $p = 0.008$, respectively). (**F**) *atfs-1* RNAi resulted in a significant decrease in the electrotaxis speed of N2 ($p < 0.001$) and *isp-1(qm150)* ($p = 0.0480$) animals whereas it had no effect on the speed of *gas-1(fc21)* ($p = 0.7929$) animals. The numbers of animals were (**A**) N2: n = 40, *isp-1(qm150)*: n = 39, *gas-1(fc21)*: n = 29, *mev-1(kn1)*: n = 40, *pink-1(ok3538)*: n = 61, *ucp-4(ok195)*: n = 40, *clk-1(e2519)*: n = 30, *sod-2(gk257)*: n = 21, *sod-3(tm760)*: n = 20, *sod-2(gk257); sod-3(tm760)*: n = 20. (**B**) N2: n = 29, *atfs-1(et15)*: n = 26, *atfs-1(gk3094)*: n = 26. (**C**) *mev-1(kn1)* untreated: n = 20, + 50 μM PQ: n = 18, + 75 μM PQ: n = 20. (**D**) *pink-1(ok3538)* untreated: n = 33, + 50 μM PQ: n = 20, + 75 μM PQ: n = 40, + 125 μM PQ: n = 27. (**E**) *ucp-4*(*ok195*) untreated: n = 20, + 50 μM PQ: n = 20, + 75 μM PQ: n = 20. (**F**) N2, L4440: n = 45**,** N2, *atfs-1* RNAi: n = 44, *isp-1(qm150),* L4440: n = 60, *isp-1(qm150), atfs-1* RNAi: n = 93, *gas-1(fc21),* L4440: n = 76, *gas-1(fc21) atfs-1* RNAi: n = 71. In all cases statistical analyses were done using one-way ANOVA with Dunnett's post hoc test.

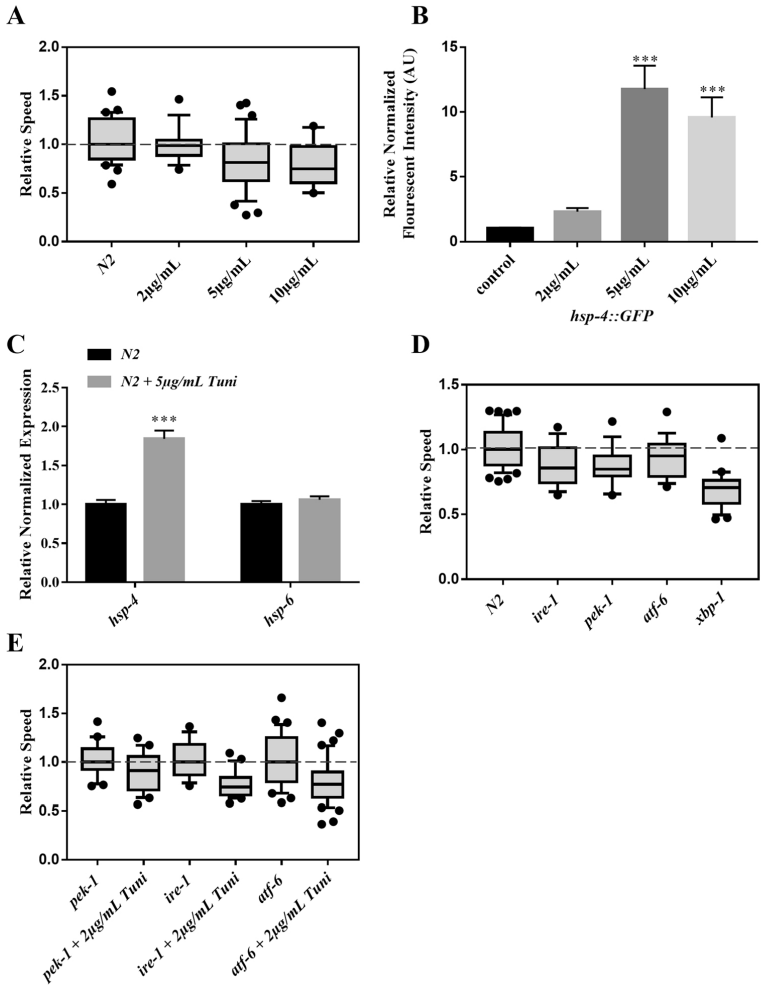

Figure 3. Electrotaxis phenotype of tunicamycin-treated animals and UPR^{ER} mutants. Refer to Fig. 1 for a description of box plot. (**A**) Wild-type (N2) animals show no speed abnormalities when exposed to 2 µg/mL of tunicamycin ($p = 0.590$), but exhibit speed deficits at higher doses, 5 µg/mL ($p = 0.002$) and 10 µg/mL ($p = 0.008$). (**B**) Fluorescence intensity of tunicamycin-treated *hsp-4::GFP* animals. The fluorescence was significantly increased following treatments with 5 µg/mL, and 10 µg/mL tunicamycin ($p < 0.001$). **C**) RT-qPCR analysis of chaperons *hsp-4* ($p = 0.003$) and *hsp-6* ($p = 0.3652$) in N2 day-1 adults following exposure to 5 µg/mL of Tunicamycin. (**D**) Electrotaxis speed of N2 and UPR^{ER} mutants. While *ire-1(v33)* ($p = 0.0144$), *pek-1(ok275)* ($p = 0.0082$) *and xbp-1(zc12)* ($p = 0.0001$) animals exhibited significant speed defects, *atf-6(ok551)* mutants were not significantly affected ($p = 0.2995$). (**E**) Responses of mutants following 2 µg/mL tunicamycin treatments., Animals showed a significant decline in the speed. P values are 0.0333 for *pek-1(ok275)*, <0.0001 for *ire-1(v33)*, and 0.0004 for *atf-6(ok551)*. The numbers of animals were: (**A**) N2 untreated: n = 30, N2 + 2 µg/mL Tuni: n = 15, N2 + 5 µg/mL Tuni: n = 32, N2 + 10 µg/mL Tuni: n = 10. (**B**) *hsp-4::GFP* untreated: n = 45, *hsp-4::GFP* + 2 µg/mL Tuni : n = 32, *hsp-4::GFP* + 5 µg/mL Tuni: n = 37, *hsp-4::GFP* + 10 µg/mL Tuni: n = 31. (**C**) N2 untreated: n = 3 batches, N2 + 5 µg/mL Tuni: n = 3 batches. (**D**) N2: n = 42, *ire-1*: n = 17, *pek-1*: n = 18, *atf-6*: n = 18, *xbp-1*: n = 23. (**E**) *pek-1:* n = *18, pek-1* + 2 µg/mL Tuni: n = 20, *ire-1:* n = *17, ire-1* + 2 µg/mL Tuni: n = 21, *atf-6*: n = *33, atf-6* + 2 µg/mL Tuni: n = 44. One-way ANOVA was performed followed by Dunnett's post hoc test for A and B, which showed that all conditions except one (i.e., control vs. 2 µg in panel B, $p = 0.7410$) were significant. Student's unpaired t-test was used for the remaining drug conditions. Data in C was analyzed using one-way ANOVA with Tukey's post hoc test.

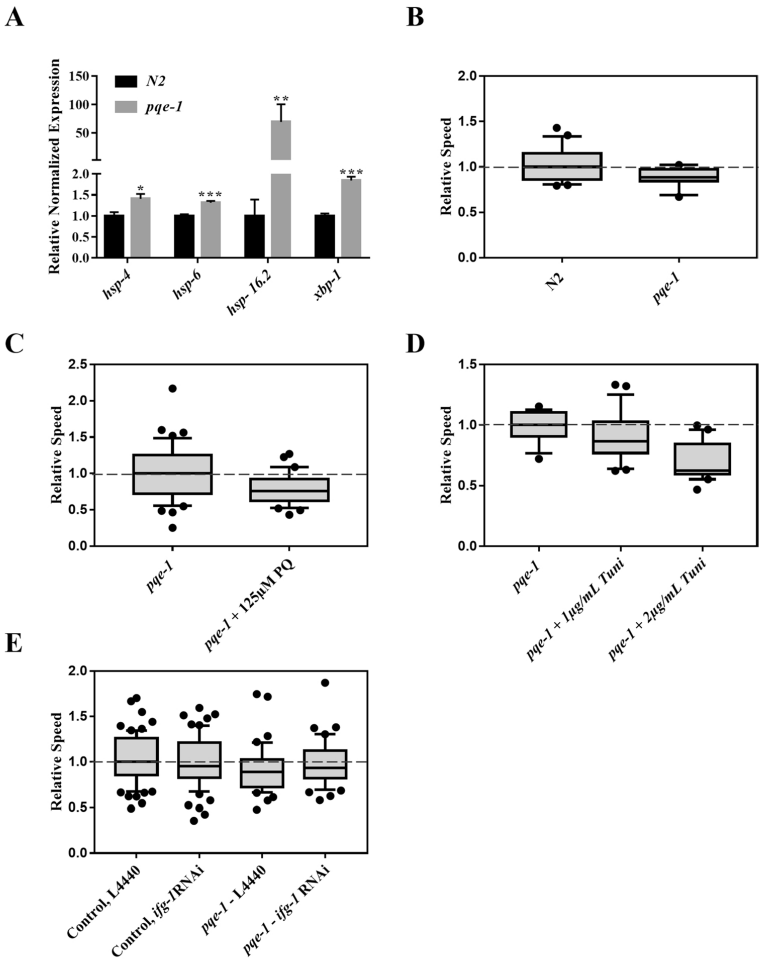

Figure 4. Analysis of *pqe-1* mutants under different stress-inducing conditions. Refer to Fig. 1 for a description of box plot. (**A**) RT-qPCR analysis showing increased expression of *hsp-4* ($p = 0.0128$), *hsp-6* ($p < 0.0001$), *hsp-16.2* ($p = 0.0012$) and *xbp-1*($p < 0.0001$) in *pqe-1*(ok1983) day-1 adults. (**B**) *pqe-1(ok1983)* animals exhibited a reduced electrotaxis speed compared to wild-type N2 ($p = 0.0053$) (**C**) The speed was further decreased following treatments with 125 µM PQ ($p = 0.007$). (**D**) The speed of *pqe-1(ok1983)* was not significantly different from untreated control ($p = 0.2461$). At 2 µg/mL exposure, *pqe-1* mutants showed a significant decrease in speed ($p = 0.0001$). (**E**) The electrotaxis speed of *ifg-1 RNAi* in control and *pqe-1(ok1983)* animals. The *ifg-1* RNAi had no effect on control animals ($p = 0.4193$) or *pqe-1* mutants ($p = 0.6676$). The numbers of animals were (**B**) N2: n = 3 batches, *pqe-1* n = 3 batches. (**C**) *pqe-1* untreated: n = 44, *pqe-1* + PQ 125 µM: n = 30. (**D**) *pqe-1: n = 16, pqe-1* + 1 µg/mL Tuni n = 21, *pqe-1* + 2 µg/mL Tuni n = 21. (**E**) Control, L4440: n = 47, Control, *ifg-1* RNAi: n = 66, *pqe-1,* L4440: n = 41, *pqe-1, ifg-1* RNAi: n = 44. Data was analyzed using one-way ANOVA with Tukey's post hoc test (A), one-way ANOVA with Dunnett's post hoc test (D), and unpaired Student's t-test (B,C,E).

Our group had previously demonstrated the role of dopaminergic neurons in mediating electrotaxis[22]. Therefore, we examined whether tunicamycin-induced ER stress will affect these neurons in our assay. The analysis of *dat-1*::YFP reporter revealed visible defects in neuronal morphology in treated animals illustrated by dendritic/axonal abnormalities and loss of cell bodies (Fig. S1A). A similar result was obtained following PQ treatment (Fig. S1B). These data suggest that toxin-induced neuronal damage may contribute to electrotaxis deficits in animals.

We further characterized ER disruption by testing the phenotypes of UPR^{ER} pathway mutants, specifically *ire-1*, *pek-1, atf-6,* and *xbp-1*. The speed was significantly lower in *ire-1(v33), xbp-1(zc12),* and *pek-1(ok275) but not atf-6(ok551)* animals compared to the control, (Fig. 3D). Interestingly, the defect was most pronounced in *xbp-1* mutants, which may be due to the gene being regulated by multiple UPR^{ER} arms. We also examined the sensitivity of UPR^{ER} mutants by exposing them to tunicamycin. Treatment with 2 µg/mL caused a significant decrease in the mobility of all three strains (Fig. 3E). A higher concentration (5 µg/mL) was found to be toxic to worms, resulting in lethality (data not shown). Taken together, the results show that electrotaxis is susceptible to ER stress-inducing conditions, and all three UPR^{ER} transducers function to facilitate this behavior.

Next, the role of *pqe-1* was investigated based on its potential link to ER stress. Earlier, *pqe-1* mutants were reported to cause an increase in transgene expression and enhance polyglutamine (poly-Q) neurotoxicity[23,24]. We speculated that both these phenotypes may be caused by proteotoxic stress due to a failure to regulate global protein synthesis. In support of this, *pqe-1(ok1983)* animals showed an increase in the expression of *hsp-4* chaperon and *xbp-1* (Fig. 4A, Fig. S2A). Interestingly, *hsp-6* and *hsp16.2* levels were also upregulated (Fig. 4A). As expected, the electrotaxis speed of mutant animals was significantly reduced (Fig. 4B), and the phenotype was exacerbated by treatment with PQ and tunicamycin (Fig. 4C,D). The sensitivity towards tunicamycin was particularly pronounced; although wild-type animals showed no abnormal electrotaxis phenotype at 2 µg/mL tunicamycin, *pqe-1* mutants exhibited a significantly reduced speed (compare Fig. 4D with 3A). Concentrations of tunicamycin above 2 µg/mL induced growth arrest and lethality in *pqe-1(ok1983)* worms (data not shown). The mutant animals also exhibited an increased degeneration of dopaminergic neurons and shorter lifespan (Fig. S2B,C).

We investigated whether reducing protein translation would lower proteotoxicity leading to a rescue of the electrotaxis defect of *pqe-1* mutant animals. This was tested by knocking down the eIF4G homolog, *ifg-1*, that encodes a component of the eIF4 complex[45]. The results showed that *ifg-1* RNAi was unable to suppress the phenotype of *pqe-1* mutant (Figs. 4E, S3). Overall, these observations provide the first evidence that *pqe-1* plays an essential role in maintaining multiple stress response pathways and electrotactic response of *C. elegans*.

Chronic heat impairs the electrotactic response. Studies have shown that heat treatments can have both positive and negative effects on animals due to activated HSR[7,46] and UPR^{ER}[7,47]. We investigated the electrotactic movement of young adults that were subjected to acute and chronic heat conditions. Worms exposed to two types of heat pulses, namely 5 h at 25 °C and 1 h at 33 °C, showed no change in their speed (Fig. 5A). Three additional treatments with a longer exposure time (i.e., 8 h each at 15 °C, 25 °C, and 28 °C), did not affect the speed either (Fig. 5B); however, all three heat shock chaperons (*hsp-4, hsp-6*, and *hsp-16.2*) were significantly upregulated (Figs. 5C, S4), suggesting the activation of UPR pathways. By contrast, chronic heat treatment at 28 °C for 3 days significantly reduced the speed (Fig. 5D). This demonstrates that unlike shorter duration (up to 8 h) of heat pulses, prolonged heat stress affects the electrotaxis speed of *C. elegans*.

One of the ways by which heat can induce stress is by interfering with the function of the heat shock transcription factor (HSF)[7]. In *C. elegans*, the HSF ortholog *hsf-1* is transcriptionally activated by a variety of stress conditions, including heat exposure[48]. In support of *hsf-1*'s involvement, we found that *hsf-1(sy441)* mutants have a significant electrotaxis speed deficit (Fig. 5E), which was further enhanced by a 1 h heat pulse at 33 °C but not by 5 h at 25 °C (Fig. 5F). There was no change in *hsp-6* and *hsp-16.2* levels in *hsf-1* mutant animals, although *hsp-4* was significantly down-regulated (Fig. 5G). Given that *hsf-1* regulates the expression of a large number of genes[49], we speculate that other heat shock chaperon(s) might mediate *hsf-1* function in electrotaxis. We also found that the *hsf-1(sy441)* phenotype was exacerbated by PQ-induced stress and L1 starvation (Figs. S5, S6), which indicates that *hsf-1* is a key regulator of diverse stress-induced responses.

Electrotactic movement decreases with reduced diet but increases after exercise. Another form of stress that we tested is starvation. Initially, the effects of two different starvation exposure protocols on electrotaxis were investigated. In one case, L1 larvae were subjected to starvation for 168 h and subsequently allowed to resume development in the presence of food. In the second case, day-1 adults were exposed to acute starvation conditions. Both nutrient deprivation treatments showed that the effect on electrotaxis was comparable to that of the controls (Fig. 6A,B).

We also investigated a chronic form of nutrient deprivation that involves reduced daily caloric intake. This treatment, termed 'dietary restriction (DR),' has been shown to be beneficial in animals such as lifespan extension, increased metabolic fitness, and reduced severity of age-related physiological decline[50–52]. To this end *eat-2* mutants were examined. *eat-2(ad1116)* animals have a longer lifespan that is attributed to chronic DR due to their slower pharyngeal pumping[33]. We found that the mutants had a significantly slower speed, suggesting that DR affects electrotaxis behavior (Fig. 6C). Since *eat-2* mutants show higher fluorescence based on *hsp-4::GFP* reporter analysis[53] but no change in *hsp-6::GFP*[54], we conclude that the sensitivity of electrotactic response to dietary restriction is likely due to the detrimental effect of persistent ER stress.

In addition to starvation and DR, we explored the effect of dietary changes on electrotaxis. Two of the bacterial strains that were initially tested were *Streptomyces venezuelae* and *Bacillus thuringiensis*. The metabolites secreted by these bacteria cause intracellular stress in *C. elegans*[55,56]. We found that neither bacteria had an impact on electrotaxis (Fig. S7). Next, worms were fed with two plant pathogens, *Agrobacterium tumefaciens* and *Pectobacterium carotovorum*[57–59] and a nonpathogenic fungus, *Cryptococcus aquaticus*. Plant pathogens have been reported to have a detrimental effect on the lifespan of worms[60]. None of these cultures had an obvious effect on electrotactic movement (Fig. S8). We also tested three commonly used *E. coli* strains, HB101, HT115, and DH5α, but, once again, observed no change in movement (Fig. S8). These results led us to conclude that electrotaxis behavior is unaffected by the above selected set of microorganisms, although the possibility of reduced nutrient

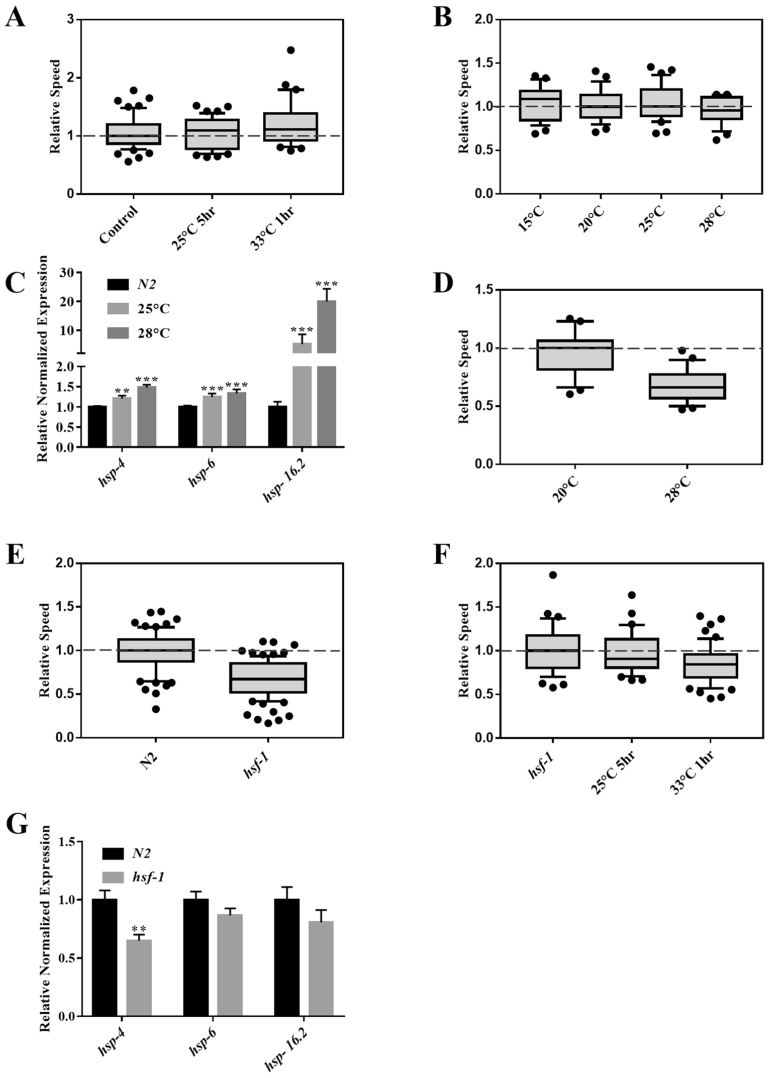

Figure 5. Effect of temperature on electrotactic response. Refer to Fig. 1 for a description of box plot. (**A**) Phenotype of animals exposed to two different heat conditions. No significant difference in speed was observed for any of the treatments (25 °C for 5 h, $p = 0.970$; 33 °C for 1 h, $p = 0.101$). (**B**) Electrotaxis of wild-type day-1 adults following exposure to heat, each for an 8 h period. No significant change was observed in the speed at 15 °C ($p = 0.9215$), 25 °C ($p = 0.9026$) and 28 °C ($p = 0.3925$). (**C**) RT-qPCR analysis of *hsp-4, hsp-6* and *hsp-16.2* in wild-type day-1 adults following 8 h exposures to 25 °C and 28 °C. The expression of the UPR chaperones was significantly increased following both treatments ($p < 0.001$). (**D**) Electrotaxis speed of wild-type animals following a chronic exposure at 28 °C for 3 days. Speed was significantly decreased ($p < 0.0001$) compared to the control grown at 20 °C. (**E**) *hsf-1(sy441)* animals exhibited significant slowness ($p < 0.001$). (**F**) *hsf-1(sy441)* animals exposed to 33 °C for 1 h exhibit significant slowness ($p = 0.0017$) while those exposed to 25 °C for 5 h had no obvious change ($p = 0.6532$). . (**G**) RT-qPCR analysis of *hsp-4, hsp-6* and *hsp-16.2* in *hsf-1* mutants. The expression of *hsp-4* was reduced ($p < 0.01$) however *hsp-6* ($p = 0.145032$) and *hsp-16.2* ($p = 0.234128$) were unaffected. The numbers of animals were (**A**) Control, untreated: n = 57, 25 °C for 5 h: n = 49, 33 °C for 1 h: n = 31. (**B**) 20 °C control: n = 26, 15 °C: n = 29, 25 °C: n = 35, 28 °C: n = 24. (**C**) Control : n = 3 batches; 25 °C: n = 3 batches, and 28 °C: n = 3 batches. (**D**) 20 °C control and 28 °C: n = 23. (**E**) N2: n = 70, *hsf-1(sy441):* n = 90. (**F**) *hsf-1(sy441)* untreated: n = 63, *hsf-1(sy441)* 25 °C for 5 h: n = 51, *hsf-1(sy441)* 33 °C for 1 h: n = 31. (**G**) N2: n = 3 batches; *hsf-1(sy441):* n = 3 batches. Statistical analyses were performed using one-way ANOVA with Dunnett's post hoc test (A,B,F), Student's t-test (D,E), and one-way ANOVA with Tukey's post hoc test (C,G).

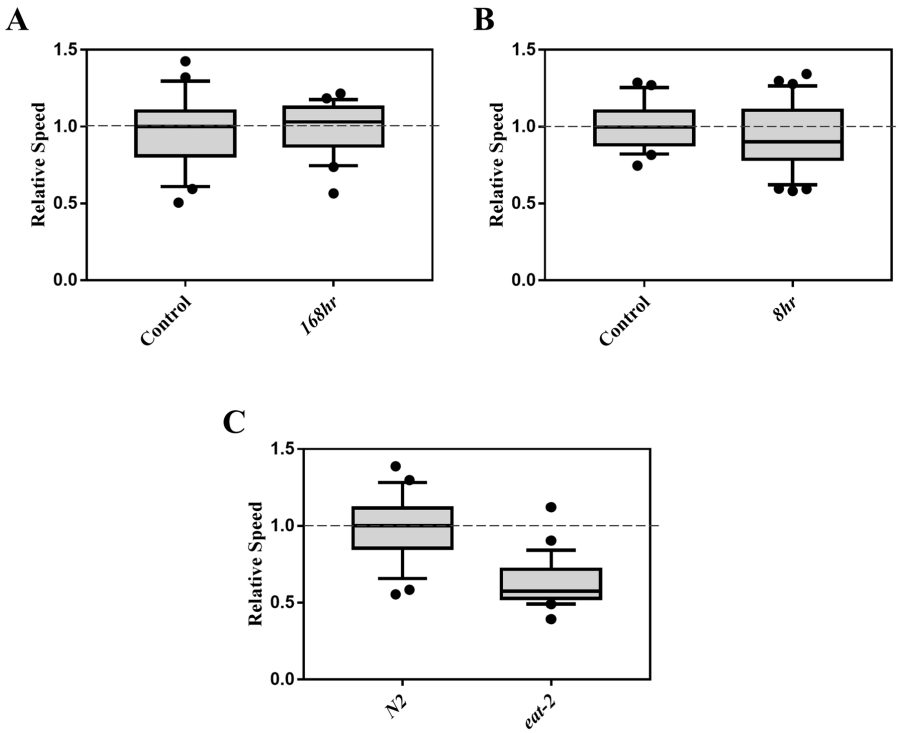

Figure 6. Effect of starvation on the electrotactic movement. Refer to Fig. 1 for a description of box plot. (**A**) Electrotaxis of animals starved for 168 h during the L1 larval stage. The speed was unaffected ($p = 0.660$). (**B**) Electrotaxis of day-1 adult wild-type animals starved for 8 h. The speed was comparable to the control ($p = 0.3350$). (**C**) The speed of *eat-2(ad1116)* adults was significantly reduced ($p < 0.0001$). The numbers of animals were (**A**) Control n = 21, 168 h n = 21. (**B**) Control n = 22, 8 h n = 25. (**C**) N2 day-1 adults n = 25, *eat-2(ad1116)* n = 29. Statistical Analysis was performed using unpaired Student's t-test.

intake in some or all cases cannot be ruled out. In the future, a larger set of microbial diets should be tested to investigate their effect on animals more thoroughly.

Finally, we investigated the effect of physical activity on the electrotactic movement of animals. The beneficial effects of exercise in humans and model organisms are well documented. In addition to improving muscle fitness, exercise also promotes neuronal health[61–63]. Since swimming activity in *C. elegans* induces known features of exercise reported in mammalian systems[62,64,65], worms were allowed to swim in M9 for 30 min daily, starting at the L3 larval stage, for a period of 7 days (see Methods for details). The results showed that animals had a significantly faster electrotaxis speed compared to controls of the same age, although they were slower compared to day-1 controls (Fig. 7A). Consistent with this, all three heat shock chaperons, *hsp-4, hsp-6,* and *hsp-16.2*, were upregulated (Fig. 7B). Additionally, we found that exercise caused a significant increase in the proportion of animals with tubular muscle mitochondria[62,66] (Fig. 7C,D). There was no change in dopaminergic neurons (Fig. S9).

Discussion

The experiments described herein are the first to demonstrate that the electrotactic response of *C. elegans* is affected by mutations and environmental conditions that increase cytosolic, mitochondrial, and ER stress. We found that the electrotaxis speed was altered by treatment with PQ and tunicamycin, two chemicals that are known to negatively impact the locomotory behavior of worms on solid media[17,67]. PQ exposure causes generation of ROS, which activates the expression of multiple chaperones such as *hsp-4* (ER stress), *hsp-6* and *hsp-60* (both mitochondrial stress), and *hsp-16.2* (cytosolic stress). The effects of PQ on mitochondrial and ER stress are well documented; hence, the effects of PQ on electrotaxis are likely due to increased stress associated with these two organelles[13,30,68].

Independent of ROS, our data show that mutations that cause mitochondrial stress also lead to decreased electrotaxis speed. The slow speed of *atfs-1(gf)* mutants indicates that the UPR^{MT} contributes to maintaining the wild-type behavior. Analysis of *ucp-4, mev-1,* and *pink-1* mutants revealed that exposure to a relatively

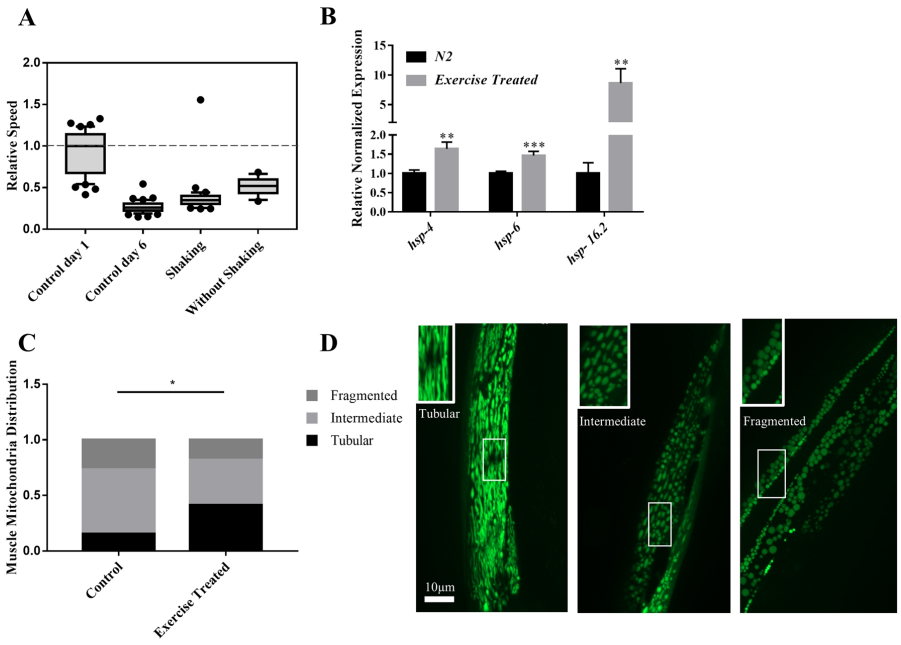

Figure 7. Effect of Exercise on electrotaxis reponse. (**A**) Worms were subjected to swimming exercise. A significant increase in the speed was observed using two different treatments (with shaking and without shaking: $p < 0.001$) compared to same age control. The speed was slower than day-1 controls ($p < 0.0001$). (**B**) RT-qPCR analysis of *hsp-4, hsp-6* and *hsp-16.2* in wild-type adults following 7 days of shaking exercise treatment. The expression of all three chaperones was significantly increased ($p < 0.01$). (**C, D**) Muscle mitochondria morphology in day-6 *myo-3::GFP(mit)* adults after shaking exercise. Animals were placed into three different categories, i.e., having mostly tubular, fragmented, and intermediate (i.e., combination of tubular and fragmented) shapes of mitochondria. These shapes correspond to mitochondrial network being normal (tubular) and defective (fragmented and intermediate). Exercise resulted in significantly more animals having tubular mitochondria ($p = 0.045$). The numbers of animals were: (**A**) Control day-1: n = 41, Control day-6: n = 48, shaking: n = 36 , without shaking: n = 14. (**B**) N2: n = 3 batches, exercise treated: n = 3 batches, (**C**) Control: n = 23, exercise treated: n = 23. Data was analyzed using one-way ANOVA with Dunnett's post hoc test (A), one-way ANOVA with Tukey's post-hoc test (B), and Chi-square test (C).

low concentration of PQ induced speed defects. In mammalian cells, mutations in UCP genes are associated with increased ROS and oxidative stress[69–71]. Interestingly, Iser and colleagues (2005) reported earlier that *ucp-4(ok195)* worms exhibit wild-type lifespan and survival in the presence of PQ, although the animals display an elevated ATP level[36,72]. Our finding that *ucp-4* mutants have defects in electrotaxis suggests that the movement response of animals may be sensitive to ROS levels. Future studies directly measuring oxidative damage following PQ exposure in different genetic backgrounds will be helpful in illuminating the relationship between ROS and electrotaxis.

isp-1 and *gas-1 mutants* exhibit reduced electrotaxis speed. While mutations in both these genes are also associated with electron transport hindrance and increased ROS generation, the *isp-1* mutant actually exhibits oxidative stress resistance due to low oxygen consumption and increased expression of mitochondrial superoxide dismutase SOD-3[36]. On the other hand, *gas-1* mutants are hypersensitive to oxidative stresses such as PQ[36,37]. The lifespan phenotypes of *isp-1* and *gas-1* mutants are also opposite, wherein *isp-1* animals have a long lifespan and *gas-1* are short-lived, possibly due to differences in ROS production and ROS-associated enzymatic activity[36]. These data suggest that electrotaxis speed is independent of pathways involved in lifespan maintenance. The *isp-1(qm150)* and *gas-1(fc21)* also both activate the UPR^{MT}[73,74], which led us to investigate the role of *atfs-1*. We found that *atfs-1* null mutant and gain-of-function mutant had a slower speed in our assay. Moreover, RNAi knock-down of *atfs-1* reduced the speed of *isp-1* mutant but not *gas-1* mutant animals. Together with known roles of *atfs-1* in regulating the expression of mitochondrial and cytosolic heat shock chaperons, these results support the conclusion that multiple stress response signaling affect the electrotaxis behavior of *C. elegans*.

The effect of ROS induced by PQ and mitochondrial mutants could also impact UPR^{ER}. Thus, we investigated the responses of animals treated with tunicamycin and observed defects in electrotaxis speed that were accompanied by an increase in the expression of the ER chaperone GRP78/BiP homolog *hsp-4*. Similar electrotaxis

phenotypes were also observed in UPR^{ER} mutants, indicating that the ER genes play a crucial role in mediating normal movement behavior. The analysis of mutants affecting the three major arms of UPR^{ER} revealed that while *ire-1, pek-1,* and *xbp-1* are needed to maintain a normal response, *atf-6* is not essential. Differences between UPR^{ER} pathway components in mediating some of the biological processes have been reported earlier. Shen et al. (2001) found that while knockdown of *pek-1* and *ire-1* affected larval development, there was no such phenotype in the case of *atf-6*[75]. Additionally, *ire-1* and *xbp-1* mutants have a short lifespan and slower development, but *pek-1* and *atf-6* mutants appear normal[56,76]. Finally, animals lacking *ire-1, xbp-1*, and *atf-6* function show high sensitivity to pore forming bacterial toxin Cry5B but *pek-1* does not appear to be involved[46]. In spite of these differences, we found that increasing the ER stress load by tunicamycin treatment exacerbated the electrotaxis defects of all three UPR^{ER} pathway mutants.

In addition to the known UPR^{ER} genes, we also tested the less well-characterized gene *pqe-1*. Mutations in *pqe-1* are thought to cause proteotoxic ER stress, possibly due to the upregulation of global protein synthesis[77]. Consistent with this idea, our results showed that *pqe-1* mutants have an abnormal electrotactic response. Studies in yeast have shown that the REXO1 (RNA exonuclease homolog 1) domain of PQE-1 functions in the processing of the 3′ ends of rRNA and tRNA[78,79], which may suggest a role of *pqe-1* in the regulation of protein translation. Since *pqe-1* localizes to the cell nucleus[23,24], it is possible that it affects genes whose products modulate the function of translation machinery. To investigate this further, we knocked-down the eIF4G homolog, *ifg-1*, a component of the initiation factor 4F (eIF4F) complex[45], but saw no suppression of the *pqe-1* mutant phenotype. This result combined with high sensitivity of mutant animals to tunicamycin and changes in the expression of multiple chaperons and *xbp-1* lead us to suggest that *pqe-1* plays an essential role in maintaining both HSR and organelle-specific stress response (UPR) pathways in *C. elegans*.

One of the ways by which stress can affect electrotaxis is by causing damage to neurons. Consistent with this, animals exposed to PQ and tunicamycin exhibited degenerated dopaminergic neurons (Fig. S1). A similar phenotype was also observed in *pqe-1* mutants (Fig. S2). These findings, along with our previous work demonstrating the role of dopaminergic neuron signaling in mediating electrotaxis behavior[22], led us to conclude that neuronal defects may in part contribute to the electrotaxis phenotype in animals as a result of stress-inducing conditions.

In addition to examining the effects of genetic mutations and compounds, we investigated whether environmental perturbations alter the electrotactic response. Among other effects , heat is reported to induce mitochondrial stress[7]. High temperatures have also been shown to modulate ER and cytosolic stress. This may involve multiple mechanisms, such as activation or repression of PERK depending on the severity of the heat regimen[47] and changes in global protein synthesis and apoptosis[47]. We exposed animals to acute heat and found that their electrotaxis was unaffected. Chronic heat, however, severely reduced the speed, suggesting that behavior is affected by prolonged heat exposure, which is consistent with cellular stress playing a role in modulating electrotaxis. The resistance to heat-induced stress appears to depend on the transcription factor *hsf-1*, since *hsf-1* mutants exhibit electrotaxis defects and are sensitive to heat treatments.

As diet can also play a role in the UPR maintenance[53,80], we subjected worms to different forms of starvation. When *C. elegans* are starved during the L1 larval stage, they enter L1 arrest, which halts the development and reproductive growth, enhances stress resistance, modifies feeding behavior, and alters metabolic flux[81,82]. Starvation during the L4 larval and adult stages has beneficial effects such as extended life span, germline cell reduction, delayed reproduction, and thermotolerance[83]. At the cellular level, starvation induces both mitochondrial and ER stress[53,80,84]. Mitochondria become fragmented in starved animals and are cleared through mitophagy[10,80,85]. Zhang et al.[86] reported that starvation caused ER stress and led to activation of PERK/eIF2α in an astrocyte cell line. Other groups have shown changes in the regulation of different ER proteins, such as chaperones[84]. Our work demonstrates that short-term DR does not affect the electrotactic response. However, *eat-2* mutants that are chronically starved, and therefore mimic a long-term DR condition, show a significantly slower electrotaxis speed. It is conceivable that a reduction in speed may aid in the long life span of *eat-2* mutants as the animals are slow feeders[53]. This line of reasoning agrees with previous findings that young adults lacking *eat-2* function move slower on solid media[33]. Furthermore, *eat-2* mutants show increased expression of *hsp-4*[53] but not *hsp-6*[54], suggesting higher ER stress levels.

The last stress condition we investigated was a daily exercise regimen. The benefits of exercise on muscular and neuronal health are well demonstrated. Healthier muscles through exercise allow animals to increase their athletic capacity[63]. At the molecular level, exercise activates the UPR^{ER} response as a protective mechanism[87]. Beneficial effects of exercise have also been demonstrated in *C. elegans*, such as a longer lifespan and improved neuronal and muscular health[62,64,65,88]. Laranjeiro et al. (2017) reported that the ER chaperone *hsp-4* is downregulated in animals subjected to exercise, which suggests a conserved role of UPR^{ER} in exercise-induced benefits[64]. Our lab showed earlier that defects in muscles reduce the electrotaxis speed of *C. elegans*[22]. Consistent with the above studies, we found that daily exercise treatment significantly improved the electrotaxis speed of *C. elegans* and resulted in increased expression of heat shock chaperons as well as better preservation of mitochondrial morphology.

In summary, the work described in this paper shows that electrotactic movement of worms is reduced by mutations in genes that affect HSR, UPR^{MT}, and UPR^{ER} as well as following chronic exposure to chemicals, heat, and reduced diet. In contrast, short bursts of daily exercise are beneficial since they resulted in a higher speed of animals and better preservation of mitochondrial morphology. Collectively, these findings lead us to conclude that conditions that elevate cellular stress for prolonged periods cause detrimental effects, whereas transient stress imparts a beneficial effect on health. The results established that a microfluidic-based assay is a reliable output of locomotory circuits and demonstrate that electrotaxis can be used to study stress response pathways in *C. elegans*.

Materials and methods

Strains and culturing. This study used the following *C. elegans* strains: N2: wild-type Bristol isolate; MQ887: *isp-1(qm150)*; CW152: *gas-1(fc21)*; TK22: *mev-1(kn1)*; CY121: *ucp-4(ok195)*; DY356: *pink-1(ok3538)*; GA184: *sod-2(gk257)*; GA186: *sod-3(tm760)*; GA480: *sod-2(gk257); sod-3(tm760)*; QC115: *atfs-1(et15)*; VC3201: *atfs-1(gk3094)*; RB545: *pek-1(ok275)*; RB772: *atf-6(ok551)*; RE666: *ire-1(v33)*; SJ17 *xbp-1(zc12) III; zcIs4 V*; SJ4100: *zcIs13(hsp-6::GFP)*; SJ4058: *zcIs9(hsp-60::GFP)*; PS3551: *hsf-1(sy441)*; DY693: *pqe-1(ok1983);zcIs4 V;* RB1611: *pqe-1(ok1983)*; SJ4005: *zcIs4(hsp-4::GFP)*; DY542: *pqe-1(ok1983); bhEx138[pGLC72(Cel-dat-1p::YFP)];* CL2070: *dvIs70[hsp-16.2::GFP + rol-6(su1006)]*; DY353: *bhEx138[pGLC72(Cel-dat-1p::YFP)];* SJ4103: *zcIs14[myo-3::GFP(mit)]* and DY356 (5x outcrossed RB2547): *pink-1(ok3538)*. RB2547 and all other strains were originally obtained from the Caenorhabditis Genetics Center (University of Minnesota, St. Paul, MN)[89].

Except where indicated, animals were grown and maintained at 20 °C on nematode growth medium (NGM) agar plates containing *E. coli* OP50 culture using previously described methods[15]. All experiments used age-synchronous populations obtained by bleach treatment[15]. Experiments involving wild-type and untreated controls were done using young adults unless stated otherwise. Growth times for all animals bearing mutations or undergoing treatments that affect developmental rate were appropriately adjusted.

Assays and treatments. The following methods were used to analyze worms in this study. Additional details are provided in supplementary methods.

Chemical treatments. Paraquat dichloride was obtained from Sigma-Aldrich (St. Louis, MO, USA) and tunicamycin was obtained from Bioshop Canada Inc (Burlington, ON, CA). Paraquat treatments were first prepared as 20 × solutions in M9 buffer; subsequently, 1 × treatment plates were produced by spreading 500 µL of the 20 × solutions across the surface of plates containing 10 mL of NGM agar. Tunicamycin treatments were first prepared as 5 mg/mL stock solutions in 100% DMSO, then diluted with water to make 20 × solutions; subsequently, 1 × treatment plates were produced by spreading 500 µL of the 20 × solutions across the surface of plates containing 10 mL of NGM agar. For chemical treatments, synchronized worms were grown on chemical-containing plates from L1 until adulthood. Young day-1 adults, based on direct observation, were used for experiments.

Heat stress. Animals were first grown at 20 °C until young adulthood. Plates were then sealed with parafilm and exposed to specific temperatures in a water bath for desired durations. Control plates were also sealed but kept at 20 °C. After the treatment, parafilm was removed and animals were allowed to recover at 20 °C for 30 min to an hour before electrotaxis assays. For 28 °C treatment, synchronized larvae were allowed to grow at 20 °C till day-1 adulthood and then shifted to 28 °C for 3 days.

Feeding bacterial and fungal cultures. *C. elegans* plates were seeded with overnight grown cultures of microorganisms. For *E. coli*, plant pathogens and fungus, L1 animals were transferred on plates and allowed to grow till adulthood. Day-1 adults were used for electrotaxis assays. In the case of *Streptomyces venezuelae* and *Bacillius thuringiensis*, L1 larvae were first fed with *E. coli* OP50 till adulthood. One day-old adults were transferred on maltose yeast extract medium (MYM) plates containing culture of *S. venezuelae* for 24 h. *Bacillus thuringiensis* culture was grown on NGM agar and fed to one day-old adults for 24 h. Electrotaxis was performed the following day. Control worms were grown in the presence of OP50 culture on NGM-Agar and MYM-Agar plates.

Starvation. Animals were first grown on OP50 until day-1 adulthood. They were then transferred to an unseeded NGM agar plate (no food) for 8 h to mimic acute starvation. Following the starvation period, electrotaxis assay was performed.

Exercise. Worms were subjected to exercise starting the L3 larval stage until day-6 adulthood (for a total of 7 days). Two different treatments were performed, each of which consisted of 30 min of daily swimming, followed by recovery on LB-agar plates. The first exercise regimen involved a belly dancer shaker in which worms, suspended in M9, were subjected to 100 rpm rotation. The second regimen consisted of keeping worms in M9 on the countertop without shaking, thereby allowing them to perform natural swimming.

Microchannel fabrication and electrotaxis assay. Microfluidic channels were fabricated as previously described[21,90]. The channel design was printed on a transparency sheet using high-resolution photoplotting to create a photomask, which was then used in conjunction with SU-8 100 negative photoresist (MicroChem Corp., MA, USA) to lithographically pattern the design onto a silicon wafer. Microchannels were then casted by pouring polydimethylsiloxane (PDMS) pre-polymer (Sylgard 184 Kit, Dow Corning Corp., MI, USA; 10:1 ratio of base and cross-linker) onto the resultant master mold and allowing 24 h for curing. The channel was then excised from the PDMS replica and fluid access ports were punched into each end. Next, the channel, a blank PDMS strip and a glass slide were oxidized via exposure to oxygen plasma for 40 s at 40 W power and stuck together to seal the microchannel. Lastly, plastic tubing and insulated copper wire were affixed to the punched reservoirs and secured with PDMS pre-polymer.

The electrotaxis assay protocol has also been described[21,90]. A syringe was attached to one of the inlet/outlet tubes of the PDMS microchannel to facilitate worm loading at the other tube. A power supply was connected via insulated copper wiring to the electrodes of the microchannel device to provide worms with electrical stimulus. A microscope, camera and monitor allowed visualization and recording of the electrotaxis experiment.

In preparation for the assay, worms were washed off of their culture plates, cleaned, and suspended in M9 buffer. Animals were then aspirated into the channel using the syringe pump. Both tubes were then laid flat at the same elevation to eliminate pressure-induced flow. Next, a 3 V/cm DC electric field was applied, and the worm's resultant behaviour recorded by camera.

Electrotaxis was carried out for up to 5 min. Animals were allowed to travel a minimum distance of 5 mm in one direction, towards the cathode, after which the field polarity was reversed to induce a turning response. Locomotory data was extracted from recorded videos using custom MATLAB-based worm tracking software. Electrotaxis speed data was plotted in box plots.

Fluorescence microscopy and quantification. Animals were mounted on 2% agar pad containing glass slides. Before placing the cover slip, they were anesthetized using a 15 µL drop of 30 mM NaN_3 mixed with a drop of M9. GFP fluorescence was visualized using a Zeiss Observer Z1 microscope equipped with an Apotome 2 and X-Cite R 120LED fluorescence illuminator. Fluorescence intensity was quantified using NIH ImageJ (http://rsbweb.nih.gov/ij/). Neurodegeneration was manually scored by counting the number of cell bodies of DAergic neurons and by assessing neurite morphologies and trajectories. Worms consist of two pairs of cephalic neurons (CEPs), a pair of anterior deirid neurons (ADE) and one pair of posterior dieirid neurons (PDE).

RNAi. The *atfs-1* RNAi plasmid (pGLC171) was constructed by inserting a 759 bp genomic fragment into the L4440 vector using the restriction enzymes *Kpn*I and *Xba*I. The fragment was obtained by PCR using the forward primer GL1649 (5'-AAGGGTACCCACTACTTGGAGAGCGACGAC-3') and reverse primer GL1650 (5'-AAGTCTAGACTACTTCTTGGAACTCCCTGC-3'). We used the RNAi gene silencing protocol described by Wu et al.[41] Since authors reported that knock-down in parental *isp-1* mutant worms caused an arrest of F1 larvae, L4-stage animals were treated with RNAi and day-2 old adults were analyzed. Synchronized worms were grown on OP50 until L4 stage and then transferred to RNAi plates containing either L4440 empty plasmid or *atfs-1* RNAi plasmid. *atfs-1* knock-down was confirmed by qPCR, which showed a range of ~2× to 10× reduction in different batches. For the *ifg-1* RNAi, animals were fed with bacteria from Ahringer library. In this RNAi paradigm synchronized animals were grown on OP50 until day-1 adult stage and then transferred to *ifg-1* RNAi plates for 48 h and analyzed right after.

Quantitative reverse transcription PCR (RT-qPCR). For RT-qPCR experiments, synchronized cultures were prepared by bleaching adult hermaphrodites twice in two successive generations to obtain highly synchronous cultures. After the second round of bleaching, eggs were grown until the day-1 adulthood. Total RNA was extracted from these animals using trizol (Catalog Number T9424, Sigma-Aldrich, Canada), according to the manufacturer's instructions. The SensiFAST cDNA Synthesis Kit (Catalog Number BIO-65053, MeridianBioscience, Canada) was used to obtain cDNA according to manufacturer's instructions. RT-qPCR was performed (in triplicate) using the Bio-Rad cycler CFX 96 machine. The primers are listed in the Supplementary table (Table S1). The reaction was set up using SensiFAST SYBR Green Kit (Catalog Number BIO-98005, BIOLINE, USA) according to the manufacturer's instructions. The expression levels of the analyzed genes were normalized to *pmp-3*.

Data analysis. GraphPad Prism 7 was used to plot the graphs. For all assays, data from repeat experiments were pooled and analyzed together. Statistical analyses were done using GraphPad Prism 7 except for RT-qPCR experiments that were analyzed using CFX Maestro 3.1 software (Bio-Rad, Canada; https://www.bio-rad.com/en-ca/product/cfx-maestro-software-for-cfx-real-time-pcr-instruments). P values less than 0.05 were considered statistically significant.

Data availability

All data generated or analysed during this study are included in this published article (and its Supplementary Information files). Additional details are available from the corresponding author on reasonable request.

Received: 11 August 2020; Accepted: 18 January 2021
Published online: 04 February 2021

References

1. Fink, G. In retrospect: eighty years of stress. *Nature* **539**, 175–176 (2016).
2. Selye, H. A syndrome produced by diverse nocuous agents. *Nature* **138**, 32 (1936).
3. Yoshino, J., Morikawa, R. K., Hasegawa, E. & Emoto, K. Neural circuitry that evokes escape behavior upon activation of nociceptive sensory neurons in drosophila larvae. *Curr. Biol.* **27**, 2499-2504.e3 (2017).
4. Ladd, C. O. *et al.* Long-term behavioral and neuroendocrine adaptations to adverse early experience. *Prog. Brain Res.* **122**, 81–103 (2000).
5. Arnsten, A. F. T. Stress signalling pathways that impair prefrontal cortex structure and function. *Nat. Rev. Neurosci.* **10**, 410–422 (2009).
6. McEwen, B. S. Mood disorders and allostatic load. *Biol. Psychiat.* **54**, 200–207 (2003).
7. Higuchi-Sanabria, R., Frankino, P. A., Paul, J. W., Tronnes, S. U. & Dillin, A. A futile battle? Protein quality control and the stress of aging. *Dev. Cell* **44**, 139–163 (2018).
8. Shpilka, T. & Haynes, C. M. The mitochondrial UPR: mechanisms, physiological functions and implications in ageing. *Nat. Rev. Mol. Cell Biol.* **19**, 109–120 (2018).
9. Fiorese, C. J. *et al.* The transcription factor ATF5 mediates a mammalian mitochondrial UPR. *Curr. Biol.* **26**, 2037–2043 (2016).
10. Melber, A. & Haynes, C. M. UPR mt regulation and output: a stress response mediated by mitochondrial-nuclear communication. *Cell Res.* **28**, 281–295 (2018).

11. Remondelli, P. & Renna, M. The endoplasmic reticulum unfolded protein response in neurodegenerative disorders and its potential therapeutic significance. *Front. Mol. Neurosci.* **10**, 187 (2017).
12. Tsuru, A., Imai, Y., Saito, M. & Kohno, K. Novel mechanism of enhancing IRE1α-XBP1 signalling via the PERK-ATF4 pathway. *Sci. Rep.* **6**, 1–8 (2016).
13. Salminen, A. & Kaarniranta, K. ER stress and hormetic regulation of the aging process. *Ageing Res. Rev.* **9**, 211–217 (2010).
14. Wang, S. & Kaufman, R. J. The impact of the unfolded protein response on human disease. *J. Cell Biol.* **197**, 857–867 (2012).
15. Brenner, S. The genetics of caenorhabditis elegans. *Genetics* **77**, 71–94 (1974).
16. Corsi, A. K., Wightman, B. & Chalfie, M. A transparent window into biology: a primer on Caenorhabditis elegans. *Genetics* **200**, 387–407 (2015).
17. Gourgou, E. & Chronis, N. Chemically induced oxidative stress affects ASH neuronal function and behavior in *C. elegans*. *Sci. Rep.* **6**, 1–9 (2016).
18. Wu, S. *et al.* Mutation of hop-1 and pink-1 attenuates vulnerability of neurotoxicity in *C. elegans*: the role of mitochondria-associated membrane proteins in Parkinsonism. *Exp. Neurol.* **309**, 67–78 (2018).
19. Cristina, D., Cary, M., Lunceford, A., Clarke, C. & Kenyon, C. A regulated response to impaired respiration slows behavioral rates and increases lifespan in caenorhabditis elegans. *PLoS Genet.* **5**, e1000450 (2009).
20. Gupta, B. P. & Rezai, P. Microfluidic approaches for manipulating, imaging, and screening C. elegans. *Micromachines* **7** (2016).
21. Rezai, P., Siddiqui, A., Selvaganapathy, P. R. & Gupta, B. P. Electrotaxis of *Caenorhabditis elegans* in a microfluidic environment. *Lab Chip* **10**, 220–226 (2010).
22. Salam, S. *et al.* A microfluidic phenotype analysis system reveals function of sensory and dopaminergic neuron signaling in *C. elegans* electrotactic swimming behavior. *Worm* **2**, e24558 (2013).
23. Faber, P. W., Voisine, C., King, D. C., Bates, E. A. & Hart, A. C. Glutamine/proline-rich PQE-1 proteins protect *Caenorhabditis elegans* neurons from huntingtin polyglutamine neurotoxicity. *Proc. Natl. Acad. Sci. USA* **99**, 17131–17136 (2002).
24. Yamada, K., Tsuchiya, J. I. & Iino, Y. Mutations in the pqe-1 gene enhance transgene expression in *Caenorhabditis elegans*. *G3 Genes Genomes Genet.* **2**, 741–751 (2012).
25. Kumsta, C., Thamsen, M. & Jakob, U. Effects of oxidative stress on behavior, physiology, and the redox thiol proteome of *Caenorhabditis elegans*. *Antioxid. Redox Signal.* **14**, 1023–1037 (2011).
26. Lee, S. J., Hwang, A. B. & Kenyon, C. Inhibition of respiration extends *C. elegans* life span via reactive oxygen species that increase HIF-1 activity. *Curr. Biol.* **20**, 2131–2136 (2010).
27. Yang, W. & Hekimi, S. A mitochondrial superoxide signal triggers increased longevity in *Caenorhabditis elegans*. *PLoS Biol.* **8**, e1000556 (2010).
28. Ortiz-Ortiz, M. A. *et al.* Curcumin enhances paraquat-induced apoptosis of N27 mesencephalic cells via the generation of reactive oxygen species. *Neurotoxicology* **30**, 1008–1018 (2009).
29. Zhang, X. F., Thompson, M. & Xu, Y. H. Multifactorial theory applied to the neurotoxicity of paraquat and paraquat-induced mechanisms of developing Parkinson's disease. *Lab. Investig.* **96**, 496–507 (2016).
30. Chinta, S. J. *et al.* Coupling endoplasmic reticulum stress to the cell death program in dopaminergic cells: effect of paraquat. *NeuroMol. Med.* **10**, 333–342 (2008).
31. Cao, S. S. & Kaufman, R. J. Endoplasmic reticulum stress and oxidative stress in cell fate decision and human disease. *Antioxid. Redox Signal.* **21**, 396–413 (2014).
32. Cooper, J. F. *et al.* Activation of the mitochondrial unfolded protein response promotes longevity and dopamine neuron survival in Parkinson's disease models. *Sci. Rep.* **7**, 1–16 (2017).
33. Bansal, A., Zhu, L. J., Yen, K. & Tissenbaum, H. A. Uncoupling lifespan and healthspan in caenorhabditis elegans longevity mutants. *Proc. Natl. Acad. Sci. USA* **112**, E277–E286 (2015).
34. Jafari, G. *et al.* Tether mutations that restore function and suppress pleiotropic phenotypes of the *C. elegans* ISP-1(qm150) Rieske iron-sulfur protein. *Proc. Natl. Acad. Sci. USA* **112**, E6148–E6157 (2015).
35. Rollins, J. A., Howard, A. C., Dobbins, S. K., Washburn, E. H. & Rogers, A. N. Assessing health span in *Caenorhabditis elegans*: lessons from short-lived mutants. *J. Gerontol. Ser. A. Biol. Sci. Med. Sci.* **72**, 473–480 (2017).
36. Feng, J., Bussière, F. & Hekimi, S. Mitochondrial electron transport is a key determinant of life span in *Caenorhabditis elegans*. *Dev. Cell* **1**, 633–644 (2001).
37. Hartman, P. S., Ishii, N., Kayser, E. B., Morgan, P. G. & Sedensky, M. M. Mitochondrial mutations differentially affect aging, mutability and anesthetic sensitivity in *Caenorhabditis elegans*. *Mech. Ageing Dev.* **122**, 1187–1201 (2001).
38. Sedensky, M. M. & Morgan, P. G. Mitochondrial respiration and reactive oxygen species in *C. elegans*. *Exp. Gerontol.* **41**, 957–967 (2006).
39. Van Raamsdonk, J. M. & Hekimi, S. Deletion of the mitochondrial superoxide dismutase sod-2 extends lifespan in Caenorhabditis elegans. *PLoS Genet.* **5** (2009).
40. Bennett, C. F. *et al.* Activation of the mitochondrial unfolded protein response does not predict longevity in *Caenorhabditis elegans*. *Nat. Commun.* **5**, 1–10 (2014).
41. Wu, Z. *et al.* Mitochondrial unfolded protein response transcription factor ATFS-1 promotes longevity in a long-lived mitochondrial mutant through activation of stress response pathways. *BMC Biol.* **16**, 147 (2018).
42. Rauthan, M., Ranji, P., Pradenas, N. A., Pitot, C. & Pilon, M. The mitochondrial unfolded protein response activator ATFS-1 protects cells from inhibition of the mevalonate pathway. *Proc. Natl. Acad. Sci. USA* **110**, 5981–5986 (2013).
43. Banerjee, A. *et al.* Unfolded protein response is required in nu/nu mice microvasculature for treating breast tumor with tunicamycin. *J. Biol. Chem.* **286**, 29127–29138 (2011).
44. Kornfeld, R. & Kornfeld, S. Assembly of asparagine-linked oligosaccharides. *Annu. Rev. Biochem.* **54**, 631–664 (1985).
45. Pan, K. Z. *et al.* Inhibition of mRNA translation extends lifespan in *Caenorhabditis elegans*. *Aging Cell* **6**, 111–119 (2007).
46. Labbadia, J. *et al.* Mitochondrial stress restores the heat shock response and prevents proteostasis collapse during aging. *Cell Rep.* **21**, 1481–1494 (2017).
47. Park, S. *et al.* Modulation of protein synthesis by eIF2α phosphorylation protects cell from heat stress-mediated apoptosis. *Cells* **7**, 254 (2018).
48. Morley, J. F. & Morimoto, R. I. Regulation of longevity in *Caenorhabditis elegans* by heat shock factor and molecular chaperones. *Mol. Biol. Cell* **15**, 657–664 (2004).
49. Brunquell, J., Morris, S., Lu, Y., Cheng, F. & Westerheide, S. D. The genome-wide role of HSF-1 in the regulation of gene expression in *Caenorhabditis elegans*. *BMC Genomics* **17**, 559 (2016).
50. Kapahi, P., Kaeberlein, M. & Hansen, M. Dietary restriction and lifespan: lessons from invertebrate models. *Ageing Res. Rev.* **39**, 3–14 (2017).
51. Honjoh, S., Yamamoto, T., Uno, M. & Nishida, E. Signalling through RHEB-1 mediates intermittent fasting-induced longevity in *C. elegans*. *Nature* **457**, 726–730 (2009).
52. Robertson, L. T. & Mitchell, J. R. Benefits of short-term dietary restriction in mammals. *Exp. Gerontol.* **48**, 1043–1048 (2013).
53. Matai, L. *et al.* Dietary restriction improves proteostasis and increases life span through endoplasmic reticulum hormesis. *Proc. Natl. Acad. Sci. USA* **116**, 17383–17392 (2019).
54. Durieux, J., Wolff, S. & Dillin, A. The cell-non-autonomous nature of electron transport chain-mediated longevity. *Cell* **144**, 79–91 (2011).

55. Ray, A., Martinez, B. A., Berkowitz, L. A., Caldwell, G. A. & Caldwell, K. A. Mitochondrial dysfunction, oxidative stress, and neurodegeneration elicited by a bacterial metabolite in a *C. elegans* Parkinson's model. *Cell Death Dis.* **5**, e984 (2014).
56. Bischof, L. J. *et al.* Activation of the unfolded protein response is required for defenses against bacterial pore-forming toxin in vivo. *PLoS Pathog.* **4** (2008).
57. Kwan, G., Charkowski, A. O. & Barak, J. D. Salmonella enterica suppresses Pectobacterium carotovorum subsp. carotovorum population and soft rot progression by acidifying the microaerophilic environment. *MBio* **4** (2013).
58. Gohlke, J. & Deeken, R. Plant responses to *Agrobacterium tumefaciens* and crown gall development. *Front. Plant Sci.* **5**, 155 (2014).
59. Ahn, S.-J., Donahue, K., Koh, Y., Martin, R. R. & Choi, M.-Y. Microbial-based double-stranded RNA production to develop cost-effective RNA interference application for insect pest management. *Int. J. Insect Sci.* **11**, 117954331984032 (2019).
60. Couillault, C. & Ewbank, J. J. Diverse bacteria are pathogens of *Caenorhabditis elegans*. *Infect. Immun.* **70**, 4705–4707 (2002).
61. Piazza, N., Gosangi, B., Devilla, S., Arking, R. & Wessells, R. Exercise-training in young drosophila melanogaster reduces age-related decline in mobility and cardiac performance. *PLoS ONE* **4**, e5886 (2009).
62. Laranjeiro, R. *et al.* Swim exercise in *Caenorhabditis elegans* extends neuromuscular and gut healthspan, enhances learning ability, and protects against neurodegeneration. *Proc. Natl. Acad. Sci. USA* **116**, 23829–23839 (2019).
63. Liu, Y. *et al.* The beneficial effects of physical exercise in the brain and related pathophysiological mechanisms in neurodegenerative diseases. *Lab. Invest.* **99**, 943–957 (2019).
64. Laranjeiro, R., Harinath, G., Burke, D., Braeckman, B. P. & Driscoll, M. Single swim sessions in *C. elegans* induce key features of mammalian exercise. *BMC Biol.* **15**, 30 (2017).
65. Hartman, J. H. *et al.* Swimming exercise and transient food deprivation in *Caenorhabditis elegans* promote mitochondrial maintenance and protect against chemical-induced mitotoxicity. *Sci. Rep.* **8** (2018).
66. Regmi, S. G., Rolland, S. G. & Conradt, B. Age-dependent changes in mitochondrial morphology and volume are not predictors of lifespan. *Aging (Albany. NY)* **6**, 118–130 (2014).
67. Kim, H. M., Do, C. H. & Lee, D. H. Taurine reduces ER stress in *C. elegans*. *J. Biomed. Sci.* **17**, 1–6 (2010).
68. Huang, C. L., Lee, Y. C., Yang, Y. C., Kuo, T. Y. & Huang, N. K. Minocycline prevents paraquat-induced cell death through attenuating endoplasmic reticulum stress and mitochondrial dysfunction. *Toxicol. Lett.* **209**, 203–210 (2012).
69. Kim-Han, J. S., Reichert, S. A., Quick, K. L. & Dugan, L. L. BMCP1: a mitochondrial uncoupling protein in neurons which regulates mitochondrial function and oxidant production. *J. Neurochem.* **79**, 658–668 (2008).
70. Krauss, S. *et al.* Superoxide-mediated activation of uncoupling protein 2 causes pancreatic β cell dysfunction. *J. Clin. Invest.* **112**, 1831–1842 (2003).
71. Vidal-Puig, A. J. *et al.* Energy metabolism in uncoupling protein 3 gene knockout mice. *J. Biol. Chem.* **275**, 16258–16266 (2000).
72. Iser, W. B., Kim, D., Bachman, E. & Wolkow, C. Examination of the requirement for ucp-4, a putative homolog of mammalian uncoupling proteins, for stress tolerance and longevity in *C. elegans*. *Mech. Ageing Dev.* **126**, 1090–1096 (2005).
73. Pujol, C., Bratic-Hench, I., Sumakovic, M., Hench, J. & Mourier, A. Succinate dehydrogenase upregulation destabilize complex i and limits the lifespan of gas-1 mutant. *PLoS ONE* **8**, 59493 (2013).
74. Nargund, A. M., Pellegrino, M. W., Fiorese, C. J., Baker, B. M. & Haynes, C. M. Mitochondrial import efficiency of ATFS-1 regulates mitochondrial UPR activation. *Science* **337**, 587–590 (2012).
75. Shen, X. *et al.* Complementary signaling pathways regulate the unfolded protein response and are required for *C. elegans* development. *Cell* **107**, 893–903 (2001).
76. Henis-Korenblit, S. *et al.* Insulin/IGF-1 signaling mutants reprogram ER stress response regulators to promote longevity. *Proc. Natl. Acad. Sci. USA* **107**, 9730–9735 (2010).
77. Yamada, K., Tsuchiya, J. I. & Iino, Y. Mutations in the pqe1 gene enhance transgene expression in *Caenorhabditis elegans*. *G3 Genes Genomes Genet.* **2**, 741–751 (2012).
78. Ozanick, S. G. *et al.* Rex1p deficiency leads to accumulation of precursor initiator tRNA Met and polyadenylation of substrate RNAs in *Saccharomyces cerevisiae*. *Nucl. Acids Res.* **37**, 298–308 (2009).
79. Copela, L. A., Fernandez, C. F., Sherrer, R. L. & Wolin, S. L. Competition between the Rex1 exonuclease and the La protein affects both Trf4p-mediated RNA quality control and pre-tRNA maturation. *RNA* **14**, 1214–1227 (2008).
80. Raut, G. K., Chakrabarti, M., Pamarthy, D. & Bhadra, M. P. Glucose starvation-induced oxidative stress causes mitochondrial dysfunction and apoptosis via Prohibitin 1 upregulation in human breast cancer cells. *Free Radic. Biol. Med.* **145**, 428–441 (2019).
81. Baugh, L. R. To grow or not to grow: Nutritional control of development during *Caenorhabditis elegans* L1 Arrest. *Genetics* **194**, 539–555 (2013).
82. Kang, C., You, N. J. & Avery, L. Dual roles of autophagy in the survival of *Caenorhabditis elegans* during starvation. *Genes Dev.* **21**, 2161–2171 (2007).
83. Angelo, G. & Van Gilst, M. R. Starvation protects germline stem cells and extends reproductive longevity in *C. elegans*. *Science.* **326**, 954–958 (2009).
84. Zhang, Y. *et al.* Inhibition of starvation-triggered endoplasmic reticulum stress, autophagy, and apoptosis in ARPE-19 cells by taurine through modulating the expression of calpain-1 and calpain-2. *Int. J. Mol. Sci.* **18**, 2146 (2017).
85. Hibshman, J. D. *et al.* Nonselective autophagy reduces mitochondrial content during starvation in *Caenorhabditis elegans*. *Am. J. Physiol. Cell Physiol.* **315**, C781–C792 (2018).
86. Zhang, A. *et al.* EIF2α and caspase-12 activation are involved in oxygen-glucose-serum deprivation/restoration-induced apoptosis of spinal cord astrocytes. *Neurosci. Lett.* **478**, 32–36 (2010).
87. Estébanez, B., De Paz, J. A., Cuevas, M. J. & González-Gallego, J. Endoplasmic reticulum unfolded protein response, aging and exercise: An update. *Front. Physiol. 9* (2018).
88. Chuang, H. S., Kuo, W. J., Lee, C. L., Chu, I. H. & Chen, C. S. Exercise in an electrotactic flow chamber ameliorates age-related degeneration in *Caenorhabditis elegans*. *Sci. Rep.* **6**, 1–11 (2016).
89. The *C. elegans* deletion mutant consortium. Large-scale screening for targeted knockouts in the caenorhabditis elegans genome. *G3 Genes, Genomes, Genet.* **2**, 1415–1425 (2012).
90. Tong, J., Rezai, P., Salam, S., Selvaganapathy, P. R. & Gupta, B. P. Microfluidic-based electrotaxis for on-demand quantitative analysis of *Caenorhabditis elegans*' locomotion. *J. Vis. Exp.* https://doi.org/10.3791/50226 (2013).

Acknowledgements

We thank Baekjun Sung for help with initial data collection, Devon Jones for adapting and fixing microfluidic channels, Sangeena Salam for some of the early experimental ideas and designs and Meghan Pepler for supplying the *Streptomyces venezuelae* culture. Some of the *C. elegans* strains were obtained from the *Caenorhabditis* Genetics Center (CGC), which is funded by NIH Office of Research Infrastructure Programs (P40 OD010440). We also acknowledge the *C. elegans* Deletion Mutant Consortium for generating the deletion strains used in this study and the Bacillus Genetics Stock Center for providing the *Bacillus thuringiensis* culture. This work was supported by the NSERC Discovery Grant to BG and a joint CIHR CHRP award to PRS, BG and RKM.

Author contributions

B.G. conceived and supervised the project. S.K.B.T., M.H.M., and J.T. performed the experiments and analyzed data. B.G., S.K.B.T., and J.T. prepared the outline. B.G., S.K.B.T., J.T. and M.H.M. wrote the manuscript. S.K.B.T. and M.H.M. created the figures. P.R.S. and R.M. provided input throughout the project and reviewed the manuscript.

Competing interests

The authors declare no competing interests.

Additional information

Supplementary Information The online version contains supplementary material available at https://doi.org/10.1038/s41598-021-82466-z.

Correspondence and requests for materials should be addressed to B.P.G.

Reprints and permissions information is available at www.nature.com/reprints.

Publisher's note Springer Nature remains neutral with regard to jurisdictional claims in published maps and institutional affiliations.

Supplementary Information

C. elegans electrotaxis behavior is modulated by heat shock response and unfolded protein response signaling pathways

Shane K. B. Taylor[1$], Muhammad H. Minhas[1$], Justin Tong[1], P. Ravi Selvaganapathy[2], Ram K. Mishra[3], and Bhagwati P. Gupta[1*]

[1]Department of Biology, McMaster University, Hamilton, ON

[2]Department of Mechanical Engineering, McMaster University, Hamilton, ON

[1]Department of Psychiatry and Behavioural Neurosciences, McMaster University, Hamilton, ON

Supplementary Methods

Lifespan Assay

Lifespan analysis was carried out at 20^0C on NGM agar plates with *E. coli* OP50 bacteria. Each strain was repeated at least twice. Each batch contained a minimum of 30 animals per strain and worms were scored for viability every day, from day 1 of adulthood. Young adult worms were transferred to fresh plates every other day and the numbers of dead worms were recorded.

GraphPad Prism software was used to calculate p values using the log-rank (Kaplan-Meier) method.

Dopaminergic neuron analysis

Neuronal phenotype was visually scored by counting cell bodies of dopaminergic (DA) neurons and observing dendritic morphologies under a Nomarski fluorescence microscope. In wild-type animals, three pairs of DA neurons (two pairs of CEPs and one pair of ADE) and their smooth dendritic/axonal projections are visible in the head region. Mutations and drug-treatments that cause defects in neurons result in fewer cell bodies and/or projections showing abnormal phenotypes such as blebbing, punctate pattern, deformed shape, faint appearance. and complete absence. Such animals were considered defective. Multiple batches of animals were scored on different days and from different culture plates to ensure that results were unbiased.

Supplementary Tables

Supplementary Table S1. List of primers used in this study.

Primer	**Gene**	**Direction (forward, FP; reverse, RP)**	**Sequence**
GL747	*pmp-3*	FP	CTTAGAGTCAAGGGTCGCAGTGGAG
GL748	*pmp-3*	RP	ACTGTATCGGCACCAAGGAAACTGG
GL1446	*xbp-1*	FP	CGCAGCCCAAAATGCTAGAG
GL1447	*xbp-1*	RP	AGATCGCGCATCACATCCTC
GL1633	*atfs-1*	FP	CGAGCCGAGAAGAAGGGAAG
GL1634	*atfs-1*	RP	GCGCCCATTTTACGAAGCTC
GL1643	*hsp-4*	FP	AAGCTTCTGAGGAGCCATCG
GL1644	*hsp-4*	RP	GGGGTTGGGTTGGGAAAGAA
GL1645	*hsp-6*	FP	AACCATTGAGCCATGCCGTA
GL1646	*hsp-6*	RP	CTTGAACAGTGGCTTGCACC
GL1647	*hsp-16.2*	FP	GTCCAGCTCAACGTTCCGT
GL1648	*hsp-16.2*	RP	TCTCAGAAGACTCAGATGGAGAGAT
GL1685	*ifg-1*	FP	CAGCAGCCATACCGTGGAAG
GL1686	*ifg-1*	RP	TCGAAGGTCTAACAACTGGTGG

Supplementary Figures

Supplementary Figure S1.

Dopaminergic (DA) neurons in young adult *dat-1::*YFP transgenic animals treated with PQ and Tunicamycin. (**A)** Quantification of neuronal degeneration following exposure to tunicamycin at different concentrations. Tunicamycin exposure caused a significantly higher dopaminergic neurodegeneration compared to untreated controls (2µg/mL p = 0.0185, 5µg/mL p = 0.0058, 10µg/mL p = 0.0008). (**B)** Quantification of neuronal degeneration following exposure to PQ at different concentrations. 125 µM PQ had no significant degeneration (p = 0.9996) but significant degeneration can be seen at 250µM (p = 0.0079). (**C-E)** Neuronal morphologies as revealed by *dat-1p::yfp* expression Arrows point to cell bodies and dashed lines represent the boundary of the head. The animal in C has normal number of neurons (3 pairs) and smooth appearance of dendritic/ axonal projections. Panels D and E show animals that are defective. In one case (D) only five cell bodies are visible. The dotted regions represent few example areas of neurodegeneration where projections can be seen having blebbing and punctate appearances. Untreated control animals **(C)**, 250 µM PQ **(D),** and 10 µg/mL tunicamycin **(E)**. Exposure to tunicamycin caused damage to dopaminergic neurons as seen by punctate and missing axons. The numbers of animals examined were: **(A)** 25 for *dat-1::YFP* untreated, 53 for Tuni 2 µg/mL, 47 for Tuni 5 µg/mL, and 42 for Tuni 10 µg/mL. (**B)** 25 for *dat-1::YFP* untreated, 27 for PQ 125 µM, and 30 for PQ 250 µM. Data in A and B was analyzed using one-way ANOVA followed by Dunnett's post hoc test.

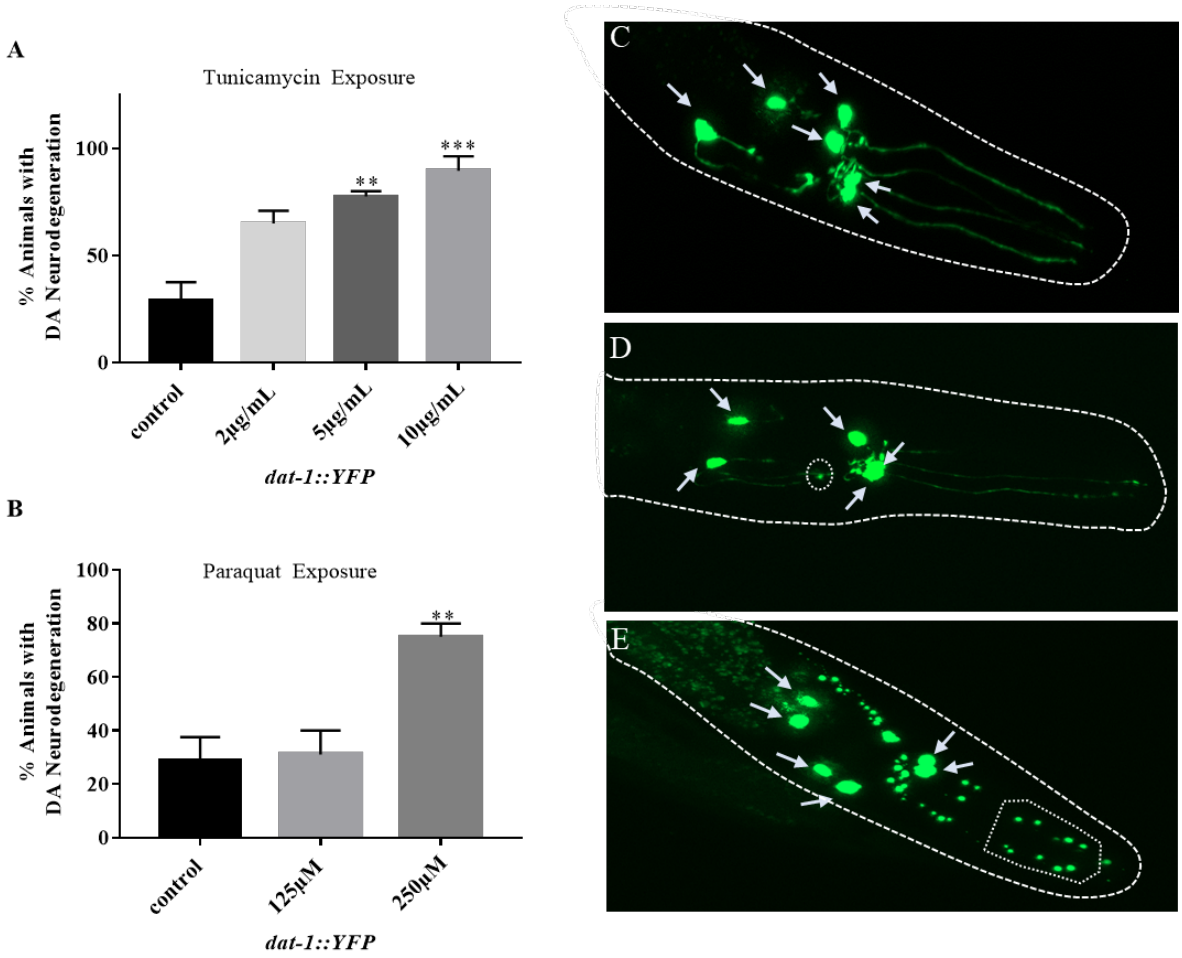
A
Tunicamycin Exposure
% Animals with DA Neurodegeneration
100
50
0
**
***
control
2µg/mL
5µg/mL
10µg/mL
dat-1::YFP
B
Paraquat Exposure
% Animals with DA Neurodegeneration
100
80
60
40
20
0
**
control
125µM
250µM
dat-1::YFP
C
D
E

Supplementary Figure S2. (A) *hsp-4::GFP* reporter analysis in *pqe-1(ok1983)* animals showed an increase in GFP fluorescence (p=0.0086, Student's t-test). **(B)** Quantification of neuronal degeneration in *pqe-1* mutants on day 1 and 3 of adulthood using the *dat-1::*YFP marker**.** Neuronal defects in mutant animals increase with age. **(C)** *pqe-1(ok1983)* animals have a shorter lifespan (mean 15.2± 0.6) compared to *N2* (mean 15.9 ± 0.6) (p = 0.0222). The numbers of animals examined were: **(A)** *N2*: n = 24, *pqe-1(ok1983)* n = 18. **(B)** *Control day 1*: n = 47, *pqe-1(ok1983)* – day 1: n = 45, Control day 3: n = 50, *pqe-1(ok1983)* – day 3: n = 51. **(C)** *N2*: n = 66, *pqe-1(ok1983)* n = 80.

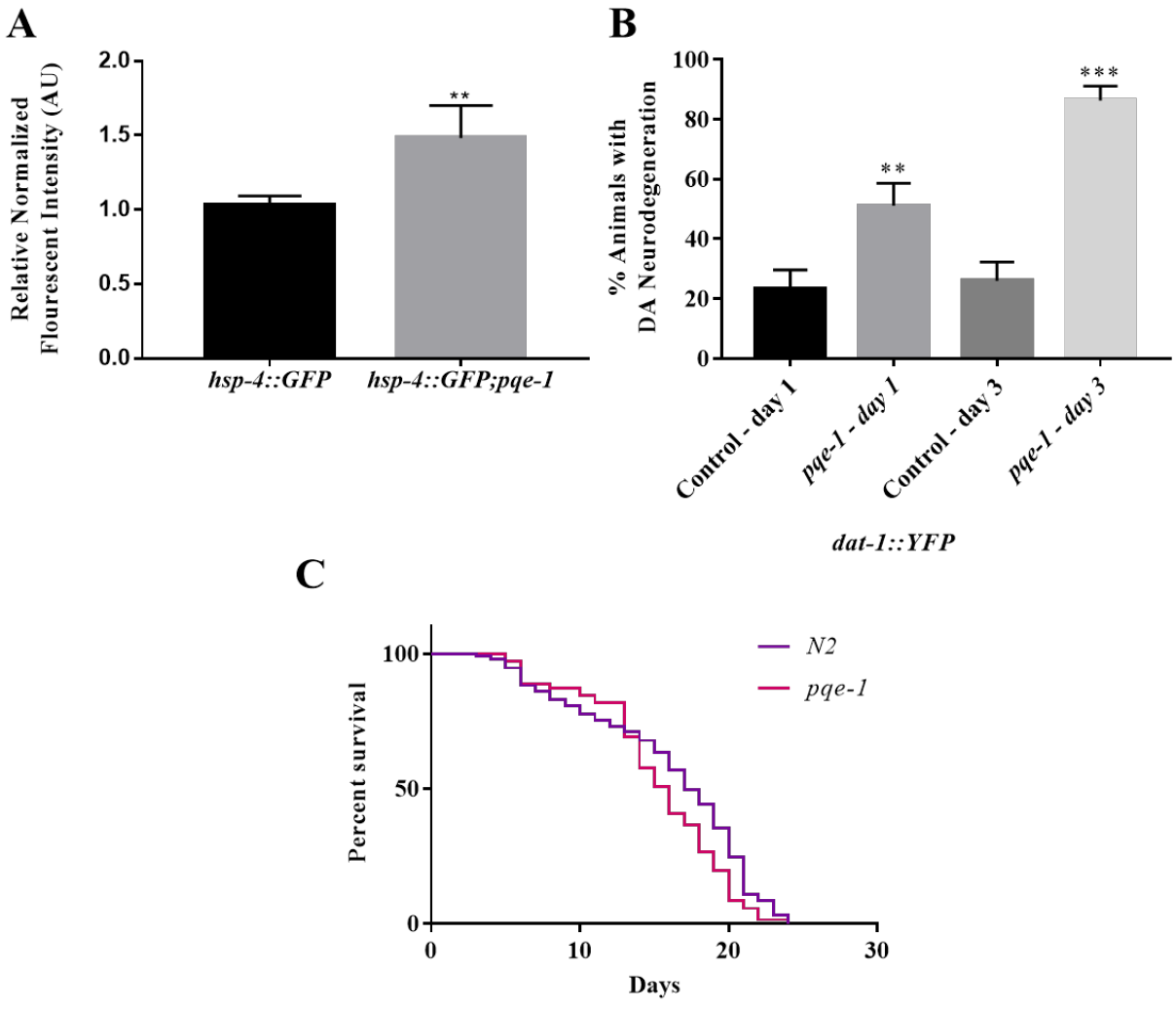

Supplementary Figure S3. RT-qPCR analysis the UPR chaperones following *ifg-1 RNAi*. The knock-down was confirmed by measuring *ifg-1* levels. **(A)** In N2 animals, *hsp-4* was unchanged. *hsp-6* was downregulated but *hsp-16.2* was increased roughly three folds (p = 0.002 and 0.03, respectively). **(B)** *ifg-1* RNAi in *pqe-1(ok1983)* animals had no effect on *hsp-4* but both *hsp-6* and *hsp-16.2* were upregulated (p = <0.001 and 0.013, respectively). While the increase in *hsp-16.2* is lower than *pqe-1* mutant alone (see Figure 4A), it is nevertheless up by 5-6 folds. Samples included: L4440 control: n = 2 batches, *ifg-1* RNAi: n = 2 batches, *pqe-1(ok1983),* L4440 control: n = 2 batches, *pqe-1(ok1983); ifg-1* RNAi: n = 2 batches. Data was analyzed using one-way ANOVA with Tukey's post hoc test.

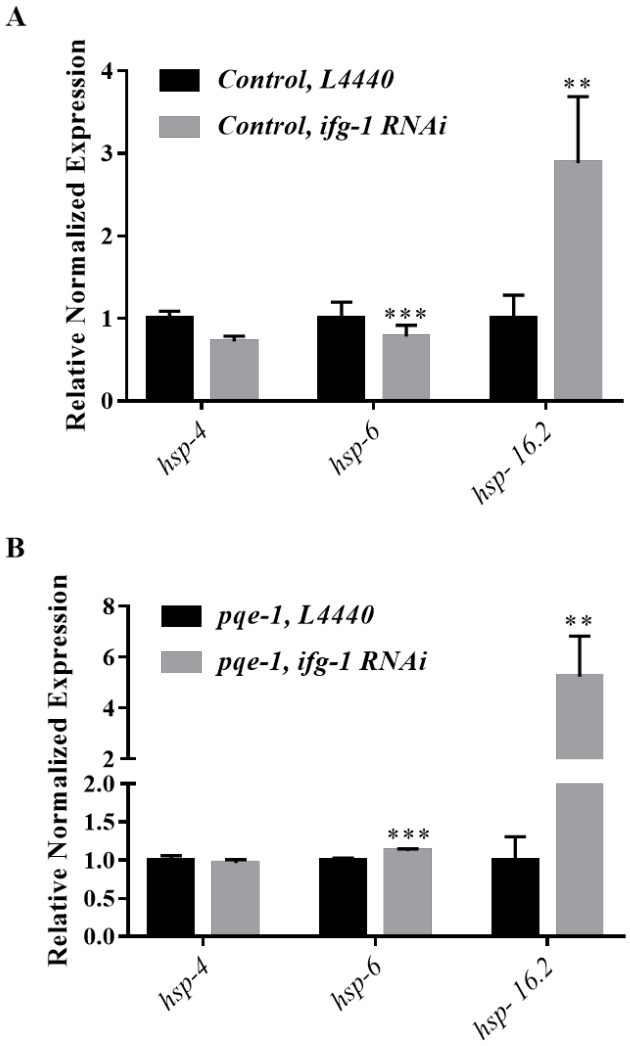

Supplementary Figure S4. Analysis of *hsp-4::GFP* reporter in wild-type N2 day-1 adults following 8 hrs exposures to 25°C and 28°C . The fluorescence was significantly increased for both temperatures (p=0.0001). Data was analyzed using one-way ANOVA followed by Dunnet's post hoc test. Control *hsp-4::GFP* : n = 20; 25°C: n = 22, *and* 28°C: n = 21.

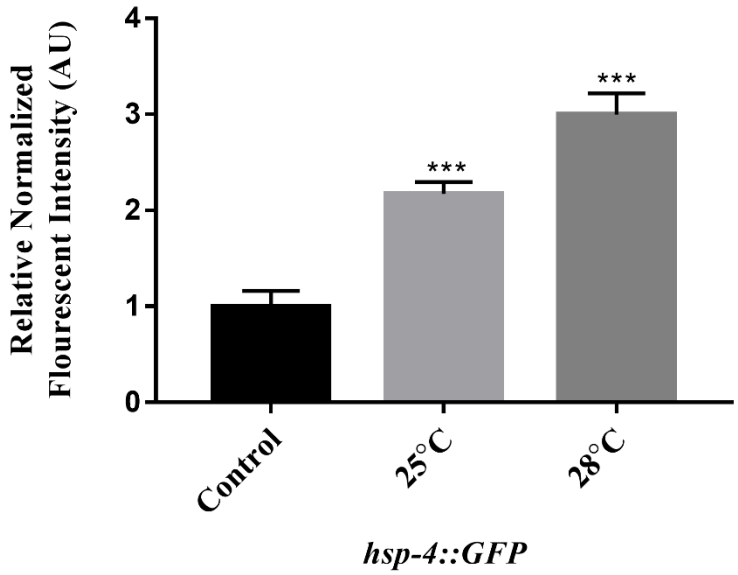

Supplementary Figure S5. Electrotaxis of PQ-treated *hsf-1* mutants. Refer to Figure 1 for a description of box plot. Speed of *hsf-1(sy441)* animals is not affected by treatment with 75 µM PQ ($p = 0.7901$) but is further depressed by treatment with 125 µM PQ ($p < 0.001$). Data was analyzed using one-way ANOVA followed by Dunnett's post hoc test. The numbers of animals examined were: *hsf-1(sy441)* untreated: n = 70, *hsf-1(sy441)* + 75 µM PQ: n = 20, *hsf-1(sy441)* + 125 µM PQ: n = 46.

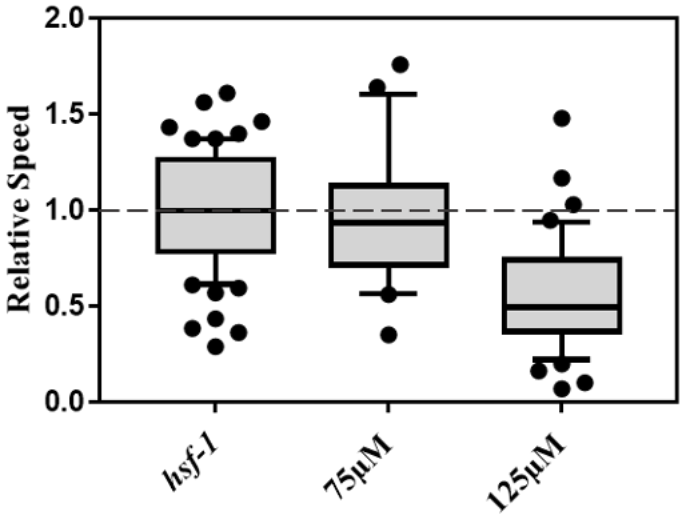

Supplementary Figure S6. Electrotaxis of adult *hsf-1* animals that have been starved in M9 for variable lengths of time at L1. Refer to Figure 1 for a description of box plot. *hsf-1(sy441)* animals arrested at L1 for 48 h or 72 h show significant slowness relative to control animals that were starved at L1 for 24 h ($p < 0.001$ in both cases). The numbers of animals examined were: *hsf-1(sy441)* starved 24h: n = 37, *hsf-1(sy441)* starved 48h: n = 24, *hsf-1(sy441)* starved 72h: n = 27. Data was analyzed using one-way ANOVA followed by Dunnett's post hoc test.

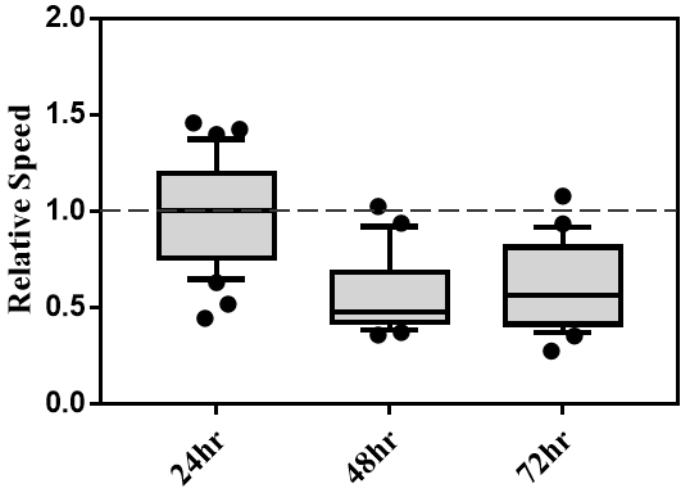

Supplementary Figure S7. Electrotaxis of animals exposed to *S. venezuelae* and *B. thuringiensis.* Refer to Figure 1 for a description of box plot. Worms fed with *E. coli* OP50 on NGM plates and MYM plates acted as controls for *S. venezuelae* fed animals. Likewise, for *B. thuringiensis*, *E. coli* OP50 on LB plate was used as a control. No significant change in *S. venezuelae* ($p = 0.3242$) and *B. thuringiensis* ($p = 0.8320$) fed animals was observed. The numbers of animals examined were: *E. coli* OP50 n = 26, *E. coli* OP50+MYM agar n = 22, *S. venezuelae* n= 27, *B. Thuringiensis* n = 24. Data was analyzed using one-way ANOVA followed by Dunnett's post hoc test.

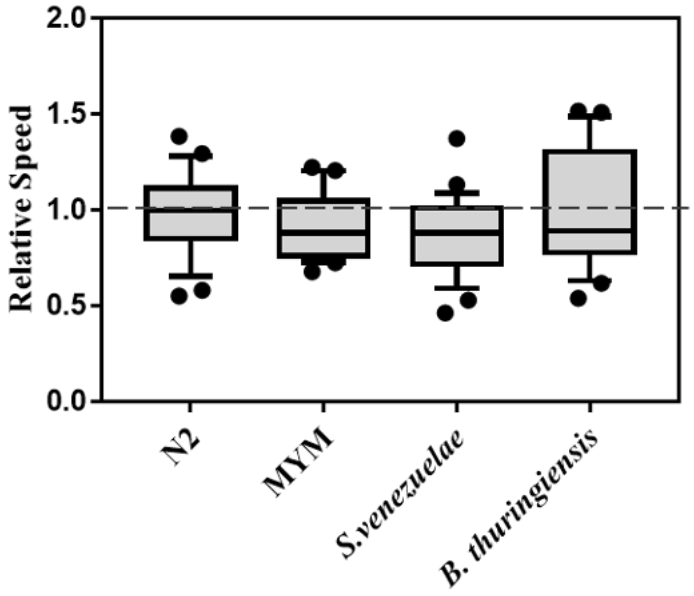

Supplementary Figure S8. Electrotaxis of wild-type animals fed with different microorganisms. Refer to Figure 1 for a description of box plot**.** No significant difference was observed between animals cultured on *E. coli* HB101 (p = 0.999), *E. coli* HT115 (p = 0.6587), *E. coli* DH5a (p = 0.9930), *C. aquaticus* DA1877 (p = 0.999), *A. tumefaciens* GV3101 (p = 0.121), or *E. carotovora* SCC3193 (p = 0.9511). The numbers of animals examined were: *E. coli* OP50 n = 20, *E. coli* HB101 n = 25, *E. coli* HT115 n = 16, *E. coli* DH5a n = 25, *C. aquaticus* DA1877 n = 30, *A. tumefaciens* GV3101 n = 25, and *P. carotovorum* SCC3193 n = 19. Data was analyzed using one-way ANOVA followed by Dunnett's post hoc test.

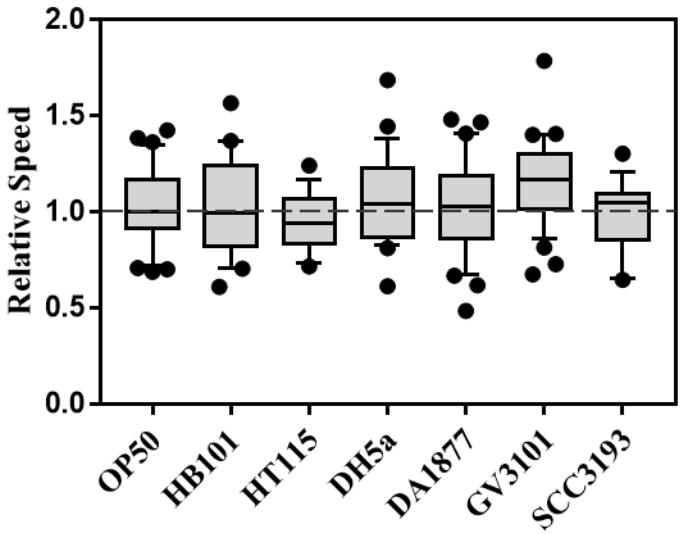

Supplementary Figure S9. Quantification of dopaminergic neurons in day-6 adults following exercise by shaking. The *dat-1::YFP* reporter was used to visualize neurons. No significant difference in neurodegeneration was observed (p = 0.7263, unpaired Student's t-test). **F)** Control n = 48, Exercise n = 47. Data was analyzed using unpaired Student's t-test.

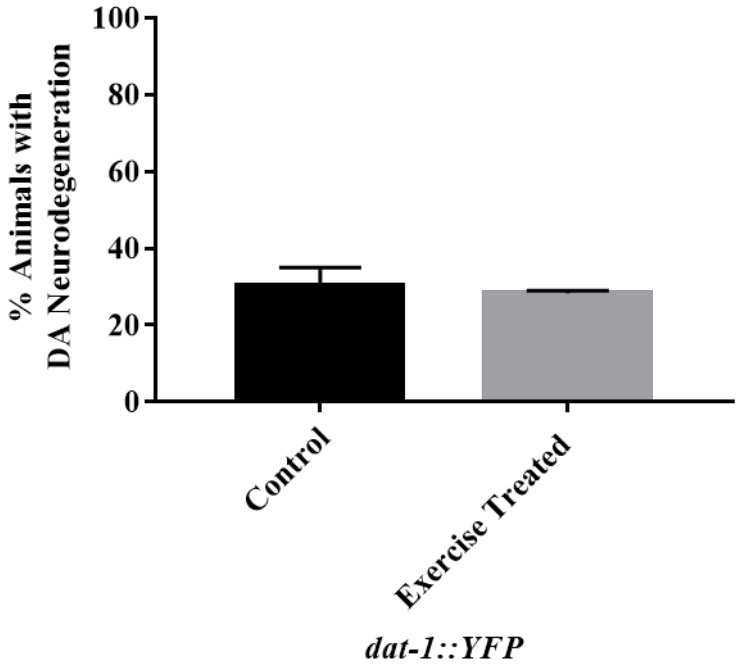

2.3 Taylor, Minhas & Gupta. 2023. microPublication Biology

microPublication BIOLOGY

9/15/2023 - *Open Access*

Effect of starvation on electrotaxis response

Shane K. B. Taylor[1§], Muhammad H. Minhas[1], Bhagwati P. Gupta[1]

[1]Biology, McMaster University, Hamilton, Ontario, Canada

[§]To whom correspondence should be addressed: taylos49@mcmaster.ca

Abstract

Caenorhabditis elegans is an ideal model for investigating the effects of extrinsic and intrinsic conditions on the behavioral changes of animals. Our group previously showed how different conditions influence the behavior of worms following an electric stimulus in a microfluidic channel, known as electrotaxis. In this study we describe the effect of starvation on the electrotaxis movement of animals. We show that acute starvation did not affect the electrotaxis response or dopaminergic neurons but extended the lifespan of animals.

microPublication BIOLOGY

9/15/2023 - *Open Access*

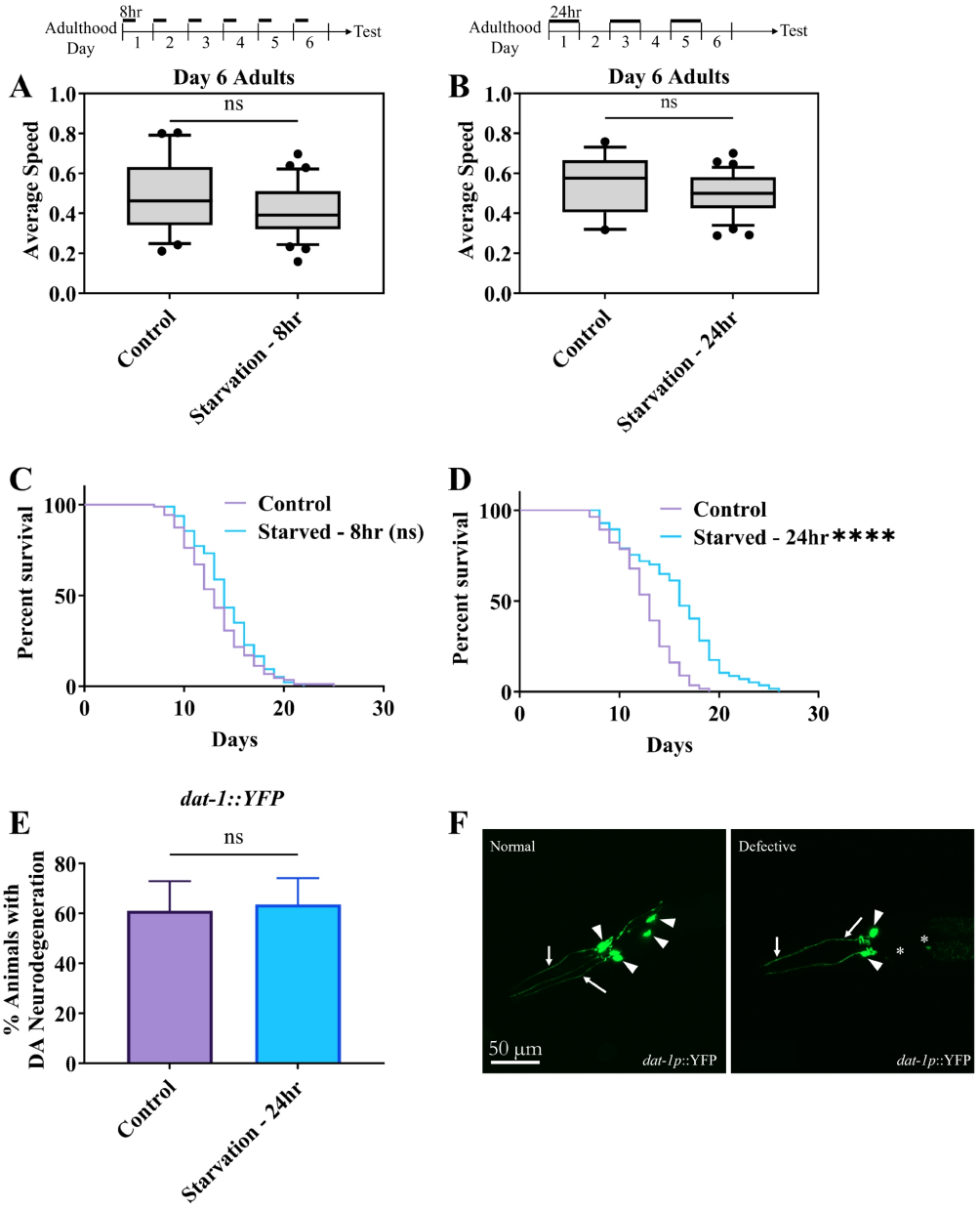

Figure 1. Effect of different starvation models on electrotaxis:

(A, B) Effect of starvation on electrotaxis speed. Boxes represent measurements from 25th to 75th percentiles, central horizontal lines represent medians, vertical lines extend to 10th and 90th percentiles, and dots represent outliers.

microPublication BIOLOGY

9/15/2023 - *Open Access*

(A) Animals are starved from day 1 adulthood everyday for 8hrs until day 6 of adulthood.

(B) Animals are starved every alternate day for 24hrs starting from day 1 until day 6 of adulthood. In **A and B** there was no significant difference in electrotaxis behaviour following starvation diets (**A,** p = 0.0592 & **B**, p = 0.1102).

(C, D) Lifespan analysis began from day 6 of adulthood.

(C) Lifespan analysis of animals starved from day 1 adulthood everyday for 8hrs until day 6 of adulthood. Mean lifespan of starved worms (mean 14.216 ± 0.318) remained unchanged compared to fed control (mean 13.205 ± 0.364) (p = 0.097).

(**D)** Lifespan analysis of animals starved every alternate day for 24hrs starting from day 1 until day 6 of adulthood. Animals starved for 24hrs had an increased mean lifespan (mean 15.754 ± 0.607) (p <0.001) compared to fed controls (12.625 ± 0.383).

(E) Quantification of neuronal degeneration of dopaminergic (DA) neurons in day-6 adults which followed the same starvation protocol as **(B and D).** There was no significant change in DA neurodegeneration compared to untreated controls (p = 0.8737).

(F) Representative images of animals showing normal and defective DA neuron morphology using *dat-1p::*YFP marker. Arrows point to dendrites and arrowheads mark cell bodies. The stars in the defective animal mark missing or faint cell bodies and axons. Note that in the defective worm dendrites are not as smooth compared to the normal animal and blebs can be seen by the arrows. Normal and defective dendrites were observed in both populations.

The numbers of animals were (**A)** Control: n = 29, Starved -8hr: n = 34. (**B)** Control: n = 17, Starved -24hr: n = 39. (**C)** Control: n = 88, Starved -8hr: n = 97. (**D)** Control: n = 56, Starved -24hr: n = 57. (**E)** Control: n = 18, Starved -24hr: n = 22. **A**, **B** and **E** were analyzed using an unpaired Student's t-test, **C** and **D** were analyzed using the log-rank (Kaplan-Meier) method for lifespan curves.

Description

Extrinsic conditions have the capability of impacting the health of organisms. To overcome this impact, animals have evolved mechanisms to protect and mitigate these harmful conditions (Higuchi-Sanabria et al. 2018; Dutta et al. 2022). Some of these protective responses involve the activation of signaling cascades collectively known as the stress response. The stress response works to maintain cellular homeostasis within the cell and prevent cell death (Taylor and Hetz 2020). However, genetic (e.g., mutations) or external factors such as starvation can impair the stress response, leaving the cell vulnerable to harmful conditions. In contrast, mild stress has been shown to have beneficial effects on organisms. This is due to a process known as hormesis, whereby mild stress can improve the tolerance of organisms towards additional stressors (Shore and Ruvkun 2013; Matai et al. 2019). For example reduced food intake (i.e., dietary restriction) has been shown to improve the health of animals through hormesis (Matai et al. 2019).

Our lab has previously shown that multiple stress response pathways contribute to the electrotaxis behaviour in *C. elegans*, which is a movement response when animals are exposed to a DC electric stimulus (Rezai et al. 2010). Specifically, the impairment of the stress response through mutations and external conditions such as heat and exercise reduced the electrotactic movement of animals (Taylor et al. 2021). We previously tested *eat-2* mutants which are chronically dietary restricted due to bacterial avoidance and other conditions including slower pharyngeal pumping (Bansal et al. 2015; Kumar et al. 2019; Matai et al. 2019). Our results showed that these animals have defects in electrotaxis (Taylor et al. 2021). However, an acute starvation treatment had no obvious effect on the electrotaxis of animals.

In this report, we describe the effect of different dietary models on worms. We utilized two different acute starvation protocols adapted from published findings (Honjoh et al. 2009). In the first dietary model, we starved animals for 8hrs every day until day 6 of adulthood. The second model involved 24hrs starvation treatment every alternate day starting from day 1 of adulthood until day 6. The examination of the electrotaxis speed and lifespan of such treated animals (i.e. 8hr and 24hr conditions) showed no significant effect on their electrotaxis behaviour **(Fig. 1A & B)**. Additionally, no change in lifespan was observed using the 8hr treatment but as expected from published studies, the lifespan of animals subjected to 24hr starvation treatment was increased **(Fig. 1C & D)** (Honjoh et al. 2009).

Dopaminergic (DA) neurons were shown previously by our group to mediate electrotaxis behaviour. Therefore, we examined these neurons in 24hr treated animals but saw no significant difference from the control **(Fig. 1E & F)**. Together with our published findings, these data demonstrate that acute starvation does not affect electrotaxis (Taylor et al. 2021). Furthermore, since *eat-2* mutants show defects in electrotaxis (Taylor et al. 2021), this suggests differences between acute and chronic dietary restriction affecting electrotaxis of animals.

Methods

microPublication BIOLOGY

9/15/2023 - *Open Access*

Strain and growth conditions

Worms were grown at 20°C on standard nematode growth media plates seeded with *E. coli* OP50. The strains used in this study are N2 (wildtype *C. elegans*) and DY353: *bhEx138[pGLC72(Cel-dat-1::yfp)]*

Starvation Protocol

This protocol was adapted from previous literature with modifications (Honjoh et al. 2009). In brief, two paradigms were tested, either 8 hrs starvation everyday or 24 hrs on alternate days. In the first paradigm, i.e., 8hr treatments, worms were washed with M9 buffer at least three times to get rid of residual bacteria. Animals were then placed on NGM plates containing no food and transferred back to OP50 bacteria containing plates at the end of the starvation period. The starvation treatment for the second paradigm was the same except that it was performed on alternate days for 24 hrs. The treatment was ended on day 6, at which point animals were tested.

Lifespan analysis

Lifespan experiments were conducted as previously described at 20°C (Mallick et al. 2020; Taylor et al. 2021). Experiments were performed on OP50 plates seeded with *E. coli*. Synchronized animals were transferred onto plates at day 6 adult stage following their respective starvation protocols. They were observed every day throughout the rest of their lifespan.

Electrotaxis Protocol

The electrotaxis assay protocol has been described previously (Tong et al. 2013). In brief, a microfluidic channel was used which is 5cm long, 300 µm wide and 80 µm deep with electrodes on both sides of the channel. A detailed description of fabricating the device was published earlier from our lab (Rezai et al. 2010; Tong et al. 2013). Worms are then suspended with M9 into a falcon tube and introduced into the microfluidic channel using a syringe under a dissecting microscope. Worms were then subjected to an electric field of 3 V/cm, which introduces a swimming response causing the worms to travel from anode to cathode resulting in electrotaxis. The electrotaxis response is recorded and locomotory data is extracted from videos using a MATLAB- based worm tracking software. The electrotaxis speed of animals is plotted as box plots.

Dopaminergic neuron analysis

Scoring of dopaminergic neurons (DA) was done using a previously published protocol (Taylor et al. 2021). In brief the number of DA cell bodies were counted, and dendritic morphology was observed under a Nomarski fluorescence microscope. Animals with reduced cell bodies, and abnormal dendrites with blebbing, punctate pattern, deformed shape, faint appearance or complete absence were counted as defective. Wildtype animals have three pairs of DA neurons and smooth dendritic projections in the head region.

Statistical analysis

For lifespan analysis, all statistics were performed using SigmaPlot software 14. Survival curves were estimated using the Kaplan-Meier test, and differences among groups were assessed using the log-rank test. Survival data are expressed relative to the control group. Other statistics were performed using Graphpad Prism 9.5.1

Acknowledgements: N2 strain was provided by Caenorhabditis Genetics Centre (CGC). We acknowledge WormBase for its database curation (PMID 19910365).

References

Bansal A, Zhu LJ, Yen K, Tissenbaum HA. 2015. Uncoupling lifespan and healthspan in *Caenorhabditis elegans* longevity mutants. Proc Natl Acad Sci U S A 112: E277-86. PubMed ID: 25561524

Dutta N, Garcia G, Higuchi-Sanabria R. 2022. Hijacking Cellular Stress Responses to Promote Lifespan. Front Aging 3: 860404. PubMed ID: 35821861

Higuchi-Sanabria R, Frankino PA, Paul JW 3rd, Tronnes SU, Dillin A. 2018. A Futile Battle? Protein Quality Control and the Stress of Aging. Dev Cell 44: 139-163. PubMed ID: 29401418

Honjoh S, Yamamoto T, Uno M, Nishida E. 2009. Signalling through RHEB-1 mediates intermittent fasting-induced longevity in *C. elegans*. Nature 457: 726-30. PubMed ID: 19079239

Kumar S, Egan BM, Kocsisova Z, Schneider DL, Murphy JT, Diwan A, Kornfeld K. 2019. Lifespan Extension in *C. elegans* Caused by Bacterial Colonization of the Intestine and Subsequent Activation of an Innate Immune Response. Dev Cell 49: 100-117.e6. PubMed ID: 30965033

microPublication BIOLOGY

9/15/2023 - *Open Access*

Mallick A, Ranawade A, van den Berg W, Gupta BP. 2020. Axin-Mediated Regulation of Lifespan and Muscle Health in *C. elegans* Requires AMPK-FOXO Signaling. iScience 23: 101843. PubMed ID: 33319173

Matai L, Sarkar GC, Chamoli M, Malik Y, Kumar SS, Rautela U, et al., Mukhopadhyay A. 2019. Dietary restriction improves proteostasis and increases life span through endoplasmic reticulum hormesis. Proc Natl Acad Sci U S A 116: 17383-17392. PubMed ID: 31413197

Rezai P, Siddiqui A, Selvaganapathy PR, Gupta BP. 2010. Electrotaxis of *Caenorhabditis elegans* in a microfluidic environment. Lab Chip 10: 220-6. PubMed ID: 20066250

Shore DE, Ruvkun G. 2013. A cytoprotective perspective on longevity regulation. Trends Cell Biol 23: 409-20. PubMed ID: 23726168

Taylor RC, Hetz C. 2020. Mastering organismal aging through the endoplasmic reticulum proteostasis network. Aging Cell 19: e13265. PubMed ID: 33128506

Taylor SKB, Minhas MH, Tong J, Selvaganapathy PR, Mishra RK, Gupta BP. 2021. *C. elegans* electrotaxis behavior is modulated by heat shock response and unfolded protein response signaling pathways. Sci Rep 11: 3115. PubMed ID: 33542359

Tong J, Rezai P, Salam S, Selvaganapathy PR, Gupta BP. 2013. Microfluidic-based electrotaxis for on-demand quantitative analysis of *Caenorhabditis elegans*' locomotion. J Vis Exp : e50226. PubMed ID: 23665669

Funding: This work was supported by NSERC Discovery grant to Bhagwati Gupta.

Author Contributions: Shane K. B. Taylor: writing - original draft, data curation, formal analysis, writing - review editing, investigation. Muhammad H. Minhas: investigation, data curation. Bhagwati P. Gupta: conceptualization, funding acquisition, writing - review editing.

Reviewed By: Ryo Sanabria

Nomenclature Validated By: Anonymous

WormBase Paper ID: WBPaper00065967

History: Received August 18, 2023 **Revision Received** September 6, 2023 **Accepted** September 12, 2023 **Published Online** September 15, 2023 **Indexed** September 29, 2023

Citation: Taylor, SKB; Minhas, MH; Gupta, BP (2023). Effect of starvation on electrotaxis response. microPublication Biology. 10.17912/micropub.biology.000962

3 More than a Neurotrophic factor: MANF regulates autophagy and lysosome function to promote proteostasis in *C. elegans*

3.1 Preface

This chapter includes the following two articles in their original published and submitted format:

1) More than a Neurotrophic factor: MANF regulates autophagy and lysosome function to promote proteostasis in *C. elegans* by Shane K. B. Taylor, Jessica H. Hartman & Bhagwati P. Gupta. Under review at Proceedings of the National Academy of Sciences (PNAS) 2024.

2) MANF and lithium paper under review at Micropublication 2024

In this chapter we primarily report on a novel regulation and mechanism for the neurotrophic factor MANF-1. This chapter discusses how MANF-1 regulates proteostasis, which may be a multifaceted approach. We discovered that MANF-1 localizes to lysosomes, regulates autophagy, the fusion of autophagosomes to lysosomes, and that the neuroprotective benefits of MANF-1 are mediated by the transcription factor for autophagy and lysosomal genes, TFEB/HLH-30. We present a novel mechanism for how MANF-1 may mediate its benefits through a lysosomal interaction that is potentially mediated by HLH-30. Additionally, we observe that MANF-1 may be regulated by other transcription factors that can be stimulated by chemical exposure. This chapter presents a new perspective on MANF-1 and new avenues for its therapeutic potential for a wide range of diseases.

3.2 Taylor, S. K. B. *et al.* 2024. In Review at PNAS.

More than a Neurotrophic factor: MANF regulates autophagy and lysosome function to promote proteostasis in *C. elegans*

Shane K. B. Taylor[1], Jessica H. Hartman[2], Bhagwati P. Gupta[1*]

[1]Department of Biology, McMaster University, Hamilton, ON L8S 4K1, Canada.

[2]Department of Biochemistry & Molecular Biology and Department of Regenerative Medicine & Cell Biology, Medical University of South Carolina, Charleston, SC 29425, USA.

[*]Author for Correspondence.

Email: guptab@mcmaster.ca; Phone: 1-905-525-9140 x26451

Running title: MANF-1 role in lysosomes and proteostasis

Keywords: MANF, MANF-1, *C. elegans*, autophagy, lysosome, ER stress, ER-UPR, Unfolded protein response, proteostasis, dopaminergic neuron, lifespan, aging, longevity

ABSTRACT

The conserved mesencephalic astrocyte-derived neurotrophic factor (MANF) protects dopaminergic neurons but also functions in several other tissues. Previously, we showed that *Caenorhabditis elegans manf-1* null mutants have defects such as increased Endoplasmic Reticulum (ER) stress, dopaminergic neurodegeneration, and abnormal protein aggregation. The multiple requirements of MANF in different systems suggest its essential role in cellular processes. However, how intracellular and extracellular MANF regulates broader cellular function remains unknown. We report a novel mechanism of action for *manf-1* that involves the autophagy transcription factor HLH-30/TFEB-mediated signaling to regulate autophagy and lysosomal function. Multiple transgenic strains overexpressing MANF-1 showed extended lifespan, reduced protein aggregation, and improved neuronal health of animals. Using a fluorescently tagged MANF-1, we observed different tissue localization of the protein, which was dependent on the ER retention signal. Further subcellular analysis showed that MANF-1 localizes within cells to the lysosomes and utilizes the endosomal pathway. Consistent with the lysosomal localization, our transcriptomic study of MANF-1 and analysis of autophagy regulators demonstrate that MANF-1 promotes proteostasis by regulating autophagic flux and lysosomal activity. Collectively, our findings establish MANF as a critical regulator of the stress response, proteostasis, and aging.

SIGNIFICANCE STATEMENT

Dysregulation of protein balance can lead to harmful protein aggregation, a key feature of age-related diseases. Neurotrophic factors such as the Mesencephalic astrocyte-derived neurotrophic Factor (MANF) play crucial roles in promoting neuronal health by protecting cells from these harmful aggregates. Given MANF's therapeutic promise, understanding its molecular mechanism is vital. Our study on nematodes demonstrates that MANF modulates autophagy and lysosome signaling, which are essential for neuron health and longevity. The cellular roles of MANF involve its interaction with vital machinery regulating protein transport and gene expression. Our findings provide new insights into MANF's critical role in maintaining cellular equilibrium, offering valuable insights into its potential applications in combating age-associated disorders.

INTRODUCTION

Nothing is perfect, and this includes the intracellular machinery of a cell. Despite their constant working, the ability of cells to maintain homeostasis declines with age [1]. Dysregulated homeostasis can cause protein misfolding and the formation of protein clumps or aggregates. Abnormal accumulation of protein aggregates is toxic to cells because it increases cellular stress, disrupts physiological processes, and eventually results in the failure of cells, tissues, and organs. Current research suggests that maintaining protein homeostasis (proteostasis) is essential for functioning cellular processes, reducing age-related diseases, and promoting healthy aging. Notably, cells can activate stress response signaling pathways, such as the unfolded protein response (UPR), to maintain proteostasis and minimize cellular damage. Although these responses work very well in most cases, they are not always efficient. Failure to eliminate toxic protein aggregates is a key hallmark of age-related diseases, including neurodegenerative diseases such as Parkinson's Disease (PD) and Huntington's Disease (HD) [1-3].

A promising approach to enhance proteostasis and protect against neurodegeneration involves the therapeutic delivery of neurotrophic factors (NTFs). NTFs are proteins that support neuronal survival, growth, and differentiation. Their anti-inflammatory and anti-apoptotic properties make them promising therapeutic candidates [4]. One family of NTFs relevant to this study is represented by two proteins, namely the cerebral dopamine neurotrophic factor (CDNF) and the mesencephalic astrocyte-derived neurotrophic factor (MANF) [5]. These two proteins are structurally and mechanistically distinct from other classical NTFs [4, 6]. Although vertebrates express both CDNF and MANF, only MANF is expressed in invertebrates.

MANF homologs have been studied in different animals including mouse, rat, zebrafish, and two leading invertebrates, *Drosophila melanogaster* and *Caenorhabditis elegans*. These studies have shown that MANF confers cytoprotection through endoplasmic reticulum (ER)-UPR regulation [5]. ER-UPR is a quality control mechanism that rectifies cellular stress by correctly folding misfolded proteins, reducing translation, and activating apoptosis when homeostasis cannot be restored [7]. Three conserved transmembrane proteins mediate the ER-UPR, inositol-requiring enzyme 1 (IRE1), protein kinase RNA (PKR)-like ER kinase (PERK), and activating transcription

factor 6 (ATF6) (*ire-1*, *pek-1*, and *atf-6*, respectively, in *C. elegans*), which activate overlapping but distinct pathways in stress responses [7, 8]. In addition, IRE1 creates a spliced form of the transcription factor X-box binding protein-1 (XBP1), the main regulator of ER-UPR. Spliced XBP-1 maintains homeostasis through the transcription of chaperones, such as GRP78/BiP (*C. elegans hsp-4*), which is affected by MANF [7-11]. Consistent with the role of MANF in ER-UPR maintenance, its sequence contains an ER retention signal [12]. Under normal conditions, MANF is retained in the ER and is secreted in response to protein misfolding or cellular stress [13].

Recent studies have indicated that MANF is also linked to other diseases with dysregulated homeostasis, more specifically, metabolic dysfunction, diabetes, ischemia, and retinal degeneration [4, 14, 15]. Accordingly, MANF is widely expressed [14-17] underscoring the protein's critical roles in multiple processes. Although MANF is secreted from the ER in response to stress, how it regulates cellular function and how extracellular MANF affects other tissues is currently unknown. Is there a common theme underlying its mechanisms of action in different cell types? The nematode *Caenorhabditis elegans* offers the necessary genetic and molecular tools to investigate these questions and functions of MANF [18-20]. Studies on the *C. elegans* MANF homolog, MANF-1, have shown that it is secreted and endocytosed upon binding to sulfatides [21]. Our group and others have demonstrated the role of MANF-1 in processes that include age-dependent protection of DA neurons [22], regulation of the ER-UPR chaperone HSP-4/BIP/GRP78, and sensitivity to bacterial pathogenesis [23, 24]. The protective role of *manf-1* may be mediated by genes affecting autophagy, ER-UPR, and immunity [23, 24].

This study reports novel findings on *C. elegans* MANF-1 and the mechanism of function. Our data indicate that *manf-1* mutants died prematurely when subjected to ER stress, and MANF-1 expression was upregulated in response to stress-inducing conditions. Further analysis revealed an essential role for this gene in regulating ER-UPR signaling. We generated multiple transgenic strains overexpressing MANF-1 and found that the animals had longer lifespans, improved proteostasis, and reduced neurodegeneration. Consistent with these results, the MANF-1::mCherry chimeric protein was widely expressed to areas including the intestine, pharynx, muscles, hypodermis, and coelomocytes. Subcellular expression studies revealed that MANF-1 was

secreted and localized to lysosomal membranes. Further characterization of MANF-1::mCherry showed differences in expression depending on the presence or absence of the ER retention signal; however, lysosomal localization was present in all of the strains. Moreover, the MANF-1 pattern was broadly similar in animals carrying the native ER sequence (KEEL) and the human version (RTDL). Interestingly, the beneficial effects of MANF-1 did not depend on the ER sequence. Consistent with these data, transcriptomic profiling of the mutant and overexpressing animals revealed significant changes in the expression of ER-UPR and lysosomal genes. We found that MANF-1 secretion and sub-cellular localization required proteins such as RAB-5 and RAB-7 mediating endosomal trafficking. Further experiments conducted to investigate autophagy in MANF-1 mutant and overexpression animals using the LGG-1 and p62/SQST-1 reporters suggest that MANF-1 regulates autophagic flux. Additionally, MANF-1 overexpression caused HLH-30/TFEB, a transcription factor that regulates autophagy and lysosomal biogenesis, to be upregulated and localized to the nucleus. Altogether, our findings establish MANF-1 as more than a neurotrophic factor, but rather as a player regulating ER-UPR, autophagy, and lysosomal function, potentially in a coordinated manner, to maintain proteostasis, neuronal health, and the lifespan of animals.

Results

Manf-1 mutants show increased ER stress sensitivity and a shorter lifespan

We reported earlier that *manf-1* mutants have increased expression of the ER-UPR reporter *hsp-4p::GFP* [22, 23]. However, the effect of additional ER stress on *manf-1* in an age dependent manner was unknown considering that the ER-UPR declines with age [1, 25]. To this end, we assessed the effect of MANF-1 in older *manf-1(tm3603)* worms by treating them with the ER stress-activating drug tunicamycin. Levels of *hsp-4p::GFP* were quantified in 1-, 4-, and 7-day old adults and found to be significantly higher than controls (Fig. 1A, D). The *hsp-4* transcription was also upregulated (Fig. 1B, C). The results led us to conclude that *manf-1* is essential in both young and older adults for the maintenance of ER-UPR. The crucial role of the gene was demonstrated through additional experiments showing that *manf-1(tm3603)* animals had significantly reduced lifespan (Fig. 1E). Additionally, tunicamycin exposure exacerbated the DA

neurodegeneration, lifespan reduction and mortality of animals (Fig. 1F-G, Supplementary Figure 1A).

Consistent with the above results, *manf-1p::GFP* expression was significantly increased following tunicamycin treatment (Fig. 1H). In support of this, *manf-1* transcription was upregulated in animals subjected to acute (8 hr) and chronic (3 days) tunicamycin treatments (Fig. 1I and J). The endogenously tagged *mKate2::manf-1* strain [23] showed a similar response (Fig. 1K).

We also examined whether *manf-1* affected the sensitivity of animals to other forms of stress in order to understand the role of the gene in other physiological processes. To this end, heat stress and oxidative stress assays were performed. Except for paraquat, where chronic exposure caused significant damage to DA neurons in *manf-1* mutants (Supplementary Figure 1D), no other difference was observed between mutant and wild-type animals (Supplementary Figure 1B, C). Taken together, the results presented in this section demonstrate that *manf-1* is necessary for the maintenance of ER-UPR and protects animals against ER stress.

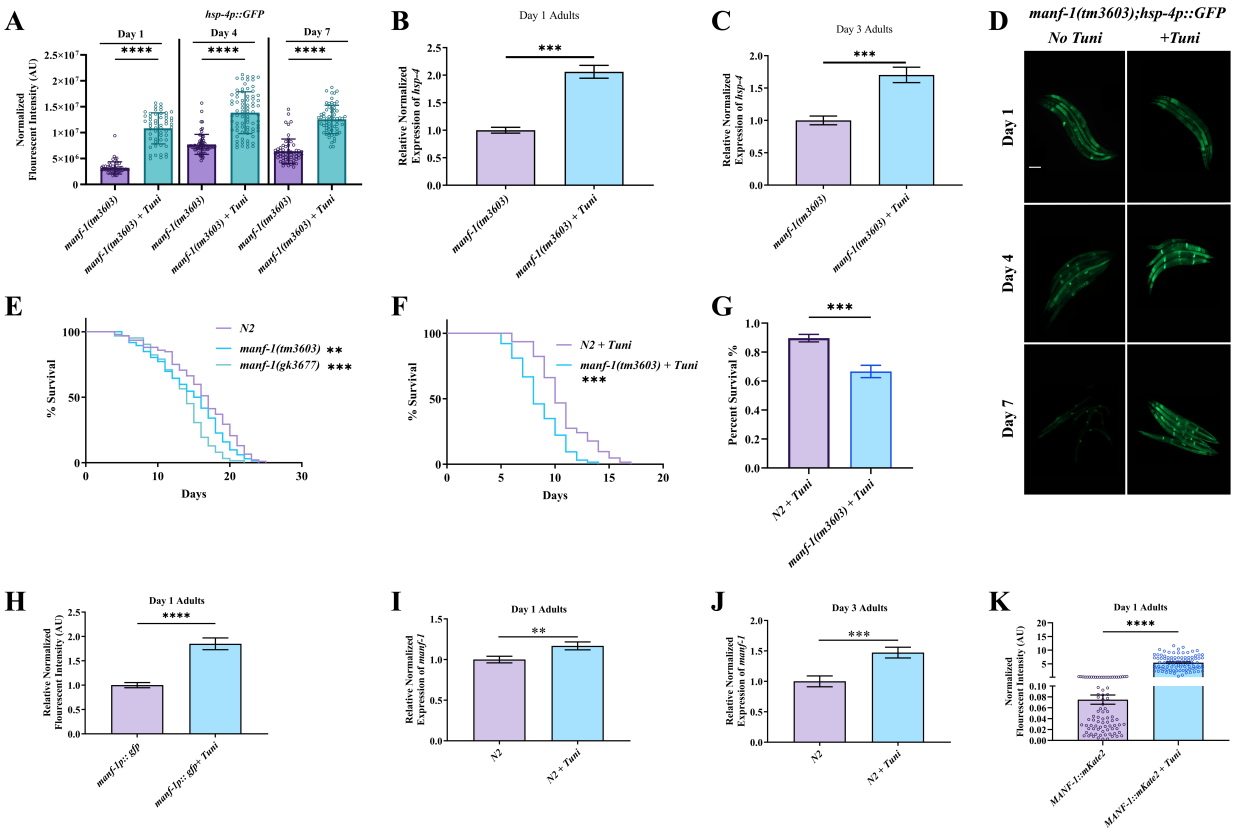

Figure 1. *manf-1* mutant phenotypes and gene expression following ER stress. **A)** GFP fluorescence in *manf-1(tm3603)*; *hsp-4p::GFP* strain with and without 4 hrs of 25 ng/µL tunicamycin exposure on day 1, 4, and 7 of adulthood. **B)** RT-qPCR analysis of *hsp-4* in day 1 *manf-1(tm3603)* adults following 8 hr exposure to 5 µg/mL tunicamycin. **C)** Same as B, except that animals were chronically exposed to 5 µg/mL tunicamycin until day 3 of adulthood. **D)** Representative images of *hsp-4p::GFP* fluorescing animals corresponding to the panel A (scale bar 100 µm). **E, F)** Lifespan analysis of *manf-1* mutants and N2 control without any treatment (E) and following chronic exposure to 25 ng/µL tunicamycin (F). Mean and max lifespan of animals are shown in the Supplementary Table 1. **G)** Percentage survival following 4 hrs exposure to 50 ng/µL tunicamycin in liquid. **(H)** Quantification of GFP fluorescence in *manf-1p::GFP* day 1 adults following an 8 hr treatment of 5 µg/mL tunicamycin. **(I)** *manf*-1 RT-qPCR analysis in day 1 N2 adults following an 8 hr treatment of 5 µg/mL tunicamycin. **J)** Same as I, except that animals were chronically exposed to 5 µg/mL tunicamycin until day 3 of adulthood. **K)** Quantification of mKate2 fluorescence in the *manf-1p:: mKate2::manf-1* transgenic strain. For results presented in panels A, E-G, H & K a total of 60 – 140 worms from three independent batches (20 worms

minimum per batch) were examined. The RT-qPCR experiments (B, C, I, J) were carried out in three independent batches. The graphs are plotted as mean ± SEM (B, C, G, H-K) and mean ± SD (E). Data was analyzed using student's t-test (A-I) and the log-rank (Kaplan-Meier) method (J and K). *p<0.05; **p<0.01; ***p<0.001; ****p<0.0001.

manf-1 mutants show enhanced protein aggregation defects

Based on the upregulation of *hsp-4* in *manf-1(tm3603)* animals, we investigated the ER-UPR genes that define each of the signaling arms, namely ATF6/*atf-6*, PERK/*pek-1*, IRE1/*ire-1*, and the downstream transcription factor XBP-1/*xbp-1* [7, 11]. The expression of all four genes was significantly upregulated in *manf-1* mutants compared to wild-type controls (Fig. 2A). The ratio of spliced to total *xbp-1* was also high (Fig. 2B). These data suggest that *manf-1* affects a wide range of processes that maintain ER homeostasis.

As ER stress affects the ability of cells to promote protein folding and reduce the accumulation of misfolded and unfolded proteins, we examined the proteostasis defects in *manf-1* mutants. To this end, transgenic animals expressing YFP reporter-tagged human α-Synuclein in body wall muscles were used. In a previous study, we demonstrated that these transgenic animals showed increased aggregation in the absence of *manf-1* [22]. Analysis of α-Synuclein::YFP in 1-, 4-, and 7-day old *manf-1 (tm3603)* adults revealed higher aggregation compared with that in wild-type controls (Fig. 2C), suggesting that *manf-1* is necessary to maintain proteostasis at different stages of adulthood. The phenotype was further enhanced by RNAi knockdown of *atf-6* and *pek-1* (Fig. 2D–F and Supplementary Figure 2A), providing evidence that ER-UPR was compromised but not eliminated in the absence of *manf-1*. Notably, the *manf-1(tm3603); xbp-1*(RNAi) animals showed an opposite effect, i.e., α-Synuclein::YFP levels were considerably reduced (Fig. 2D–F and Supplementary Figure 2A). Although the precise reasons are unknown, we noted that the animals were unhealthy and exhibited slower growth, abnormal movement, reduced viability, and a tendency to frequently burst open through the vulval opening (see Methods and Supplementary Figure 3). These observations suggest that *xbp-1* knockdown significantly compromised the physiological processes in *manf-1* mutants, leading to reduced α-Synuclein aggregation. The synthetic interaction between *manf-1* and *xbp-1* was consistent with that observed in a previous study that

reported that *manf-1; ire-1* double mutants and *xbp-1* RNAi-treated *manf-1* mutants were lethal or sterile [23].

We used another protein aggregation system to examine the effects of *manf-1*, which consists of glutamine repeats (polyQ) and serves as a *C. elegans* HD model [26]. To this end, two polyQ strains, Q35::YFP (AM140) and Q40::YFP (AM141), that express fusion proteins in body wall muscles under the *unc-54* promoter were utilized [26]. Similar to α-Synuclein, both polyQ carrying strains exhibited a significant increase in protein aggregation in *manf-1* mutants (Fig. 2G, H and Supplementary Figure 2B, C). Thrashing defects in the polyQ35 animals, due to aggregates accumulating in muscles, were also enhanced (Fig. 2I). Thus, *manf-1* is necessary for regulating ER-UPR signaling and preventing protein aggregation.

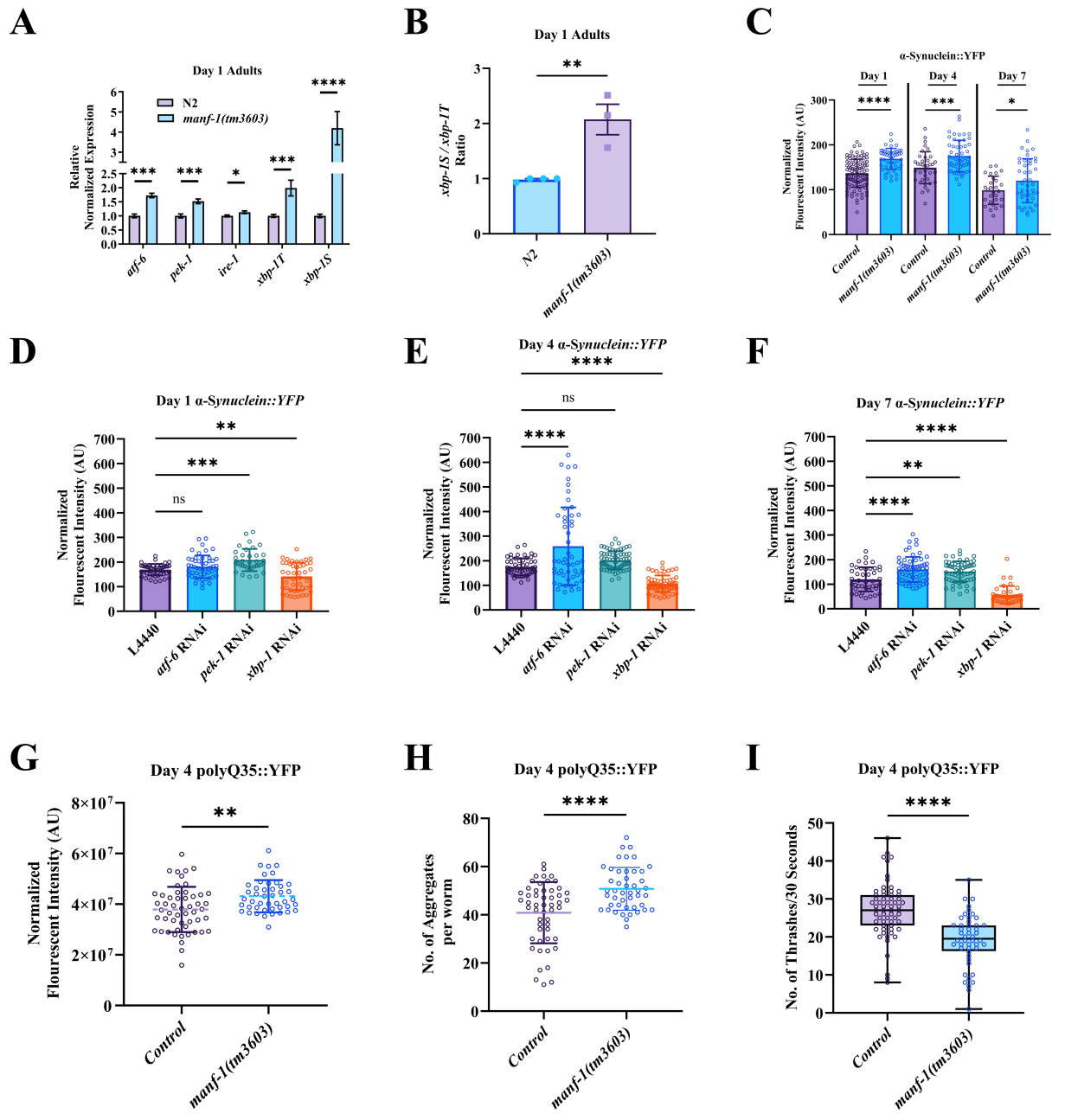

Figure 2. Effect of RNAi knockdown of ER-UPR components on α-Synuclein and polyQ aggregation in *manf-1(tm3603)* animals. **A)** RT-qPCR analysis of ER-UPR genes (*atf-6, pek-1,ire-1* and *xbp-1)* in N2 and *manf-1(tm3603)* day 1 adults. *Xbp-1* total and spliced forms are indicated by *xbp-1T* and *xbp-1S*, respectively. **B)** The ratio of spliced *xbp-1* to total *xbp-1* in *manf-1(tm3603)* day 1 adults. **C)** The fluorescence intensity of α-Synuclein::YFP in body wall muscles was measured in day 1, 4 and 7 adults of *manf-1(tm3603)* and control genotypes. **D-F)** α-Synuclein::YFP fluorescence intensities in day 1 (D), day 4 (E) and day 7 (F) animals, following

knockdowns of *atf-6, pek-1* and *xbp-1***.** L4440 is an empty vector RNAi control. **G-I)** polyQ35 protein aggregation phenotype in *manf-1(tm3603)* animals on day 4 of adulthood compared to wild-type. The total fluorescent intensity measurement of polyQ35::YFP (G) and number of aggregates (H) in body wall muscles. The thrashing response of animals over a 30 second interval (I). Results in panels A and B are based on pooled worms from 3 batches. For panels C-J, at least 3 batches were analyzed (10-20 worms per batch). Results are shown as mean ± SEM (A, B) and mean ± SD (C-I). Panel I shows a box plot containing all data points, mean, and 25th and 75th quartile boundaries. Data was analyzed using student's *t*-test (A-C, G-I) and one-way ANOVA with Dunnett's test (D-F). *p<0.05; **p<0.01; ***p<0.001; ****p<0.0001. ns: not significant.

Overexpression of *manf-1* reduces protein aggregation, improves neuronal survival, and extends lifespan

The essential role of *manf-1* in stress response maintenance and proper protein folding raises the possibility that overexpression of this gene in animals may have beneficial and protective effects. To test this hypothesis, we used different approaches to activate *manf-1* expression. One of these involves treating animals with bioactive compounds such as curcumin and lithium. Recently, these two chemicals were reported to increase *manf* transcription in mammalian cells [27, 28]. Similar experiments in worms also showed increased *manf-1* levels, albeit only modestly (SKBT, unpublished). Other approaches involve the use of transgenic strains that express *manf-1* under the control of either the heat-shock *hsp-16.41* promoter *(hsp::manf-1)* or the native promoter (*manf-1p::manf-1* and *manf-1p::manf-1::mCherry*) (see Methods).

For the *hsp::manf-1* strain, we tested whether induction of *manf-1* expression had a cytoprotective effect in animals. The transgenic worms showed a robust response to heat treatments because a 1 hr 31-°C exposure caused a significant increase in *manf-1* transcription (Fig. 3A). Notably, heat shock was not required at later stages as 3- and 7-day old adults showed a significant expression without any treatment (Fig. 3B), likely due to basal activity of the promoter at room temperature.

Phenotypic analysis of day 7 *hsp::manf-1; dat-1p::YFP* adults showed increased protection of DA neurons following heat treatment. Specifically, these animals had a much higher proportion of morphologically normal dendritic processes and cell bodies (Fig. 3C). Quantification of neuronal defects revealed fewer animals with defective dendritic and cell body morphologies, demonstrating the beneficial effects of *manf-1* in promoting neuronal health. Interestingly, animals without heat treatment also showed comparable neuroprotection (Fig. 3C), suggesting that a mild increase in MANF-1 levels is sufficient to protect DA neurons. In addition, the *hsp::manf-1* transgene caused a significantly lower α-Synuclein::YFP fluorescence in *hsp::manf-1; α-Synuclein::YFP* animals, suggesting a reduction in protein aggregation defects in older adults (Fig. 3D). Finally, the lifespan was significantly enhanced (approximately 5% in heat-treated animals and 21% in untreated animals; Fig. 3E, Supplementary Table 1).

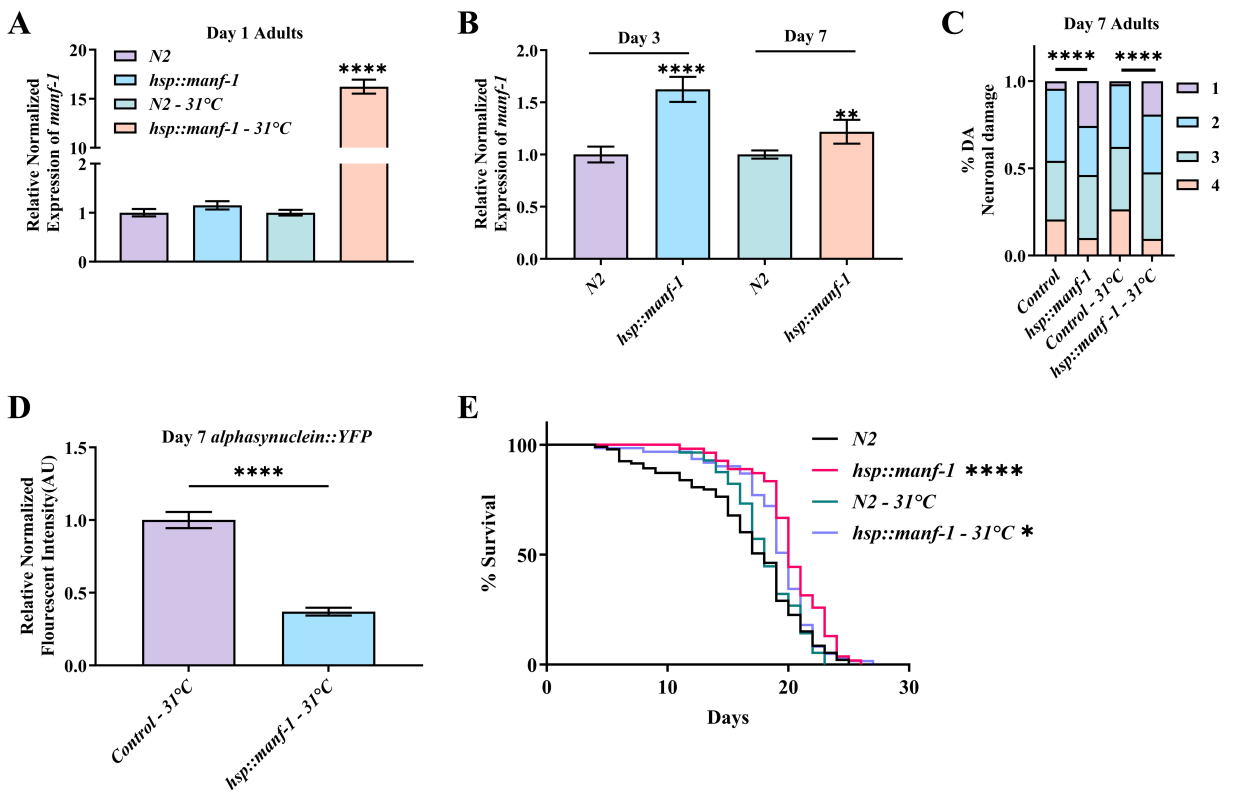

Figure 3. Effect of *manf-1* overexpression on *hsp::manf-1* animals. **A)** RT-qPCR analysis of *manf-1* expression in day 1 *hsp::manf-1* and N2 adults maintained either at 20°C or subjected to 1 hr heat shock at 31°C. **B)** RT-qPCR analysis of day 3 and day 7 adults grown at 20°C. **C)** Neuronal analysis in day 7 adults. An odd day heat treatment at 31°C starting on day 1 until day 7 was used to activate *hsp::manf-1*. Neurons were scored as described in Methods (1: normal cell bodies and dendrites, 2: dendritic damage, 3: cell body missing or abnormally shaped, 4: both dendrites and cell bodies defective). **D)** The effect of MANF-1 overexpression on α-Synuclein aggregation. The fluorescent intensity of α-Synuclein::YFP was measured in day 7 adults following the same heat treatment as in panel C. **E)** The lifespan analysis of animals after subjecting them to heat treatments as in panels C and D. Mean and max lifespan are in the Supplementary Table 1. Data in panels A-C include three different batches. For α-Synuclein and lifespan analyses, three batches with 20-30 animals per batch were examined. Results are expressed as mean ± SEM (A, B, D). Data was analyzed using one-way ANOVA with Tukey's test (A, B). Chi square test (C), Student's *t*-test (D), and log-rank (Kaplan-Meier) method (E). *p<0.05; **p<0.01; ***p<0.001; ****p<0.0001.

Next, we examined the phenotype of *manf-1p::MANF-1::mCherry* transgenic animals (termed as *MANF-1*$^{KEEL::mCherry}$; see methods). The *MANF-1*$^{KEEL::mCherry}$ worms showed high levels of secreted MANF-1 in three different lines examined (see next section and Methods). One of these lines showing high transgene transmission (DY759, *bhEx304*) was analyzed in detail. While *hsp-4* transcripts were not significantly affected in these animals, the *hsp-4p::GFP* transgene was activated resulting in increased GFP fluorescence, which suggests that *manf-1* overexpression caused a modest activation of ER-UPR (Fig. 4A and B). We also observed an increase in both the total and spliced *xbp-1* transcripts, whereas *pek-1* levels were reduced (Supplementary Figure 4). However, *MANF-1*$^{KEEL::mCherry}$ suppressed the ER stress phenotype of *manf-1(tm3603)* mutants based on *hsp-4::GFP* analysis (Fig. 4A and B).

To determine if *MANF-1*$^{KEEL::mCherry}$ had protective capabilities, we analyzed the DA neuron morphology, α-Synuclein and polyQ aggregation, movement, and lifespan of animals. The results indicated that *manf-1* overexpression conferred significant protection on DA neurons (Fig. 4D) and reduced the aggregation of α-Synuclein (Fig. 4E) and polyQ35 & polyQ40 (Fig. 4G, H, J and Supplementary Figure 2C). Additionally, the thrashing response of muscular polyQ35-expressing worms significantly improved (Fig. 4I). Similar to *hsp::manf-1* animals; the *MANF-1*$^{KEEL::mCherry}$ animals had a significantly increased lifespan (19.2% higher; mean lifespan 19.9 ± 0.5 days compared with 16.7 ± 0.4 days for controls) (Fig. 4K, Supplementary Table 1). In addition, they showed higher resistance to chronic ER stress (Fig. 4L). The increase in lifespan was also observed in another independently generated *manf-1* overexpression strain (*manf-1p::manf-1*, termed as *MANF-1*^{HAR}*;* mean lifespan 18.5 ± 0.9 days compared with 15.9 ± 0.5 days for controls) (Supplementary Figure 5). Overall, these results demonstrate the multiple beneficial effects of MANF-1 in *C. elegans*.

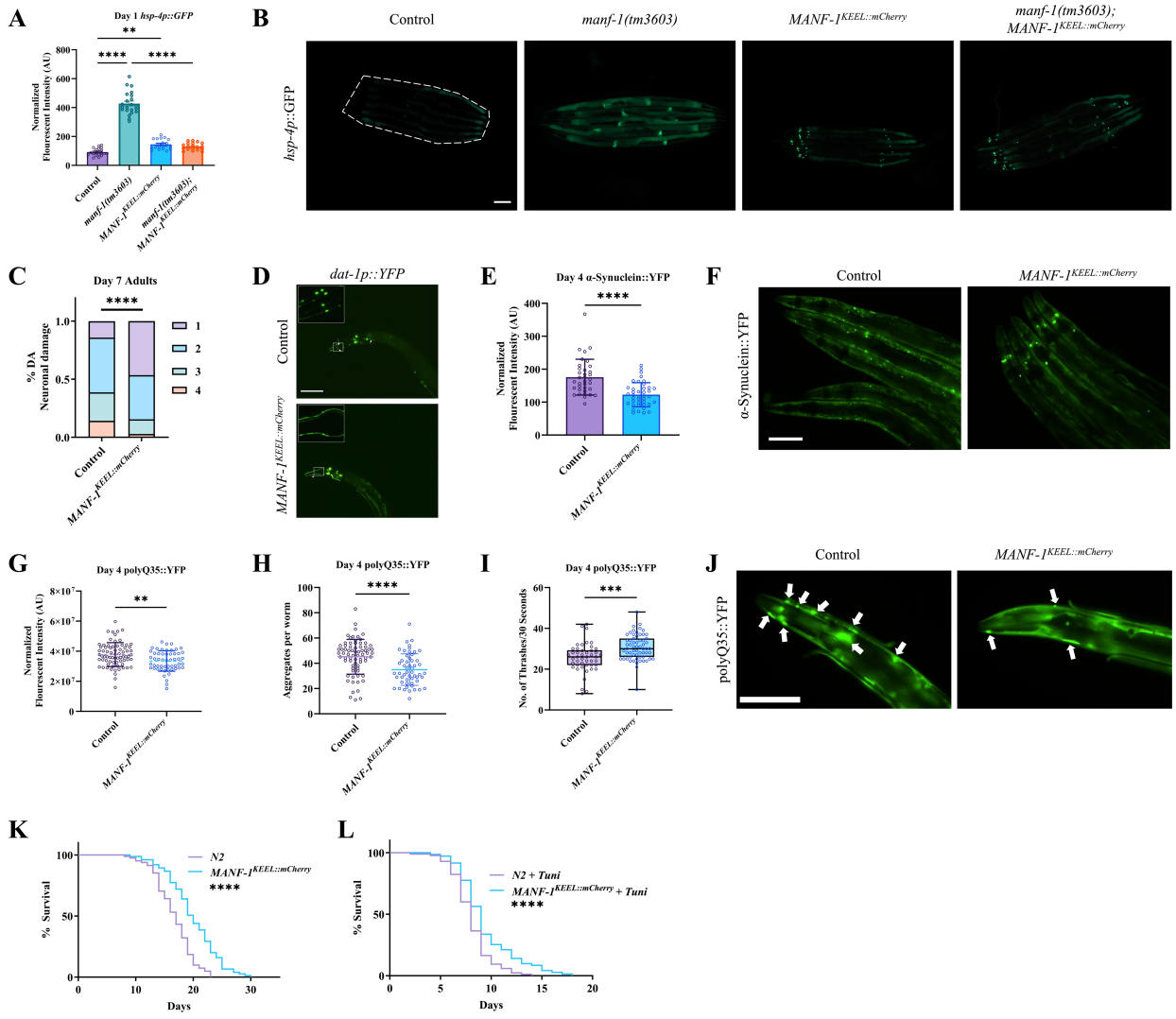

Figure 4. Effect of *manf-1* overexpression on neurons, stress response, and lifespan of animals. **A-B)** *hsp-4p::GFP* reporter expression in wild-type, *manf-1(tm3603)*, *MANF-1*$^{KEEL::mCherry}$, and *manf-1(tm3603); MANF-1*$^{KEEL::mCherry}$ day 1 adults. Quantification of GFP fluorescence (A) and representative images (scale bar 100 µm) (B). **C, D)** Analysis of dopaminergic neurons in day 7 adults. (C) Neurons were classified into four different categories based on defects in cell bodies and dendrites. See Figure 3 legend and Methods for details. (D) Corresponding images of dopaminergic neurons (scale bar 100 µm). **E, F)** The effect of *MANF-1*$^{KEEL::mCherry}$ on α-Synuclein::YFP aggregation in body wall muscles of day 4 adults. (E) The α-Synuclein::YFP fluorescence intensity was measured in day 4 adults; (F) Representative images of day 4 adults showing α-Synuclein::YFP fluorescence (scale bar 100 µm). **G-J)** The effect of *MANF-1*$^{KEEL::mCherry}$ on polyQ35::YFP aggregation in body wall muscles of day 4 adults. Quantification

of polyQ35::YFP fluorescence intensity (G) and protein aggregates (H). (I) Thrashing response over a 30 sec interval. (J) Representative images of day 4 adults (scale bar 100 μm). Arrows mark aggregates in the head region. **K, L)** Lifespan analysis of wild-type N2 and *MANF-1*$^{KEEL::mCherry}$ animals without any treatment (K) and in the presence of 25 ng/μL tunicamycin (L). The mean and max lifespan are shown in the Supplementary Table 1. At least three batches with 10-30 worms per batch were examined for panels A-I and three batches with 20-30 animals per batch for panels K, L. Data in A is expressed as mean ± SEM and in E-H as mean ± SD. Panel I shows a box plot containing all data points along with the mean and 25th and 75th quartile boundaries. Data was analyzed using one-way ANOVA with Tukey's test (A), Chi-square test (C), Student's *t*-test (E-J), and log-rank (Kaplan-Meier) method (K & L). *p<0.05; **p<0.01; ***p<0.001; ****p<0.0001.

MANF-1 is expressed broadly, secreted, and localizes to lysosomes independent of the ER retention signal

Previously, we reported that *manf-1* is ubiquitously expressed in tissues such as the pharynx, hypodermis, and intestine [22, 23]. To further expand on these studies, we sought to provide novel insight into the mechanism of *manf-1* function. Moreover, we reasoned that altering the ER retention capability of MANF would be a suitable target for further investigation. For MANF to localize to ER, the protein must have a signal peptide at the N-terminus and a KDEL sequence (KEEL in worms) at the C-terminus. We generated several new transgenic strains expressing MANF-1::mCherry chimeric proteins using an endogenous promoter (Supplementary Figure 6). Two such strains contained either an obstructed or deleted retention signal with mCherry fused at the C-terminus (*MANF-1*$^{KEEL::mCherry}$ and *MANF-1*$^{\Delta KEEL::mCherry}$, respectively); one carried an unobstructed and functional ER retention signal after mCherry (*MANF-1*$^{mCherry::KEEL}$), and in the other one, a functional human version of the retention signal (*MANF-1*$^{mCherry::RTDL}$) (Supplementary Figure 6). These different strains allowed us to investigate the subcellular localization of MANF-1 and how it might confer a protective response in animals.

The examination of *MANF-1*$^{KEEL::mCherry}$ and *MANF-1*$^{\Delta KEEL::mCherry}$ animals with putatively secreted MANF protein revealed that the chimeric protein was present throughout the body, including the hypodermis, pharynx, coelomocytes, and the extracellular space (Fig. 5A–F' and Supplementary Figure 7A). A detailed examination identified fluorescent vesicles in the hypodermal cells as lysosomes based on colocalization studies. Specifically, the MANF-1::mCherry pattern overlapped with the lysosomal dye, LysoTracker Green and the lysosomal membrane marker *scav-3::GFP* [29] (Fig. 5Gi). Similar to the hypodermis, MANF-1 localization in coelomocytes was confirmed to be lysosomal by colocalization with another lysosomal membrane marker *lmp-1::GFP* [30] (Fig. 5Giv). These data provide the first evidence that MANF-1 is localized to the lysosomal membrane. The protein is secreted in the extracellular space that allows it to be taken up by other cells and coelomocytes.

An identical expression pattern was observed in two additional independently generated *MANF-1*$^{KEEL::mCherry}$ strains with lower amounts of *manf-1::mCherry* (see Methods) (Supplementary Figure 7A, B). The MANF-1::mCherry positive structures in these and the *MANF-1*$^{\Delta KEEL::mCherry}$ strain were indistinguishable (Supplementary Figure 7C, D). Similar to *MANF-1*$^{KEEL::mCherry}$, *MANF-1*$^{\Delta KEEL::mCherry}$ animals showed significant lifespan extension and ER stress resistance (Supplementary Figure 7E, F). Another CRISPR-generated transgenic strain NK2548 (*manf-1p:: mKate2:: manf-1*) carrying *mKate2* reporter downstream of the endogenous *manf-1* signal sequence [23] also exhibited lysosomal localization of the chimeric protein upon treatment with tunicamycin (Supplementary Figure 8A). Additionally, detailed examination of both the mKate2::MANF-1 and the previously existing *manf-1p::GFP* transcriptional line showed coelomocyte localization (Supplementary Figure 8A, B).

Further characterization of *manf-1* expression during aging revealed a dynamic pattern. As reported earlier for lysosomes [31], MANF-1::mCherry structures changed with age from a vesicular to tubular-like morphology (Fig. 5H & I). No significant overlap was observed with MANS::GFP (golgi body) [30], *vha-6p::GFP::C34B2.10* (ER) [32], GFP::LGG-1 (autophagosomes) [33] mitoGFP (mitochondria) [34], and Bodipy 493/503 (lipid droplets) (Supplementary Figure 9A-E). Additionally, MANF-1::mCherry was not detected in the neurons

based on the DA neuronal marker *dat-1p::YFP* and pan-neuronal marker *unc-119p::GFP* [35, 36] (Supplementary Figure 9F, G).

We also examined MANF-1::mCherry localization in *MANF-1*$^{mCherry::KEEL}$ and *MANF-1*$^{mCherry::RTDL}$ animals, both of which contain functional ER retention signal sequences (Figs. 5J–M and Supplementary Figure 10). The expression patterns of these strains were like the observations of the two secreted MANF strains, *MANF-1*$^{KEEL::mCherry}$ and *MANF-1*$^{\Delta KEEL::mCherry}$. In addition, we observed bright fluorescence in the intestine in a pattern resembling ER-like morphology, which is consistent with the role of *manf-1* in ER-UPR maintenance, and in other tissues, such as the spermatheca and muscles (Fig. 5K-M and Supplementary Figure 10A, B). Fluorescence was also observed in several neuron-like cells in the ventral cord (data not shown). Intestinal and muscle expression was faint in early-stage larvae but became more prominent from the late larval stage and during adulthood. Both spermatheca were visible in adults and coincided with the egg-laying stage of the animals. Expression in lysosome-like structures became more prominent as the animals progressed from early larval to adult stages. *MANF-1*$^{mCherry::RTDL}$ animals exhibited a slightly more diffuse pattern of MANF-1::mCherry in the lysosomes (Supplementary Figure 10C-I).

Taken together, these data demonstrate that MANF-1 is broadly expressed and secreted. Its presence in various tissues is affected by both native and human versions of the ER retention signal. Intracellular MANF-1 localizes to lysosomes within hypodermal cells, where it may interact with other proteins to regulate lysosome function and proteostasis. These findings lead us to conclude that MANF-1 confers protective benefits on animals beyond its previously described role in the ER.

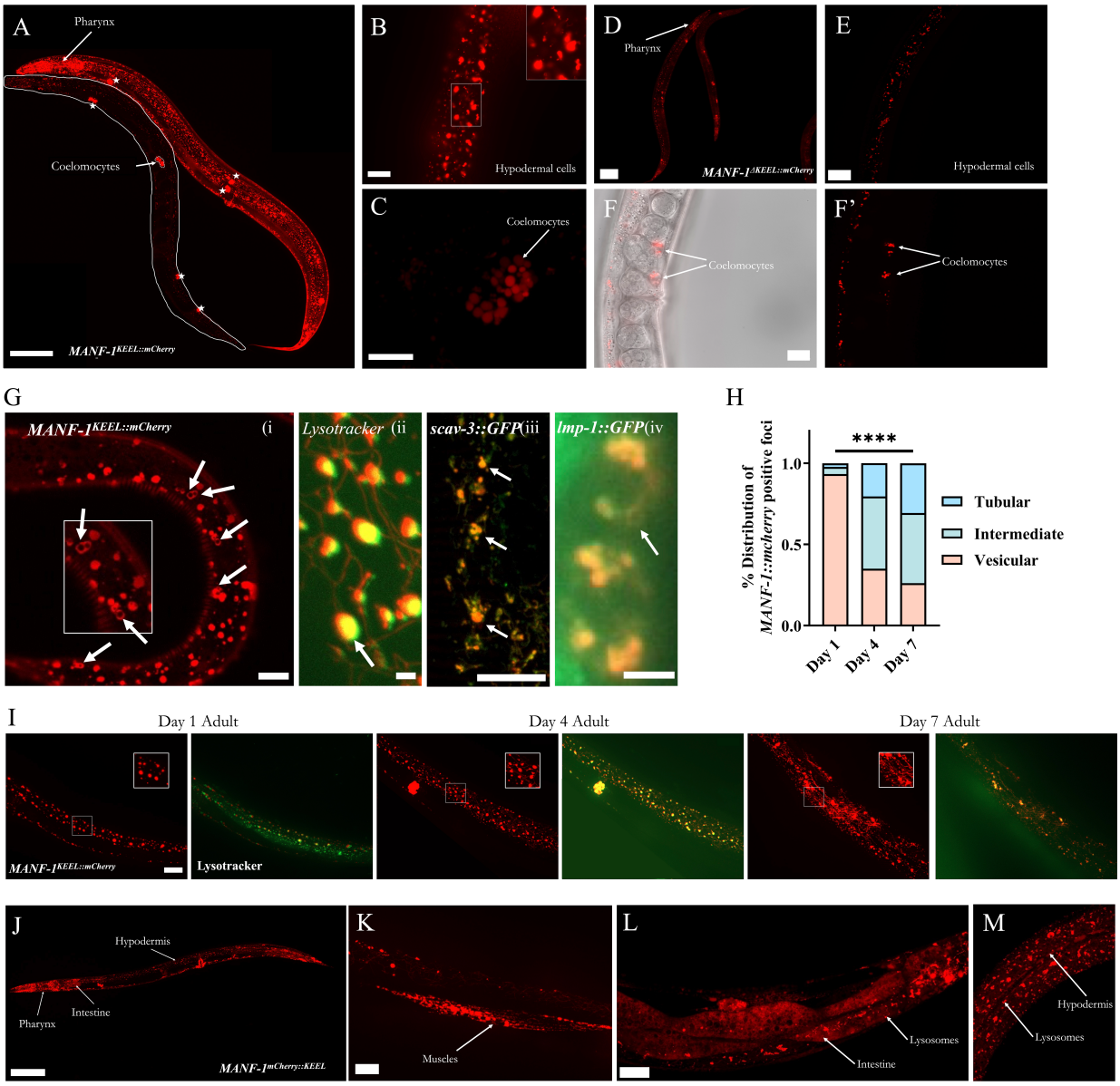

Figure 5. MANF-1 expression pattern in *MANF-1*$^{KEEL::mCherry}$ transgenic animals. **A)** Two *MANF-1*$^{KEEL::mCherry}$ day 1 adults. The hypodermal region is in focus. Fluorescence is visible throughout the body including the pharynx and coelomocytes (arrows and stars). The outlined worm has a weak fluorescence compared to the one next to it. Scale bar 100 µm. **B-C)** Enlarged areas of animals showing fluorescence in hypodermal cells in clusters of varying sizes (scale bar 20 µm) (B) and in coelomocytes (scale bar 10 µm) (C). **D-F')** *MANF-1*$^{\Delta KEEL::mCherry}$ animals at day 1 of adulthood. Fluorescence is similar to that seen in the *MANF-1*$^{KEEL::mCherry}$ line and observed in the pharynx (scale bar 100 µm) (D), hypodermal cells (scale bar 20 µm) (E), and coelomocytes (scale bar 10 µm) (F and F'). **Gi-iv)** Colocalization of MANF-1::mCherry with subcellular markers in

hypodermal cells of day 1 adults. **Gi)** A single confocal slice showing lysosomes. Arrows point to structures where MANF-1 appears to be on the lysosomal membrane. Scale bar 10 µm. **Gii)** MANF-1::mCherry colocalization with LysoTracker™ Green DND-26. **Giii)** Confocal image showing colocalization with SCAV-3::GFP. Arrows point to MANF-1 and SCAV-3 overlapping areas on lysosome membranes. Scale bar 20 µm. **Giv)** Colocalization with LMP-1::GFP in coelomocytes. The arrow points to a ring structure within coelomocytes showing an overlap of MANF-1::mCherry with LMP-1::GFP. Scale bar 5 µm. **H)** Quantification of MANF-1::mCherry fluorescing structures at different stages of adulthood. The foci were classified as vesicular, intermediate, or tubular and plotted as a stacked histogram. Worms were scored in at least three batches with 10 per batch. Data was analyzed using Chi-squared test. *p<0.05; **p<0.01; ***p<0.001; ****p<0.0001. **I)** *MANF-1*$^{KEEL::mCherry}$ animals at day 1, 4 and 7 of adulthood (scale bar 20 µm). Each animal was imaged for MANF-1::mCherry alone (red) and together with lysotracker (green). In all cases, hypodermal cells near the posterior region are shown. Insets show zoomed in view of MANF-1::mCherry foci that change from vesicular to tubular-looking structures. **J-M)** *MANF-1*$^{mCherry::KEEL}$ animals showing the chimeric protein. Fluorescence in this animal is visible in the pharynx, hypodermis, and one of the intestinal cells (J) (scale bar 100 µm). (K) Zoomed in view of MANF-1::mCherry in a muscle fiber (scale bar 20 µm). Confocal images of an animal showing fluorescence in the intestinal (L) and hypodermal (M) regions. MANF-1::mCherry appears diffused with lysosomes appearing as bright fluorescing dots.

MANF-1 affects lysosome formation and expression of lysosomal genes

The expression pattern of *manf-1* along with the phenotypic studies of mutant and transgenic animals prompted us to use a transcriptomic approach to understand the changes in gene expression associated with various cellular and molecular processes. To this end, we examined the differentially expressed (DE) genes in *manf-1(tm3603)* and MANF-1^{HAR} animals obtained from the Hartman lab. A comparison of downregulated DE genes in *MANF-1*^{HAR} and upregulated *in manf-1(tm3603)*, revealed 16 genes that were linked to terms such as ER function and ER-UPR maintenance (Fig. 6A and B and Supplementary File 2). An inverse of this analysis, that is, genes upregulated in MANF-1^{HAR} (5,943) with downregulated genes in *manf-1(tm3603)* (776) identified an overlapping set of 388 genes that were enriched in various GO, KEGG, and WormCat terms

including lysosome, lipid metabolism, metabolism, and other processes (Fig. 6C and D and Supplementary File 2). The list consisted of proteases such as *cpr-6, asp-2, asp-5, asp-8,* and *asp-12*; the V-ATPase *vha-6*, and the ABC transporter *haf-9*.

Following up on the transcriptomic results, we examined the lysosomes in *manf-1* null mutants. LysoTracker staining of *manf-1(tm3603)* animals revealed significantly fewer stained acidic organelles when compared with N2 and *MANF-1*$^{KEEL::mCherry}$ adults (Fig. 6E and F). Another lysosomal marker *nuc-1::mCherry* [31] showed that lysosomes were smaller but present in a larger number in *manf-1* mutant worms (Fig. 6G–I). There are several possibilities for differences in the LysoTracker and *nuc-1::mCherry* results. For example, *manf-1* mutants may have less efficient lysosomes regarding material uptake leading to *nuc-1::mCherry* expressing structures being smaller and with a reduced lysosomal storage capacity. Additionally, not all lysosomes may be acidic enough to stain efficiently with LysoTracker in *manf-1* mutants and with the lysosome size being smaller, would make it difficult to visualize them adequately. The lysosomal defect also included increased tubular morphology of *nuc-1::mCherry* in older adults (Supplementary Figure 11).

As lysosomes regulate lipid metabolism and *manf-1* transcriptomes contained misregulated lipid-related genes (Supplementary File 2), we investigated whether lipid content was affected by the gene. The results showed that while *manf-1* mutants had more lipids, the phenotype was opposite in *MANF-1*$^{KEEL::mCherry}$ animals (Fig. 6J-M, Supplementary Figures 12A, B). Altogether, these data support the role of *manf-1* in lysosomal maintenance and its potential involvement in the autophagy lysosomal pathway.

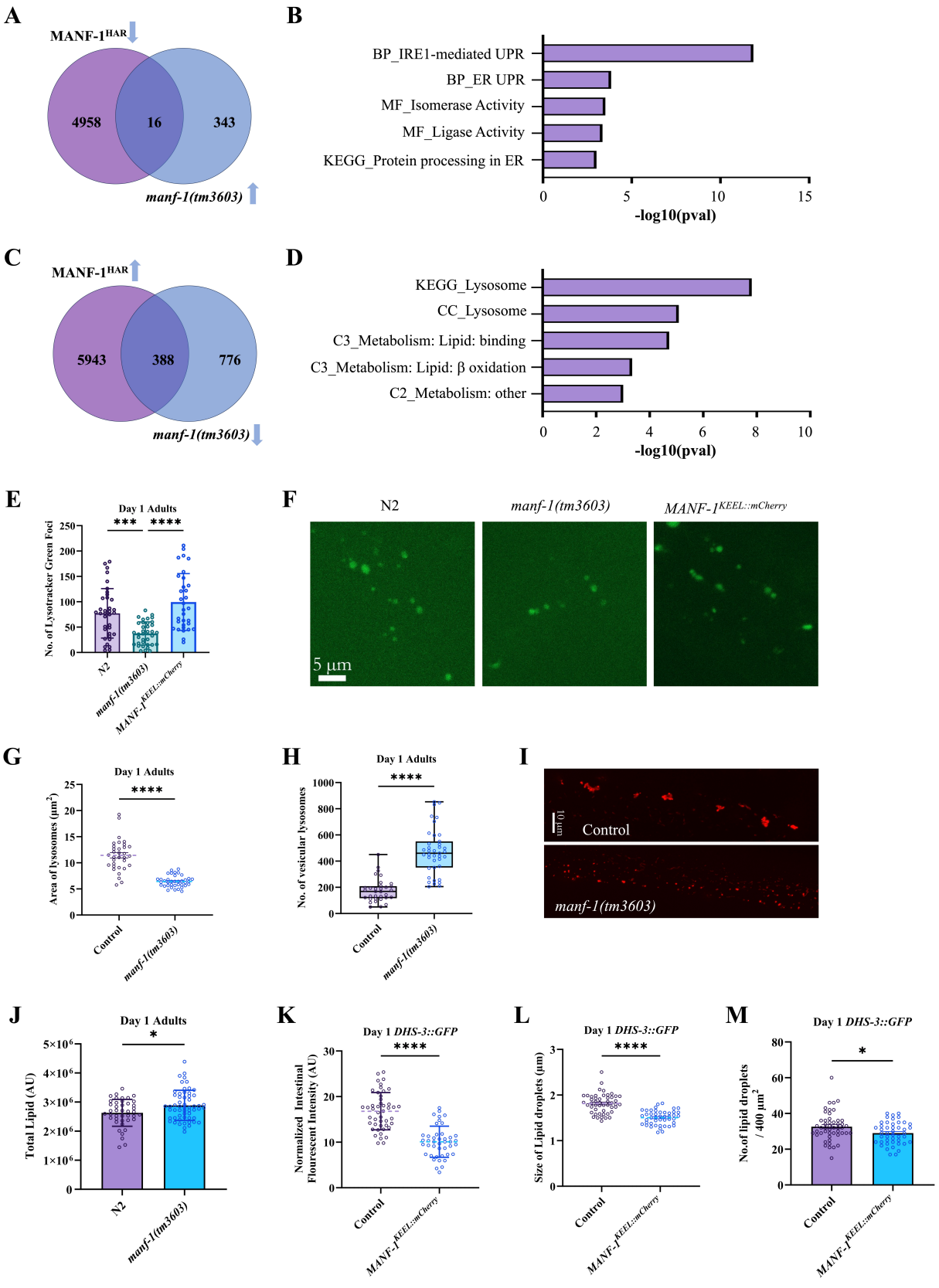
A
MANF-1HAR
4958
16
343
manf-1(tm3603)
B
BP_IRE1-mediated UPR
BP_ER UPR
MF_Isomerase Activity
MF_Ligase Activity
KEGG_Protein processing in ER
0
5
10
15
-log10(pval)
C
MANF-1HAR
5943
388
776
manf-1(tm3603)
D
KEGG_Lysosome
CC_Lysosome
C3_Metabolism: Lipid: binding
C3_Metabolism: Lipid: β oxidation
C2_Metabolism: other
0
2
4
6
8
10
-log10(pval)
E
Day 1 Adults
***
****
No. of Lysotracker Green Foci
N2
manf-1(tm3603)
MANF-1KEEL::mCherry
F
N2
manf-1(tm3603)
MANF-1KEEL::mCherry
5 µm
G
Day 1 Adults
****
Area of lysosomes (µm2)
Control
manf-1(tm3603)
H
Day 1 Adults
****
No. of vesicular lysosomes
Control
manf-1(tm3603)
I
10 µm
Control
manf-1(tm3603)
J
Day 1 Adults
*
Total Lipid (AU)
N2
manf-1(tm3603)
K
Day 1 DHS-3::GFP
****
Normalized Intestinal Flourescent Intensity (AU)
Control
MANF-1KEEL::mCherry
L
Day 1 DHS-3::GFP
****
Size of Lipid droplets (µm)
Control
MANF-1KEEL::mCherry
M
Day 1 DHS-3::GFP
*
No.of lipid droplets / 400 µm2
Control
MANF-1KEEL::mCherry

Figure 6. Transcriptome profiling of *manf-1* mutant and overexpression strains and the analysis of lysosomes. **A, B)** An overlapping set of 16 genes that were downregulated in MANF-1^{HAR} and upregulated in *manf-1(tm3603)* animals. Venn diagram (A) and selected GO, KEGG and WormCat categories generated using easyGSEA from the eVITTA toolbox (B). **C, D)** An overlapping set of 388 genes that were upregulated in MANF-1^{HAR} and downregulated in *manf-1(tm3603)* animals. Data is plotted similar to panels A and B. **E-F)** Lysotracker staining of N2, *manf-1(tm3603)* and *MANF-1$^{KEEL::mCherry}$* animals at day 1 of adulthood. Quantification of total number of lysosomes stained (E) and representative images (F). Scale bar 5 μm. **G-I)** Lysosome size and count based on the *nuc-1::mCherry* reporter in day 1 adult animals. Measurement of lysosomal area (G) and number (H) in the hypodermis. (I) Representative Images corresponding to panels G and H showing changes in lysosomal size and area. Scale bar 10 μm. **J)** Lipid quantification using Oil Red O staining. **K-M)** Lipid quantification in the intestine using DHS-3::GFP. (K) Normalized GFP fluorescent intensity, (L) Lipid droplets, and (M) number in a 400μM^2 area. For panels E, G and H, at least three batches with 10-12 worms per batch were examined. K-M, a minimum of three batches with 30-40 worms per batch were examined. Data is expressed as mean ± SD (E, J, K) and mean ± SEM (G, H, L, M). Panel H shows a box plot containing all data points along with the mean and 25th and 75th quartile boundaries. Data was analyzed using one-way ANOVA with Tukey's test (E) and Student's *t*-test (G & H, J-M). *p<0.05; **p<0.01; ***p<0.001; ****p<0.0001.

MANF-1 affects autophagic flux and requires endosomal pathway and HLH-30/TFEB for its function

Prompted by the MANF-1 expression pattern, mutant phenotype, and transcriptomic data, we analyzed the effect of the gene on autophagic process using two known factors LGG-1/LC3 and SQST-1/p62. While LGG-1 is involved in autophagosome formation, SQST-1 is an autophagy receptor that facilitates the degradation of ubiquitinated protein cargo [37, 38]. The results showed that although the *lgg-1/LC3* and *sqst-1/*p62 transcripts were unaffected in *MANF-1$^{KEEL::mCherry}$* worms (Fig. 7A), a significant reduction was noted in GFP::LGG-1 and SQST-1::GFP fluorescent puncta (Fig. 7B–E), consistent with increased autophagic clearance [39]. In agreement with this, *manf-1(tm3603)* mutants exhibited an increased number of autophagosomes (Fig. 7H and I).

We also used a tandem mCherry::GFP::LGG-1 reporter, which differentially marks autophagosomes (APs) and autolysosomes (ALs), to examine the effect of *manf-1* on autophagy. In this transgenic line, APs emit both green (GFP) and red (mCherry) fluorescence whereas ALs emit only red fluorescence as the GFP signal is quenched [40]. The results showed that *manf-1* RNAi caused a significant increase in APs compared to the control and a corresponding reduction in ALs (Fig. 7F and G). These results suggest that in the absence of *manf-1*, autophagy is blocked and fewer APs fuse to lysosomes.

Next, we investigated the involvement of endosomal pathway components in mediating MANF-1's role in autophagy and its lysosomal localization. To this end, RAB-5 and RAB-7, two Rab GTPases affecting early and late trafficking, respectively, were examined. RNAi knockdown of *rab-7* resulted in *MANF-1*$^{KEEL::mCherry}$ worms having the same amount of autophagosomes as controls, suggesting that autophagy was blocked (Fig. 7H). A similar phenotype was observed following *rab-5* RNAi (Fig. 7I), however the animals showed additional defects. Unlike control worms where MANF-1::mCherry fluorescence was present predominantly in vesicle-like structures, *rab-5* RNAi caused a striking change in mCherry localization such that the fluorescence was significantly diffused (Fig. 7J,K). We also observed that coelomocytes were much brighter in these animals (data not shown). Additionally, abnormally large MANF-1::mCherry structures were present in hypodermal and seam cells, indicative of defects in MANF-1 transport (Fig. 7L). In some cases, GFP::LGG-1 fluorescence overlapped with MANF-1::mCherry (Fig. 7M). Thus, endosomal components play an essential role in MANF-1 secretion and subcellular localization.

In addition to RNAi experiments, we studied the colocalization of MANF-1 with markers of the endosomal trafficking system. One of these, RME-8::GFP, localizes to endosomal membranes in coelomocytes and structures in hypodermal cells that may be cytoplasmic [41]. Our results showed that the cytoplasmic RME-8::GFP within the hypodermis appeared to surround MANF-1::mCherry fluorescence (Fig. 7N) While the colocalization of two proteins needs to be investigated in greater detail, these data together with Rab GTPase requirements lead us to conclude that MANF-1 utilizes the endo-lysosomal system for secretion and intracellular transport.

Finally, we analyzed HLH-30/TFEB, a transcription factor that regulates autophagy and lysosomal genes in *C. elegans* [42]. The analysis of *MANF-1*$^{KEEL::mCherry}$ animals revealed that HLH-30 was predominantly localized to nucleus (Fig. 7O and P). As a positive control, animals subjected to

starvation showed a significant increase in nuclear HLH-30/TFEB (Fig. 7O and P). Additionally, the expression of *hlh-30* was upregulated (Fig. 7A). Consistent with the essential role of *hlh-30* in mediating *manf-1* function, *hlh-30(tm1978); MANF-1*$^{KEEL::mCherry}$ animals had smaller MANF-1::mCherry puncta (Fig. 7Q and R), a slower thrashing rate (Fig. 7S), and a shorter lifespan compared to the *MANF-1*$^{KEEL::mCherry}$ alone (Fig. 7T). These results demonstrate that MANF-1 utilizes the HLH-30-mediated pathway to promote autophagy and lysosomal activity to promote proteostasis and longevity in animals.

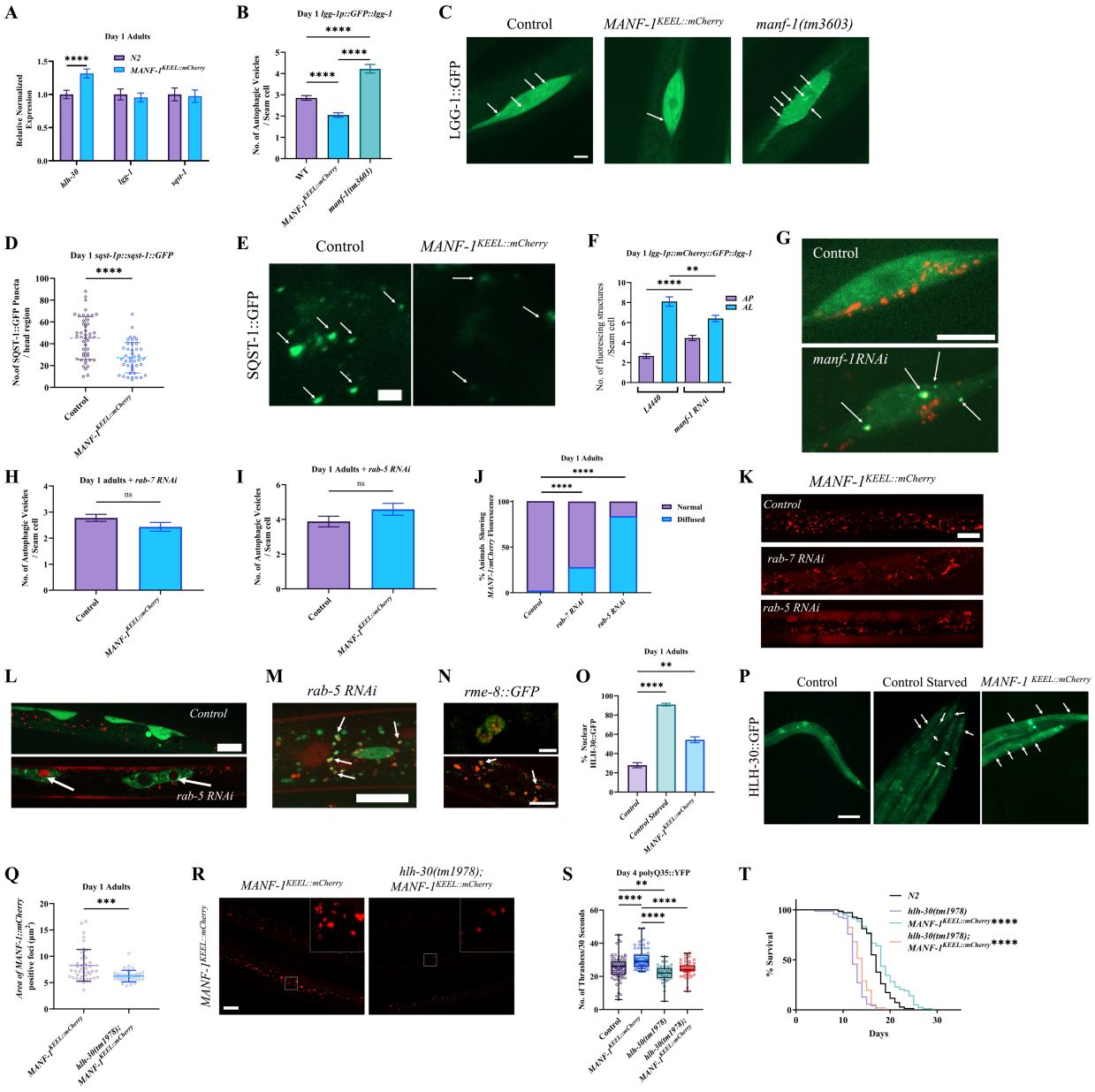

Figure 7. Analysis of autophagy, endosomal trafficking, and HLH-30 role in MANF-1 function. **A)** RT-qPCR Analysis of *hlh-30, lgg-1* and *sqst-1* transcripts. **B)** Quantification of GFP::LGG-1 puncta in seam cells. **C)** Representative images showing GFP fluorescence corresponding to panel B. Fluorescent puncta in GFP::LGG-1 seam cells are visible (arrows). Scale bar 5 µm. **D)** Quantification of SQST-1::GFP puncta in the head region. **E)** Representative images corresponding to (D) showing the posterior pharyngeal bulb region. Arrows point to puncta in a 30 µm x30 µm region, scale bar 5 µm. **F)** Quantification of *lgg-1p::mCherry::GFP:lgg-1* tandem reporter in day 1 adults following *manf-1 RNAi*. **G)** Representative images (enlarged)

corresponding to panel F. *manf-1* RNAi causes autophagy defects. Fluorescing structures represent autophagosomes (APs) carrying both mCherry and GFP and autolysosomes (ALs) with only mCherry. Arrows in the lower panel point to mCherry and GFP overlap in seam cells. Scale bar 10 µm. **H, I)** Quantification of GFP::LGG-1 puncta in seam cells following *rab-7* (H) and *rab-5* (I) *RNAi*. **J)** Quantification of MANF-1::mCherry distribution. The distribution was classified as either normal or diffused and plotted as a stacked histogram. **K)** Representative images showing fluorescing foci distribution corresponding to panel J. Scale bar 20 µm. **L)** Representative images showing defects in MANF-1::mCherry foci following *rab-5* RNAi. Arrows in the lower panel point to abnormal structures in seam cells. The left arrow shows an abnormally large MANF-1::mCherry aggregate. The right arrow points to a hollow appearance. Scale bar 20 µm. **M)** Colocalization of MANF-1::mCherry with GFP::LGG-1 puncta (arrows) following *rab-5* RNAi. Scale bar 20 µm. **N)** No colocalization was observed with the endosome marker RME-8::GFP in coelomocytes (top panel) but arrows point to cytoplasmic RME-8::GFP (bottom panel) surrounding MANF-1::mCherry in the hypodermal region. Scale bar 10 µm. **O)** Quantification of HLH-30::GFP nuclear localization in *MANF-1*$^{KEEL::mCherry}$ day 1 adults. Wild-type and starved animals were used as negative and positive controls, respectively. Graph is plotted as cumulative percentage of animals with nuclear localization. **P)** Representative fluorescent images corresponding to (O). Arrows point to areas of intestinal nuclear localization, scale bar 100 µm. **Q)** MANF-1::mCherry foci size in the hypodermis. **R)** Representative images of MANF-1::mCherry foci corresponding to Q, scale bar 20 µm. **S)** Thrashing rates of animals expressing polyQ35::YFP in a 30 sec interval. **T)** Lifespan analysis. Mean and max lifespan are in the Supplementary Table 1. A, three batches of pooled worms. B, D, O, Q, S, T, three batches with 30-40 worms per batch were examined. F-J three batches, with n= 10 to 15 worms per batch. Data are expressed as mean ± SEM (A, B, F, H, I, O) and mean ± SD (D, Q). Panel S shows a box plot containing all data points along with the mean and 25th and 75th quartile boundaries. Data was analyzed using one-way ANOVA with Dunnett's test (B & O), Student's t-test (A, D, F, H, I, Q), Chi-squared test (J), one-way ANOVA with Tukey's test (S), and log-rank (Kaplan-Meier) method (T). *p<0.05; **p<0.01; ***p<0.001; ****p<0.0001.

DISCUSSION

The neurotrophic factor MANF was originally identified for its role in promoting dopaminergic neuron survival but subsequently was also found to affect other processes [4, 14, 15, 43, 44]. Much work on MANF has focused on its ER localization and regulation of ER-UPR. Although this aspect of MANF function has been studied in considerable detail, recent data point to additional novel mechanisms. This is supported by expression studies in animal models showing the cellular presence of MANF in many tissues and extracellular regions [16, 21, 45-47].

We and others previously reported that *C. elegans* MANF-1 plays an essential role in protecting dopaminergic neurons from increased ER stress [21-23]. In this study, we present a novel understanding of MANF function in stress response maintenance, proteostasis, and longevity. We found that *manf-1* mutants exhibit chronic ER-UPR activation, and when subjected to ER stress, they exhibit enhanced neurodegeneration and a shorter lifespan. Additionally, both the transcript and protein levels of MANF-1 increased in response to ER stress, similar to findings in other systems [9, 48-51]. As ER-UPR helps cells to manage stress through multiple mechanisms, including enhanced protein folding and clearance of nonfunctional proteins [7, 52], we examined whether *manf-1* mutant animals have defects in these processes. The results showed increased protein aggregation in PD and HD models that express human α-Synuclein and polyQ, respectively. These phenotypes were exacerbated in older adults lacking *manf-1* and resulted in abnormal locomotion, suggesting an age-dependent breakdown of proteostasis.

Our work demonstrates that *manf-1* overexpression through different paradigms offers cytoprotective benefits leading to increased neuronal survival and healthy aging. We found that MANF-1 is expressed at different stages and in different cell types. Although there was no obvious overlap between MANF-1-expressing cells and DA neurons, the neurons may be protected by the uptake of the protein from the extracellular environment [21] since MANF-1::mCherry is seen at high levels in the pharynx and surrounding areas. Subcellular studies showed that MANF-1 is predominantly present in the intestine, pharynx, muscles, hypodermal cells, and coelomocytes. A similar expression pattern was observed in strains carrying endogenous *manf-1p::mKate2::manf-1* and transcriptional *manf-1p::GFP* reporters. It is worth mentioning that our *manf-1* expression results are supported by recent transcriptomic and proteomic studies [53, 54].

We found that MANF-1 expression was altered when the ER retention signal was blocked or deleted. Such sequence manipulations resulted in a weak or no localization of the protein in the intestine, muscles, and other areas, likely because it was secreted to the extracellular space. Previous studies involving cell cultures had shown that removal of the ER retention sequence caused higher levels of MANF being released in the culture media [45, 48]. The novel shift in MANF-1::mCherry expression in transgenic animals lacking ER signals, in conjunction with our results and rescue experiments, lead us to suggest that MANF-1 may be secreted from the intestinal ER and localizes to lysosomes of different cells to elicit its cytoprotective function. Furthermore, the identification of the intestine as a likely synthesis point for MANF and the hypodermis as a target tissue for exported MANF opens the door for future inquiry into the cell-non-autonomous function of MANF *in vivo*.

Our analysis of *C. elegans* MANF-1 was supported by transcriptomic data in which lysosomal genes were repressed in mutant animals and activated in those overexpressing *manf-1*. A previous study in the fruit fly *Drosophila melanogaster* also identified lysosomal genes that were downregulated in the MANF mutant [47]. In addition, the authors studied MANF localization in Schneider-2 cells, which revealed structures such as endosomes. Our work identified specific endosomal pathway components RAB-5, RAB-7, and RME-8 that are involved in MANF-1 transport in *C. elegans*. Overall, the data suggest that MANF transport via the endosomal pathway and its role in lysosome function may be conserved.

This study also provides the first evidence of MANF-1 expression in coelomocytes. Proteins in coelomocytes, which are scavenger cells, play a role in the efficient uptake of materials from the pseudocoelom and endosomal to lysosomal trafficking [55]. Following uptake by coelomocytes, molecules travel through endocytic compartments and eventually enter lysosomes for degradation [56]. Although the exact mechanism underlying the role of MANF-1 in coelomocytes is unknown, it is likely to affect lysosomal function to maintain proteostasis. In support of this, Sousa et al. recently reported the GO enrichment of lysosomal and endosomal terms in MANF-deficient macrophages [57]. The authors also showed that recombinant MANF in older adults improved phagocytosis-induced lysosomal activity [57].

Recent work has shown that lysosomes act as signaling hubs inside cells, and the dysregulation of lysosomal function and autophagy are associated with various defects and neurodegenerative

diseases [58, 59]. The autophagy-lysosomal pathway is instrumental in clearing toxic protein aggregates. We found that *MANF-1*$^{KEEL::mCherry}$ affects the gene expression and nuclear localization of HLH-30/TFEB, a transcriptional regulator of lysosomal and autophagy genes [60], which is necessary for lifespan extension conferred by Insulin/IGF-1 signaling and other longevity pathways [42]. HLH-30 is essential for the lifespan and proteostasis benefits of overexpressed MANF in MANF-1::mCherry animals. Previous studies have shown that the calcium released from lysosomes can activate calcineurin to dephosphorylate TFEB, leading to its nuclear localization [60]. Additionally, lysosomal calcium can trigger ER calcium release and signaling [58, 60]. These data, together with the observation that changes in ER calcium can promote MANF secretion [48], provide support to a model where MANF is part of a network that facilitates ER and lysosome crosstalk to regulate the TFEB-mediated activation of autophagy and proteostasis (Fig. 8). Interestingly, we observed a reduction in the size of MANF-1-positive foci in *hlh-30* mutants, raising the possibility of a feedback mechanism. In support of this, the *manf-1* promoter contains sequences that overlap with the HLH-30 CLEAR-binding motif. Thus, similar to the lysosomal gene targets of TFEB [42], it is conceivable that *manf-1* is transcriptionally regulated by *hlh-30* and forms a positive regulatory network.

The role of MANF-1 in lysosome-mediated signaling and the involvement of HLH-30/TFEB in this process led us to investigate the role of LGG-1/Atg8/LC3 and SQST-1/p62 in regulating autophagy [38, 61-64]. While an increase in LGG-1 and SQST-1 puncta may be caused by a blockage of autophagy, a reduction in both types of puncta is indicative of an increase in autophagic flux. We found that *MANF-1*$^{KEEL::mCherry}$ animals exhibited reduced GFP::LGG-1 and SQST-1::GFP puncta, suggesting that MANF-1 promotes autophagy. Similarly, *manf-1(tm3603)* animals showed an increase in the number of GFP::LGG-1 puncta. A double fluorescent reporter strain, mCherry::GFP::LGG-1, was also used which showed an increase in autophagosomes with a concomitant decrease in autolysosomes. Consistent with these data, a recent study reported that MANF overexpression in mouse kidney cells promoted autophagy and mitochondrial biogenesis [39]. The authors also observed a decrease in p62 abundance and found that p-AMPK and FOXO3 play roles in promoting mitochondrial biogenesis. However, whether *C. elegans* AAK-2/AMPK and DAF-16/FOXO are involved in MANF-1-mediated processes remains unclear.

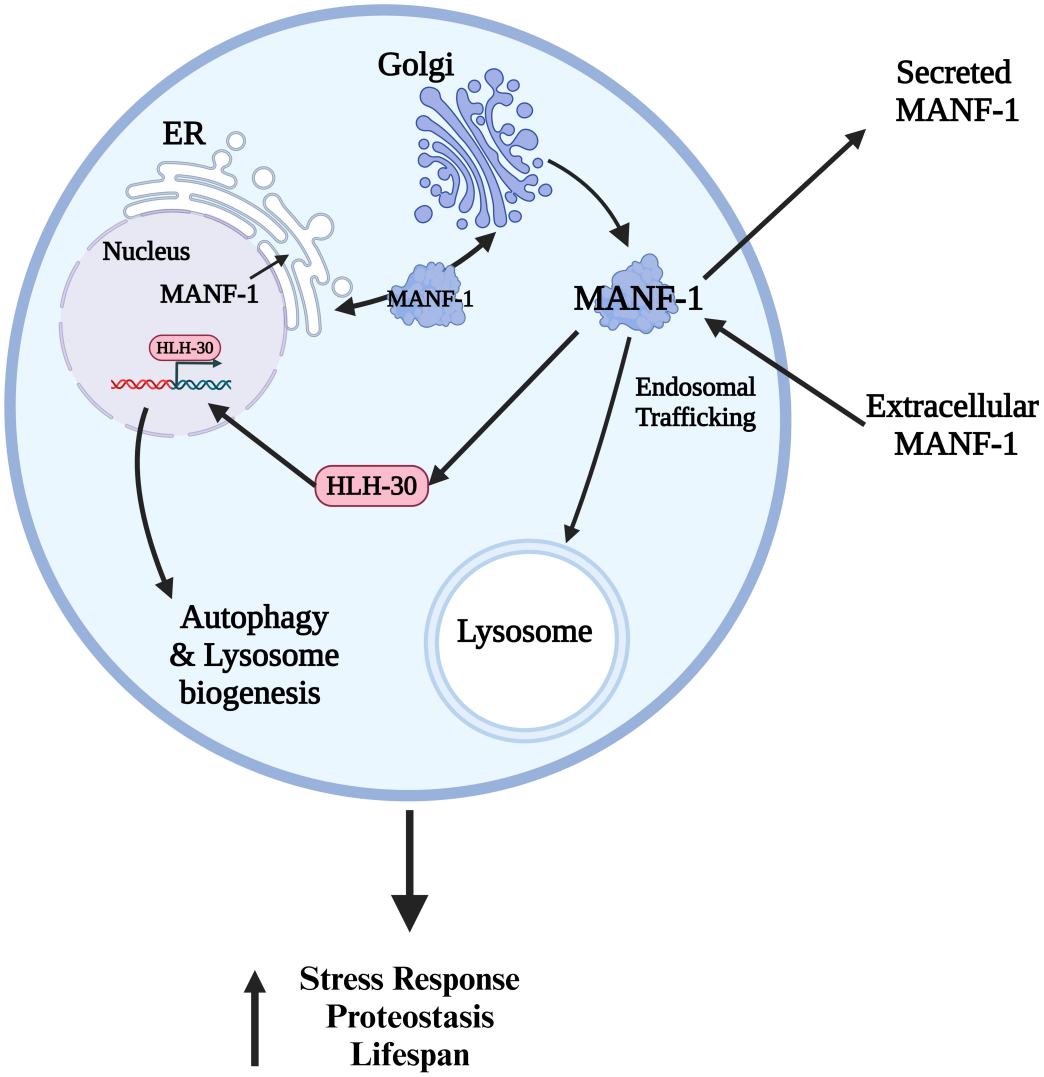

Figure 8. A proposed model for MANF action. MANF-1 can be synthesized by cells or taken up from their extracellular environment. Within the cell, MANF-1 is retained in the ER through its native ER retention sequence and released in response to stress-inducing conditions. Once released from the ER, MANF-1 localizes to lysosomes as well as secreted out. The intracellular transport and secretion are mediated by the endosomal trafficking. The cytoprotective benefits of MANF-1 depend on the HLH-30-mediated signaling. Image created with BioRender.com.

Our findings on HLH-30-mediated MANF-1 function were also supported by lipid analysis. As ER-UPR, autophagy, and lysosomes affect lipid metabolism [65-67] and *manf-1* transcriptomes identified lipid-related genes, we examined neutral lipids in *manf-1* mutants and found that levels were significantly higher. As expected, *MANF-1*$^{KEEL::mCherry}$ animals exhibited the opposite phenotype, which was accompanied by a reduction in the number and size of lipid droplets. Earlier, TFEB was shown to be necessary for the clearance of lipid droplets and regulation of lipid catabolism [60]; in relation to this, mammalian TFEB and worm HLH-30 were found to regulate lysosomal genes and fusion of lipid droplets to lysosomes in a process called lipophagy [68, 69]. These data underscore the importance of MANF-1-HLH-30 signaling in multiple lysosome-mediated processes.

The presence of MANF-1 on lysosomes and its interactions with HLH-30 to mediate proteostasis raises various questions such as how MANF-1 gets to lysosomes? And how could MANF-1 cause HLH-30 to translocate to the nucleus? Firstly, MANF-1 needs to be secreted from the ER to be cytoprotective. One likelihood is that MANF-1 is trafficked through the Golgi to enter the endo-lysosomal pathway, reaching lysosomes. Furthermore, once in this pathway, MANF-1 may affect autophagic flux through enhanced lysosome function. This model is supported by *manf-1 RNAi* blocking autophagy and reducing the number of lysosomes which impacts the health of animals overall. MANF-1 may also follow the endosomal pathway, as discussed above, to localize to lysosomes where it may interact with other membrane proteins. It would be interesting to investigate whether MANF-1 affects the calcium channel MCOLN1 to release lysosomal calcium into the cytoplasm and/or interacts with MTOR components, thereby causing HLH-30's nuclear localization [58, 60]. Further experiments are needed to study these possibilities.

Our results have broad implications for understanding the function of MANF in higher eukaryotes and manipulating its role in promoting healthy aging and treat diseases including lysosomal disorders. In this regard, it is worth noting that *manf* expression is downregulated in Niemann-Pick and Gaucher disease models [70, 71]. Future work will help to understand the precise mechanisms of MANF localization, HLH-30/TFEB interaction, and stress response signaling that collectively promote neuronal health, proteostasis maintenance, and longevity.

ACKNOWLEDGEMENTS

This work was supported by the Natural Sciences and Engineering Research Council of Canada Discovery grant to BPG and partially supported by the National Institutes of Health (R00-ES029552 to JHH). Some of the strains were obtained from the *Caenorhabditis* Genetics Center, which is funded by the NIH Office of Research Infrastructure Programs (P40 OD010440). The pGLC130 plasmid was made by Komal Prajapati. We thank WormBase for its citation database on individual genes (PMID 19910365) and the McMaster biology department confocal resource for assistance with imaging. Ram Mishra and Ravi Selvaganapathy provided feedback on some of the experiments. We thank Dr. Kacy Gordon (University of North Carolina-Chapel Hill) for her assistance with generating the MANF-1^{HAR} overexpression line.

AUTHOR CONTRIBUTIONS

S.K.B.T. carried out the experiments and generated most reagents for the study. J.H. generated the *MANF-1^{HAR}* strain and examined the lifespan of animals. RNA-Seq was carried out in J.H. laboratory. S.K.B.T., J.H. and B.P.G. analyzed the data. S.K.B.T wrote the first draft of the manuscript, S.K.B.T., J.H. and B.P.G. worked together to revise the manuscript. All authors reviewed the final version. B.P.G. supervised the study.

COMPETING INTERESTS

The authors declare no competing interests.

MATERIALS AND METHODS

Strains and culturing

Strains were cultured on standard NGM (nematode growth media) agar plates using established protocols. Plates were seeded with *E. coli* bacterial strain OP50 as a food source [18]. Worms were grown and maintained at standard culture temperature (20°C) unless stated otherwise. Age-synchronized animals were obtained by using a standard bleaching protocol and treating gravid hermaphrodites with a mixture of sodium hypochlorite and sodium hydroxide (3:2::NaOCl:NaOH) [72]. The Bristol isolate of *C. elegans* (N2) was used as a wild-type control. Strains generated as part of this study and those obtained from the *Caenorhabditis* Genetics Center (University of Minnesota, St. Paul, MN) are listed along with full genotypes in the Supplementary File 1.

Plasmid construction, site-directed mutagenesis, and transgenic strains

The plasmid pGLC72 (dat-*1p::YFP)* was described earlier [73]. Three others, pGLC130 (*hsp-16.41::manf-1*), pGLC180 (*manf-1p::MANF-1::mCherry*, carrying an obstructed or non-functional ER retention signal), and HAR002 (*manf-1p::manf-1*) were generated to study MANF-1 expression and its effect on cellular processes. For the pGLC130, a 507 bp cDNA fragment of *manf-1* was amplified by PCR using primers GL1041 and GL1042. The fragment was subcloned into pPD49.83 (a gift from Andrew Fire, Addgene plasmid # 1448; http://n2t.net/addgene:1448 ; RRID:Addgene_1448) using *BamH1* and *Nco1* restriction sites. The pGLC180 was created by PCR amplification of a 3,429 bp genomic fragment containing 2,713 bp of the *manf-1* promoter and *manf-1* gene (705 bp) using primers GL1749 and GL1750. The fragment was cloned into an *mCherry* reporter carrying vector, pHT101 (a gift from Casonya Johnson, Addgene plasmid # 61021; http://n2t.net/addgene:61021; RRID: Addgene_61021) using *Pst1* and *Age1* restriction sites. The third plasmid, HAR002, contains full-length *manf-1* genomic DNA driven by the *manf-1* promoter. The DNA fragment was subcloned into the Fire vector pPD95.75 using directional cloning upstream of the *unc-54* 3'UTR. The resulting plasmid was confirmed by sequencing.

Three additional *manf-1* plasmids were generated by site-directed mutagenesis that affect the ER retention signal sequence. This involved creating deletions and insertions in the gene using NEB Q5® Site directed mutagenesis kit (E0554). Mutagenic primers were designed using the online tool NEBaseChanger™ and the provided annealing temperature was used for the PCR. As per the kit instructions, 1 ng/µL of pGLC180 was amplified using Q5 hot start high-fidelity 2x master mix and routine PCR thermocycling conditions. The PCR product was then incubated at 24°C for an hour in the NEB KLD enzyme mix and introduced into NEB DH5α cells by transformation. The plasmid pGLC189 (*manf-1p::MANF-1ΔKEEL::mCherry*) was created by deleting the 12 bp of native ER retention sequence (KEEL) of *MANF-1* in pGLC180 using primers GL1908 and GL1909. The pGLC189 was subsequently used as a base plasmid to generate pGLC196 (*manf-1p::MANF-1::mcherry::KEEL*) and pGLC197 (*manf-1p::MANF-1::mcherry::RTDL*) that carry 12 bp native ER retention sequence (KEEL) and the corresponding human sequence (RTDL), respectively. The primer pairs GL1983 & GL1984 and GL1987 & GL1988 created a 12bp insertion of pGLC189 to give pGLC196 and pGLC197 respectively. All plasmids were sequenced before generating transgenic strains. The primers are listed in the Supplementary File 1.

The HAR002 plasmid was injected at 50 ng/µl concentration into the gonad of adult *unc-119(ed4)* animals along with the *unc-119* rescue plasmid (50 ng/µl), and 50 ng/µl EcoRI-cut salmon sperm DNA. Once extrachromosomal lines were established, plasmid was integrated by gamma irradiation as previously described [74]. The integrated line jhhIs001 was outcrossed with N2 to remove possible background mutations. All other plasmids were injected into the germline of adult N2 hermaphrodites using *dat-1p::YFP* (pGLC72; 25-50 ng/µL range) as a co-injection marker [73]. The pGLC130 (50 ng/µL) was used to generate two independent lines DY695 (*bhEx291*) and DY696 (*bhEx292*), both with genotype *hsp::manf-1; dat-1p::YFP* (See Supplementary File 1). One of these, DY695, was selected for detailed studies and RT-qPCR analysis showed roughly 15x increase in *manf-1* expression following 1 hr heat shock at 31°C. The pGLC180 (30 ng/µL) was used to generate three independent lines, DY757 (*bhEx302*), DY758 (*bhEx303*) and DY759 (*bhEx304*), with transcript levels ranging from 3x to 6x determined by RT-qPCR (data not shown). Additional transgenic animals were generated by injecting lower concentrations of pGLC180: DY798 (*bhEx305*) 10 ng/µL and DY800 (*bhEx306*) 1 ng/µL. The genotype of these animals was *manf-1p::manf-1::mCherry; dat-1p::YFP*. The pGLC189 was injected at 20 ng/µL to create DY807 (*bhEx307*), DY808 (*bhEx308*) and DY809 (*bhEx309*) strains with the genotype: *manf-*

1p::MANF-1ΔKEEL::mCherry; dat-1p::YFP. The pGLC196 (25 ng/µL) plasmid was used to create DY819 (*bhEx310*) and DY820 (*bhEx311*) with the genotype: *manf-1p::MANF-1::mCherry:: KEEL; dat-1p::YFP.* And, finally, pGLC197 (25 ng/µL) was used to create DY821 (*bhEx312*) and DY823 (*bhEx314*) with the genotype: *manf-1p::MANF-1::mCherry::RTDL; dat-1p::YFP*.

RNA extraction and RT-qPCR

Total RNA was extracted from adults using Trizol (Sigma-Aldrich Canada, Catalog Number T9424). In brief, animals were bleach synchronized at desired adult stages. Worms were collected and washed with M9. Trizol was added followed by flash freezing in liquid nitrogen and then thawed in a 37°C water bath. The flash freeze and thaw steps were repeated three to four times. Chloroform was added, mixed, and then centrifuged to collect the aqueous phase. Isopropanol was used to precipitate RNA followed by two washes in 75% ethanol. Samples were allowed to air dry to remove any remaining ethanol. Extracted samples were treated with TURBO DNA-free™ Kit (Catalog Number: AM1907, ThermoFisher Scientific) according to manufacturer's instructions. The resulting samples were used to obtain cDNA using the SensiFAST cDNA Synthesis Kit (Catalog Number BIO-65053, Meridian Bioscience) following kit instructions.

RT-qPCR was performed (in triplicate) using the Bio-Rad cycler CFX 96 and the SensiFAST SYBR Green Kit (Catalog Number BIO-98005, BIOLINE, USA). Gene expression levels were normalized to housekeeping genes *pmp-3*, *iscu-1* (*Y45F10D.4*) and *cdc-42.* The primers are listed in the Supplementary File 1. qPCR involving extrachromosomal lines was done by enriching cultures for worms carrying the reporter of interest. For this, 30 fluorescent day 1 adults were picked and allowed to lay eggs overnight. The progenies were grown to gravid adults and bleached to obtain F2 worms. For the DY759 strain, 200 of these F2 fluorescent day 1 adult worms were individually picked and used for RNA extraction.

RNAi

RNAi-mediated gene silencing was carried out using an established protocol in our lab [75]. Knockdowns were performed from the egg stage unless stated otherwise. Worms were fed with an empty plasmid (L4440)-containing *E. coli* HT115 culture or a gene-specific plasmid culture from the Ahringer library. The *manf-1* RNAi plasmid (pGLC176) was constructed by inserting a 720 bp genomic fragment into the L4440 vector using the restriction enzymes *Kpn*I and *Sal*I. The fragment was amplified by PCR using a primer pair GL1739 and GL1740.

Lifespan assay

All lifespan assays were carried out at 20°C on NGM agar plates seeded with *E. coli* OP50 bacteria as previously described [76]. Assays were repeated in triplicates. Each batch contained roughly 30 animals per strain. Worms were scored every day for survival starting from day 1 adulthood. They were transferred to fresh plates on alternate days until no progeny were seen. Cases involving escaping, bursting at vulva, and progeny hatching internally were censored. Survival curves were estimated using the Kaplan-Meir method (see the statistical analysis section). Mean and max lifespan of strains used in this study are presented in the Supplementary Table 1.

Heat shock treatments

Animals were grown at room temperature until young adulthood, they were then transferred to a 35°C incubator for 2 hrs and assayed for their survival 24 hrs later. The *hsp::manf-1* transgenic worms (DY695) were age synchronized and grown till adulthood. One-day old adults were heat shocked at 31°C for 1 hr. For lifespan assays, animals were treated every other day starting from day 1 until day 7 of adulthood.

Normarski fluorescence microscopy and fluorescence quantification

Worms were mounted onto glass slides containing 2% agar pad. Animals were anaesthetized using 30 mM stock solution of NaN_3, if necessary. Fluorescence was visualized using a Zeiss Observer Z1 microscope equipped with an Apotome 2 and X-Cite R 120LED fluorescence illuminator (unless stated otherwise). Images were also taken using a Leica SP5 confocal and are specified in figure legends. Zeiss Zen2 blue (https://www.zeiss.com/microscopy/en/products/software/zeiss-zen.html) and NIH ImageJ (*http://rsbweb.nih.gov/ij/*) software were used to capture and analyze images. Subcellular structures were examined in age synchronized animals at 63x magnification. For co-localization studies involving MANF-1::mCherry and other subcellular markers, individual stacks were examined.

Analysis of LysoTracker, MANF-1::mCherry, and NUC-1::mCherry fluorescence involved taking 10 to 15 Z stacks per image. For LysoTracker Green stained structures, the total number of fluorescent foci within the field of view were counted in the hypodermis of individual animals. In the case of MANF-1::mCherry and NUC-1::mCherry fluorescing structures, the maximum projection was used to count the number of foci and to quantify their morphology in the hypodermis. The number of foci within the field of view per animal were quantified using Cell Profiler [77]. The lysosomal morphology in hypodermal cells was grouped into three categories: tubular, intermediate, and vesicular. A Chi-square test was used to analyze the data.

DA neurons were scored using a protocol that we described earlier [75] and refined in this study. Specifically, the *dat-1p::GFP* reporter was used to visualize neuronal cell bodies and dendrites [73]. To quantify neurodegeneration, we used the following four morphological categories: 1: normal-looking neuronal cell bodies and dendrites (wild-type pattern), 2: dendritic damage (blebs, puncta, faint appearance, missing, etc.) but cell bodies appearing normal, 3: one or more cell bodies missing, faint, or abnormally shaped but dendrites appearing normal, and 4: type 2 and 3 combined. At least 3 independent batches of animals were scored with a minimum of 20 animals per batch.

For *hsp-4p::GFP* strain, whole animal images were taken to quantify GFP fluorescence following different treatments. Using the polygon tool of ImageJ (*http://rsbweb.nih.gov/ij/*), the total fluorescence of a selected area was obtained. Samples were analyzed in triplicate, a minimum of n = 15 per batch.

To quantify α-Synuclein::YFP fluorescence in *unc-54p::α-Synuclein::YFP* animals, we used a protocol published earlier by our lab [22]. A fixed area of the head region with the pharynx in focus was selected and images were captured at an optimal exposure rate. Total fluorescent intensity was obtained using the polygon and measure tool of ImageJ. Samples were analyzed in triplicate, with a minimum of n = 15 per batch.

To quantify fluorescence intensity and no. of aggregates in *unc-54p::polyQ35::YFP* and *unc-54p::polyQ40::YFP* animals was analyzed similar to α-Synuclein::YFP as described above. Images were taken of the entire worm with the pharynx in focus. Total whole worm fluorescent intensity was obtained using ImageJ's polygon and measure tool. To count aggregates, the "Find Maxima" function in ImageJ was used. Samples were examined in triplicate, with a minimum of n = 10 per batch.

The *hlh-30p::hlh-30::GFP* strain was used to count fluorescing intestinal nuclei in one-day old adults using published protocols [42]. As a positive control, animals were starved by transferring them to an unseeded NGM agar plate for 24 hrs that induced nuclear location of HLH-30. Samples were analyzed in triplicate, a minimum of n = 20 per batch.

The GFP puncta in *lgg-1p::GFP::lgg-1* animals were quantified using published protocols [37, 61, 63]. Z stack images at 63x magnification were taken at optimal slice intervals determined by the Zeiss Zen2 blue software. The maximum projection was acquired and the GFP puncta were counted in 4 seam cells per animal. Samples were analyzed in triplicate, a minimum of n = 10 per batch. A similar method was used to quantify mCherry and GFP foci in *lgg-1p::mCherry::GFP::lgg-1* animals.

The SQST-1::GFP puncta in *sqst-1p::sqst-1::GFP* animals were examined using a protocol based on published studies [38, 61]. Z stack images were taken at optimal slice intervals determined by the Zeiss Zen2 blue software. A maximum projection of the Z stacks was obtained and GFP positive puncta were counted in the posterior pharynx of the head region using ImageJ "Find Maxima" function. Samples were analyzed in triplicate, a minimum of n = 10 per batch.

The *dhs-3p::dhs-3::GFP* strain [78] was used to quantify lipid droplets in age synchronized one-day-old adults. Z-stack images were captured at 63x magnification. The images ranged from 8 to 12 stacks per image at optimal slice intervals determined by the Zeiss Zen2 blue software. As per

the published protocol [79], a 400 μM^2 region of interest was selected in the tail region of worms. All visible lipid droplets were counted, and their diameter was measured using the line tool in software. Samples were analyzed in triplicate, n = 14 animals per batch.

LysoTracker™ Green staining

LysoTracker™ Green DND-26 dye (Catalog Number: L7526, ThermoFisher Scientific) was used to stain the lysosomes in age synchronized worms as described earlier [31]. A stock solution of 250 μM was made. Worms were washed with M9 and placed in a 1.5 mL microcentrifuge tube containing 80 μL of dye in M9 buffer (working concentration 60 μM). The tube was wrapped in an aluminum foil. Animals were placed in a rotator for 1 hr and then transferred to an aluminum foil wrapped NGM plate seeded with OP50 bacteria. The plates were placed in the 20°C incubator for 2 hrs and animals were imaged.

Oil Red O staining

Neutral lipids in one-day-old synchronized adults were visualized by Oil Red O dye (Thermo Fisher Scientific, USA) staining using a published protocol [80]. Images were acquired using a Nikon 80i Eclipse Nomarski fluorescence microscope fitted with a Micropublisher 3.3 RTV color camera and Q-imaging software. ImageJ was used to quantify the images [80]. Samples were analyzed in triplicate, n = 15 to 20 animals per batch.

Bodipy 493/503 staining

Bodipy 493/503 (Catalog Number: D3922, Invitrogen) was used to stain lipid droplets in age synchronized worms as described earlier [81]. Worms were washed in M9 buffer prior to a 15 min incubation in 4% paraformaldehyde fixative. They were then flash frozen in liquid nitrogen and thawed in a 37°C water bath. The freeze-thaw cycle was repeated three times. In the end, worms were washed three times with M9. A stock solution of 1mg/mL BODIPY 493/503 in DMSO was diluted to a working concentration of 1 μg/mL. The animals were incubated in the BODIPY solution for 1 hr at room temperature, washed three times with M9, and imaged.

Thrashing Assay

The thrashing rate of polyQ35::YFP animals was quantified using a published protocol [82]. Age synchronized day 4 adults were placed in 10 µL of M9 buffer and the number of thrashes in 30 seconds were counted. Samples were analyzed in triplicate, a minimum of n = 15 per batch.

Chemical treatments

Age synchronized day 1 adults were used for chemical treatments unless stated otherwise. Animals were exposed to desired concentrations of drugs as described earlier [75]. For *manf-1* and *hsp-4* expression assays, animals were exposed to tunicamycin on culture plates. The duration and concentration are mentioned in figure legends. Acute treatments of tunicamycin (50 ng/µL) and paraquat (200 mM) were carried out in liquid by exposing animals for 4 hrs as described earlier [76].

Lifespan and *hsp-4p::GFP* reporter assays were performed using published protocols [25]. For lifespan, day 1 adults were transferred to plates containing 25 ng/µL concentration of the drug. Viability was scored daily. Samples were analyzed in duplicate, each batch containing a minimum of 30 animals. The *hsp-4p::GFP* animals were placed in a 1.5 mL microcentrifuge tube containing 25 ng/µL of tunicamycin in M9 buffer and incubated on a rotator for 4 hrs. Samples were analyzed in triplicate, each batch containing a minimum of 20 animals.

RNA Sequencing Analysis

RNA-seq data was processed using the TrimGalore toolkit (http://www.bioinformatics.babraham.ac.uk/projects/trim_galore/) which employs Cutadapt [83] to trim low quality bases and Illumina sequencing adapters from the 3' end of the reads. Only reads that were 20nt or longer after trimming were kept for further analysis. Reads were mapped to the WBcel235r95 version of the worm genome and transcriptome using the STAR RNA-seq alignment tool [84]. Reads were kept for subsequent analysis if they mapped to a single genomic location. Gene counts were compiled using the HTSeq tool [85]. Only genes that had at least 10 reads in any given library were used in subsequent analysis. Normalization and differential

expression were carried out using the DESeq2 Bioconductor package [86, 87] with the R statistical programming environment. The false discovery rate was calculated to control for multiple hypothesis testing. Gene set enrichment analysis [88] was performed to identify gene ontology terms associated with altered gene expression for each of the comparisons performed. We used eVITTA to perform a gene enrichment analysis on the genes that were common between *manf-1 (tm3603)* and MANF-1^{HAR} [89]. Specifically, the easyGSEA tool generated the enrichment terms in Figures 6C and D (Supplementary File 2).

Statistical analyses

GraphPad Prism 9.5.1 was used to plot all the graphs and perform statistical analyses. The Student's *t*-test or analysis of variance (ANOVA) with a multiple comparisons test were performed depending on the number of conditions and comparisons to be made. Data from repeat experiments were pooled and analyzed together. Graphs were plotted with either standard deviation (SD) or standard error of mean (SEM) as appropriate (see figures). RT-qPCR results were analyzed using CFX Manager 3.1 software (Bio-Rad, Canada; https://www.bio-rad.com/en-ca/sku/1845000-cfx-manager-software?ID=1845000), which performed an ANOVA or *t*-test. SigmaPlot 14 was used to calculate the mean lifespan using the log-rank (Kaplan-Meier) method.

REFERENCES

1. Taylor, R.C. and A. Dillin, *Aging as an event of proteostasis collapse.* Cold Spring Harb Perspect Biol, 2011. **3**(5).

2. Hetz, C. and S. Saxena, *ER stress and the unfolded protein response in neurodegeneration.* Nat Rev Neurol, 2017. **13**(8): p. 477-491.

3. Remondelli, P. and M. Renna, *The Endoplasmic Reticulum Unfolded Protein Response in Neurodegenerative Disorders and Its Potential Therapeutic Significance.* Front Mol Neurosci, 2017. **10**: p. 187.

4. Nasrolahi, A., et al., *Neurotrophic factors hold promise for the future of Parkinson's disease treatment: is there a light at the end of the tunnel?* Rev Neurosci, 2018. **29**(5): p. 475-489.

5. Pakarinen, E. and P. Lindholm, *CDNF and MANF in the brain dopamine system and their potential as treatment for Parkinson's disease.* Front Psychiatry, 2023. **14**: p. 1188697.

6. Lindahl, M., M. Saarma, and P. Lindholm, *Unconventional neurotrophic factors CDNF and MANF: Structure, physiological functions and therapeutic potential.* Neurobiol Dis, 2017. **97**(Pt B): p. 90-102.

7. Walter, P. and D. Ron, *The unfolded protein response: from stress pathway to homeostatic regulation.* Science, 2011. **334**(6059): p. 1081-6.

8. Mercado, G., P. Valdes, and C. Hetz, *An ERcentric view of Parkinson's disease.* Trends Mol Med, 2013. **19**(3): p. 165-75.

9. Eesmaa, A., et al., *The cytoprotective protein MANF promotes neuronal survival independently from its role as a GRP78 cofactor.* J Biol Chem, 2021. **296**: p. 100295.

10. Kovaleva, V., et al., *MANF regulates neuronal survival and UPR through its ER-located receptor IRE1alpha.* Cell Rep, 2023. **42**(2): p. 112066.

11. Taylor, R.C. and C. Hetz, *Mastering organismal aging through the endoplasmic reticulum proteostasis network.* Aging Cell, 2020. **19**(11): p. e13265.

12. Lohelaid, H., et al., *UPR Responsive Genes Manf and Xbp1 in Stroke.* Front Cell Neurosci, 2022. **16**: p. 900725.

13. Jäntti, M. and B.K. Harvey, *Trophic activities of endoplasmic reticulum proteins CDNF and MANF.* Cell Tissue Res, 2020. **382**(1): p. 83-100.

14. Neves, J., et al., *Immune modulation by MANF promotes tissue repair and regenerative success in the retina.* Science, 2016. **353**(6294): p. aaf3646.

15. Sousa-Victor, P., et al., *MANF regulates metabolic and immune homeostasis in ageing and protects against liver damage.* Nat Metab, 2019. **1**(2): p. 276-290.

16. Danilova, T., et al., *Mesencephalic Astrocyte-Derived Neurotrophic Factor (MANF) Is Highly Expressed in Mouse Tissues With Metabolic Function.* Front Endocrinol (Lausanne), 2019. **10**: p. 765.

17. Peled, M., et al., *Mesencephalic astrocyte-derived neurotrophic factor is secreted from interferon-gamma-activated tumor cells through ER calcium depletion.* PLoS One, 2021. **16**(4): p. e0250178.

18. Brenner, S., *The genetics of Caenorhabditis elegans.* Genetics, 1974. **77**: p. 71-94.

19. Corsi, A.K., B. Wightman, and M. Chalfie, *A Transparent window into biology: A primer on Caenorhabditis elegans.* WormBook, 2015: p. 1-31.

20. Liang, J.J.H., I.A. McKinnon, and C.H. Rankin, *The contribution of C. elegans neurogenetics to understanding neurodegenerative diseases.* J Neurogenet, 2020. **34**(3-4): p. 527-548.

21. Bai, M., et al., *Conserved roles of C. elegans and human MANFs in sulfatide binding and cytoprotection.* Nat Commun, 2018. **9**(1): p. 897.

22. Richman, C., et al., *C. elegans MANF Homolog Is Necessary for the Protection of Dopaminergic Neurons and ER Unfolded Protein Response.* Front Neurosci, 2018. **12**: p. 544.

23. Hartman, J.H., et al., *MANF deletion abrogates early larval Caenorhabditis elegans stress response to tunicamycin and Pseudomonas aeruginosa.* Eur J Cell Biol, 2019. **98**(5-8): p. 151043.

24. Zhang, Z., et al., *MANF protects dopamine neurons and locomotion defects from a human alpha-synuclein induced Parkinson's disease model in C. elegans by regulating ER stress and autophagy pathways.* Exp Neurol, 2018. **308**: p. 59-71.

25. Taylor, R.C. and A. Dillin, *XBP-1 is a cell-nonautonomous regulator of stress resistance and longevity.* Cell, 2013. **153**(7): p. 1435-47.

26. Morley, J.F., et al., *The threshold for polyglutamine-expansion protein aggregation and cellular toxicity is dynamic and influenced by aging in Caenorhabditis elegans.* Proc Natl Acad Sci U S A, 2002. **99**(16): p. 10417-22.

27. Abu-Hijleh, F.A., et al., *Novel mechanism of action for the mood stabilizer lithium.* Bipolar Disord, 2021. **23**(1): p. 76-83.

28. Nawar, K. and R.K. Mishra, *MANF, ER stress and the pathophysiology of Parkinson's disease*, in *Neuroscience*. 2019, McMaster University. p. 78.

29. Li, Y., et al., *The lysosomal membrane protein SCAV-3 maintains lysosome integrity and adult longevity.* J Cell Biol, 2016. **215**(2): p. 167-185.

30. Treusch, S., et al., *Caenorhabditis elegans functional orthologue of human protein h-mucolipin-1 is required for lysosome biogenesis.* Proc Natl Acad Sci U S A, 2004. **101**(13): p. 4483-8.

31. Sun, Y., et al., *Lysosome activity is modulated by multiple longevity pathways and is important for lifespan extension in C. elegans.* Elife, 2020. **9**.

32. Xu, N., et al., *The FATP1-DGAT2 complex facilitates lipid droplet expansion at the ER-lipid droplet interface.* J Cell Biol, 2012. **198**(5): p. 895-911.

33. Lapierre, L.R., et al., *Autophagy and lipid metabolism coordinately modulate life span in germline-less C. elegans.* Curr Biol, 2011. **21**(18): p. 1507-14.

34. Labrousse, A.M., et al., *C. elegans dynamin-related protein DRP-1 controls severing of the mitochondrial outer membrane.* Mol Cell, 1999. **4**(5): p. 815-26.

35. Nass, R., et al., *Neurotoxin-induced degeneration of dopamine neurons in Caenorhabditis elegans.* Proc Natl Acad Sci U S A, 2002. **99**(5): p. 3264-9.

36. Maduro, M. and D. Pilgrim, *Identification and cloning of unc-119, a gene expressed in the Caenorhabditis elegans nervous system.* Genetics, 1995. **141**(3): p. 977-88.

37. Kumsta, C., et al., *The autophagy receptor p62/SQST-1 promotes proteostasis and longevity in C. elegans by inducing autophagy.* Nat Commun, 2019. **10**(1): p. 5648.

38. Ploumi, C., A. Sotiriou, and N. Tavernarakis, *Monitoring autophagic flux in Caenorhabditis elegans using a p62/SQST-1 reporter.* Methods Cell Biol, 2021. **165**: p. 73-87.

39. Kim, Y., et al., *MANF stimulates autophagy and restores mitochondrial homeostasis to treat autosomal dominant tubulointerstitial kidney disease in mice.* Nat Commun, 2023. **14**(1): p. 6493.

40. Chang, J.T., et al., *Spatiotemporal regulation of autophagy during Caenorhabditis elegans aging.* Elife, 2017. **6**.

41. Zhang, Y., B. Grant, and D. Hirsh, *RME-8, a conserved J-domain protein, is required for endocytosis in Caenorhabditis elegans.* Mol Biol Cell, 2001. **12**(7): p. 2011-21.

42. Lapierre, L.R., et al., *The TFEB orthologue HLH-30 regulates autophagy and modulates longevity in Caenorhabditis elegans.* Nat Commun, 2013. **4**: p. 2267.

43. Petrova, P., et al., *MANF: a new mesencephalic, astrocyte-derived neurotrophic factor with selectivity for dopaminergic neurons.* J Mol Neurosci, 2003. **20**(2): p. 173-88.

44. Voutilainen, M.H., et al., *Mesencephalic astrocyte-derived neurotrophic factor is neurorestorative in rat model of Parkinson's disease.* J Neurosci, 2009. **29**(30): p. 9651-9.

45. Henderson, M.J., et al., *Mesencephalic astrocyte-derived neurotrophic factor (MANF) secretion and cell surface binding are modulated by KDEL receptors.* J Biol Chem, 2013. **288**(6): p. 4209-25.

46. Lindholm, P., et al., *MANF is widely expressed in mammalian tissues and differently regulated after ischemic and epileptic insults in rodent brain.* Mol Cell Neurosci, 2008. **39**(3): p. 356-71.

47. Palgi, M., et al., *Gene expression analysis of Drosophilaa Manf mutants reveals perturbations in membrane traffic and major metabolic changes.* BMC Genomics, 2012. **13**: p. 134.

48. Glembotski, C.C., et al., *Mesencephalic astrocyte-derived neurotrophic factor protects the heart from ischemic damage and is selectively secreted upon sarco/endoplasmic reticulum calcium depletion.* J Biol Chem, 2012. **287**(31): p. 25893-904.

49. Lindstrom, R., et al., *Exploring the Conserved Role of MANF in the Unfolded Protein Response in Drosophila melanogaster.* PLoS One, 2016. **11**(3): p. e0151550.

50. Tadimalla, A., et al., *Mesencephalic astrocyte-derived neurotrophic factor is an ischemia-inducible secreted endoplasmic reticulum stress response protein in the heart.* Circ Res, 2008. **103**(11): p. 1249-58.

51. Xu, S., et al., *Mesencephalic astrocyte-derived neurotrophic factor (MANF) protects against Abeta toxicity via attenuating Abeta-induced endoplasmic reticulum stress.* J Neuroinflammation, 2019. **16**(1): p. 35.

52. Hetz, C., E. Chevet, and H.P. Harding, *Targeting the unfolded protein response in disease.* Nat Rev Drug Discov, 2013. **12**(9): p. 703-19.

53. Tan, C.-H., et al., *Single tissue proteomics in Caenorhabditis elegans reveals proteins resident in intestinal lysosome-related organelles.* bioRxiv, 2023.

54. Schorr, A.L., et al., *An updated C. elegans nuclear body muscle transcriptome for studies in muscle formation and function.* Skelet Muscle, 2023. **13**(1): p. 4.

55. Fares, H. and I. Greenwald, *Genetic analysis of endocytosis in Caenorhabditis elegans: coelomocyte uptake defective mutants.* Genetics, 2001. **159**(1): p. 133-45.

56. Gee, K., et al., *Regulators of Lysosome Function and Dynamics in Caenorhabditis elegans.* G3 (Bethesda), 2017. **7**(3): p. 991-1000.

57. Sousa, N.S., et al., *Aging disrupts MANF-mediated immune modulation during skeletal muscle regeneration.* Nat Aging, 2023. **3**(5): p. 585-599.

58. Bonam, S.R., F. Wang, and S. Muller, *Lysosomes as a therapeutic target.* Nat Rev Drug Discov, 2019. **18**(12): p. 923-948.

59. Lawrence, R.E. and R. Zoncu, *The lysosome as a cellular centre for signalling, metabolism and quality control.* Nat Cell Biol, 2019. **21**(2): p. 133-142.

60. Napolitano, G. and A. Ballabio, *TFEB at a glance.* J Cell Sci, 2016. **129**(13): p. 2475-81.

61. Henis-Korenblit, S. and A. Melendez, *Methods to Determine the Role of Autophagy Proteins in C. elegans Aging.* Methods Mol Biol, 2019. **1880**: p. 561-586.

62. Palmisano, N.J. and A. Melendez, *Detection of Autophagy in Caenorhabditis elegans.* Cold Spring Harb Protoc, 2016. **2016**(2): p. pdb top070466.

63. Palmisano, N.J. and A. Melendez, *Detection of Autophagy in Caenorhabditis elegans Using GFP::LGG-1 as an Autophagy Marker.* Cold Spring Harb Protoc, 2016. **2016**(1): p. pdb prot086496.

64. Ploumi, C., E. Kyriakakis, and N. Tavernarakis, *Coupling of autophagy and the mitochondrial intrinsic apoptosis pathway modulates proteostasis and ageing in Caenorhabditis elegans.* Cell Death Dis, 2023. **14**(2): p. 110.

65. Moncan, M., et al., *Regulation of lipid metabolism by the unfolded protein response.* J Cell Mol Med, 2021. **25**(3): p. 1359-1370.

66. Singh, R., et al., *Autophagy regulates lipid metabolism.* Nature, 2009. **458**(7242): p. 1131-5.

67. Xu, J. and S. Taubert, *Beyond Proteostasis: Lipid Metabolism as a New Player in ER Homeostasis.* Metabolites, 2021. **11**(1).

68. O'Rourke, E.J. and G. Ruvkun, *MXL-3 and HLH-30 transcriptionally link lipolysis and autophagy to nutrient availability.* Nat Cell Biol, 2013. **15**(6): p. 668-76.

69. Settembre, C., et al., *TFEB controls cellular lipid metabolism through a starvation-induced autoregulatory loop.* Nat Cell Biol, 2013. **15**(6): p. 647-58.

70. Cougnoux, A., et al., *Single Cell Transcriptome Analysis of Niemann-Pick Disease, Type C1 Cerebella.* Int J Mol Sci, 2020. **21**(15).

71. Dasgupta, N., et al., *Gaucher disease: transcriptome analyses using microarray or mRNA sequencing in a Gba1 mutant mouse model treated with velaglucerase alfa or imiglucerase.* PLoS One, 2013. **8**(10): p. e74912.

72. Wood, W.B., *The Nematode Caenorhabditis elegans*. 1988, New York: Cold Spring Harbor Laboratory.

73. Salam, S., et al., *A microfluidic phenotype analysis system reveals function of sensory and dopaminergic neuron signaling in C. elegans electrotactic swimming behavior.* Worm, 2013. **2**(2): p. e24558.

74. Sherwood, D.R., et al., *FOS-1 promotes basement-membrane removal during anchor-cell invasion in C. elegans.* Cell, 2005. **121**(6): p. 951-62.

75. Taylor, S.K.B., et al., *C. elegans electrotaxis behavior is modulated by heat shock response and unfolded protein response signaling pathways.* Sci Rep, 2021. **11**(1): p. 3115.

76. Mallick, A., et al., *Cabin1 domain-containing gene picd-1 interacts with pry-1/Axin to regulate multiple processes in Caenorhabditis elegans.* Sci Rep, 2022. **12**(1): p. 12029.

77. Stirling, D.R., et al., *CellProfiler 4: improvements in speed, utility and usability.* BMC Bioinformatics, 2021. **22**(1): p. 433.

78. Zhang, P., et al., *Proteomic study and marker protein identification of Caenorhabditis elegans lipid droplets.* Mol Cell Proteomics, 2012. **11**(8): p. 317-28.

79. Clark, J.F., et al., *Caenorhabditis elegans DBL-1/BMP Regulates Lipid Accumulation via Interaction with Insulin Signaling.* G3 (Bethesda), 2018. **8**(1): p. 343-351.

80. Ranawade, A., A. Mallick, and B.P. Gupta, *PRY-1/Axin signaling regulates lipid metabolism in Caenorhabditis elegans.* PLoS One, 2018. **13**(11): p. e0206540.

81. Klapper, M., et al., *Fluorescence-based fixative and vital staining of lipid droplets in Caenorhabditis elegans reveal fat stores using microscopy and flow cytometry approaches.* J Lipid Res, 2011. **52**(6): p. 1281-1293.

82. Grushko, D., et al., *Temporal requirements of SKN-1/NRF as a regulator of lifespan and proteostasis in Caenorhabditis elegans.* PLoS One, 2021. **16**(7): p. e0243522.

83. Martin, M., *Cutadapt Removes Adapter Sequences From High-Throughput Sequencing Reads.* EMBnet.journal, 2011. **17**(1).

84. Dobin, A., et al., *STAR: ultrafast universal RNA-seq aligner.* Bioinformatics, 2013. **29**(1): p. 15-21.

85. Anders, S., P.T. Pyl, and W. Huber, *HTSeq--a Python framework to work with high-throughput sequencing data.* Bioinformatics, 2015. **31**(2): p. 166-9.

86. Love, M.I., W. Huber, and S. Anders, *Moderated estimation of fold change and dispersion for RNA-seq data with DESeq2.* Genome Biol, 2014. **15**(12): p. 550.

87. Huber, W., et al., *Orchestrating high-throughput genomic analysis with Bioconductor.* Nat Methods, 2015. **12**(2): p. 115-21.

88. Mootha, V.K., et al., *PGC-1alpha-responsive genes involved in oxidative phosphorylation are coordinately downregulated in human diabetes.* Nat Genet, 2003. **34**(3): p. 267-73.

89. Cheng, X., et al., *eVITTA: a web-based visualization and inference toolbox for transcriptome analysis.* Nucleic Acids Res, 2021. **49**(W1): p. W207-W215

PNAS

Supporting Information for

More than a Neurotrophic factor: MANF regulates autophagy and lysosome function to promote proteostasis in *C. elegans*

Shane K. B. Taylor, Jessica H. Hartman, Bhagwati P. Gupta

Corresponding Author: Bhagwati P. Gupta

Email: guptab@mcmaster.ca

This PDF file includes:

Supplementary Text

Figs. S1 to S12

Tables S1

Other supporting materials for this manuscript include the following:

Dataset S1 & S2

Please contact Dr. Bhagwati Gupta (guptab@mcmaster.ca) for these files.

List of supplementary tables and figures

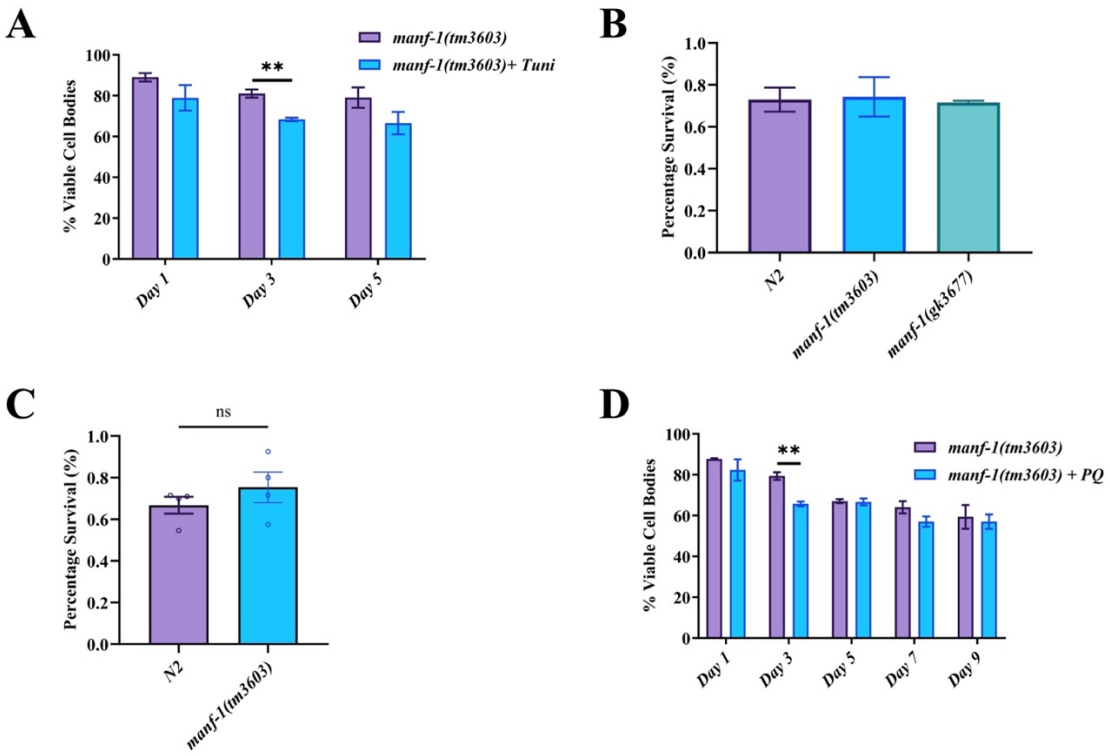

Figure S1. Effect of chemicals and heat on *manf-1* mutants. **A)** *manf-1* mutants were exposed to 5 µg/mL tunicamycin. The treatment reduced the percentage of viable DA neuron cell bodies by day 3. The neuronal damage plateaued by day 5. **B)** Survival of *manf-1* mutants following heat treatment at 35°C for 2hrs. Survival was examined after 24 hrs of recovery. *manf-1* mutants behave similarly to N2 worms. **C)** *manf-1* mutants were exposed to 200 mM paraquat for a 4 hrs period. **D)** *manf-1* mutants were exposed to 250 µM of paraquat. The treatment reduced the percentage of viable DA neuron cell bodies by day 3**.** For each assay, at least 3 batches of animals were examined with 10 - 30 per batch. Values are expressed as mean ± SEM. Data was analyzed using two-way ANOVA with Sidak's test (A and D), one-way ANOVA with Tukey's test (B), and Student's *t*-test (C). *p<0.05; **p<0.01; ***p<0.001; ****p<0.0001.

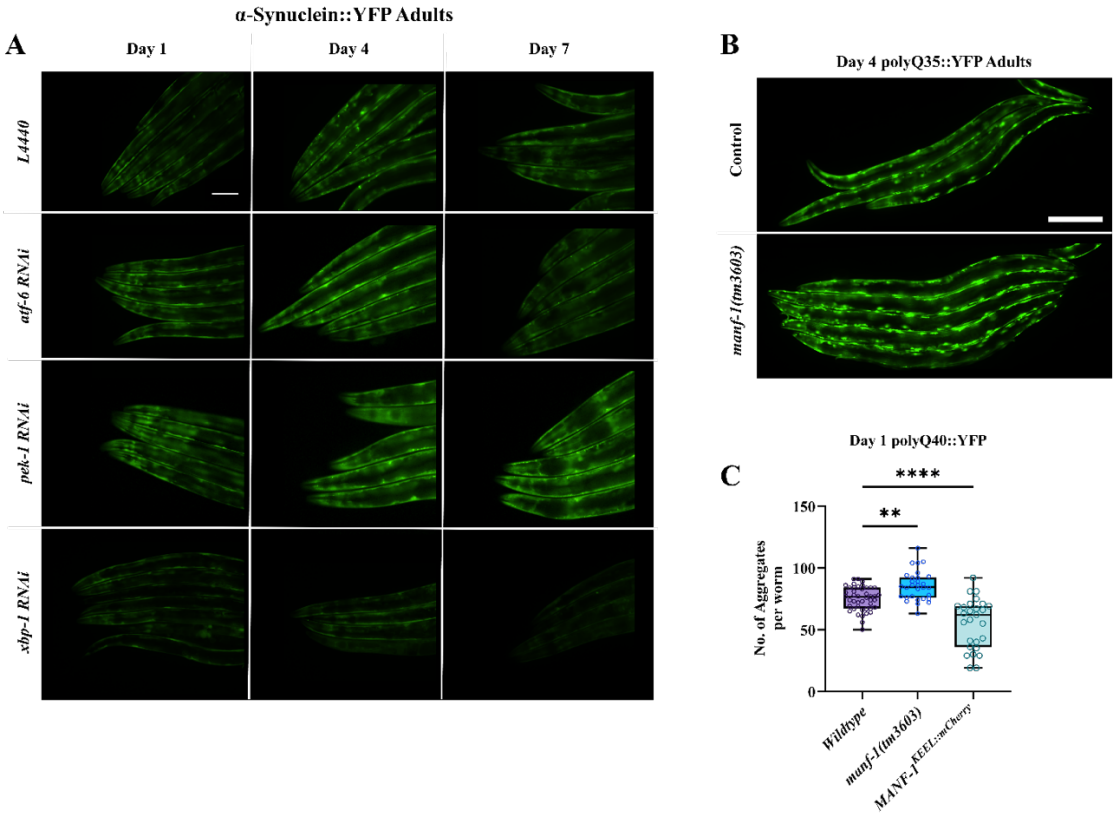

Figure S2. *manf-1(tm3603)* animals show increased aggregation of α-Synuclein::YFP and polyQ::YFP. **A)** Representative images of α-Synuclein::YFP fluorescence in *manf-1(tm3603)* animals measured on day 1, 4 and 7, following RNAi knockdown of *atf-6, pek-1* and *xbp-1***.** L4440 refers to an empty vector control RNAi. Images correspond to panels D-F in Figure 2. Scale bar 100 µm. **B)** Representative images of polyQ35::YFP aggregation in *manf-1(tm3603)* and wild-type animals (control) on day 4 of adulthood. The images correspond to panels G-I in Figure 2. Scale bar 100 µm. **C)** Total number of polyQ40::YFP aggregates was significantly increased in *manf-1(tm3063)* but decreased in MANF-1$^{KEEL::mCherry}$ day 1 adults when compared to wild-type controls. n = 15-20 worms per batch (2 batches). Box plots showing all data points along with mean and 25th and 75th quartiles. Data was analyzed using one-way ANOVA with Dunnett's test or Student's *t*-test. *p<0.05; **p<0.01; ***p<0.001; ****p<0.0001.

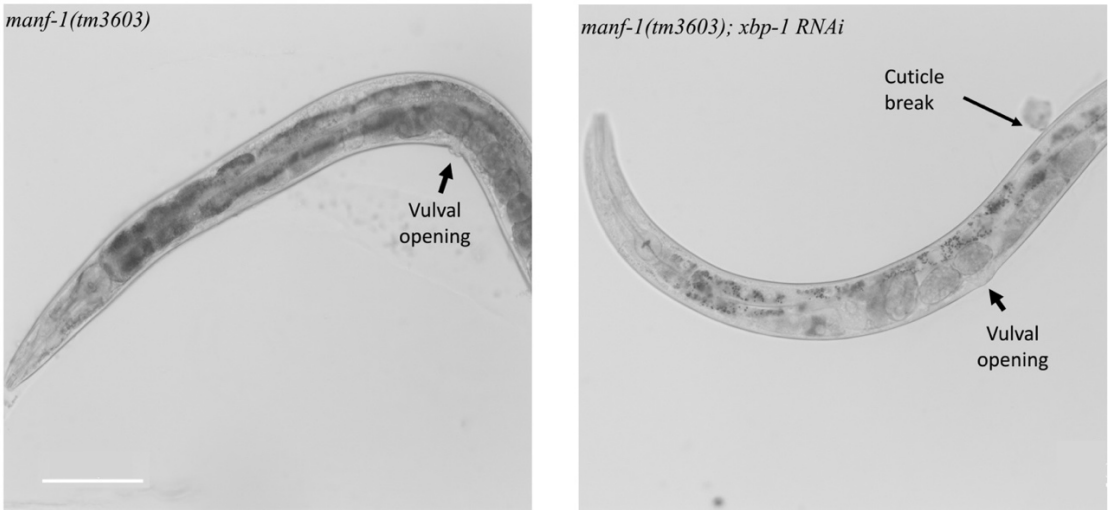

Figure S3. Effect of *xbp-1* RNAi knockdown on *manf-1* mutants. The *xbp-1* RNAi caused *manf-1(tm3603)* animals to become unhealthy. Representative images of day 1 adult animals are shown. The *manf-1(tm3603); xbp-1(RNAi)* animal is skinnier and more transparent compared to the *manf-1(tm3603)* control. In addition, the cuticle was weaker. The arrow points to an area where the cuticle was ruptured while mounting on the glass slide, causing internal contents to leak out. Head is towards the left in both panels. Scale bar is 100 µm.

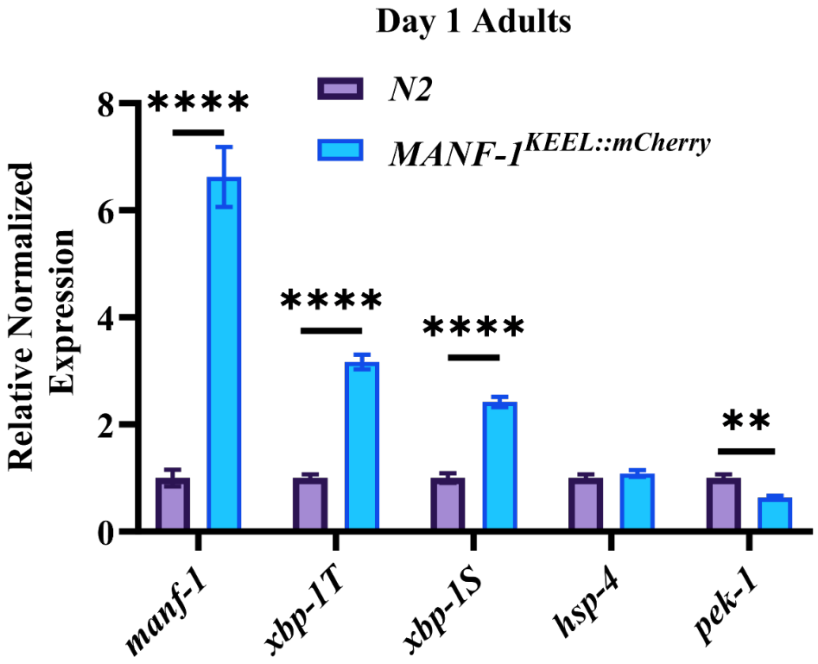

Figure S4. Transcript analysis of ER-UPR genes in *MANF-1* KEEL::mCherry animals. Expression levels were determined by RT-qPCR. **A)** *MANF-1* KEEL::mCherry had increased spliced *xbp-1 (xbp-1S)* and total *xbp-1 (xbp-1T),* but *hsp-4* gene expression was comparable to N2 and *pek-1* was reduced. The animals show ~6.5 fold increase in *manf-1* transcripts. Results are expressed as mean ± SEM. Data was analyzed using student's *t*-test. *p<0.05; **p<0.01; ***p<0.001; ****p<0.0001.

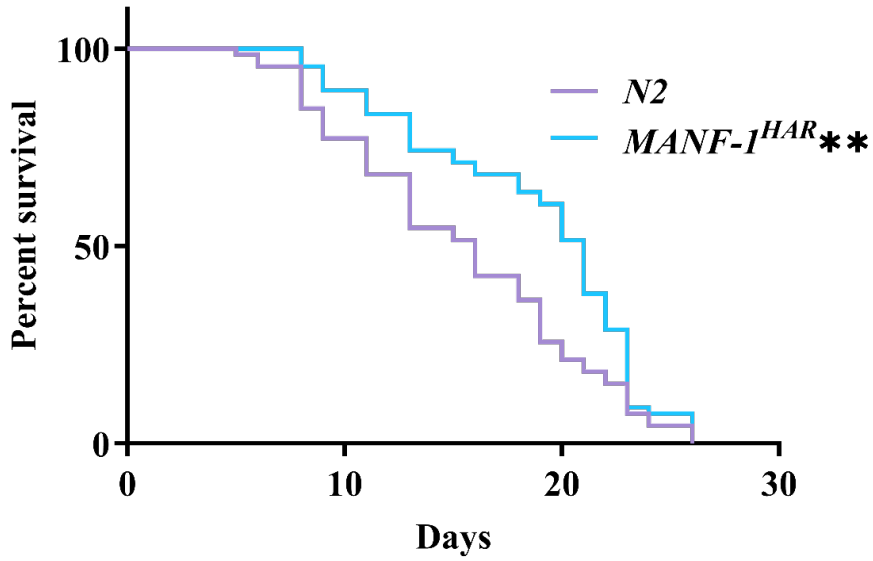

Figure S5. Lifespan analysis of MANF-1^{HAR} worms. The strain carries full-length *manf-1* gene under the control of the native promoter, which results in *manf-1* overexpression. The mean lifespan of MANF-1^{HAR} animals is 18.5 ± 0.9 days compared with 15.9 ± 0.5 days for controls. Approximately 30 worms were scored per batch and data from two independent batches was pooled. Statistical analysis was performed using the log-rank (Kaplan-Meier) method. *p<0.05; **p<0.01; ***p<0.001; ****p<0.0001.

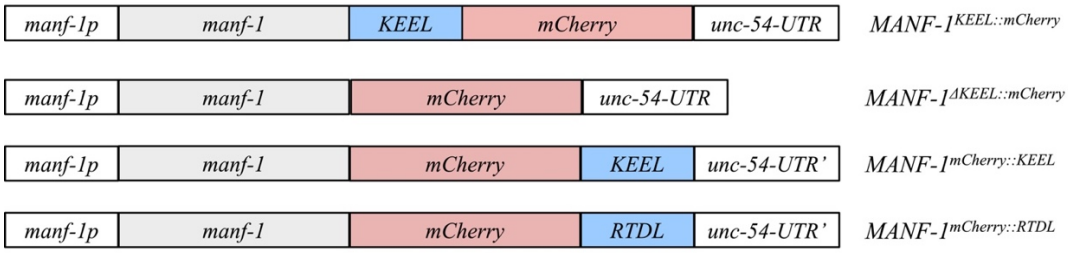

Figure S6. A schematic of different forms of *manf-1* gene fused to the *mCherry* reporter. In all cases, the *unc-54* 3' UTR is located at the 3' end and *manf-1* expression is driven by the endogenous promoter. The constructs differ in the presence and location of the ER retention signal sequence (KEEL: native sequence, RTDL: human sequence). The plasmids were injected into the N2 background to generate transgenic worms overexpressing chimeric MANF-1::mCherry. The strain names are listed on the right side of each construct and the full genotypes of animals are in the Supplementary File 1.

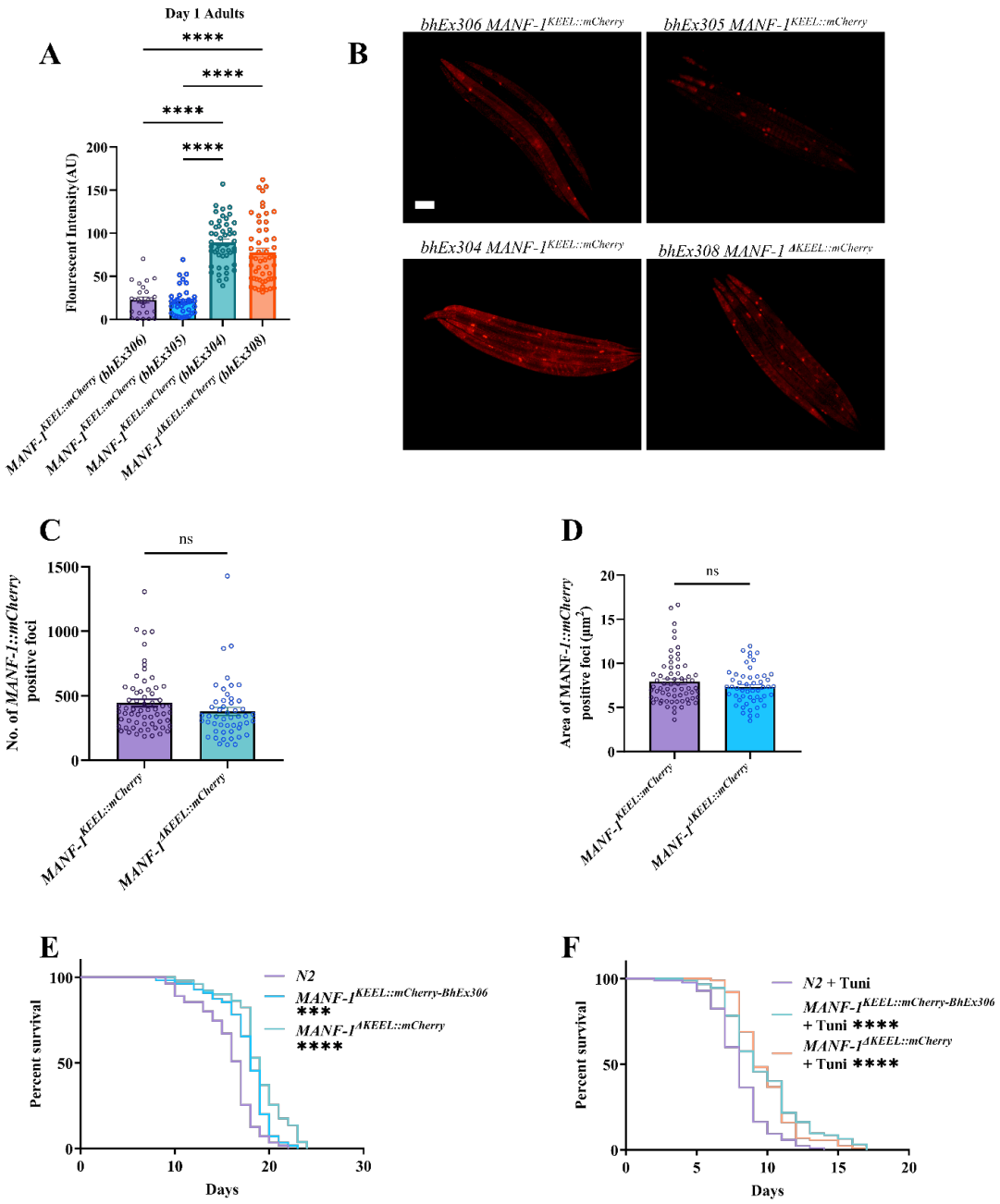

Figure S7. MANF-1::mCherry expression in various transgenic strains and lifespan phenotype of animals. **A)** Fluorescence intensity in *bhEx306* (pGLC180), *bhEx305* (pGLC180), *bhEx304* (pGLC180), and *bhEx308*(*ΔKEEL*) transgenic worms at day 1 of adulthood. **B)** Representative images of animals corresponding to panel A. Scale bar 100 µm. **C, D)** MANF-1::mCherry foci number (C) and area (D) in day 1 adults of *MANF-1*$^{KEEL::mCherry}$ *bhEx304* and *MANF-*

1$^{\Delta KEEL::mCherry}$ bhEx308 lines. **E)** Lifespan analysis of *MANF-1$^{KEEL::mCherry}$ bhEx306 and MANF-1$^{\Delta KEEL::mCherry}$ bhEx308* at 20°C. Mean lifespans were as follows: N2 = 15.8 ± 0.408 days, *MANF-1$^{KEEL::mCherry}$ bhEx306* 17.673 ± 0.376 days, and *MANF-1$^{\Delta KEEL::mCherry}$ bhEx308* 18.843 ± 0.414 days. **F)** Lifespan analysis of *MANF-1$^{KEEL::mCherry}$ bhEx306 and* MANF-1$^{\Delta KEEL::mCherry}$ *bhEx308* following chronic tunicamycin exposure (25 ng/µL). Mean lifespan were as follows: N2 = 8.024 ± 0.212 days, *MANF-1$^{KEEL::mCherry}$ bhEx306* 9.783 ± 0.299 days, *MANF-1$^{\Delta KEEL::mCherry}$* bhEx308 9.828 ± 0.227 days. A, C-F: n = 10 to 30 worms per batch (2 to 3 batches), Data in A, C, D is expressed as mean ± SEM. Comparisons were done using one-way ANOVA with Tukey's test (A), Student's t-test (C & D) and log-rank (Kaplan-Meier) method (E & F). *p<0.05; **p<0.01; ***p<0.001; ****p<0.0001.

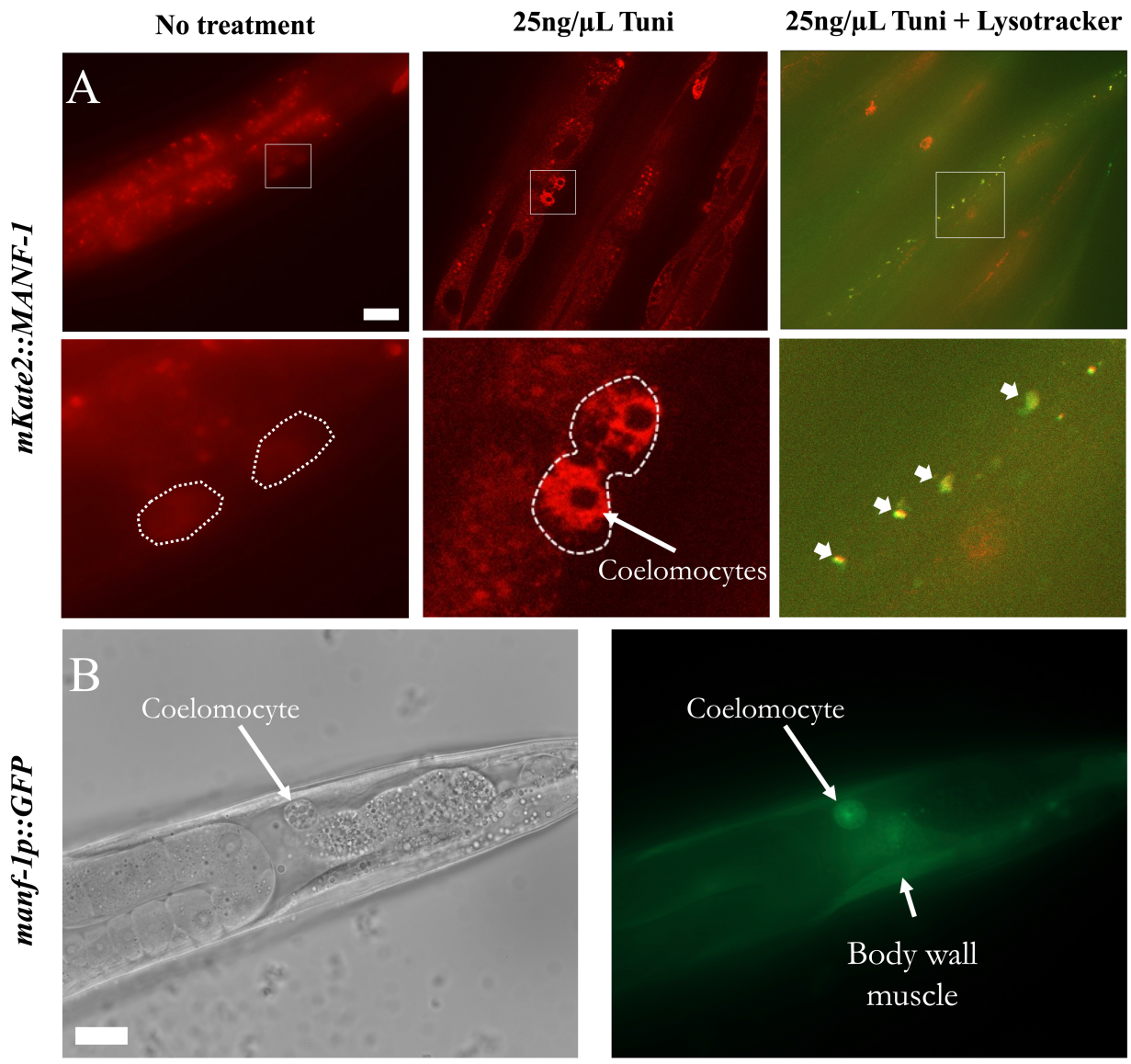

Figure S8. Reporter gene expression in *manf-1p:: mKate2::manf-1* and *manf-1p::GFP* transgenic animals at day 1 of adulthood. **A**) The second row shows enlarged views of white boxed regions in the upper panel. The fluorescence is faint and diffused. Regions containing coelomocytes are marked. Treatment with 25ng/µL tunicamycin increased MANF-1 levels, thereby revealing an overlap with lysosomes (arrowheads). Scale bar 20 µm. **B)** Nomarski and GFP fluorescence images of a transcriptional *manf-1p::GFP* one-day old adult. The animal has GFP fluorescence in a coelomocyte and body wall muscle in the posterior region (arrows). Scale bar 20µm. Head is towards the left in all cases.

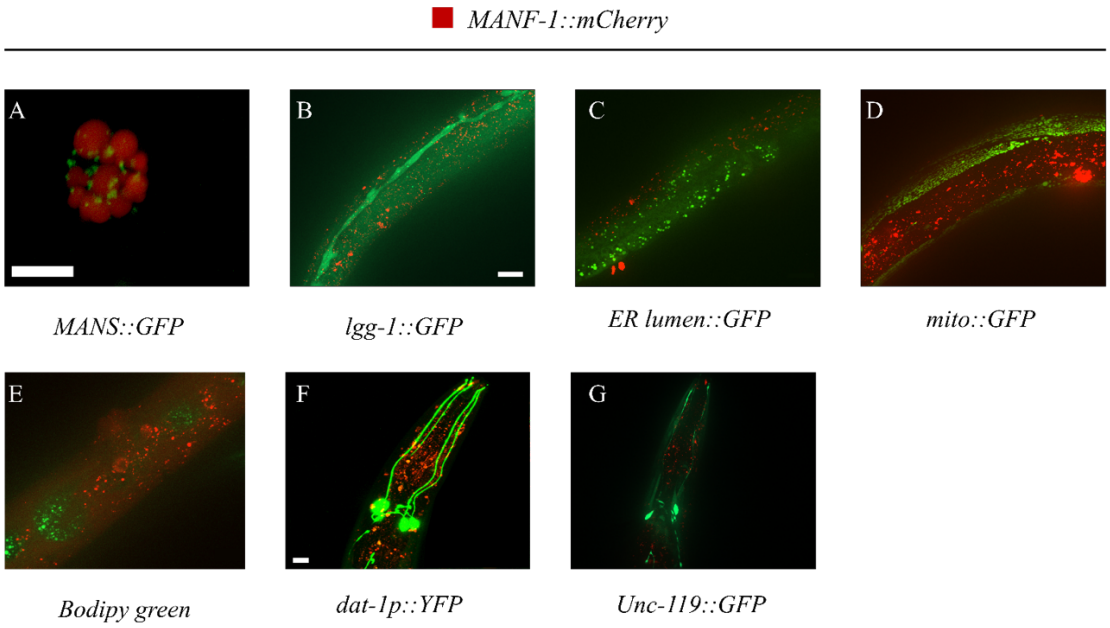

Figure S9. MANF-1::mCherry fluorescence analysis in *MANF-1*$^{KEEL::mCherry}$ animals. Representative images are shown. **A-G)** No colocalization was observed with a Golgi body marker MANS::GFP (coelomocyte) (A). autophagosome marker *lgg-1p::GFP::lgg-1* (B), intestinal ER lumen marker *vha-6p::GFP::C34B2.10(SP12)* (C), mitochondria marker *myo-3p::GFP*(mit) (D), lipid droplet marker *Bodipy green 493/503* (E), dopaminergic neuronal marker *dat-1p::YFP* ((F), and the pan-neuronal marker *unc-119p::GFP* (G). Scale bars in A-D and F are 20 µm. A & E were imaged with a Leica confocal microscope, scale bar 10 µm.

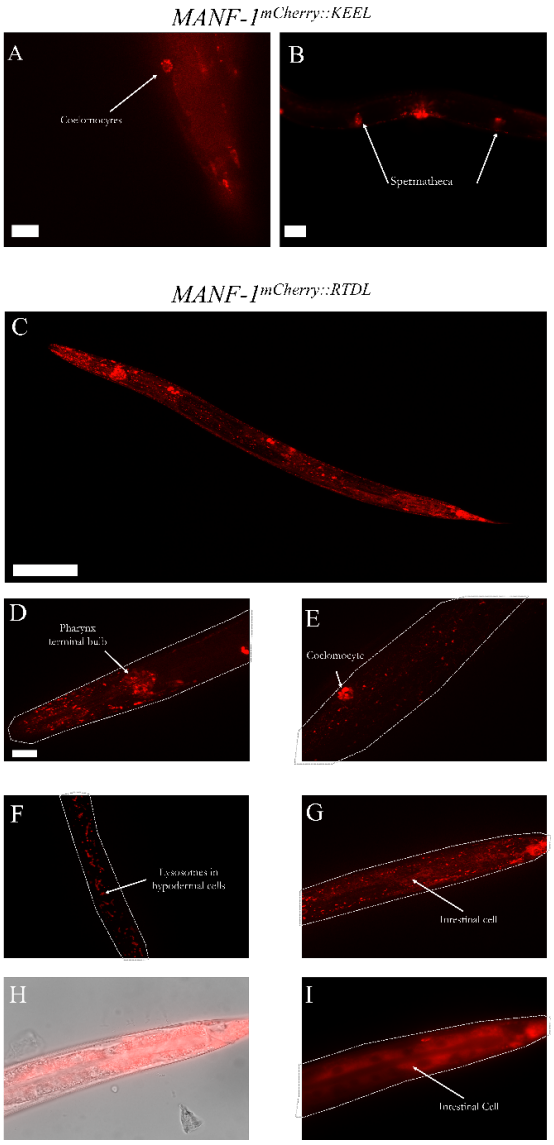

Figure S10. MANF-1::mCherry expression analysis in animals carrying the native ER retention sequence, KEEL and the human version RTDL. Panels show *MANF-1*$^{mCherry::KEEL}$ (**A, B**) and *MANF-1*$^{mCherry::RTDL}$ (**C-I**) transgenic worms. **A, B)** Expression in coelomocytes (A, scale bar 20 µm) and spermatheca (B, scale bar 50 µm). **C**) Expression pattern, which is similar to that observed in the *MANF-1*$^{mCherry::KEEL}$ line with fluorescence visible throughout the body, scale bar 100 µm. Close up images of tissues showing fluorescence in the pharynx **(D)**, coelomocytes **(E)**, hypodermal lysosomes **(F)** and the intestine **(G-I)**. The panel F shows an overlap of brightfield and fluorescent signals. scale bar 20 µm.

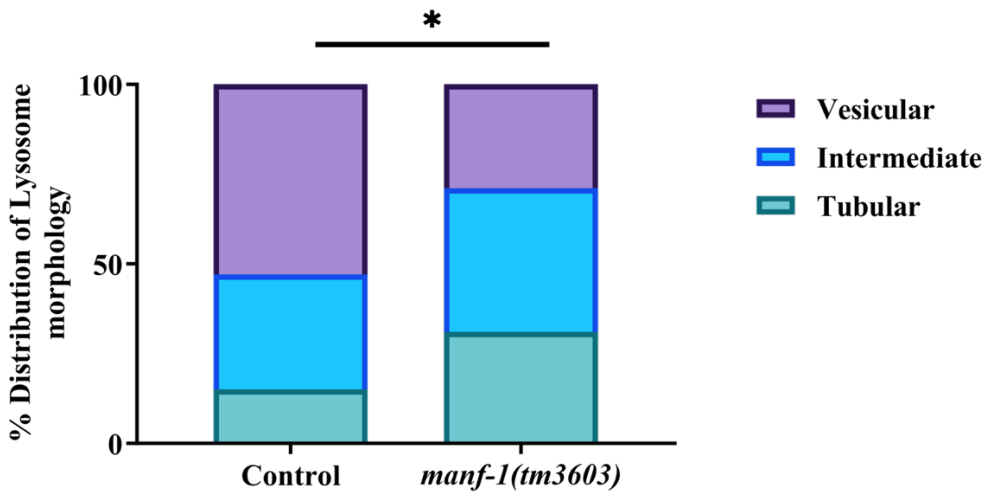

Figure S11. Loss of *manf-1* affects lysosomal morphology. Quantification of NUC-1::mCherry structures in *manf-1(tm3063)* four-day old adults. The lysosomes were analyzed and classified as vesicular, intermediate, or tubular and plotted as a stacked histogram. A total of three batches, n= 20 to 25 worms per batch, were plotted as stacked histograms. Data was analyzed using Chi-squared test. *p<0.05; **p<0.01; ***p<0.001; ****p<0.0001.

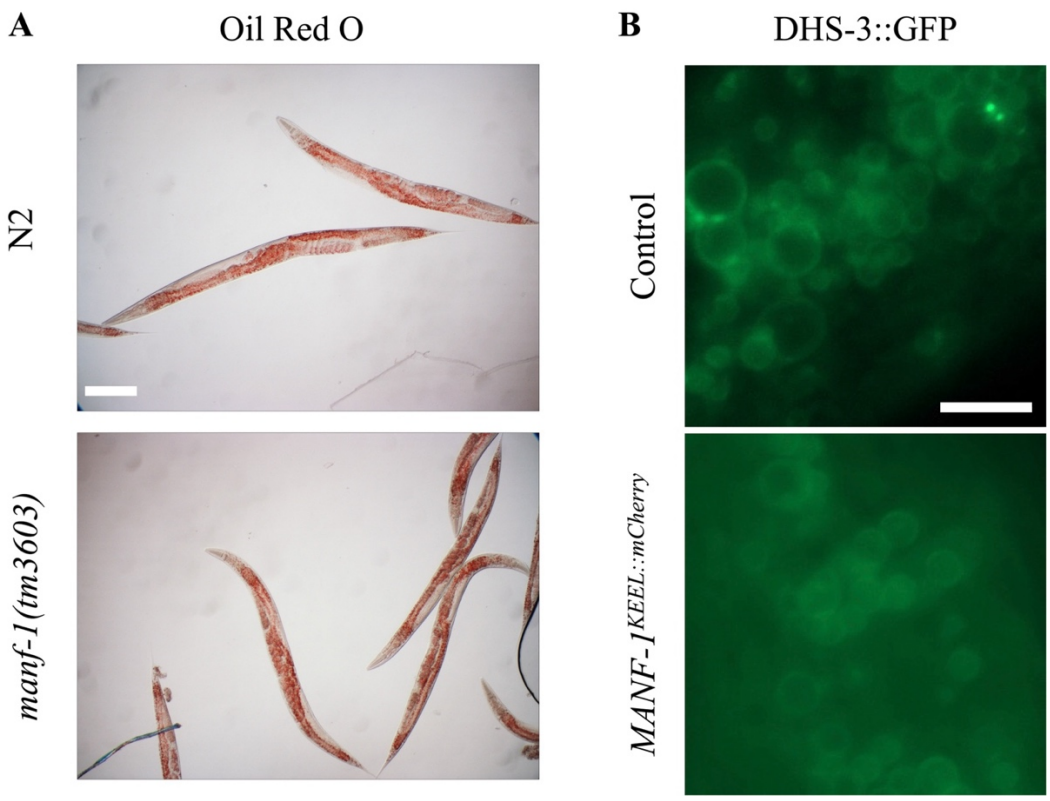

Figure S12. Representative images of animals showing Oil Red O staining and expression of the lipid droplet marker *dhs-3p::dhs-3::GFP*. (**A**) Oil Red O staining of day 1 *manf-1(tm3603)* mutants and N2. scale bar 10 µm. (**B**) Representative images of the lipid droplets in the tail region of day 1 *MANF-1*$^{KEEL::mCherry}$ adults, scale bar 5 µm.

Table S1.

Mean and max lifespans of animals along with treatments. The *p* values were calculated based on wild-type N2 or respective controls. SEM: Standard Error of Mean. N: number of animals examined, combined from at least 3 independent batches.

Genotype	Treatment	Mean Lifespan ± SEM	Max Lifespan	N	*p* value
N2	-	16.0 ± 0.5	25	92	-
manf-1(tm3603)	-	14.5 ± 0.4	24	132	0.0183
manf-1(gk3677)	-	13.5 ± 0.5	22	62	<0.0001
N2	25 ng/µL tunicamycin	10.7 ± 0.3	17	62	-
manf-1(tm3603)	25 ng/µL tunicamycin	8.6 ± 0.3	14	63	<0.001
N2	-	16.7 ± 0.5	25	93	-
hsp::manf-1	-	20.2 ± 0.4	26	54	<0.0001
N2	31°C	18.1 ± 0.4	23	56	-
hsp::manf-1	31°C	19.0 ± 0.5	27	61	0.048
N2	-	16.7 ± 0.4	23	81	-
MANF-1$^{KEEL::mCherry}$	-	19.9 ± 0.5	30	75	<0.0001
N2	-	17.0 ± 0.4	25	69	-
hlh-30(tm1978)	-	12.5 ± 0.3	17	70	<0.0001
MANF-1$^{KEEL::mCherry}$	-	18.5 ± 0.5	29	78	-
MANF-1$^{KEEL::mCherry}$; hlh-30(tm1978)	-	13.5 ± 0.2	19	97	<0.0001
N2	-	15.8 ± 0.4	22	55	-
MANF-1$^{KEEL::mCherry}$; bhEx306	-	17.7 ± 0.4	23	55	<0.0001
MANF-1$^{\Delta KEEL::mCherry}$	-	18.8 ± 0.4	24	51	<0.0001
N2	25 ng/µL tunicamycin	8.0 ± 0.2	14	85	-

MANF-1$^{KEEL::mCherry}$	25 ng/µL tunicamycin	9.4 ± 0.3	18	71	<0.001
MANF-1$^{KEEL::mCherry}$*; bhEx306*	25 ng/µL tunicamycin	9.8 ± 0.3	17	92	<0.0001
MANF-1$^{\Delta KEEL::mCherry}$	25 ng/µL tunicamycin	9.8 ± 0.2	17	87	<0.0001
N2	-	15.9 ± 0.5	26	66	-
MANF-1^{HAR}	-	18.5 ± 0.9	26	66	0.004

Dataset S1 (separate file).

Supplementary File 1 (primers and strains) – Microsoft Excel document

Dataset S2 (separate file).

Supplementary File 2 (RNA-seq) – Microsoft Excel document

3.3 Taylor, S. K. B *et* al. 2024. In Review at microPublication Biology

Effect of bioactive compounds and genetic factors on *manf-1* expression

Shane Taylor* and Bhagwati P Gupta

Department of Biology, McMaster University, Hamilton, ON L8S-4K1, Canada

*Author for Correspondence

Meta data: Expression data, Genomic data, Genotype data, Interaction data

Email: taylos49@mcmaster.ca; Phone: 1-905-525-9140 x26451

Abstract

Mesencephalic **A**strocyte Derived **N**eurotrophic **F**actor (MANF) is a novel family of neurotrophic factors in metazoans that promotes neuronal health and helps maintain cellular homeostasis. Using bioactive compounds to increase *MANF* expression is a promising therapeutic strategy. We examined the effect of curcumin, the most abundant polyphenolic compound present in the *Curcuma longa* (turmeric) rhizome, and lithium, a small alkali metal, on the nematode *Caenorhabditis elegans manf-1* expression. Our results showed that both curcumin and lithium increased *manf-1* expression. In the case of lithium, the effect was dependent on AP1 transcription factors ATF-6 and FOS-1.

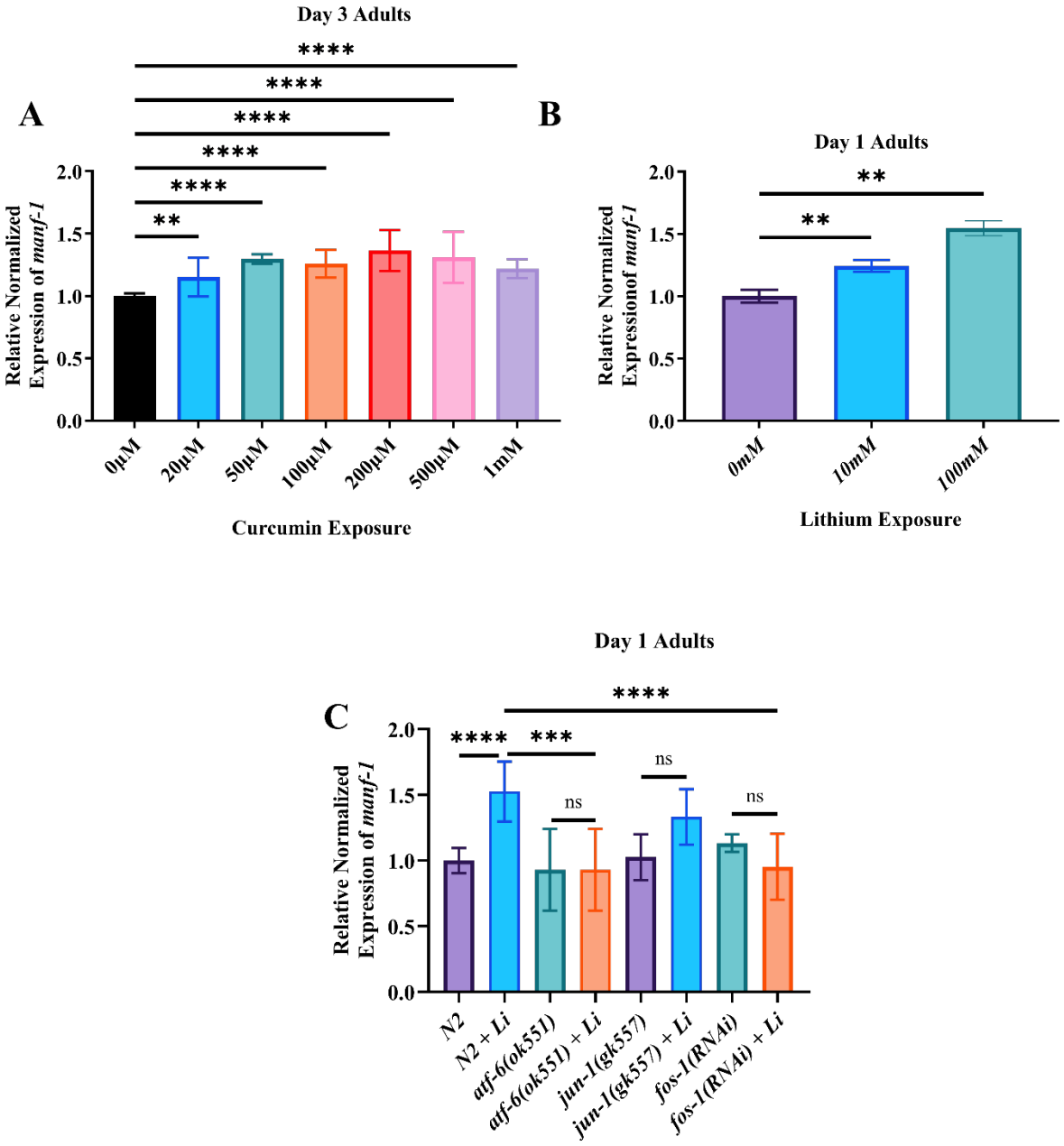

Figure 1. Analysis of *manf-1* expression in adult worms following curcumin and lithium exposure. **A)** qRT-PCR Analysis of chronic curcumin exposure on *manf-1* expression using DY611. Animals were exposed to curcumin from day 1 of adulthood until day 3 at concentrations ranging from 1mM to 20µM and significantly increased *manf-1* expression. **B)** Lithium (Li) Exposure of N2 significantly increases the expression of *manf-1* at 10mM and 100mM. **C)** Analysis of AP-1 family of proteins on *manf-1* expression. The increased expression of *manf-1* due to 10mM lithium (Li) is not observed in *atf-6* mutants and *fos-1(RNAi)* but is seen in *jun-1* mutants. *atf-6, jun-1 and fos-1* do not affect *manf-1* expression. **A-C**: n = 2-3 batches of pooled worms. **A-C** Results are expressed as mean ± SEM. **A-C**: Data was analyzed using one-way ANOVA with Dunnett's post hoc test (*p<0.05; **p<0.01; *** p<0.001; ****p<0.0001)

Description

Neurotrophic factors promote the survival and differentiation of neurons (Nasrolahi et al., 2018). The **M**esencephalic **A**strocyte **D**erived **N**eurotrophic **F**actor (MANF) is of great interest as it is conserved in eukaryotes and its absence in animal models including *C. elegans* (worm) has been shown to phenocopy symptoms of Parkinson's Disease (Palgi et al., 2009; Richman et al., 2018; Voutilainen et al., 2009). While the decline or the absence of MANF accelerates dopaminergic (DA) neurodegeneration, its overexpression protects neurons (Taylor et al., 2024). Thus, MANF is a good candidate for therapeutic treatment of neurodegenerative diseases (Eesmaa et al., 2021; Renko et al., 2018; Voutilainen et al., 2009).

Utilizing existing chemicals that increase MANF expression may be a promising strategy to promote neuroprotection. To this end, we examined the effects of curcumin and lithium exposure on the *C. elegans* MANF homolog, *manf-1*. Curcumin was selected based on its widespread use and popularity as an anti aging drug to be protective whereas lithium was selected due to its role in bipolar disorder(Abu-Hijleh et al., 2020; Liao et al., 2011; McColl et al., 2008; Monroy et al., 2013)

Wild-type animals were exposed to six different concentrations of curcumin starting from day 1 adulthood until day 3. Examination of day 3 worms revealed a significant increase in *manf-1* expression (15 to 30%) **(Fig. 1A)**. The highest increase in gene expression was observed at 200µM. These data add support to existing literature that describe the benefits of inducing MANF expression (Pakarinen & Lindholm, 2023). Since curcumin affects the endoplasmic reticulum-unfolded protein response (ER-UPR) similar to *manf-1* (Hartman et al., 2019; Kovaleva et al., 2023; Richman et al., 2018; Shakeri et al., 2019), it is conceivable that curcumin may exert its effect on the ER-UPR in part through *manf-1* activation.

Next, we examined the effect of lithium on *manf-1* transcript levels. Previous work in rats and cellular models reported that lithium can increase *MANF* expression and is neuroprotective (Abu-Hijleh et al., 2020). We found that lithium promoted *manf-1* expression in *C. elegans* at different concentrations **(Fig. 1C)**. Studies investigating the mechanism of action of lithium on *MANF* expression have reported the involvement of the activating protein-1 (AP-1) family of transcription factors (TFs). Previously, AP-1 binding sites were identified in the human *MANF* promoter region (Wang et al., 2018). In support of this, work in rats and cells demonstrated that AP-1 inhibitors suppress the effect of lithium on MANF induction (Abu-Hijleh et al., 2020).

The AP-1 family consists of many TFs, including JUN, FOS, and ATF whose *C. elegans* homologs are JUN-1, FOS-1 and ATF-6, respectively (Garces de Los Fayos Alonso et al., 2018; Harris et al., 2009). These proteins possess a basic leucine zipper domain and form a dimeric complex. It is worth noting that ATF-6 is a major component of the ER-UPR, which *manf-1* intricately regulates (Hartman et al., 2019; Kovaleva et al., 2023; Richman et al., 2018; Walter & Ron, 2011). We performed *in silico* analysis of the MANF promoter regions from *C. elegans*, *Drosophila melanogaster*, and *Mus musculus* using the CIS-BP database (Weirauch et al., 2014). While consensus sites for JUN, FOS, and ATF were found *in D. melanogaster* and *M. musculcus*, only the ATF-6 site was present in the *C. elegans* promoter **(Table 1)**. This analysis suggested differences in *MANF* transcriptional regulation and raised the possibility that ATF-6 may be involved in regulating *manf-1* expression in *C. elegans*. As expected, we found that *manf-1* levels were not increased in *atf-6(ok551)* animals following lithium treatment **(Fig. 1D)**. Interestingly, *fos-1(RNAi)* showed a similar response **(Fig. 1D)**. No such effect was observed in *jun-1(gk557)* animals **(Fig. 1D)**. In control experiments loss of these three TFs did not alter *manf-1* expression **(Fig. 1E).** While more work is needed to determine the precise mechanism of *atf-6* and *fos-1* function, these results suggest that lithium-induced *manf-1* expression in *C. elegans* is mediated by the AP-1 proteins.

It is worth mentioning that curcumin regulates AP-1 family members in mammalian systems. However, the mechanism appears to be more complex since both positive and negative effects on the expression of AP-1 family members have been reported (Balasubramanian & Eckert, 2007; Dickinson et al., 2003; Yang et al., 2012). Whether AP-1 homologs in *C. elegans* play a role in curcumin-mediated *manf-1* expression, remains to be investigated.

Overall, our findings have revealed important roles of curcumin and lithium in activating *manf-1* transcription and provide preliminary data to further investigate the roles of ATF-6 and FOS-1 in this process.

Table 1. Transcription factor binding site prediction based on CIS-BP database

Organism	Family	TF ID	Name	Motif ID	GeneID	Sequence	From	To	Direction	Score
C. elegans	bZIP	T069395_2.00	*atf-6*	M00594_2.0	WBGene00000222	ACACGTCAG	1316	1324	R	11.404
C. elegans	bZIP	T069395_2.00	*atf-6*	M00594_2.0	WBGene00000222	ATGACGTGG	557	565	F	11.202
C. elegans	bZIP	T069395_2.00	*atf-6*	M00594_2.0	WBGene00000222	TCACGTAAA	611	619	R	8.678
Mouse	bZIP	T060468_2.00	*Atf6*	M04042_2.0	ENSMUSG00000026	ATCCACGTGGTA	1545	1556	F	9.17
Mouse	bZIP	T060455_2.00	*Atf6b*	M04042_2.0	ENSMUSG00000015	ATCCACGTGGTA	1545	1556	F	9.17
Mouse	bZIP	T060459_2.00	*Fos*	M04333_2.0	ENSMUSG00000021	GATCATTCAGG	229	239	R	8.732
Mouse	bZIP	T060459_2.00	*Fos*	M01809_2.0	ENSMUSG00000021	CAGTCATC	460	467	R	9.098
Mouse	bZIP	T060459_2.00	*Fos*	M04338_2.0	ENSMUSG00000021	GATGGCACA	495	503	F	8.127
Mouse	bZIP	T060459_2.00	*Fos*	M01805_2.0	ENSMUSG00000021	AACTGACTTAA	902	912	F	9.771
Mouse	bZIP	T060459_2.00	*Fos*	M01805_2.0	ENSMUSG00000021	AACTGACTCCC	1048	1058	F	8.649
Mouse	bZIP	T060459_2.00	*Fos*	M04336_2.0	ENSMUSG00000021	GATGCAGCATA	1904	1914	F	9.17
Mouse	bZIP	T060453_2.00	*Fosb*	M04333_2.0	ENSMUSG00000003	GATCATTCAGG	229	239	R	8.732
Mouse	bZIP	T060453_2.00	*Fosb*	M01809_2.0	ENSMUSG00000003	CAGTCATC	460	467	R	9.098
Mouse	bZIP	T060453_2.00	*Fosb*	M04338_2.0	ENSMUSG00000003	GATGGCACA	495	503	F	8.127
Mouse	bZIP	T060453_2.00	*Fosb*	M01805_2.0	ENSMUSG00000003	AACTGACTTAA	902	912	F	9.771
Mouse	bZIP	T060453_2.00	*Fosb*	M01805_2.0	ENSMUSG00000003	AACTGACTCCC	1048	1058	F	8.649
Mouse	bZIP	T060453_2.00	*Fosb*	M04336_2.0	ENSMUSG00000003	GATGCAGCATA	1904	1914	F	9.17
Mouse	bZIP	T060493_2.00	*Jun*	M01842_2.0	ENSMUSG00000052	CAGACTCAC	320	328	F	9.867
Mouse	bZIP	T060493_2.00	*Jun*	M01001_2.0	ENSMUSG00000052	CTGACTTAA	904	912	F	11.102
Mouse	bZIP	T060493_2.00	*Jun*	M07834_2.0	ENSMUSG00000052	AATATCTGGCAACTGAC	1038	1057	F	10.777
Mouse	bZIP	T060493_2.00	*Jun*	M07834_2.0	ENSMUSG00000052	GACTGCTGTGATGTGAA	1074	1093	F	8
Mouse	bZIP	T060493_2.00	*Jun*	M01000_2.0	ENSMUSG00000052	TCGAGTCAAT	1692	1701	R	8.846
Mouse	bZIP	T060494_2.00	*Junb*	M01842_2.0	ENSMUSG00000052	CAGACTCAC	320	328	F	9.867
Mouse	bZIP	T060494_2.00	*Junb*	M01001_2.0	ENSMUSG00000052	CTGACTTAA	904	912	F	11.102
Mouse	bZIP	T060494_2.00	*Junb*	M07834_2.0	ENSMUSG00000052	AATATCTGGCAACTGAC	1038	1057	F	10.777
Mouse	bZIP	T060494_2.00	*Junb*	M07834_2.0	ENSMUSG00000052	GACTGCTGTGATGTGAA	1074	1093	F	8
Mouse	bZIP	T060494_2.00	*Junb*	M01000_2.0	ENSMUSG00000052	TCGAGTCAAT	1692	1701	R	8.846
Mouse	bZIP	T060504_2.00	*Jund*	M01842_2.0	ENSMUSG00000071	CAGACTCAC	320	328	F	9.867
Mouse	bZIP	T060504_2.00	*Jund*	M01001_2.0	ENSMUSG00000071	CTGACTTAA	904	912	F	11.102
Mouse	bZIP	T060504_2.00	*Jund*	M07834_2.0	ENSMUSG00000071	AATATCTGGCAACTGAC	1038	1057	F	10.777
Mouse	bZIP	T060504_2.00	*Jund*	M07834_2.0	ENSMUSG00000071	GACTGCTGTGATGTGAA	1074	1093	F	8
Mouse	bZIP	T060504_2.00	*Jund*	M01000_2.0	ENSMUSG00000071	TCGAGTCAAT	1692	1701	R	8.846
Drosophila	bZIP	T062079_2.00	*Atf6*	M03651_2.0	FBgn0033010	CTAATGACGTCGT	373	385	F	9.892
Drosophila	bZIP	T062071_2.00	*kay (fos homolog*	M06019_2.0	FBgn0001297	GCTTAGTCATC	412	422	F	13.402
Drosophila	bZIP	T062071_2.00	*kay (fos homolog*	M03638_2.0	FBgn0001297	GGTGATGTCATA	959	970	F	11.235
Drosophila	bZIP	T062070_2.00	*Jra*	M07834_2.0	FBgn0001291	GGAATCACCACCTTGAA	41	60	R	10.848
Drosophila	bZIP	T062070_2.00	*Jra*	M04342_2.0	FBgn0001291	TATGTCTCACT	161	171	R	8.519
Drosophila	bZIP	T062070_2.00	*Jra*	M05837_2.0	FBgn0001291	ATGAAGTAAAT	277	287	R	9.08
Drosophila	bZIP	T062070_2.00	*Jra*	M03636_2.0	FBgn0001291	AATGACGTCGTT	375	386	F	12.092
Drosophila	bZIP	T062070_2.00	*Jra*	M06018_2.0	FBgn0001291	GCTTAGTCATC	412	422	F	13.402
Drosophila	bZIP	T062070_2.00	*Jra*	M07834_2.0	FBgn0001291	CATGCTGGTTCGGTGAG	441	460	F	9.566
Drosophila	bZIP	T062070_2.00	*Jra*	M04037_2.0	FBgn0001291	ATGACACAT	663	671	F	12.075
Drosophila	bZIP	T062070_2.00	*Jra*	M08072_2.0	FBgn0001291	TGAGTGATGTAAC	778	790	R	12.523
Drosophila	bZIP	T062070_2.00	*Jra*	M08838_2.0	FBgn0001291	CTGATTAAT	799	807	F	8.415
Drosophila	bZIP	T062070_2.00	*Jra*	M09487_2.0	FBgn0001291	TGGTGATGTCAT	958	969	R	15.743
Drosophila	bZIP	T062070_2.00	*Jra*	M01816_2.0	FBgn0001291	ATACGTAAA	1225	1233	R	9.194
Drosophila	bZIP	T062070_2.00	*Jra*	M04037_2.0	FBgn0001291	AGGACTCAC	1356	1364	F	10.201
Drosophila	bZIP	T062070_2.00	*Jra*	M04282_2.0	FBgn0001291	GACTACGTCACG	1702	1713	R	11.327
Drosophila	bZIP	T062070_2.00	*Jra*	M04281_2.0	FBgn0001291	CGCGCGTGATT	1791	1801	R	8.369
Drosophila	bZIP	T062070_2.00	*Jra*	M01816_2.0	FBgn0001291	CTGCGTAAA	1823	1831	R	8.803
Drosophila	bZIP	T062070_2.00	*Jra*	M04281_2.0	FBgn0001291	GATGCCTGACC	1959	1969	R	8.395

Methods

Strain and growth conditions

Worms were grown at 20°C on standard nematode growth media plates seeded with *E. coli* OP50. The strains used in this study are N2 (wildtype *C. elegans*) and, RB772 *atf-6(ok551)* and VC1200 *jun-1(gk557)*. DY611 bhEx260[pGLC135(*manf-1p::GFP*) + pRF4 *(rol-6 (su1006)*)]; *otIs181* [*dat-1::mCherry + tax-3::mCherry*]

Chemical Exposure

For all chemical exposures animals were maintained at 20°C until young adulthood where they were then harvested for RNA isolation at the required stage and *manf-1* levels quantified by RT-qPCR. These chemical exposures were done at two different times.

Lithium Exposure

N2 eggs were bleach isolated and transferred NGM agar plates with OP50 until they reached the L4 stage. Using an adapted protocol (McColl et al., 2008) the culture of L4 worms was then transferred onto NGM plates with and without 10mM or 100mM of Lithium Chloride (LiCl).

Curcumin Exposure

A stock solution of 200mM Curcumin was prepared in DMSO and then diluted to the required concentration by directly adding to the liquid agar media before it solidified prior to pouring. OP50 was seeded on the plate the following day and allowed to grow for a day before placing day 1 adults and allowing animals to develop to the required stage for analysis. Day 3 adults were chosen for gene expression analysis to allow adequate curcumin exposure and day 5 adults were chosen for neuronal analysis. Animals were transferred to fresh curcumin plates when necessary.

Dopaminergic neuron analysis

Method to score DA neurons has been described previously in our paper (Taylor et al., 2021). In brief, cell bodies and dendritic morphology were observed under a Nomarski fluorescence microscope. Wildtype animals have three pairs of DA neurons and smooth dendritic projections in the head region. Animals with fewer cell bodies and abnormal dendrites with blebbing, punctate pattern, deformed shape, faint appearance or complete absence were counted as defective.

RNAi

The Ahringer library was used to feed worms bacteria containing *fos-1* RNAi. Animals were bleached synchronized, and eggs were placed on *fos-1* RNAi plates. They were allowed to grow to adulthood and collected for RNA extraction. The *fos-1* knockdown was confirmed visually as animals were observed to be 100% sterile.

RNA extraction and RT-qPCR

Total RNA was extracted from adults using Trizol (Catalog Number T9424, Sigma-Aldrich, Canada), as described previously in(Taylor et al., 2021). In brief, animals were bleached synchronized to acquire day 1 adults. Worms were collected in 1.5mL tubes following M9 washes. Approximately 4x the amount of Trizol was added to the collected worm pellet volume. This was followed with flash freezing in liquid nitrogen and then thawed in a 37°C water bath. This step was repeated three to four times. Chloroform was added, mixed, and then spun to obtain the aqueous phase. Isopropanol was used to precipitate RNA and two 75% ethanol washes removed impurities. Samples were air dried to remove remaining ethanol. Extracted samples were treated with TURBO DNA-free™ Kit (Catalog Number: AM1907, ThermoFisher Scientific) according to manufacturer's instructions. The resulting samples were used for cDNA synthesis using the SensiFAST cDNA Synthesis Kit (Catalog Number BIO-65053, MeridianBioscience) following kit instructions.

RT-qPCR was performed using the Bio-Rad cycler CFX 96 and the SensiFAST SYBR Green Kit (Catalog Number BIO-98005, BIOLINE, USA). Gene expression levels were normalized to housekeeping gene *pmp-3* and *manf-1* expression was measured. Primers are as follows:

Table 2. List of qRT-PCR Primers

Gene	Oligo Name	**Direction (forward, FP; reverse, RP)**	Sequence (5’ to 3’)
pmp-3	GL747	FP	CTTAGAGTCAAGGGTCGCAGTGGAG
	GL748	RP	ACTGTATCGGCACCAAGGAAACTGG
manf-1	GL916	FP	AGCCGACTCGTCCTTCTCAT
	GL1232	RP	GCATCTGGCTTGGATTTGTCG

Statistical analysis

GraphPad Prism 9.5.1 was used to plot all the graphs and perform statistical analysis. A *t*-test or analysis of variance (ANOVA) with a multiple comparison's test was performed depending on the number of conditions and comparisons to be made. Data from repeat experiments were pooled and analyzed together. Graphs are plotted with either SD or SEM and are indicated in figure legends.

Acknowledgments

N2 strain was provided by Caenorhabditis Genetics Centre (CGC). We acknowledge WormBase for its database curation (PMID 19910365). We thank the anonymous reviewer for providing valuable comments which helped to improve the manuscript.

Funding

This work was supported by NSERC Discovery grant to Bhagwati Gupta.

Author Contributions

B.G. conceived and supervised the project. S.K.B.T. performed the experiments. S.K.B.T wrote the original draft, analyzed the data, and created the figures.

References

Abu-Hijleh, F. A., Prashar, S., Joshi, H., Sharma, R., Frey, B. N., & Mishra, R. K. (2020). Novel mechanism of action for the mood stabilizer lithium. *Bipolar Disorders*, 1–8. https://doi.org/10.1111/bdi.13019

Balasubramanian, S., & Eckert, R. L. (2007). Curcumin suppresses AP1 transcription factor-dependent differentiation and activates apoptosis in human epidermal keratinocytes. *Journal of Biological Chemistry*, *282*(9), 6707–6715. https://doi.org/10.1074/jbc.M606003200

Dickinson, D. A., Iles, K. E., Zhang, H., Blank, V., & Forman, H. J. (2003). Curcumin alters EpRE and AP-1 binding complexes and elevates glutamate-cysteine ligase gene expression. *FASEB Journal : Official Publication of the Federation of American Societies for Experimental Biology*, *17*(3), 473–475. https://doi.org/10.1096/FJ.02-0566FJE

Eesmaa, A., Yu, L. Y., Göös, H., Nõges, K., Kovaleva, V., Hellman, M., Zimmermann, R., Jung, M., Permi, P., Varjosalo, M., Lindholm, P., & Saarma, M. (2021). The cytoprotective protein MANF promotes neuronal survival independently from its role as a GRP78 cofactor. *Journal of Biological Chemistry*, *296*, 100295. https://doi.org/10.1016/j.jbc.2021.100295

Garces de Los Fayos Alonso, I., Liang, H. C., Turner, S. D., Lagger, S., Merkel, O., & Kenner, L. (2018). The role of activator protein-1 (AP-1) family members in CD30-positive lymphomas. In *Cancers* (Vol. 10, Issue 4). Multidisciplinary Digital Publishing Institute (MDPI). https://doi.org/10.3390/cancers10040093

Harris, T. W., Antoshechkin, I., Bieri, T., Blasiar, D., Chan, J., Chen, W. J., De la Cruz, N., Davis, P., Duesbury, M., Fang, R., Fernandes, J., Han, M., Kishore, R., Lee, R., Müller, H. M., Nakamura, C., Ozersky, P., Petcherski, A., Rangarajan, A., … Sternberg, P. W. (2009). Wormbase: A comprehensive resource for nematode research. *Nucleic Acids Research*, *38*((Database issue)), D463–D467. https://doi.org/10.1093/nar/gkp952

Hartman, J. H., Richie, C. T., Gordon, K. L., Mello, D. F., Castillo, P., Zhu, A., Wang, Y., Hoffer, B. J., Sherwood, D. R., Meyer, J. N., & Harvey, B. K. (2019). MANF deletion abrogates early larval Caenorhabditis elegans stress response to tunicamycin and Pseudomonas aeruginosa. *European Journal of Cell Biology*, *98*(5–8), 1–12. https://doi.org/10.1016/j.ejcb.2019.05.002

Kovaleva, V., Yu, L. Y., Ivanova, L., Shpironok, O., Nam, J., Eesmaa, A., Kumpula, E. P., Sakson, S., Toots, U., Ustav, M., Huiskonen, J. T., Voutilainen, M. H., Lindholm, P., Karelson, M., & Saarma, M. (2023). MANF regulates neuronal survival and UPR through its ER-located receptor IRE1α. *Cell Reports*, *42*(2). https://doi.org/10.1016/j.celrep.2023.112066

Liao, V. H. C., Yu, C. W., Chu, Y. J., Li, W. H., Hsieh, Y. C., & Wang, T. T. (2011). Curcumin-mediated lifespan extension in Caenorhabditis elegans. *Mechanisms of Ageing and Development*, *132*(10), 480–487. https://doi.org/10.1016/j.mad.2011.07.008

McColl, G., Killilea, D. W., Hubbard, A. E., Vantipalli, M. C., Melov, S., & Lithgow, G. J. (2008). Pharmacogenetic analysis of lithium-induced delayed aging in Caenorhabditis elegans. *Journal of Biological Chemistry*, *283*(1), 350–357. https://doi.org/10.1074/jbc.M705028200

Monroy, A., Lithgow, G. J., & Alavez, S. (2013). Curcumin and neurodegenerative diseases. *Biofactors*, *39*(1), 122–132. https://doi.org/10.1002/biof.1063

Nasrolahi, A., Mahmoudi, J., Akbarzadeh, A., Karimipour, M., Sadigh-Eteghad, S., Salehi, R., & Farhoudi, M. (2018). Neurotrophic factors hold promise for the future of Parkinson's disease treatment: is there a light at the end of the tunnel? *Reviews in the Neurosciences*, *29*(5), 475–489. https://doi.org/10.1515/revneuro-2017-0040

Pakarinen, E., & Lindholm, P. (2023). CDNF and MANF in the brain dopamine system and their potential as treatment for Parkinson's disease. *Frontiers in Psychiatry*, *14*. https://doi.org/10.3389/fpsyt.2023.1188697

Palgi, M., Lindstrom, R., Peranen, J., Piepponen, T. P., Saarma, M., & Heino, T. I. (2009). Evidence that DmMANF is an invertebrate neurotrophic factor supporting dopaminergic neurons. *Proceedings of the National Academy of Sciences*, *106*(7), 2429–2434. https://doi.org/10.1073/pnas.0810996106

Renko, J. M., Bäck, S., Voutilainen, M. H., Piepponen, T. P., Reenilä, I., Saarma, M., & Tuominen, R. K. (2018). Mesencephalic Astrocyte-Derived Neurotrophic Factor (MANF) Elevates Stimulus-Evoked Release of Dopamine in Freely-Moving Rats. *Molecular Neurobiology*, *55*(8), 6755–6768. https://doi.org/10.1007/s12035-018-0872-8

Richman, C., Rashid, S., Prashar, S., Mishra, R., Selvaganapathy, P. R., & Gupta, B. P. (2018). C. elegans MANF Homolog Is Necessary for the Protection of Dopaminergic Neurons and ER Unfolded Protein Response. *Frontiers in Neuroscience*, *12*(AUG), 1–11. https://doi.org/10.3389/fnins.2018.00544

Shakeri, A., Zirak, M. R., Wallace Hayes, A., Reiter, R., & Karimi, G. (2019). Curcumin and its analogues protect from endoplasmic reticulum stress: Mechanisms and pathways. *Pharmacological Research*, *146*(June), 104335. https://doi.org/10.1016/j.phrs.2019.104335

Taylor, S. K. B., Hartman, J. H., & Gupta, B. P. (2024). The neurotrophic factor MANF regulates autophagic flux and lysosome function to promote proteostasis in C. elegans. *BioRxiv*, 1–58. https://doi.org/10.1101/2023.07.31.551399

Taylor, S. K. B., Minhas, M. H., Tong, J., Selvaganapathy, P. R., Mishra, R. K., & Gupta, B. P. (2021). C. elegans electrotaxis behavior is modulated by heat shock response and unfolded protein response signaling pathways. *Scientific Reports*, *11*(1), 1–17. https://doi.org/10.1038/s41598-021-82466-z

Voutilainen, M. H., Back, S., Porsti, E., Toppinen, L., Lindgren, L., Lindholm, P., Peranen, J., Saarma, M., & Tuominen, R. K. (2009). Mesencephalic Astrocyte-Derived Neurotrophic Factor Is Neurorestorative in Rat Model of Parkinson's Disease. *Journal of Neuroscience*, *29*(30), 9651–9659. https://doi.org/10.1523/jneurosci.0833-09.2009

Walter, P., & Ron, D. (2011). The unfolded protein response: From stress pathway to homeostatic regulation. In *Science* (Vol. 334, Issue 6059, pp. 1081–1086). American Association for the Advancement of Science. https://doi.org/10.1126/science.1209038

Wang, C. H., Jiang, T. C., Qiang, W. M., Zhang, L., Feng, L. J., Shen, Y. J., & Shen, Y. X. (2018). Activator protein-1 is a novel regulator of mesencephalic astrocyte-derived neurotrophic factor transcription. *Molecular Medicine Reports*, *18*(6), 5765–5774. https://doi.org/10.3892/mmr.2018.9601

Weirauch, M. T., Yang, A., Albu, M., Cote, A. G., Montenegro-Montero, A., Drewe, P., Najafabadi, H. S., Lambert, S. A., Mann, I., Cook, K., Zheng, H., Goity, A., van Bakel, H., Lozano, J. C., Galli, M., Lewsey, M. G., Huang, E., Mukherjee, T., Chen, X., … Hughes, T. R. (2014). Determination and inference of eukaryotic transcription factor sequence specificity. *Cell*, *158*(6), 1431–1443. https://doi.org/10.1016/j.cell.2014.08.009

Yang, C. W., Chang, C. L., Lee, H. C., Chi, C. W., Pan, J. P., & Yang, W. C. (2012). Curcumin induces the apoptosis of human monocytic leukemia THP-1 cells via the activation of JNK/ERK Pathways. *BMC Complementary and Alternative Medicine*, *12*(1), 1–8. https://doi.org/10.1186/1472-6882-12-22/FIGURES/5

4 MANF-1 plays an essential role in muscle maintenance and function

4.1 Preface

This chapter includes the following manuscript draft to be submitted to a peer reviewed journal.

1) MANF-1 plays an essential role in muscle maintenance and function by Shane K. B. Taylor, Gurtaaj Gill, Jessica H. Hartman & Bhagwati P. Gupta.

In this chapter we discuss the role of neurotrophic factor MANF-1 and its contribution to maintaining muscle health in animals. Utilizing existing transcriptomic data sets, I show that MANF-1 is enriched for genes related to muscle function. This chapter demonstrates the impact that loss of MANF-1 has on the physiology of animals, showing reduced thrashing and burrowing capacity. This chapter shows that the loss of MANF-1 in animals elicits an age dependent decline in the behavior of animals. The current data in this chapter implicates MANF as being a necessary component to maintain muscle health with age.

4.2 Taylor, S. K. B *et* al. 2024. To be Submitted.

MANF-1 plays an essential role in muscle maintenance and function in *C. elegans*

Shane K. B. Taylor[1], Gurtaaj S. Gill[1], Jessica H. Hartman[2], Bhagwati P. Gupta[1*]

[1]Department of Biology, McMaster University, Hamilton, ON L8S 4K1, Canada.

[2]Department of Biochemistry & Molecular Biology and Department of Regenerative Medicine & Cell Biology, Medical University of South Carolina, Charleston, SC 29425, USA.

[*]Author for Correspondence.

Email: guptab@mcmaster.ca; Phone: 1-905-525-9140 x26451

Keywords: MANF, MANF-1, *C. elegans*, muscles, mitochondria, proteostasis, sarcopenia, muscle aging, muscle health

ABSTRACT

Muscle function declines with age. Healthy muscles can be maintained through exercise and genetic manipulations that promote cellular homeostasis. We recently discovered that the *C. elegans* homolog of the conserved neurotrophic factor, mesencephalic astrocyte-derived neurotrophic factor (MANF), is expressed in muscles. MANF protects against age-dependent neurodegeneration in different animal models. Work from our lab and others has shown that MANF is neuroprotective in *C. elegans* against age-dependent protein aggregation and extends lifespan. Expression of MANF in muscles suggests that the protein may be involved in regulating muscle maintenance and health in these animals. Here, we report that MANF affects the expression of genes involved in muscle function, and that loss of MANF impacts muscle morphology, as well as animals' burrowing and thrashing capacity. These findings support the role of MANF in muscle function, establishing its requirement in maintaining muscle health with age.

Introduction

Maintaining muscle function is critically important to promote healthy aging and has been shown to extend the longevity of animals. Unfortunately, muscle health naturally declines with age, a phenomenon known as sarcopenia (Christian & Benian, 2020). There are multiple reported mechanisms that lead to the onset of sarcopenia (Fernando et al., 2018). The collapse of proteostasis, a key hallmark of aging, is one such pathway that has been attributed to the decline in muscle health with age (Fernando et al., 2018; López-Otín et al., 2023). The increase in protein aggregation and the decline of proteasome activity with age could severely impact the muscle health of animals (Fernando et al., 2018). Loss of muscle function with age is also associated with some neurodegenerative disorders which cause both muscle stiffness and loss of muscle control due to a decline in neuronal function (Hetz & Saxena, 2017; Nasrolahi et al., 2018). Exercise can be used as an intervention for sarcopenia, as it promotes neuromuscular health and is associated with longevity in both humans and animal models (Christian & Benian, 2020; Hartman et al., 2018; Laranjeiro et al., 2019).

The nematode *Caenorhabditis elegans* is an excellent model for the study of the interplay between exercise and genetics, including those controlling muscle aging (Campos et al., 2023;

Christian & Benian, 2020; Gieseler et al., 2017; Laranjeiro et al., 2019). This is due to the conservation of disease-related genes, transparent body, and easy of visualization of muscles (Christian & Benian, 2020; Corsi et al., 2015; Gieseler et al., 2017). It is a useful tool for applying knowledge of muscle function to other animals including humans. Fluorescent reporters facilitate detailed examination of the muscle structures within *C. elegans*. Muscle structure and function, as well as the genetic pathways required for muscle health are conserved from *C. elegans* to vertebrates (Gieseler et al., 2017).

Body wall muscle development in vertebrates is regulated similarly compared to *C. elegans.* The ortholog of MyoD, *hlh-1,* is a myogenic regulatory factor which exists in *C. elegans* to facilitate muscle development. There are 95 striated muscles within *C. elegans* which are functionally similar to skeletal muscles of vertebrates. The muscles of vertebrates and *C. elegans* are made up of thick myosin containing filaments and thin actin filaments. The body wall muscles in *C. elegans* also undergo sarcopenia, as the sarcomeres can become disorganized with age (Gieseler et al., 2017). Additionally, the lack of muscle stem cells within *C. elegans* makes them incapable of muscle regeneration. However, this has made them an excellent model for investigating mechanisms to maintain muscle mass and function with age (Christian & Benian, 2020). *C. elegans* has been found to experience age associated loss of muscle function, but interventions such as genetic manipulations and exercise have previously been found to improve muscle health and movement in animals (Laranjeiro et al., 2019; Mergoud dit Lamarche et al., 2018).

While investigating the role of MANF in neuroprotection and proteostasis, we discovered its potential role in muscle function. The neurotrophic factor, mesencephalic astrocyte derived neurotrophic factor (MANF) is an ideal candidate for studying muscle health in animals through genetic manipulations. As a neurotrophic factor MANF is neuroprotective in multiple neurodegenerative models (Pakarinen & Lindholm, 2023). Additionally, recent work on MANF has demonstrated that it is a regulator of the stress response and can reduce the age-dependent decline of proteostasis within animals (Taylor et al., 2024). MANF is expressed in many tissues and much work has focused on its protective effect on neurons (Pakarinen & Lindholm, 2023). In mice MANF appears to have a role in muscle regeneration, however the specific function of MANF in muscles in other model systems remains to be examined (Sousa et al., 2023). The muscle

expression of MANF potentially demonstrates additional requirements of MANF in *C. elegans* (Taylor et al., 2024). More work is needed to investigate the role of MANF in the muscles of *C. elegans* muscles as they do not regenerate but deteriorate with age. This presents an opportunity to understand the age dependent role of MANF in muscle maintenance.

In this report, we investigate the role of MANF in maintaining muscle health in *C. elegans.* Utilizing existing whole worm transcriptomic data, we show that MANF regulates a subset of muscle genes which are required for age dependent muscle function. Consistent with this, a separate transcriptomic data specific to muscles, identified MANF as a muscle protein coding gene (Schorr et al., 2023). This further supports the role of MANF in muscle maintenance. We assessed the functional muscle health of animals using thrashing and burrowing assays (Gaffney et al., 2014; Lesanpezeshki et al., 2019, 2021; Volovik et al., 2014). Additionally, we assessed the muscle mitochondrial morphology of animals. Overall, this work provides new insights into age dependent requirements of MANF for maintenance of muscle health in animals.

Results

MANF-1 regulates expression of muscle-related genes

We analyzed existing databases to investigate the muscle role of the *C. elegans* MANF homolog, *manf-1*. Initially, we utilized an existing RNAseq dataset consisting of day 8 worms which identified genes that are upregulated following *manf-1* overexpression and are downregulated in *manf-1* mutants (Taylor et al., 2024). Utilizing this dataset, we found several significantly enriched muscle terms, including muscle function, myosin complex, striated muscle dense body, and sarcomere (Fig. 1A). Additionally, we examined the genes (13) identified within the muscle function enrichment term (Fig. 1B). Some of these genes, which constitute the sarcomere, are involved in myosin thick filament assembly (*myo-3*, *mlc-1, mlc-2, mlc3, unc-15, unc-54,)* myosin thin filament formation (*unc-87, pat-10*), M line formation (*unc-89),* dense body formation (*dim-1*) (Fig. 1C). Other genes such as *mup-2* are part of the troponin complex; *hum-4* is predicted to be part of the myosin heavy complex; however, *cpna-2,* which is expressed in muscles, is predicted to be involved in protein ubiquitination.

We next examined a tissue specific transcriptome database. This database allowed us to examine tissue specific expression of *manf-1* that was based on microarray and RNAseq datasets

within *C. elegans* (Kaletsky et al., 2018). We found that within *C. elegans, manf-1* is broadly expressed as previously reported in several tissues (Fig. 1C) (Lindholm et al., 2008; Pakarinen et al., 2022). Additionally, an updated transcriptomic study for muscle function and formation identified *manf-1* as a muscle expressed gene (Schorr et al., 2023). Taken together, the data demonstrate the potential role of MANF-1 in maintaining muscle function, providing a basis for the following work.

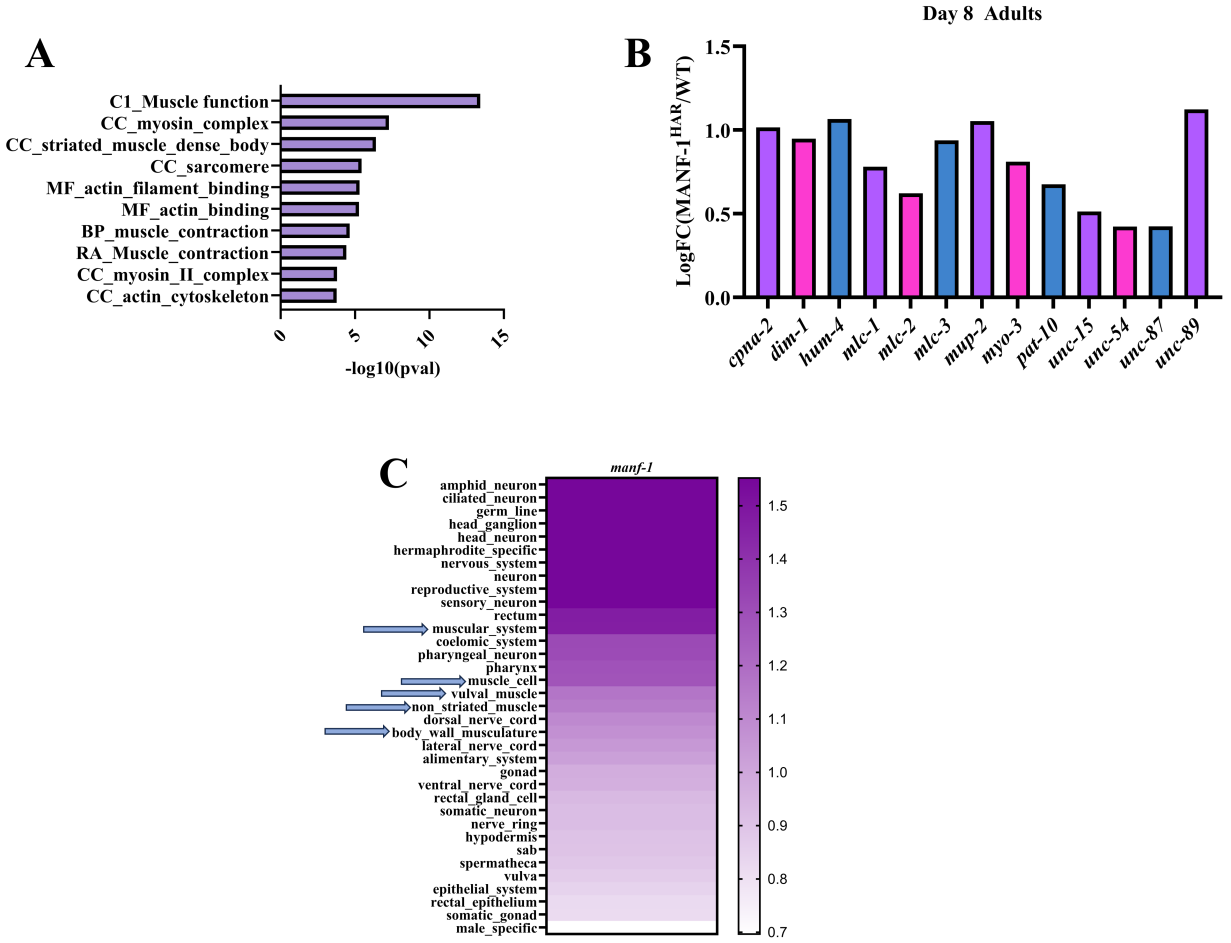

Figure 1. *In Silico* analysis of *manf-1* expression and function in muscles. **A)** Transcriptomic data set of overexpression and loss of *manf-1* showing enriched GO, KEGG and WormCat categories using easyGSEA **B)** The log fold change of the 13 genes from the enriched Muscle function Category of (A). **C)** The tissue specific gene **e**xpression prediction of *manf-1* within *C. elegans* using Worm Tissue (https://worm.princeton.edu/). The list shows 35 out of 76 tissues based on the software. The blue arrows point to the different muscle tissues with predicted *manf-1* expression.

Manf-1 **is expressed in diverse muscles types**

The *in-silico* analysis (Fig. 1C) using the Worm tissue database, predicted MANF-1 expression within muscles. To this end, we followed up with *in vivo* analysis using MANF-1::mCherry transgenic animals to identify specific areas with MANF-1 expression in the muscles of *C. elegans.* We found that MANF-1::mCherry animals show expression within the pharynx, body wall muscle, vulva muscles, and anal muscles (Fig. 2A-D). Additionally, Worm Tissue software predicted that MANF is expressed in the alimentary system of *C. elegans,* and we observed expression in cells in the area of the rectal gland and anal depressor muscles (Fig. 2D). We also observed that the muscle expression of MANF-1 is easily visible from the L4 stage but becomes more prominent during adulthood. Furthermore, the localization of MANF-1 to muscles was dependent on a functional ER retention signal (Taylor et al., 2024). To further assess the localization of MANF-1 to muscles, we crossed MANF-1::mCherry worms with a muscle mitochondria marker (*myo-3p::GFP(mit))*. We observed that in *MANF-1*$^{mCherry::KEEL}$ animals, the expression of MANF-1 was dispersed between the mitochondria within the muscles appearing circular in shape. However, this was not the case for *MANF-1*$^{KEEL::mCherry}$ animals where the ER retention signal was disrupted (Fig. 2E-F). These spherical structures may represent lysosomes in the muscles of animals and could potentially implicate a role for MANF in mitophagy. Altogether, the muscle localization suggests MANF could have a role in maintaining muscle health of animals.

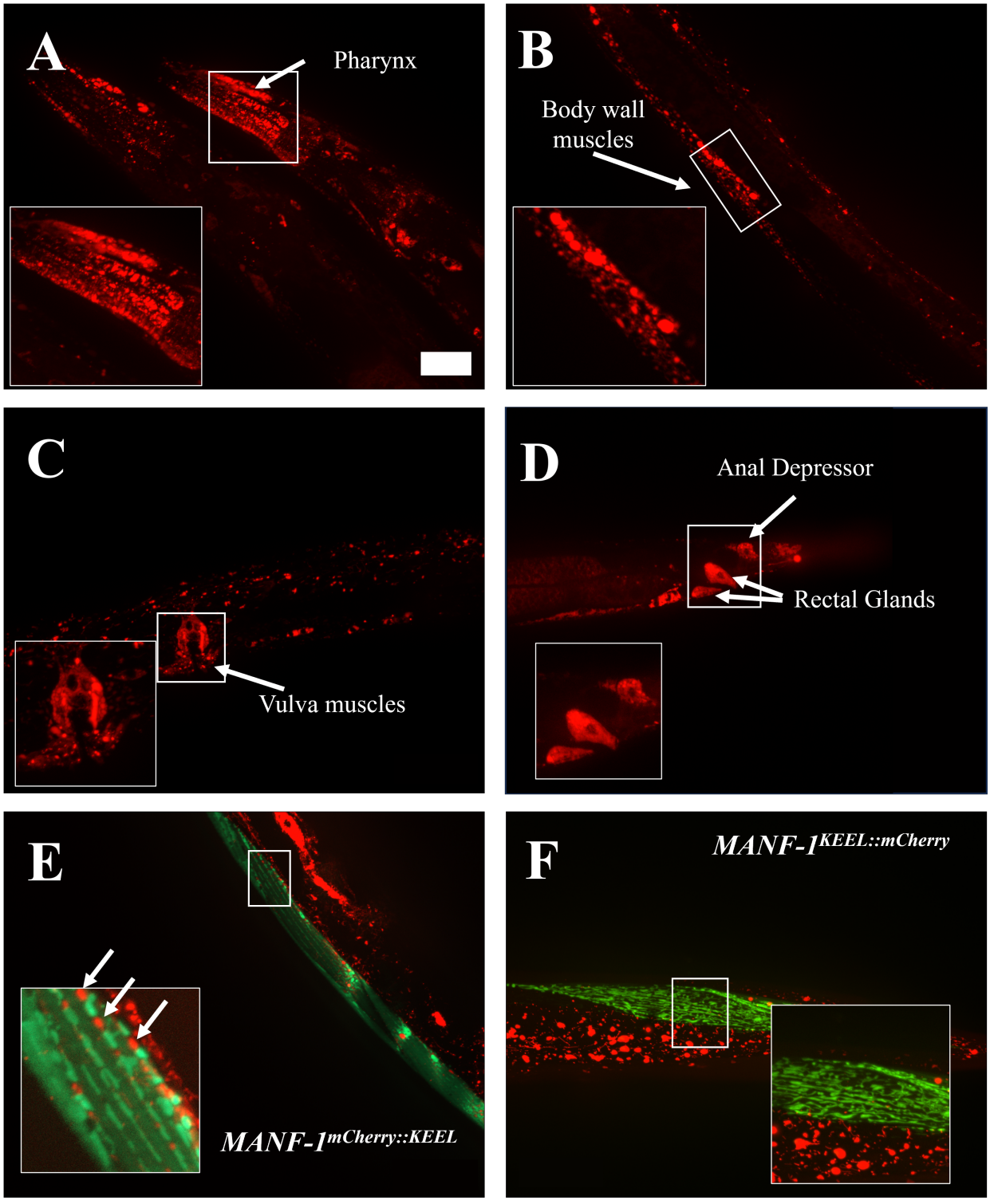

Figure 2. The muscle expression pattern of MANF-1::mCherry. **A-D)** *MANF-1*$^{mCherry::KEEL}$ animals showing fluorescent expression in muscles of the pharynx (A), body wall (B), vulva (C) and anal depressor (D) in adult *C. elegans*. **E-F)** MANF-1::mCherry colocalization with

mitochondria marker *myo-3p::GFP(mit)*. *MANF-1*$^{mCherry::KEEL}$ animals show fluorescent expression interspersed between the muscle mitochondria (E), arrows within inset, point to MANF-1::mCherry foci between the mitochondria. *MANF-1*$^{KEEL::mCherry}$ animals do not show fluorescence within the muscle mitochondria (F). Scale bar = 20µm for A-F.

Manf-1 **is required for normal muscle function**

Following the identification of *manf-1* expression in different tissues and muscle types, we sought to examine the functional impact of loss of *manf-1* on muscle function, using thrashing and burrowing assays (Laranjeiro et al., 2019; Lesanpezeshki et al., 2019, 2021). The thrashing assay and burrowing assays measure changes in the muscle health and function of animals. We tested two *manf-1* mutants, the *tm3603* allele which deletes exon 3 causing a premature stop codon and the *gk3677* allele which is a CRISPR knockout of *manf-1*(Richman et al., 2018). We found that both mutants of *manf-1* significantly increased the thrashing rate in day 1 adults compared to wildtype (Fig. 3A). This hyperactivity of thrashing could potentially be due to altered neuromuscular activity in these animals. This change in thrashing was no longer seen in day 7 *manf-1(tm3603)* adults but *manf-1(gk3677)* animals showed significantly reduced activity compared to wildtype (Fig. 3B). Overall, this suggests that their muscle function capacity had decreased due to the absence of *manf-1*.

Next, we analyzed the burrowing capacity of *manf-1* mutants using a Pluronic gel assay. This gel assay uses OP50 as an attractant, forcing worms to crawl to the surface of a substance that turns from liquid to gel at room temperature (Laranjeiro et al., 2019; Lesanpezeshki et al., 2019). Previous work has demonstrated that this measurement of crawling behavior is a readout of neuromuscular health muscle in *C. elegans* (Laranjeiro et al., 2019; Lesanpezeshki et al., 2019). Using this assay, we were able to quantify the proportion of worms that are able to reach the surface after a 1hr and 2hr time period. First we confirmed that the burrowing assay is functional for our purposes. More WT animals should reach the surface over time, which we observed. We also observed that the ability of animals to reach the surface of the gel significantly declined with age from day 1 to day 7 of adulthood (Fig. 3C). This suggests that neuromuscular health declines with age. We then analyzed *manf-1(gk3677)* mutants and saw a significant reduction in the burrowing capacity of day 1 and day 7 adults reaching the surface of the gel (Fig. 3C). However, this was not the case for *manf-1(tm3603)* (Fig. 3C). Additionally, no day 7 *manf-1(gk3677)* worms were able

to reach the surface during the first hour of the assays. The *gk3677* allele of *manf-1* may exhibit a stronger phenotype due to it being a null mutation. Similar data was observed following lifespan analysis of *manf-1* mutants showing the *gk3677* allele having a greater reduction in lifespan compared to control animals (Taylor et al., 2024). Overall, this data suggests the impact of *manf-1* on maintaining muscle function with age.

A hallmark of age dependent muscle degeneration is dysfunctional mitochondria in animals (Regmi et al., 2014). Our observation of decreased muscle function in *manf-1* mutants therefore lead us to investigate if *manf-1* alters the health of mitochondria in the muscles of animals. We utilized a fluorescent reporter to examine mitochondria morphology specifically in the muscles. We chose to focus on *manf-1(gk3677)* due to the more significant impact it has on muscle function. Interestingly, we found that *manf-1* mutants had a significantly increased distribution in tubular mitochondrial morphology compared to control animals (Fig. 4A-B). However, analysis of worms which overexpress MANF-1 exhibited similar mitochondrial morphology compared to control (Fig. 4C).

Altogether, these results suggest that MANF-1 plays an essential role in muscle maintenance. This effect on muscle health may be due in part to the role of MANF-1 in proteostasis and as a regulator of the UPR.

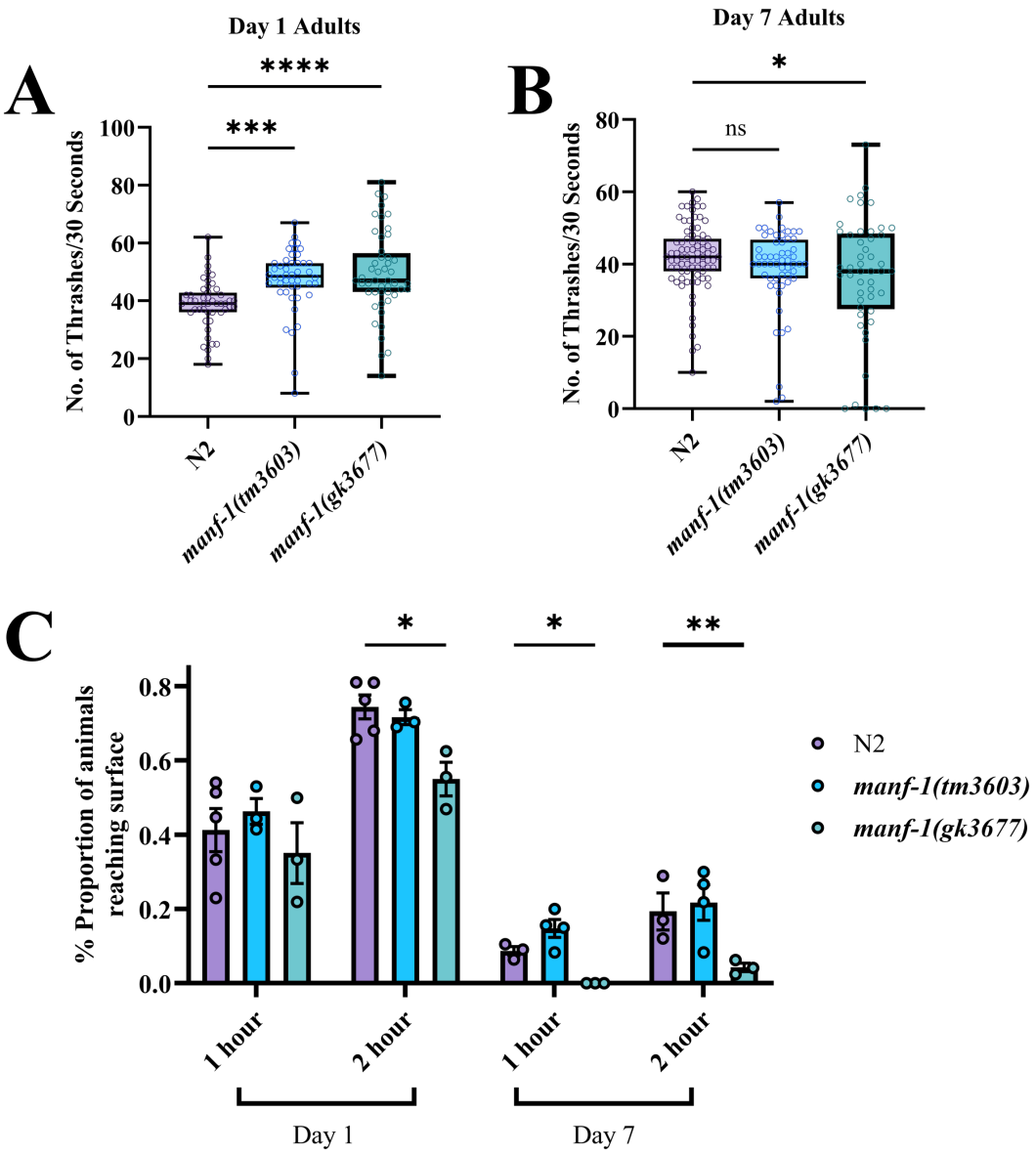

Figure 3. The functional analysis of muscles within *manf-1* mutants. **A, B)** The thrashing response of animals at day 1 and day 7 of adulthood over a 30 second interval. **C)** The proportion of day 1 and day 7 adults that reached the surface of the gel after 1hr and 2hr intervals. A-C: A minimum of 3 individual batches were performed. A & B: n=12-15 worms per batch were analyzed. C, n=30-40 worms per batch. A and B show box plots containing all data points along with the mean and 25th and 75th quartile boundaries. C is expressed as mean ± SEM. Data was analyzed using Student's *t*-test (A), a one-way ANOVA with Dunnett's test (B) and a mixed effects two-way ANOVA with Dunnet's test (C). *p<0.05; **p<0.01; ***p<0.001; ****p<0.0001.

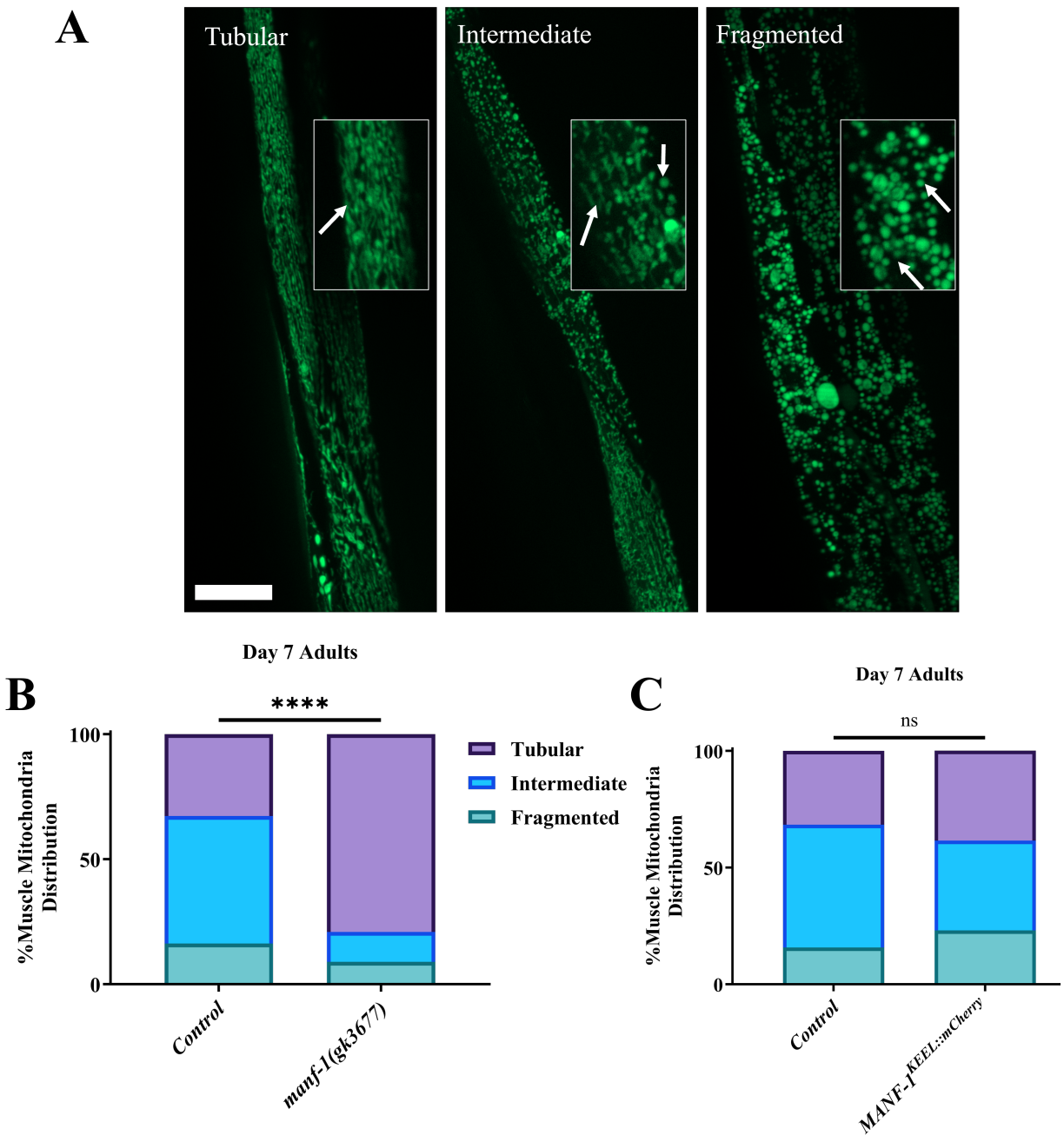

Figure 4. Muscle Mitochondria Morphology of *manf-1(gk3677)* and *MANF-1*$^{KEEL::mCherry}$ animals **A)** Three different categories for muscle mitochondria morphology were used for scoring. The mitochondria in the muscles were classified as either tubular, intermediate or fragmented with tubular being the most preserved morphology and fragmented being the least preserved. **B, C)** Quantification of muscle morphology at day 7 of adulthood in *manf-1(gk3677)* (B) and *MANF-1*$^{KEEL::mCherry}$ (C) worms. Plotted as a stacked histogram. B: Worms were scored in at least three

batches with 15 to 20 per batch. C: This is one batch of preliminary scoring with 12-15 worms in each group. Data was analyzed using Fisher's exact test. *p<0.05; **p<0.01; ***p<0.001; ****p<0.0001.

Discussion

MANF-1 is expressed in multiple tissues and a tremendous amount of work has been done to characterize its function, mechanism of action, and its association with various diseases. Specifically, MANF-1 has been investigated for its role in dopaminergic neurodegeneration in PD models, and other neurodegenerative disorders (Abu-Hijleh et al., 2020; Kovaleva & Saarma, 2021; Pakarinen & Lindholm, 2023; Y. Wang et al., 2021). My recent work has shown changes in MANF tissue localization that is dependent on the ER retention signal (Taylor et al., 2024). A non-functional ER retention signal causes MANF to be expressed predominantly in the hypodermis whereas the functional ER retention signal results in the muscular localization of MANF, among other tissues. The data described in this paper reinforces the importance of MANF function in muscles. Furthermore, this current study examining MANF in muscles adds to the growing body of literature investigating the collapse of proteostasis and its effect on muscle health (Christian & Benian, 2020; Fernando et al., 2018). The decline of MANF-1 with age could also be a contributing factor in sarcopenia. Overall, as a regulator of proteostasis with age, MANF-1 is a suitable candidate for investigating how to maintain muscle function and potentially morphology with age.

The work in this paper demonstrates the requirements of MANF-1 as an age-dependent regulator of muscle maintenance. Here, we show that MANF-1 regulates the expression of several muscle function genes in older adults. Interestingly, expression of genes such as *mlc-1*, *mlc-2*, *mlc-3, myo-3, mup-4, pat-10, unc-15, unc-54,* and *unc-87* are reported to decline with age (Mergoud dit Lamarche et al., 2018). These genes are considered sarcomeric genes and their downregulation may be a contributing factor in early muscle aging (Mergoud dit Lamarche et al., 2018). However, overexpression of MANF-1 is able to maintain high levels of these genes in older adults. Additionally, *mlc-1, unc-54* and *unc-87* are upregulated following an exercise regimen (Laranjeiro et al., 2019). Altogether this data suggests that MANF contributes not only to the age dependent neuronal health of animals, but also age dependent muscle health.

In support of this decline in expression of muscle function genes with age, we found that loss of MANF-1 is associated with loss of muscle function in animals. The burrowing assay demonstrated that the severity of muscle dysfunction correlated with the different mutant alleles of *manf-1*. The full deletion led to a significant reduction in the animal's burrowing capability. The burrowing assay is a measure of neuromuscular health as animals sense the food at the surface (Lesanpezeshki et al., 2019). This assay was a direct read out of muscle function in *manf-1* mutants. It is important to mention that *manf-1* does not affect the chemotactic response of animals (Richman et al., 2018).

Interestingly, the *manf-1* mutants showed an increased thrashing response at day 1 of adulthood but this declined with age while the *tm* allele was comparable to WT and the GK was less functional than WT by day 7. This could potentially be due to the increased UPR activity that *manf-1* mutants exhibit (Richman et al., 2018). High UPR activity has been reported to allow *manf-1* animals to develop in the presence of tunicamycin when wildtype worms cannot (Hartman et al., 2019). This suggests that day 1 *manf-1* mutants may be experiencing high UPR activation which may cause the hyperactive thrashing behaviour of animals.

Muscle function may be affected by changes in muscle morphology. In *C. elegans* mitochondrial morphology can be used as a readout of muscle health following exercise regimen and drug treatment (Hewitt et al., 2018; Laranjeiro et al., 2019). Our results provide the first evidence of the effect of *manf-1* mutations on muscle mitochondrial morphology. We observed that *manf-1(gk3677)* animals retained a tubular mitochondrial morphology with age, which was unexpected as their muscle function was severely impacted. Interestingly, ER stress has been reported to cause dynamic remodeling of mitochondrial morphology in cell cultures (Lebeau et al., 2018). The loss of *manf-1* has been shown previously to induce ER stress (Hartman et al., 2019; Richman et al., 2018) This increased ER stress maybe forcing a constant or adaptive remodeling of the mitochondria i.e. changes in mitochondrial dynamics or morphology. Previous research has shown that mutations in proteins which regulate mitochondrial dynamics (fission and fusion of mitochondria), disrupt the muscle mitochondrial morphology. Interestingly, double mutants for both mitochondrial fission (*drp-1*) and mitochondrial fusion (*eat-3)* result in normal muscle mitochondrial morphology. However, the genetic combination of loss of both *drp-1* and *fzo-1,* another mitochondrial fusion gene, retained the fragmented mitochondrial morphology seen in

single mutants (Byrne et al., 2019). This data suggests that *manf-1* may potentially regulate mitochondrial dynamics and mitophagy within animals. It is possible *manf-1* may directly affect mitochondrial fission or fusion within animals by affecting the expression of *drp-1, fzo-1* and *eat-3.*

My previous work shows that *manf-1* mutants have reduced autophagy (Taylor et al., 2024), which could be a contributing factor to the unexpected mitochondrial morphology of *manf-1* mutants. Moreover, muscle autophagy is reported to decline with age, and increases in autophagosome number is considered a marker of aging (Mergoud dit Lamarche et al., 2018). Similar to this, loss of MANF increases autophagosomes number as well (Taylor et al., 2024). RNAi of the muscle transcription factor *unc-120/*SRF increases muscle autophagosomes with age and dysregulates muscle genes (Mergoud dit Lamarche et al., 2018; Taylor et al., 2024). This suggests that MANF may potentially influence autophagy in muscles for efficient function.

A transcriptomic study on muscles in *C. elegans* identified MANF-1 as a muscle gene (Schorr et al., 2023). This same study also identified *xbp-1* and *hlh-30* as muscle specific transcription factors and these are known to affect MANF regulation (Schorr et al., 2023; Taylor et al., 2024; D. Wang et al., 2018). This indicates that the requirements of MANF in muscles may be dependent on regulation by these two transcription factors, *xbp-1* and *hlh-30*.

Taken together, the work in this paper points to a novel role of MANF-1 in regulating muscle maintenance in animals. This research highlights different avenues such as mitophagy and muscle gene regulation, that *manf-1* may utilize in promoting muscle homeostasis. Overall, this provides evidence that further study of MANF-1 may demonstrate its utility as an intervention for the improvement and maintenance of muscles during aging.

AUTHOR CONTRIBUTIONS

Experiments were performed by S.K.B.T. and G.G.. The majority of reagents for the study were created by S.K.B.T.. Data was analyzed by S.K.B.T. and G.G. The first draft of the manuscript was written by S.K.B.T. and was subsequently revised in collaboration with G.G. J.H. and B.P.G. The final version was reviewed by all authors for submission and B.P.G. supervised the study.

COMPETING INTERESTS

The authors declare no competing interests.

Method

Strains and culturing

Worms were grown and maintained at standard culture temperature (20°C) unless stated otherwise. All strains were cultured on standard NGM (nematode growth media) agar plates seeded with *E. coli* bacterial strain OP50 as a food source unless otherwise indicated. To obtain age-synchronized cultures, gravid hermaphrodites were exposed to a mixture of sodium hypochlorite and sodium hydroxide (3:2::NaOCl:NaOH) which followed a standard bleaching protocol. Worm strains that were obtained from the *Caenorhabditis* Genetics Center (University of Minnesota, St. Paul, MN) and those that were created during this study are as follows: Bristol isolate N2, DY487 *manf-1(tm3603),* DY699 *manf-1(gk3677), SJ4103 zcIs14 [myo-3::GFP(mit)],* DY711 *manf-1(gk3677); zcIs[myo-3::GFP(mit)],* DY759 *bhEx304[pGLC180(manf-1p::MANF-1::KEEL::mcherry)+pGLC72(dat-1p::YFP)],* DY819 *bhEx310[pGLC196(manf-1p::manf-1ΔKEEL::mCherry::KEEL)+pGLC72(dat-1p::YFP)],* DY761 *zcIs14 [myo-3::GFP(mit)];bhEx304[pGLC180(manf-1p::MANF-1::KEEL::mcherry)+pGLC72(dat-1p::YFP)],* DY828 *zcIs14 [myo-3::GFP(mit)];bhEx310[pGLC196(manf-1p::manf-1ΔKEEL::mCherry::KEEL)+pGLC72(dat-1p::YFP)].*

Burrowing Assay

The burrowing capacity of animals was adapted from existing protocols(Laranjeiro et al., 2019; Lesanpezeshki et al., 2019). In brief, 30 to 40 worms were placed via picking or washing into a 12 well plate which contained 20 μL of Pluronic F-127 gel that was at 15°C. After the worms were added, an additional 3mL of Pluronic gel was added to the top and allowed to solidify at room

temperature (25°C). Following this 20 µL of *E. coli* OP50 at an OD of 0.12 was placed onto the surface of the gel as a chemoattractant for worms. Worms that reached the surface of the gel were counted every hour on the hour for 2hrs.

Thrashing Assay

The thrashing rate of animals was quantified using a established lab protocols. Age synchronized day 1 or day 7 adults were placed in 10 µL of M9 buffer and the number of thrashes in 30 seconds were counted. Samples were analyzed across 3 bathces.

Bioinformatic Analysis

We used eVITTA to perform a gene enrichment analysis on the genes that were common between *manf-1 (tm3603)* and MANF-1^{HAR}. Specifically, the easyGSEA tool generated the enrichment terms in Figures

Fluorescence microscopy and quantification

Animals were mounted on 2% agar pad containing glass slides**.** They were then anesthetized with 30mM of NaN3. *myo-3::GFP(mit*) GFP fluorescence was visualized using a Zeiss Observer Z1 microscope equipped with an Apotome 2 and X-Cite R 120LED fluorescence illuminator. Analysis of mitochondrial morphology was done by blinding the observer to the genotype and condition of the worm. The researcher then quantified the mitochondrial morphology under the microscope.

Statistical analyses

GraphPad Prism 10.2 was used to plot all the graphs and perform statistical analyses. The Student's *t*-test or analysis of variance (ANOVA) with a multiple comparisons test were performed depending on the number of conditions and comparisons to be made. Data from repeat experiments were pooled and analyzed together. Graphs were plotted with either standard deviation (SD) or standard error of mean (SEM) as appropriate (see figures).

References

Abu-Hijleh, F. A., Prashar, S., Joshi, H., Sharma, R., Frey, B. N., & Mishra, R. K. (2020). Novel mechanism of action for the mood stabilizer lithium. *Bipolar Disorders*, 1–8. https://doi.org/10.1111/bdi.13019

Byrne, J. J., Soh, M. S., Chandhok, G., Vijayaraghavan, T., Teoh, J. S., Crawford, S., Cobham, A. E., Yapa, N. M. B., Mirth, C. K., & Neumann, B. (2019). Disruption of mitochondrial dynamics affects behaviour and lifespan in Caenorhabditis elegans. *Cellular and Molecular Life Sciences*, *76*(10), 1967–1985. https://doi.org/10.1007/s00018-019-03024-5

Campos, J. C., Bozi, L. H. M., Krum, B., Bechara, L. R. G., Ferreira, N. D., Arini, G. S., Albuquerque, R. P., Traa, A., Ogawa, T., van der Bliek, A. M., Beheshti, A., Chouchani, E. T., Van Raamsdonk, J. M., Blackwell, T. K., & Ferreira, J. C. B. (2023). Exercise preserves physical fitness during aging through AMPK and mitochondrial dynamics. *Proceedings of the National Academy of Sciences of the United States of America*, *120*(2), e2204750120.

Christian, C. J., & Benian, G. M. (2020). Animal models of sarcopenia. *Aging Cell*, *19*(10). https://doi.org/10.1111/acel.13223

Corsi, A. K., Wightman, B., & Chalfie, M. (2015). A Transparent window into biology : A primer on Caenorhabditis elegans. *WormBook*, *200*(2), 1–31. https://doi.org/10.1895/wormbook.1.177.1

Fernando, R., Drescher, C., Nowotny, K., Grune, T., & Castro, P. (2018). *Impaired proteostasis during skeletal muscle aging*. https://doi.org/10.1016/j.freeradbiomed.2018.08.037

Gaffney, C. J., Bass, J. J., Barratt, T. F., & Szewczyk, N. J. (2014). Methods to Assess Subcellular Compartments of Muscle in C. elegans. *Journal of Visualized Experiments*, *93*. https://doi.org/10.3791/52043

Gieseler, K., Qadata, H., & Benian, G. M. (2017). Development, structure, and maintenance of C. elegans body wall muscle. *WormBook*, 1–59. https://doi.org/10.1895/wormbook.1.81.2

Hartman, J. H., Richie, C. T., Gordon, K. L., Mello, D. F., Castillo, P., Zhu, A., Wang, Y., Hoffer, B. J., Sherwood, D. R., Meyer, J. N., & Harvey, B. K. (2019). MANF deletion abrogates early larval Caenorhabditis elegans stress response to tunicamycin and Pseudomonas aeruginosa.

European Journal of Cell Biology, *98*(5–8), 1–12. https://doi.org/10.1016/j.ejcb.2019.05.002

Hartman, J. H., Smith, L. L., Gordon, K. L., Laranjeiro, R., Driscoll, M., Sherwood, D. R., & Meyer, J. N. (2018). Swimming Exercise and Transient Food Deprivation in Caenorhabditis elegans Promote Mitochondrial Maintenance and Protect Against Chemical-Induced Mitotoxicity. *Scientific Reports*, *8*(1). https://doi.org/10.1038/s41598-018-26552-9

Hetz, C., & Saxena, S. (2017). ER stress and the unfolded protein response in neurodegeneration. *Nature Reviews Neurology*, *13*(8), 477–491. https://doi.org/10.1038/nrneurol.2017.99

Hewitt, J. E., Pollard, A. K., Lesanpezeshki, L., Deane, C. S., Gaffney, C. J., Etheridge, T., Szewczyk, N. J., & Vanapalli, S. A. (2018). Muscle strength deficiency and mitochondrial dysfunction in a muscular dystrophy model of Caenorhabditis elegans and its functional response to drugs. *Disease Models & Mechanisms*, *11*(12). https://doi.org/10.1242/DMM.036137

Kaletsky, R., Yao, V., Williams, A., Runnels, A. M., Tadych, A., Zhou, S., Troyanskaya, O. G., & Murphy, C. T. (2018). Transcriptome analysis of adult Caenorhabditis elegans cells reveals tissue-specific gene and isoform expression. *PLoS Genetics*, *14*(8). https://doi.org/10.1371/journal.pgen.1007559

Kovaleva, V., & Saarma, M. (2021). Endoplasmic Reticulum Stress Regulators: New Drug Targets for Parkinson's Disease. *Journal of Parkinson's Disease*, *11*(s2), S219–S228. https://doi.org/10.3233/JPD-212673

Laranjeiro, R., Harinath, G., Hewitt, J. E., Hartman, J. H., Royal, M. A., Meyer, J. N., Vanapalli, S. A., & Driscoll, M. (2019). Swim exercise in Caenorhabditis elegans extends neuromuscular and gut healthspan, enhances learning ability, and protects against neurodegeneration. *Proceedings of the National Academy of Sciences of the United States of America*, *116*(47), 23829–23839. https://doi.org/10.1073/pnas.1909210116

Lebeau, J., Saunders, J. M., Moraes, V. W. R., Madhavan, A., Madrazo, N., Anthony, M. C., & Wiseman, R. L. (2018). The PERK Arm of the Unfolded Protein Response Regulates Mitochondrial Morphology during Acute Endoplasmic Reticulum Stress. *Cell Reports*, *22*(11), 2827–2836. https://doi.org/10.1016/j.celrep.2018.02.055

Lesanpezeshki, L., Hewitt, J. E., Laranjeiro, R., Antebi, A., Driscoll, M., Szewczyk, N. J., Blawzdziewicz, J., Lacerda, C. M. R., & Vanapalli, S. A. (2019). Pluronic gel-based burrowing assay for rapid assessment of neuromuscular health in C. elegans. *Scientific Reports*, *9*(1). https://doi.org/10.1038/s41598-019-51608-9

Lesanpezeshki, L., Qadota, H., Darabad, M. N., Kashyap, K., Lacerda, C. M. R., Szewczyk, N. J., Benian, G. M., & Vanapalli, S. A. (2021). Investigating the correlation of muscle function tests and sarcomere organization in C. elegans. *Skeletal Muscle*, *11*(1), 1–15. https://doi.org/10.1186/s13395-021-00275-4

Lindholm, P., Peränen, J., Andressoo, J. O., Kalkkinen, N., Kokaia, Z., Lindvall, O., Timmusk, T., & Saarma, M. (2008). MANF is widely expressed in mammalian tissues and differently regulated after ischemic and epileptic insults in rodent brain. *Molecular and Cellular Neuroscience*, *39*(3), 356–371. https://doi.org/10.1016/j.mcn.2008.07.016

López-Otín, C., Blasco, M. A., Partridge, L., Serrano, M., & Kroemer, G. (2023). Hallmarks of aging: An expanding universe. *Cell*, *186*(2), 243–278. https://doi.org/10.1016/j.cell.2022.11.001

Mergoud dit Lamarche, A., Molin, L., Pierson, L., Mariol, M. C., Bessereau, J. L., Gieseler, K., & Solari, F. (2018). UNC-120/SRF independently controls muscle aging and lifespan in Caenorhabditis elegans. *Aging Cell*, *17*(2). https://doi.org/10.1111/acel.12713

Nasrolahi, A., Mahmoudi, J., Akbarzadeh, A., Karimipour, M., Sadigh-Eteghad, S., Salehi, R., & Farhoudi, M. (2018). Neurotrophic factors hold promise for the future of Parkinson's disease treatment: is there a light at the end of the tunnel? *Reviews in the Neurosciences*, *29*(5), 475–489. https://doi.org/10.1515/revneuro-2017-0040

Pakarinen, E., & Lindholm, P. (2023). CDNF and MANF in the brain dopamine system and their potential as treatment for Parkinson's disease. *Frontiers in Psychiatry*, *14*. https://doi.org/10.3389/fpsyt.2023.1188697

Pakarinen, E., Lindholm, P., Saarma, M., & Lindahl, M. (2022). CDNF and MANF regulate ER stress in a tissue-specific manner. *Cellular and Molecular Life Sciences*, *79*(2), 1–18. https://doi.org/10.1007/s00018-022-04157-w

Regmi, S. G., Rolland, S. G., & Conradt, B. (2014). Age-dependent changes in mitochondrial morphology and volume are not predictors of lifespan. *Aging*, *6*(2), 118–130. https://doi.org/10.18632/aging.100639

Richman, C., Rashid, S., Prashar, S., Mishra, R., Selvaganapathy, P. R., & Gupta, B. P. (2018). C. elegans MANF Homolog Is Necessary for the Protection of Dopaminergic Neurons and ER Unfolded Protein Response. *Frontiers in Neuroscience*, *12*(AUG), 1–11. https://doi.org/10.3389/fnins.2018.00544

Schorr, A. L., Mejia, A. F., Miranda, M. Y., & Mangone, M. (2023). An updated C. elegans nuclear body muscle transcriptome for studies in muscle formation and function. *Skeletal Muscle*, *13*(1), 1–14. https://doi.org/10.1186/s13395-023-00314-2

Sousa, N. S., Brás, M. F., Antunes, I. B., Lindholm, P., Neves, J., & Sousa-Victor, P. (2023). Aging disrupts MANF-mediated immune modulation during skeletal muscle regeneration. *Nature Aging 2023*, 1–15. https://doi.org/10.1038/s43587-023-00382-5

Taylor, S. K. B., Hartman, J. H., & Gupta, B. P. (2024). The neurotrophic factor MANF regulates autophagic flux and lysosome function to promote proteostasis in C. elegans. *BioRxiv*, 1–58. https://doi.org/10.1101/2023.07.31.551399

Volovik, Y., Marques, F. C., & Cohen, E. (2014). The nematode Caenorhabditis elegans: A versatile model for the study of proteotoxicity and aging. *Methods*, *68*(3), 458–464. https://doi.org/10.1016/J.YMETH.2014.04.014

Wang, D., Hou, C., Cao, Y., Cheng, Q., Zhang, L., Li, H., Feng, L., & Shen, Y. (2018). XBP1 activation enhances MANF expression via binding to endoplasmic reticulum stress response elements within MANF promoter region in hepatitis B. *The International Journal of Biochemistry & Cell Biology*, *99*, 140–146. https://doi.org/10.1016/j.biocel.2018.04.007

Wang, Y., Wen, W., Li, H., Clementino, M., Xu, H., Xu, M., Ma, M., Frank, J., & Luo, J. (2021). MANF is neuroprotective against ethanol-induced neurodegeneration through ameliorating ER stress. *Neurobiology of Disease*, *148*, 105216. https://doi.org/10.1016/j.nbd.2020.105216

5 Discussion and Future Directions

5.1 Major Findings of Thesis

Each chapter discussed within my doctoral thesis has added to the current field of stress response signaling and how it relates to MANF. Understanding the underlying mechanisms by which genes interact with each other to regulate multiple stress responses is essential to ensure survival against stress response dysregulation, a key hallmark of several diseases. This research supports future work investigating the role of stress response regulating proteins within the context of behaviour and organism survival. In this thesis, I have laid the foundation for future research to explore organelle-specific regulation of the stress response by MANF in order to promote organism survival.

Analysis of electrotaxis behaviour (**Chapter 2**) demonstrated that changes in UPR activity significantly impact the behaviour of animals following a variety of external insults. These stressors cause animals to adapt their behaviour through reduction or increase in speed, but also activate multiple stress response chaperones to maintain organismal health. Though chaperone activity represents an active stress response, it does not necessarily indicate whether a behavioural response will be detrimental or beneficial. The coupling of changes in UPR activity with electrotaxis behaviour allowed us to understand the severity or benefits due to cellular changes caused by our internal and external environment.

Chapter 3 of my thesis provides an in-depth investigation of MANF-1, the stress-regulating neurotrophic factor. *In vivo* analysis of MANF performed here presents a new interpretation for how MANF works within tissues and at the subcellular level of various organelles. This research redefines MANF as not only a neurotrophic factor but also as a central player in facilitating communication between the ER and lysosomes within multiple tissues. Furthermore, localization analysis of MANF within **Chapter 3** provides groundwork for the requirement of MANF in multiple tissues to be cytoprotective.

As a follow up to this work, **Chapter 4** began our first line of investigation into the tissue specific roles of MANF. **Chapter 4** describes the importance of the localization of MANF to muscles. Interestingly, loss of MANF downregulates genes that are required for muscle function and health. To this end, we observed that mutations in *manf-1* reduced the neuromuscular ability of animals in an age-dependent manner, suggesting that MANF may have a different role within various tissues to maintain animal fitness.

Overall, this thesis reveals the impact of the stress response on behaviour and that understanding how MANF acts to control cellular mechanisms provides novel avenues for how stress responses can be altered to mitigate various diseases. It also suggests that crosstalk between different cellular compartments is crucial for appropriate function of the cell with aging, and that dysregulation of this system causes a detriment to behaviour, neurons, muscles, and longevity.

The results described here provide the groundwork for future study on how animals co-ordinate tissue-to-tissue stress response signaling and how this impacts behaviour. Future work on MANF should investigate its tissue-specific function, its interaction with the other organelles to maintain organismal health, its transcriptional regulation, and the interacting proteins that MANF utilizes to be cytoprotective.

5.2 The HSR, MT-UPR, and ER-UPR modulate electrotaxis behavior

This chapter demonstrated that mutations in the major transcription factors that regulate the ER-UPR (*xbp-1)*, MT-UPR (*atfs-1*), and HSR (*hsf-1*) caused significant defects in animal behaviour, reducing electrotactic movement. These same mutations are also known to impact animal health (Bennett et al., 2014; Hajdu-Cronin et al., 2004; Henis-Korenblit et al., 2010; Morley & Morimoto, 2004; Wu et al., 2018). The findings of this chapter showed that various stressors such as chemical, heat, starvation, and exercise increased the expression of organelle-specific stress response chaperones. These external stressors affected the behaviour of animals, resulting in either a hypoactive or hyperactive response. This suggests that modulation of electrotaxis behaviour is potentially rooted in stress response signaling.

One of the genes that impaired UPR and HSR activity was *pqe-1.* Mutations in *pqe-1* enhance polyglutamine (polyQ) toxicity and dysregulate the stress response, causing increased *hsp-4*, *hsp-6* and *hsp-16.2* chaperone expression. Consequently, this led to a reduction in the movement response of animals. In contrast, exercise treatment from larval stages, which also increase expression of the previously mentioned chaperones, enhanced the electrotaxis behaviour of animals and improved muscle mitochondrial morphology. Interestingly, wildtype animals and *hsf-1* mutants which were given a chronic heat shock and a 1hr heat treatment respectively reduced electrotaxis speed but also had reduced chaperone expression (**Figure A1).** However, the chronic heat treatment caused an upregulation of *hsp-16.2* (**Figure A1)**. This suggests the stress response has collapsed in the face of chronic stressors, including mutations, affecting the behaviour of animals. Overall, I found that the difference in the behaviour of animals appears to depend on the

type of stressor, in this case mutations or external stressors. How the cell determines which behaviour to elicit is likely a tightly regulated network that changes overall animal physiology and can impact the electrotaxis response.

The work in this chapter has laid the foundation for electrotaxis as a means to study changes in the behaviour of animals to promote organismal survival, following manipulations of the stress response. Furthermore, it provides a basis for understanding the requirement of UPR activity in controlling the behaviour of animals for organismal survival.

5.3 The Future of Electrotaxis and Behaviour

5.3.1 Potential mechanisms by which the stress response modulates behaviour

The stress response coordinates changes at the cellular level to maintain homeostasis. Research shows that neuronal overexpression of the stress response modulates proteostasis and organismal health in animals via cell-nonautonomous signaling (Dutta et al., 2022). Therefore, future studies should examine how cell non-autonomous signaling by the stress response via different tissues modulates behaviour. Neurons are of particular interest due to their ability to communicate to tissues to promote organismal survival (Dutta et al., 2022).

Utilizing neuronal overexpression of the MT-UPR, ER-UPR, and HSR we can investigate how cell-nonautonomous signaling by the stress response affects the behaviour of animals. Neuronal signaling caused by the different stress responses is reported to lead to the release of neuropeptides from neurons to signal to other tissues to extend lifespan and maintain proteostasis (Dutta et al., 2022). It is plausible that these same neuropeptides signaling may additionally regulate animal behaviour. This will provide insight into how the UPR modulates locomotory behaviour in animals. In support of this, both the ER-UPR and HSR appear to influence different types of behaviour in mammals such as memory and foraging (Özbey et al., 2021). However, the impact of neuronal MT-UPR signaling on behaviour in mammals has not been investigated (Özbey et al., 2021). Activation of MT-UPR can promote longevity and better mitochondrial function in animals which may translate to changes in the behaviour of animals (Dutta et al., 2022; Schulz & Haynes, 2015; Wu et al., 2018; Q. Zhang et al., 2018).

Future work can also examine how neuronal expression of the stress response works to adapt the behaviour of animals in response to stress inducing conditions such as chemicals and environmental changes. This can provide a more complete understanding of how the cell non-autonomous signaling of the stress response by neurons alters the behavior of animals in response

to detrimental stimuli. Additionally, it can elucidate which stress response pathways and genes may be critical for behavioural responses to stress. For example, exercise has been shown to activate the stress response and improve electrotaxis response. By utilizing different neuronal overexpression lines of the organelle specific stress responses, we can investigate the specific pathways regulating the stress response in this exercise scenario. This will allow us to understand which stress responses pathways are activated to mediate behaviour under various conditions.

5.3.2 *pqe-1* regulation of the stress response

In addition to examining the effects of exercise we can investigate if a potential gene harnesses a specific stress response pathway to modulate behaviour. One potential candidate is the understudied gene, *pqe-1,* which enhances proteotoxicity in cells and causes neuronal damage impacting the health of animals. Loss of *pqe-1* also activates the stress response and modulates the electrotaxis behaviour of animals. Future work should perform genetic knockdown of *pqe-1* in combination with different transgenic lines which overexpress transcription factors associated with the different stress responses (e.g. XBP-1, HSF-1 and ATFS-1). We can ascertain which stress response pathway can rescue defects in *pqe-1* loss. Additionally, this will provide insight into the pathways which require *pqe-1* to maintain homeostasis and modulate behaviour in animals. It can also give us perspective on how *pqe-1* acts as a regulator of the stress response to promote organismal health.

Electrotaxis presents as a means for monitoring these behavioral adaptations following a multitude of stress response manipulations. Overall, this can allow us to couple the precise stress response tissue signaling with behaviour.

5.4 MANF-1 regulates autophagy and lysosome-mediated proteostasis

My work demonstrates that overexpression of MANF promotes longevity, neuronal health, and maintains proteostasis in *C. elegans* through regulating both the stress response and lysosomal function. Other eukaryotic models have demonstrated that overexpression or supplementation of MANF is cytoprotective (Bai et al., 2018; Eesmaa et al., 2021; S. K. B. Taylor et al., 2024). The work in this chapter sought to elucidate the relationship between MANF/MANF-1 and the UPR and to gain an understanding of its mechanism of action. Furthermore, this chapter demonstrated a novel function of MANF-1 in mediating autophagic flux and its essential role in lysosome-mediated organismal survival.

I observed an age-dependent accumulation in the ER-UPR chaperone *hsp-4* within *manf-1* mutants. The chronic activation of *hsp-4* with age is likely detrimental to animals, which could contribute to the reduced lifespan of *manf-1* mutants (R. C. Taylor & Dillin, 2013). Additionally, this is the first study showing *manf-1* mutants are sensitive to tunicamycin during adulthood, causing reduced lifespan. Larvae of *manf-1* mutants show resistance to tunicamycin, conceivably due to the increased ER-UPR activity due to loss of *manf-1* (Hartman et al., 2019; Richman et al., 2018). Larvae experience increased resistance, but chronic activation of stress response pathways is detrimental to health long-term, as evidenced by the shortened lifespan.

Chapter 3 provides new lines of evidence regarding the genetic interaction between *manf-1* and ER-UPR components (Hartman et al., 2019). Loss of *manf-1* caused an age-dependent increase in α-Synuclein aggregation, which was exacerbated by loss of ER-UPR components. Chronic activation of the ER-UPR is a contributing factor in the age-dependent protein aggregation of *manf-1* mutants. Consistent with this, I demonstrated that loss of *manf-1* enhances polyQ aggregation in HD disease models in *C. elegans.* Additionally, knockdown of MANF is reported to enhance amyloidβ toxicity, a hallmark of AD (S. Xu et al., 2019). These data support the potential role of MANF in multiple neurodegenerative diseases to reduce aggregation of misfolded proteins. My results also demonstrate that MANF-1 overexpression reduces the accumulation of misfolded proteins in different neurodegenerative models. Furthermore, this beneficial effect of overexpression of MANF-1 extends to protection of DA neurons, reduces ER stress, and extends lifespan in *C. elegans.* Thus MANF-1 likely functions to confer protective benefits in whole body maintenance, not just in neuroprotection. MANF therefore represents a potential therapeutic target for promoting whole organism survival *in vivo*.

5.4.1 MANF-1 Expression Pattern

Knowing that MANF-1 has a role in maintaining multiple aspects of health in the entire organism, elucidating its mechanism became more crucial. We investigated this by examining whole animal protein expression pattern of MANF-1. We observed that it is strongly expressed within the pharynx, hypodermis, intestine, muscles, and also possesses a previously uncharacterized localization to the coelomocytes. Interestingly, the localization pattern of MANF-1 varied depending on the presence of the ER retention signal. However, the removal of the ER retention signal results in MANF-1 predominantly localizing to the hypodermis, coelomocytes,

and pharynx. Despite this, the ER retention is not required for MANF-1 to elicit its cytoprotective function.

At a subcellular level we also observed localization of MANF-1 to the lysosomal membrane. This is the first time MANF-1 has been reported to have a role in lysosomal function. In support of this, RNAseq data analyzing differentially expressed genes in both *manf-1* mutants and *manf-1* overexpression contained several enriched terms, one being lysosomal function. Some of the enriched genes were proteases, which are required for lysosomal protein degradation (Saftig & Puertollano, 2021). In particular, MANF-1 increased an aspartyl protease, *asp-12,* by roughly 20-fold (**Figure A2**). Increases in lysosomal proteases can aid in the protection against misfolded proteins (Imanikia, Özbey, et al., 2019). This suggests that the native role of MANF-1 is likely to promote cellular proteostasis.

5.4.2 Potential Mechanism of MANF-1: How and why is it going to lysosomes?

By localizing to the lysosomes MANF-1 stimulates autophagy and lysosomal function, reducing toxic protein aggregation. The research in **Chapter 3** revealed a potential mechanism for "how" MANF-1 localizes to lysosomes. I found that MANF-1 utilizes the endo-lysosomal pathway to reach the lysosomal surface. Specifically, the RAB proteins *rab-5* and *rab-7* are involved in the translocation of MANF-1 to lysosomes. In support of the role of MANF in lysosomes, I observed that MANF-1 overexpression causes TFEB/HLH-30 (the main transcriptional regulator of autophagy and lysosomal biogenesis) to move from the cytoplasm to the nucleus. We found that this translocation is essential for the lifespan benefits and neuroprotection conferred by MANF-1.

Altogether, this data illustrates a novel model for the mechanism of action of MANF-1. As a regulator of the UPR, MANF-1 starts within the ER but gets secreted out to target cells to be beneficial, leading to its lysosomal localization. Activated MANF-1 appears to regulate lysosomal function and is not just a regulator of ER stress. This model for MANF-1 addresses some of the existing questions for its mode of action. It provides a missing link for what MANF-1 does when it localizes to target cells to execute a protective function. Furthermore, it broadens our areas of investigation for identifying either a bonafide receptor of MANF-1 or multiple receptors that are context dependent for MANF-1 binding. Additionally, this study presents novel regions of exploration for the role of MANF-1 in stress response regulation.

In summary, MANF may utilize the lysosome as a signaling hub to execute its cytoprotective function. This chapter provides the basis for the idea that MANF is more than a neurotrophic

factor, and enhances our knowledge of its mechanism of action in diverse tissues and gene regulatory networks.

5.5 The Future of MANF

5.5.1 Tissue specific role of MANF

Despite MANF being expressed in many tissues, the bulk of existing research has focused on its protective role within neurons. However, recent work has begun analyzing the broad requirements of MANF within different tissues such as kidneys and muscles (Danilova et al., 2019; Neves et al., 2016; Peled et al., 2021; Sousa-Victor et al., 2019). As more than an NTF, **Chapter 3** demonstrated the broad expression pattern of MANF which suggests it functions in multiple tissues. Future work should examine the tissue specific regulation and function of MANF. Follow up to this discovery can revolve around the following question: Do specific tissues have different requirements of MANF expression level?

Using tissue specific promoters such as those expressed in the coelomocytes, hypodermis, intestine, muscles, and neurons we can specifically overexpress MANF in these tissues. This will allow us to examine if tissue specific overexpression of MANF in wildtype animals is sufficient to promote longevity, proteostasis, neuronal health, and maintenance of the stress response with age. We can examine if tissue specific MANF expression mediates UPR activity of organelle specific chaperones such as *hsp-4* (ER), *hsp-6* (mitochondria), and *hsp-16.2* (cytosolic). Furthermore, we can investigate a cell non-autonomous mechanism for the requirements of MANF to regulate the stress response in animals. This could involve either tissue specific knockdown or overexpression of MANF and would provide detailed analysis of how MANF regulates the ER-UPR in different tissues. These experiments will provide answers regarding the requirements of MANF in a tissue dependent manner.

5.5.2 Organelle specific requirements of MANF-1

MANF is an ER resident protein which is secreted to other tissues to serve a protective function (Jäntti & Harvey, 2020). My work suggests that MANF begins in the ER and is eventually shuttled to the lysosomal membrane to promote proteostasis (**Chapter 3)**. Interestingly, the ER protein ATF-6 can stimulate mitochondrial function, which ultimately leads to longevity in animals (Burkewitz et al., 2020). It remains to be explored if MANF can affect mitochondrial function. Chapter 3 shows that MANF plays a role in autophagy and recent work shows that MANF regulates proteins involved in mitophagy (Y. Kim et al., 2023). Using different conditions

such as genetic or chemical disruption of the electron transport chain which are known to damage mitochondria and activate the MT-UPR, we can ascertain if MANF protects against mitochondrial dysfunction through clearance of damaged mitochondria. It is worth examining if after different chemical insults loss of *manf-1* accelerates the damage to the mitochondria, similarly to how it accelerates neurodegeneration in animals (Richman et al., 2018). Additionally, it remains to be explored if MANF can interact with the cytosolic HSR to promote organismal health. We can examine if loss or overexpression of HSF-1 will reduce *hsp-4* chaperone activity in MANF-1, and the impact that will have on survival.

Chapter 3 demonstrates that *manf-1* affects lysosome number and function. However, the conditions under which MANF acts to maintain lysosomal homeostasis can be further explored. To this end, we can attempt to block entry of MANF to lysosomes through genetic or chemical inhibition and examine the health of animals. We can knockdown different genetic components of the endosomal pathway or use chloroquine which blocks autophagosome fusion to lysosome (Mauthe et al., 2018). We can also inhibit the function of calcium channel proteins or VATPases on the lysosome membrane to examine changes in MANF cytoprotective capabilities, and potentially its localization. An RNAi screen can be conducted to examine endo-lysosomal components that may inhibit the lysosomal localization of MANF and potentially the proteostasis benefits conferred by MANF overexpression. These experiments will allow us to elucidate what other components of the trafficking system MANF utilizes.

Overall, these experiments can provide insight into the different organelles that may require MANF for maintenance and function. Furthermore, the above experiments highlight the different biological processes MANF uses to promote organismal health through organelle crosstalk.

5.5.3 Receptors of MANF

NTFs are known to bind to specific receptors (Ibáñez, 1998), however no specific receptor for MANF has been identified to date. It has been reported that MANF may bind to NPTN and the IRE1 receptor, which are involved in the inflammatory response and ER-UPR activity respectively (Kovaleva et al., 2023; Yagi et al., 2020). These studies report that MANF requires these receptors to be protective in the cell (Kovaleva et al., 2023; Yagi et al., 2020). The necessity of these receptors for the function of MANF has yet to be confirmed within *C. elegans. C. elegans* appear to lack an NPTN receptor, which suggests the existence of a potentially unidentified MANF-binding receptor. However, the IRE1 receptor is conserved within *C. elegans.* Due to the level of

conservation in the function of MANF between species, it is expected that the IRE1 receptor would play a similar role in *C. elegans*. It should be noted that worms with mutations in both *ire-1* and *manf-1* exhibit larval lethality. However, it remains to be examined if inhibiting *ire-1* function in MANF-1 overexpression worms can impede MANF localization and its cytoprotective abilities within *C. elegans.*

The aforementioned receptors, however, may not be able explain the broad role of MANF across an organism in regulating cellular processes. It is possible that MANF may have multiple binding receptors. Using the fluorescent constructs of MANF-1 that I have created, we can perform biochemical analysis to pull down protein complexes of MANF and potentially identify other receptors and interacting partners. These strains could also be used to perform a genetic screen for potential receptors that block or shift MANF localization and examine their impact on organismal health.

Chapter 3 demonstrated that without the KDEL signal, MANF overexpression is still beneficial. It would be interesting to analyze the binding affinity of the KDEL receptors within *C. elegans*. Previous research showed that MANF trafficking involved KDEL receptors and its paralog CDNF also binds to KDEL receptors at the cell membrane (Henderson et al., 2013; Maciel et al., 2021). Future analysis can investigate if overexpression of KDEL receptors can affect MANF trafficking by retaining MANF within the ER, potentially inhibiting its ability to affect the health of animals. Analysis of novel receptors for MANF should also focus on looking at its interaction with lysosome transmembrane proteins. Taken together, the above experiments would allow us to further understand what signaling components MANF activates to facilitate its lysosomal function and be cytoprotective.

5.5.4 Transcriptional Regulation of MANF

Future work on MANF should investigate novel transcriptional regulators HLH-30 and AP-1 transcription factors. My data described in **Chapter 3.3 (micropublication)** and other published studies show that AP-1 transcription factors can regulate the expression of MANF-1 following pharmacological induction (Abu-Hijleh et al., 2020; C. H. Wang et al., 2018). The ER transmembrane protein ATF6 is part of the AP-1 transcription factor family and is a transcriptional regulator of MANF-1, similar to XBP1 (Oh-Hashi et al., 2013; D. Wang et al., 2018). A follow-up investigation for the transcriptional regulation of MANF could involve assessing the

requirements of AP1 family members in mediating the stress response regulation of MANF and its protective benefits.

One can also consider a potential complex signaling cascade involving XBP-1, HLH-30, and MANF-1. Similar to MANF-1 overexpression, neuronal overexpression of XBP-1 causes TFEB/HLH-30 nuclear localization, ultimately causing expression of genes involved in lysosomal biogenesis and function (Imanikia, Özbey, et al., 2019). One of these lysosomal genes could be MANF-1, which is also induced by XBP-1. This interaction suggests that MANF-1 may be regulated by different transcription factors under different conditions. Does ER-stress cause transcription of MANF by XBP-1? Does lysosomal stress cause transcription of MANF by HLH-30? To this end, future experiments should examine the binding affinity of XBP1 and HLH-30 with MANF under basal conditions and stress inducing conditions. Using ER stress-inducing drugs such as tunicamycin and thapsigargin, or drugs which inhibit lysosome function such as bafilomycin or chloroquine we can examine the binding affinity of XBP-1 and HLH-30 to MANF. This would allow us to examine the conditions required for transcriptional regulation of MANF, advancing our understanding of its function. Genetic interaction experiments can also be used to examine if either XBP-1 or HLH-30 preferentially regulates MANF under specific stress-inducing conditions to maintain cellular health.

5.5.5 MANF interacting proteins

There are several lysosomal membrane protein complexes (Saftig & Puertollano, 2021) which MANF-1 could conceivably utilize to regulate a lysosomal stress response to maintain proteostasis. The identification of MANF on the lysosome membrane has opened the door for various potential interacting partners. Proteins such as MTOR, AMPK, and calcium channel pumps are also found on the lysosome membrane (Napolitano & Ballabio, 2016; Saftig & Puertollano, 2021). Assessing the interaction of MANF with these proteins can provide further evidence for how MANF is able to cause nuclear localization of TFEB/HLH-30. Using a combination of fluorescent colocalization and biochemical analysis such as mCherry pulldown, co-immunoprecipitation, and mass spectrometry, we can determine potential binding partners of MANF. Additionally, membrane proteins such as VATPases and calcium channels are also potential areas of binding for MANF, especially considering that MANF is activated in response to calcium efflux (Glembotski et al., 2012). Additionally, I propose that performing genetic

knockdown of AMPK, MTOR components, or calcium channel pumps in MANF overexpression animals will allow us to examine their role in MANF mediated cytoprotection.

5.5.6 The interaction between MANF and Axin/PRY1

Another potential interacting partner of MANF-1 is the *C. elegans* Axin homolog *pry-1*. Axin/PRY1 is expressed in many tissues and is well studied in our research group (Mallick et al., 2019, 2020, 2022). Research on Axin has shown that it acts as a scaffolding protein on the lysosome membrane (Saftig & Puertollano, 2021). This localization points to the possibility of a MANF-1 interaction with Axin at the lysosomal surface. Additionally, preliminary work in **Appendix E** shows that *pry-1* mutants have reduced *manf-1* expression (Mallick et al., 2019). MANF-1 overexpression partially rescues the defect of *pry-1* mutants, extending lifespan, and improving the neuronal health of these animals (**Figure C1**).

Colocalization analysis of MANF-1 and AXIN/PRY-1 should be performed to determine if these two proteins are co-expressed in multiple tissues, and also if they localize together on the lysosomal membrane. Future work should also examine if MANF-1 overexpression can reduce the detrimental activation of the stress response within *pry-1* mutants or *vice versa*. This will allow us to build a model defining the role of these two proteins which regulate the stress response and promote health by acting together. Additionally, utilizing transcriptomic datasets between these two proteins can identify candidate genes that might be commonly regulated between MANF-1 and PRY-1. Such genes could then be analyzed to explore how MANF-1 and PRY-1 act to maintain organismal fitness and regulate the stress response. This will further build the interaction network between MANF-1 and PRY-1, two proteins which can be beneficial to organismal health.

5.5.7 Potential role of MANF in proteasomal degradation

The collapse of proteostasis is hallmark of aging. When proteostasis cannot be achieved proteins are targeted for degradation. This can occur via the ubiquitin proteasome system (UPS) and autophagy. These are the two main protein degradation pathways in the cell. Current research on MANF demonstrates its role in the autophagy pathway (**Chapter 3**), but the UPS remains to be explored. Currently, fluorescent transgenic strains in *C. elegans* exist which allow us to monitor the rate of proteasomal degradation with age based on fluorescent protein accumulation. Using this tool, we can study how loss and overexpression of MANF impacts proteasomal degradation as animals age. Preliminary data in **Appendix A** shows that MANF overexpression upregulates *rpn-6.1,* a component of the 26S/30S proteasome (**Figure A2**). Overexpression of *rpn-6.1* increases proteasome activity, extends lifespan and reduces protein aggregation in animals

(Vilchez et al., 2012). Genetic interactions can be used to study if MANF requires *rpn-6.1* or other components of the UPS system for survival or reducing protein aggregation. Furthermore, we can examine the impact of UPS components on MANF expression and localization. The study of the UPS will allow us to determine the existence of additional processes that MANF uses to clear the cell of protein aggregates.

5.6 MANF-1 causes age dependent decline in muscle function

The results of **Chapter 3** demonstrate that MANF-1 is localized to many tissues, including muscles. RNA seq analysis in **Chapter 4** found that MANF-1 regulates a subset of muscle genes that are known to be upregulated following exercise (Laranjeiro et al., 2019). Maintaining muscle function as we age is associated with longevity in animals (Campos et al., 2023; Laranjeiro et al., 2019). The results in **Chapter 4** provide the first evidence of the requirements of *C. elegans* MANF-1 to maintain muscle morphology and function with age.

By examining different markers of muscle health in worms, we observed that loss of MANF-1 causes muscle dysfunction in an age-dependent manner. The loss of MANF-1 reduced the burrowing capacity in an age-dependent manner but increased the thrashing ability of day 1 adults compared to WT. However, by day 7 of adulthood they were worse than WT, notably thrashing less. The unexpected thrashing behaviour on day 1 could result from an elevation in ER-UPR activity due to the loss of MANF-1. Once correctly regulated the high ER-UPR may be beneficial to animals in a transient manner, but chronic activation is to the detriment of the animal. The work in **Chapter 4** observed a novel phenomenon, in that *manf-1* mutants retain tubular mitochondrial muscle morphology with age. Tubular morphology suggests that these animals have functional mitochondria and good muscle function (Hartman et al., 2018; Laranjeiro et al., 2019). However, this appears to not be the case due to the decline in muscle function of *manf-1* mutants. It is possible that we are observing an accumulation of mitochondria. Research in **Chapter 3** demonstrated that MANF-1 regulates autophagy. It is possible that MANF-1 may regulate the selective autophagy process of mitophagy (Galluzzi et al., 2017) and is required for efficient clearing of dysfunctional mitochondria.

These analyses provide a basis for age-dependent requirements of MANF-1 to maintain muscle health. My studies in *C. elegans* complement recent research showing that MANF is also required for skeletal muscle repair in young mice (Sousa et al., 2023). Sousa *et al.* (2023) also demonstrated that supplementation of MANF in aged mice can restore muscle health following

impairment (Sousa et al., 2023). Together, these results highlight not only the cytoprotective capability and requirements of MANF at different stages in animals but also the therapeutic potential from modulating MANF expression. Based on my findings and current research we believe MANF is a suitable intervention target for the improvement of muscles as we age.

5.7 The Future of MANF in muscle health maintenance

5.7.1 Does MANF-1 have a muscle specific role?

This section provides a detailed discussion of future work to investigate the effect of MANF on muscle function. It presents an opportunity to examine the muscle-specific roles and requirements of MANF in animals. To address this question, both muscle specific RNAi and muscle specific overexpression should be utilized to analyze how changes in MANF expression impact the muscle health of animals. Using a muscle specific promoter we can create a muscular overexpression of MANF-1 in *C. elegans.* Following this we can examine how stress response genes such as *hsp-4, hsp-6,* and *hsp-16.2* are regulated by tissue specific MANF expression (as **described in 5.5.1**). A similar experiment can be performed using a muscle specific knockdown of MANF. Furthermore, we can examine how MANF impacts the body wall muscle fibers of animals in an age-dependent manner. Data in **Chapter 4** demonstrates that loss of MANF causes an age-dependent decline in neuromuscular health. Muscle specific overexpression of MANF may be able to rescue the age dependent decline in muscle health of *manf-1* mutants.

Chapter 4 shows that MANF is distributed in spherical puncta throughout the muscle mitochondria in animals. These are likely to be lysosomes in muscle cells. Future experiments using lysosome staining should aim to confirm if MANF also localizes to the lysosomes of muscles. Interestingly, lysosomes were one of the cellular component GO terms that were enriched in macrophages taken from muscles deficient in MANF (Sousa et al., 2023). Lysosomes are a central signaling hub that can act as a platform for several signaling molecules including AMPK (Saftig & Puertollano, 2021). AMPK is a sensor of energy levels and is known to improve muscle health and function in animals (Campos et al., 2023; Saftig & Puertollano, 2021). The genetic interaction between MANF and AMPK can be examined to determine if AMPK overexpression can rescue the muscle defects exhibited by *manf-1* mutants.

Overall, this analysis can provide a better understanding of the different processes that MANF may utilize to maintain muscle health in animals.

5.8 Concluding Remarks

The research that I have completed throughout my Ph.D. tenure has addressed gaps in our understanding of the effect of the stress response on behaviour and stress regulating proteins such as MANF. MANF is integral for regulating the stress response and proteostasis to ensure the survival of organisms. The data presented in this thesis builds a stronger connection between MANF and different processes that regulate the stress response. These results further emphasize the novel roles of MANF in lysosome trafficking and signaling, tissue-to-tissue communication, and its potential interacting partners. Additionally, this work highlights the involvement of MANF in other disease processes through regulation of the stress response. The extensive characterization of MANF in *C. elegans* provides a strong base for further experiments in *C. elegans* and other model systems to look at the novel regulatory networks that I have presented in this thesis. Understanding the detailed mechanism of action of MANF could assist with the development of novel therapeutics to prevent or attenuate age-related disorders. From originally being described as exclusively a neurotrophic factor, to a UPR regulator gene, and now a potential mediator of lysosomal function, our understanding of MANF has grown dramatically. Due to its all-encompassing function within the cell, it is evident that MANF is more than a neurotrophic factor. By leveraging knowledge of MANF, the stress response and overall proteostasis, there is an opportunity to develop novel therapeutics to enhance human health and our standard of living throughout our lifespan.

Bibliography

Abu-Hijleh, F. A., Prashar, S., Joshi, H., Sharma, R., Frey, B. N., & Mishra, R. K. (2020). Novel mechanism of action for the mood stabilizer lithium. *Bipolar Disorders*, 1–8. https://doi.org/10.1111/bdi.13019

Airavaara, M., Shen, H., Kuo, C.-C., Peranen, J., Sarma, M., Hoffer, B., & Wang, Y. (2009). *mesencephalic astrocyte-derived neurotrophic factor (MANF) reduces ischemic brain injury and promotes behavioral recovery in rats*. *515*(1), 116–124. https://doi.org/10.1002/cne.22039.Mesencephalic

Apostolou, A., Shen, Y., Liang, Y., Luo, J., & Fang, S. (2008). Armet, a UPR-upregulated protein, inhibits cell proliferation and ER stress-induced cell death. *Experimental Cell Research*, *314*(13), 2454–2467. https://doi.org/10.1016/j.yexcr.2008.05.001

Appenzeller-Herzog, C., & Hall, M. N. (2012). Bidirectional crosstalk between endoplasmic reticulum stress and mTOR signaling. *Trends in Cell Biology*, *22*(5), 274–282. https://doi.org/10.1016/J.TCB.2012.02.006

Bai, M., Vozdek, R., Hnízda, A., Jiang, C., Wang, B., Kuchar, L., Li, T., Zhang, Y., Wood, C., Feng, L., Dang, Y., & Ma, D. K. (2018). Conserved roles of C. elegans and human MANFs in sulfatide binding and cytoprotection. *Nature Communications*, *9*(1), 1–11. https://doi.org/10.1038/s41467-018-03355-0

Bennett, C. F., Vander Wende, H., Simko, M., Klum, S., Barfield, S., Choi, H., Pineda, V. V., & Kaeberlein, M. (2014). Activation of the mitochondrial unfolded protein response does not predict longevity in Caenorhabditis elegans. *Nature Communications*, *5*(3483), 1–10. https://doi.org/10.1038/ncomms4483

Burkewitz, K., Feng, G., Dutta, S., Kelley, C. A., Steinbaugh, M., Cram, E. J., & Mair, W. B. (2020). Atf-6 Regulates Lifespan through ER-Mitochondrial Calcium Homeostasis. *Cell Reports*, *32*(10), 108125. https://doi.org/10.1016/j.celrep.2020.108125

Cabral-Miranda, F., & Hetz, C. (2017). ER stress in neurodegenerative disease: from disease mechanisms to therapeutic interventions. *Endoplasmic Reticulum Stress in Diseases*, *4*(1), 11–26. https://doi.org/10.1515/ersc-2017-0002

Caldwell, K. A., Willicott, C. W., & Caldwell, G. A. (2020). Modeling neurodegeneration in Caenorhabditis elegans. *DMM Disease Models and Mechanisms*, *13*(10). https://doi.org/10.1242/dmm.046110

Campos, J. C., Bozi, L. H. M., Krum, B., Bechara, L. R. G., Ferreira, N. D., Arini, G. S., Albuquerque, R. P., Traa, A., Ogawa, T., van der Bliek, A. M., Beheshti, A., Chouchani, E. T., Van Raamsdonk, J. M., Blackwell, T. K., & Ferreira, J. C. B. (2023). Exercise preserves physical fitness during aging through AMPK and mitochondrial dynamics. *Proceedings of the National Academy of Sciences of the United States of America*, *120*(2), e2204750120.

Chen, Y. C., Sundvik, M., Rozov, S., Priyadarshini, M., & Panula, P. (2012). MANF regulates dopaminergic neuron development in larval zebrafish. *Developmental Biology*, *370*(2), 237–249. https://doi.org/10.1016/j.ydbio.2012.07.030

Chmielarz, P., & Saarma, M. (2020). Neurotrophic factors for disease-modifying treatments of Parkinson's disease: gaps between basic science and clinical studies. In *Pharmacological Reports* (Vol. 72, Issue 5, pp. 1195–1217). Springer. https://doi.org/10.1007/s43440-020-00120-3

Corsi, A. K., Wightman, B., & Chalfie, M. (2015). A Transparent window into biology : A primer on Caenorhabditis elegans. *WormBook*, *200*(2), 1–31. https://doi.org/10.1895/wormbook.1.177.1

Danilova, T., Belevich, I., Li, H., Palm, E., Jokitalo, E., Otonkoski, T., & Lindahl, M. (2019). MANF Is Required for the Postnatal Expansion and Maintenance of Pancreatic b-Cell Mass in Mice. *Diabetes*, *68*, 66–80. https://doi.org/10.2337/db17-1149

Dong, G., Liu, Y., Zhang, L., Huang, S., Ding, H. F., & Dong, Z. (2015). mTOR contributes to ER stress and associated apoptosis in renal tubular cells. *American Journal of Physiology - Renal Physiology*, *308*(3), F267. https://doi.org/10.1152/AJPRENAL.00629.2014

Dong, Y., Zhang, M., Liang, B., Xie, Z., Zhao, Z., Asfa, S., Choi, H. C., & Zou, M. H. (2010). Reduction of AMP-activated Protein Kinase Alpha 2 Increases Endoplasmic Reticulum Stress and Atherosclerosis In Vivo. *Circulation*, *121*(6), 792. https://doi.org/10.1161/CIRCULATIONAHA.109.900928

Douglas, P. M., Baird, N. A., Simic, M. S., Uhlein, S., McCormick, M. A., Wolff, S. C., Kennedy, B. K., & Dillin, A. (2015). Heterotypic Signals from Neural HSF-1 Separate Thermotolerance from Longevity. *Cell Reports*, *12*(7), 1196–1204. https://doi.org/10.1016/J.CELREP.2015.07.026

Ducray, A., Krebs, S. H., Schaller, B., Seiler, R. W., Meyer, M., & Widmer, H. R. (2006). GDNF family ligands display distinct action profiles on cultured GABAergic and serotonergic neurons of rat ventral mesencephalon. *Brain Research*, *1069*(1), 104–112. https://doi.org/10.1016/j.brainres.2005.11.056

Durieux, J., Wolff, S., & Dillin, A. (2011). The cell-non-autonomous nature of electron transport chain-mediated longevity. *Cell*, *144*(1), 79–91. https://doi.org/10.1016/j.cell.2010.12.016

Dutta, N., Garcia, G., & Higuchi-Sanabria, R. (2022). Hijacking Cellular Stress Responses to Promote Lifespan. *Frontiers in Aging*, *3*(March), 1–21. https://doi.org/10.3389/fragi.2022.860404

Eesmaa, A., Yu, L. Y., Göös, H., Nõges, K., Kovaleva, V., Hellman, M., Zimmermann, R., Jung, M., Permi, P., Varjosalo, M., Lindholm, P., & Saarma, M. (2021). The cytoprotective protein MANF promotes neuronal survival independently from its role as a GRP78 cofactor. *Journal of Biological Chemistry*, *296*, 100295. https://doi.org/10.1016/j.jbc.2021.100295

Fiorese, C. J., Schulz, A. M., Lin, Y. F., Rosin, N., Pellegrino, M. W., & Haynes, C. M. (2016). The Transcription Factor ATF5 Mediates a Mammalian Mitochondrial UPR. *Current Biology*, *26*(15), 2037–2043. https://doi.org/10.1016/j.cub.2016.06.002

Frakes, A. E., Metcalf, M. G., Tronnes, S. U., Bar-Ziv, R., Durieux, J., Gildea, H. K., Kandahari, N., Monshietehadi, S., & Dillin, A. (2020). Four glial cells regulate ER stress resistance and

longevity via neuropeptide signaling in C. elegans. *Science*, *367*(6476), 436–440. https://doi.org/10.1126/SCIENCE.AAZ6896

Galluzzi, L., Baehrecke, E. H., Ballabio, A., Boya, P., Bravo-San Pedro, J. M., Cecconi, F., Choi, A. M., Chu, C. T., Codogno, P., Colombo, M. I., Cuervo, A. M., Debnath, J., Deretic, V., Dikic, I., Eskelinen, E., Fimia, G. M., Fulda, S., Gewirtz, D. A., Green, D. R., … Kroemer, G. (2017). Molecular definitions of autophagy and related processes. *The EMBO Journal*, *36*(13), 1811–1836. https://doi.org/10.15252/embj.201796697

Gildea, H. K., Frankino, P. A., Tronnes, S. U., Pender, C. L., Durieux, J., Dishart, J. G., Choi, H. O., Hunter, T. D., Cheung, S. S., Frakes, A. E., Sukarto, E., Wickham, K., & Dillin, A. (2022). Glia of C. elegans coordinate a protective organismal heat shock response independent of the neuronal thermosensory circuit. *Science Advances*, *8*(49). https://doi.org/10.1126/SCIADV.ABQ3970

Glembotski, C. C., Thuerauf, D. J., Huang, C., Vekich, J. A., Gottlieb, R. A., & Doroudgar, S. (2012). Mesencephalic astrocyte-derived neurotrophic factor protects the heart from ischemic damage and is selectively secreted upon sarco/endoplasmic reticulum calcium depletion. *Journal of Biological Chemistry*, *287*(31), 25893–25904. https://doi.org/10.1074/jbc.M112.356345

Gomez-Pastor, R., Burchfiel, E. T., & Thiele, D. J. (2018). Regulation of heat shock transcription factors and their roles in physiology and disease. In *Nature Reviews Molecular Cell Biology* (Vol. 19, Issue 1, pp. 4–19). Nature Publishing Group. https://doi.org/10.1038/nrm.2017.73

Hajdu-Cronin, Y. M., Chen, W. J., & Sternberg, P. W. (2004). The L-type cyclin CYL-1 and the heat-shock-factor HSF-1 are required for heat-shock-induced protein expression in Caenorhabditis elegans. *Genetics*, *168*(4), 1937–1949. https://doi.org/10.1534/genetics.104.028423

Hartman, J. H., Richie, C. T., Gordon, K. L., Mello, D. F., Castillo, P., Zhu, A., Wang, Y., Hoffer, B. J., Sherwood, D. R., Meyer, J. N., & Harvey, B. K. (2019). MANF deletion abrogates early larval Caenorhabditis elegans stress response to tunicamycin and Pseudomonas aeruginosa. *European Journal of Cell Biology*, *98*(5–8), 1–12. https://doi.org/10.1016/j.ejcb.2019.05.002

Hartman, J. H., Smith, L. L., Gordon, K. L., Laranjeiro, R., Driscoll, M., Sherwood, D. R., & Meyer, J. N. (2018). Swimming Exercise and Transient Food Deprivation in Caenorhabditis elegans Promote Mitochondrial Maintenance and Protect Against Chemical-Induced Mitotoxicity. *Scientific Reports*, *8*(1). https://doi.org/10.1038/s41598-018-26552-9

Hellman, M., Arumäe, U., Yu, L. Y., Lindholm, P., Peränen, J., Saarma, M., & Permi, P. (2011). Mesencephalic astrocyte-derived neurotrophic factor (MANF) has a unique mechanism to rescue apoptotic neurons. *Journal of Biological Chemistry*, *286*(4), 2675–2680. https://doi.org/10.1074/jbc.M110.146738

Henderson, M. J., Richie, C. T., Airavaara, M., Wang, Y., & Harvey, B. K. (2013). Mesencephalic astrocyte-derived neurotrophic factor (MANF) secretion and cell surface binding are modulated by KDEL receptors. *Journal of Biological Chemistry*, *288*(6), 4209–

4225. https://doi.org/10.1074/jbc.M112.400648

Henis-Korenblit, S., Zhang, P., Hansen, M., McCormick, M., Lee, S. J., Cary, M., & Kenyon, C. (2010). Insulin/IGF-1 signaling mutants reprogram ER stress response regulators to promote longevity. *Proceedings of the National Academy of Sciences of the United States of America*, *107*(21), 9730–9735. https://doi.org/10.1073/pnas.1002575107

Hetz, C., & Saxena, S. (2017). ER stress and the unfolded protein response in neurodegeneration. *Nature Reviews Neurology*, *13*(8), 477–491. https://doi.org/10.1038/nrneurol.2017.99

Hetz, C., Zhang, K., & Kaufman, R. J. (2020). Mechanisms, regulation and functions of the unfolded protein response. *Nature Reviews Molecular Cell Biology*, *21*(8), 421–438. https://doi.org/10.1038/s41580-020-0250-z

Higuchi-Sanabria, R., Frankino, P. A., Paul, J. W., Tronnes, S. U., & Dillin, A. (2018). A Futile Battle? Protein Quality Control and the Stress of Aging. *Developmental Cell*, *44*(2), 139–163. https://doi.org/10.1016/j.devcel.2017.12.020

Huttunen, H. J., Booms, S., Sjögren, M., Kerstens, V., Johansson, J., Holmnäs, R., Koskinen, J., Kulesskaya, N., Fazio, P., Woolley, M., Brady, A., Williams, J., Johnson, D., Dailami, N., Gray, W., Levo, R., Saarma, M., Halldin, C., Marjamaa, J., … Svenningsson, P. (2023). Intraputamenal Cerebral Dopamine Neurotrophic Factor in Parkinson's Disease: A Randomized, Double-Blind, Multicenter Phase 1 Trial. *Movement Disorders*, *38*(7), 1209–1222. https://doi.org/10.1002/MDS.29426

Ibáñez, C. F. (1998). Emerging themes in structural biology of neurotrophic factors. *Trends in Neurosciences*, *21*(10), 438–444. https://doi.org/10.1016/S0166-2236(98)01266-1

Imanikia, S., Özbey, N. P., Krueger, C., Casanueva, M. O., & Taylor, R. C. (2019). Neuronal XBP-1 Activates Intestinal Lysosomes to Improve Proteostasis in C. elegans. *Current Biology*, *29*, 2322–2338. https://doi.org/10.1016/j.cub.2019.06.031

Imanikia, S., Sheng, M., Castro, C., Griffin, J. L., & Taylor, R. C. (2019). XBP-1 Remodels Lipid Metabolism to Extend Longevity. *Cell Reports*, *28*(3), 581-589.e4. https://doi.org/10.1016/j.celrep.2019.06.057

Jovaisaite, V., Mouchiroud, L., & Auwerx, J. (2014). The mitochondrial unfolded protein response, a conserved stress response pathway with implications in health and disease. *Journal of Experimental Biology*, *217*(1), 137–143. https://doi.org/10.1242/jeb.090738

Jäntti, M., & Harvey, B. K. (2020). Trophic activities of endoplasmic reticulum proteins CDNF and MANF. In *Cell and Tissue Research* (Vol. 382, Issue 1, pp. 83–100). Springer Science and Business Media Deutschland GmbH. https://doi.org/10.1007/s00441-020-03263-0

Kenyon, C., Chang, J., Gensch, E., Rudner, A., & Tabtiang, R. (1993). A C. elegans mutant that lives twice as long as wild type. *Nature*, *366*(6454), 461–464. https://doi.org/10.1038/366461a0

Kim, H., Moon, S. Y., Kim, J. S., Baek, C. H., Kim, M., Min, J. Y., & Lee, S. K. (2015). Activation of AMP-activated protein kinase inhibits ER stress and renal fibrosis. *American Journal of Physiology - Renal Physiology*, *308*(3), F226–F236. https://doi.org/10.1152/AJPRENAL.00495.2014/ASSET/IMAGES/LARGE/ZH200415750

60010.JPEG

Kim, J., & Guan, K. L. (2019). mTOR as a central hub of nutrient signalling and cell growth. *Nature Cell Biology*, *21*(1), 63–71. https://doi.org/10.1038/s41556-018-0205-1

Kim, Y., Li, C., Gu, C., Fang, Y., Tycksen, E., Puri, A., Pietka, T. A., Sivapackiam, J., Kidd, K., Park, S. J., Johnson, B. G., Kmoch, S., Duffield, J. S., Bleyer, A. J., Jackrel, M. E., Urano, F., Sharma, V., Lindahl, M., & Chen, Y. M. (2023). MANF stimulates autophagy and restores mitochondrial homeostasis to treat autosomal dominant tubulointerstitial kidney disease in mice. *Nature Communications*, *14*(1), 1–22. https://doi.org/10.1038/s41467-023-42154-0

Kovaleva, V., Yu, L. Y., Ivanova, L., Shpironok, O., Nam, J., Eesmaa, A., Kumpula, E. P., Sakson, S., Toots, U., Ustav, M., Huiskonen, J. T., Voutilainen, M. H., Lindholm, P., Karelson, M., & Saarma, M. (2023). MANF regulates neuronal survival and UPR through its ER-located receptor IRE1α. *Cell Reports*, *42*(2). https://doi.org/10.1016/j.celrep.2023.112066

Lakpa, K. L., Khan, N., Afghah, Z., Chen, X., & Geiger, J. D. (2021). Lysosomal Stress Response (LSR): Physiological Importance and Pathological Relevance. In *Journal of Neuroimmune Pharmacology* (Vol. 16, Issue 2, pp. 219–237). Springer. https://doi.org/10.1007/s11481-021-09990-7

Lamptey, R. N. L., Chaulagain, B., Trivedi, R., Gothwal, A., Layek, B., & Singh, J. (2022). A Review of the Common Neurodegenerative Disorders: Current Therapeutic Approaches and the Potential Role of Nanotherapeutics. *International Journal of Molecular Sciences*, *23*(3). https://doi.org/10.3390/ijms23031851

Lapierre, L. R., De Magalhaes Filho, C. D., McQuary, P. R., Chu, C. C., Visvikis, O., Chang, J. T., Gelino, S., Ong, B., Davis, A. E., Irazoqui, J. E., Dillin, A., & Hansen, M. (2013). The TFEB orthologue HLH-30 regulates autophagy and modulates longevity in Caenorhabditis elegans. *Nature Communications*, *4*. https://doi.org/10.1038/NCOMMS3267

Laranjeiro, R., Harinath, G., Hewitt, J. E., Hartman, J. H., Royal, M. A., Meyer, J. N., Vanapalli, S. A., & Driscoll, M. (2019). Swim exercise in Caenorhabditis elegans extends neuromuscular and gut healthspan, enhances learning ability, and protects against neurodegeneration. *Proceedings of the National Academy of Sciences of the United States of America*, *116*(47), 23829–23839. https://doi.org/10.1073/pnas.1909210116

Lawrence, R. E., & Zoncu, R. (2019). The lysosome as a cellular centre for signalling, metabolism and quality control. *Nature Cell Biology*, *21*(2), 133–142. https://doi.org/10.1038/s41556-018-0244-7

Li, T. Y., Wang, Q., Gao, A. W., Li, X., Sun, Y., Mottis, A., Shong, M., & Auwerx, J. (2023). Lysosomes mediate the mitochondrial UPR via mTORC1-dependent ATF4 phosphorylation. *Cell Discovery*, *9*(1), 92. https://doi.org/10.1038/s41421-023-00589-1

Lindahl, M., Danilova, T., Palm, E., Lindholm, P., Võikar, V., Hakonen, E., Ustinov, J., Andressoo, J. O., Harvey, B. K., Otonkoski, T., Rossi, J., & Saarma, M. (2014). MANF Is Indispensable for the Proliferation and Survival of Pancreatic β Cells. *Cell Reports*, *7*(2), 366–375. https://doi.org/10.1016/j.celrep.2014.03.023

Lindahl, M., Saarma, M., & Lindholm, P. (2017). Unconventional neurotrophic factors CDNF and MANF: Structure, physiological functions and therapeutic potential. *Neurobiology of Disease*, *97*, 90–102. https://doi.org/10.1016/j.nbd.2016.07.009

Lindström, R., Lindholm, P., Kallijärvi, J., Palgi, M., Saarma, M., & Heino, T. I. (2016). Exploring the conserved role of MANF in the unfolded protein response in Drosophila melanogaster. *PLoS ONE*, *11*(3), 1–18. https://doi.org/10.1371/journal.pone.0151550

Lindström, R., Lindholm, P., Kallijärvi, J., Yu, L. ying, Piepponen, T. P., Arumäe, U., Saarma, M., & Heino, T. I. (2013). Characterization of the Structural and Functional Determinants of MANF/CDNF in Drosophila In Vivo Model. *PLoS ONE*, *8*(9). https://doi.org/10.1371/journal.pone.0073928

Lõhelaid, H., Anttila, J. E., Liew, H. K., Tseng, K. Y., Teppo, J., Stratoulias, V., & Airavaara, M. (2022). UPR Responsive Genes Manf and Xbp1 in Stroke. In *Frontiers in Cellular Neuroscience* (Vol. 16, p. 252). Frontiers. https://doi.org/10.3389/fncel.2022.900725

López-Otín, C., Blasco, M. A., Partridge, L., Serrano, M., & Kroemer, G. (2023). Hallmarks of aging: An expanding universe. *Cell*, *186*(2), 243–278. https://doi.org/10.1016/j.cell.2022.11.001

Maciel, L., De Oliveira, D. F., Mesquita, F., Da Silva Souza, H. A., Oliveira, L., Christie, M. L. A., Palhano, F. L., De Carvalho, A. C. C., Nascimento, J. H. M., & Foguel, D. (2021). New cardiomyokine reduces myocardial ischemia/reperfusion injury by PI3K-AKT pathway via a putative KDEL-receptor binding. *Journal of the American Heart Association*, *10*(1), 1–35. https://doi.org/10.1161/JAHA.120.019685

Mair, W., Morantte, I., Rodrigues, A. P. C., Manning, G., Montminy, M., Shaw, R. J., & Dillin, A. (2011). Lifespan extension induced by AMPK and calcineurin is mediated by CRTC-1 and CREB. *Nature*, *470*(7334), 404–408. https://doi.org/10.1038/nature09706

Mallick, A., Ranawade, A., van den Berg, W., & Gupta, B. P. (2020). Axin-Mediated Regulation of Lifespan and Muscle Health in C. elegans Requires AMPK-FOXO Signaling. *IScience*, *23*(12), 101843. https://doi.org/10.1016/j.isci.2020.101843

Mallick, A., Taylor, S. K. B., Mehta, S., & Gupta, B. P. (2022). Cabin1 domain-containing gene picd-1 interacts with pry-1/Axin to regulate multiple processes in Caenorhabditis elegans. *Scientific Reports 2022 12:1*, *12*(1), 1–18. https://doi.org/10.1038/s41598-022-15873-5

Mallick, A., Taylor, S. K. B., Ranawade, A., & Gupta, B. P. (2019). Axin Family of Scaffolding Proteins in Development: Lessons from C. elegans. *Journal of Developmental Biology*, *7*(4), 20. https://doi.org/10.3390/jdb7040020

Martin-Montalvo, A., Mercken, E. M., Mitchell, S. J., Palacios, H. H., Mote, P. L., Scheibye-Knudsen, M., Gomes, A. P., Ward, T. M., Minor, R. K., Blouin, M. J., Schwab, M., Pollak, M., Zhang, Y., Yu, Y., Becker, K. G., Bohr, V. A., Ingram, D. K., Sinclair, D. A., Wolf, N. S., … De Cabo, R. (2013). Metformin improves healthspan and lifespan in mice. *Nature Communications 2013 4:1*, *4*(1), 1–9. https://doi.org/10.1038/ncomms3192

Martínez, G., Duran-Aniotz, C., Cabral-Miranda, F., Vivar, J. P., & Hetz, C. (2017). Endoplasmic reticulum proteostasis impairment in aging. *Aging Cell*, *16*(4), 615–623.

https://doi.org/10.1111/acel.12599

Mauthe, M., Orhon, I., Rocchi, C., Zhou, X., Luhr, M., Hijlkema, K.-J., Coppes, R. P., Engedal, N., Mari, M., & Reggiori, F. (2018). Chloroquine inhibits autophagic flux by decreasing autophagosome-lysosome fusion. *Autophagy*, *14*(8), 1435–1455. https://doi.org/10.1080/15548627.2018.1474314

Mizobuchi, N., Hoseki, J., Kubota, H., Toyokuni, S., Nozaki, J., Naitoh, M., Koizumi, A., & Nagata, K. (2007). ARMET is a Soluble ER Protein Induced by the Unfolded Protein Response via ERSE-II Element. *Cell Structure and Function*, *32*(1), 41–50. https://doi.org/10.1247/csf.07001

Morley, J. F., & Morimoto, R. I. (2004). Regulation of Longevity in Caenorhabditis elegans by Heat Shock Factor and Molecular Chaperones. *Molecular Biology of the Cell*, *15*(2), 657–664. https://doi.org/10.1091/mbc.E03-07-0532

Napolitano, G., & Ballabio, A. (2016). TFEB at a glance. *Journal of Cell Science*, *129*(13), 2475–2481. https://doi.org/10.1242/jcs.146365

Naresh, N. U., & Haynes, C. M. (2019). Signaling and Regulation of the Mitochondrial Unfolded Protein Response. *Cold Spring Harbor Perspectives in Biology*, *11*(6). https://doi.org/10.1101/CSHPERSPECT.A033944

Nargund, A. M., Fiorese, C. J., Pellegrino, M. W., Deng, P., & Haynes, C. M. (2015). Mitochondrial and nuclear accumulation of the transcription factor ATFS-1 promotes OXPHOS recovery during the UPRmt. *Molecular Cell*, *58*(1), 123–133. https://doi.org/10.1016/j.molcel.2015.02.008

Nasrolahi, A., Mahmoudi, J., Akbarzadeh, A., Karimipour, M., Sadigh-Eteghad, S., Salehi, R., & Farhoudi, M. (2018). Neurotrophic factors hold promise for the future of Parkinson's disease treatment: is there a light at the end of the tunnel? *Reviews in the Neurosciences*, *29*(5), 475–489. https://doi.org/10.1515/revneuro-2017-0040

Neves, J., Zhu, J., Sousa-Victor, P., Konjikusic, M., Riley, R., Chew, S., Qi, Y., Jasper, H., & Lamba, D. A. (2016). Immune modulation by MANF promotes tissue repair and regenerative success in the retina. *Science*, *353*(6294). https://doi.org/10.1126/science.aaf3646

O'Brien, D., & Van Oosten-Hawle, P. (2016). Regulation of cell-non-autonomous proteostasis in metazoans. *Essays in Biochemistry*, *60*(2), 133–142. https://doi.org/10.1042/EBC20160006

O'Reilly, L. P., Benson, J. A., Cummings, E. E., Perlmutter, D. H., Silverman, G. A., & Pak, S. C. (2014). Worming our way to novel drug discovery with the Caenorhabditis elegans proteostasis network, stress response and insulin-signaling pathways. *Expert Opinion on Drug Discovery*, *9*(9), 1021–1032. https://doi.org/10.1517/17460441.2014.930125

O'Rourke, E. J., & Ruvkun, G. (2013). MXL-3 and HLH-30 transcriptionally link lipolysis and autophagy to nutrient availability. *Nature Cell Biology 2013 15:6*, *15*(6), 668–676. https://doi.org/10.1038/ncb2741

Oh-Hashi, K., Hirata, Y., & Kiuchi, K. (2013). Transcriptional regulation of mouse mesencephalic astrocyte-derived neurotrophic factor in Neuro2a cells. *Cellular and*

Molecular Biology Letters, *18*(3), 398–415. https://doi.org/10.2478/s11658-013-0096-x

Ottens, F., Franz, A., & Hoppe, T. (2021). Build-UPS and break-downs: metabolism impacts on proteostasis and aging. *Cell Death and Differentiation*, *28*(2), 505. https://doi.org/10.1038/S41418-020-00682-Y

Özbey, N. P., Thompson, M. A., & Taylor, R. C. (2021). The regulation of animal behavior by cellular stress responses. *Experimental Cell Research*, *405*(2), 112720. https://doi.org/10.1016/J.YEXCR.2021.112720

Pakarinen, E., & Lindholm, P. (2023). CDNF and MANF in the brain dopamine system and their potential as treatment for Parkinson's disease. *Frontiers in Psychiatry*, *14*. https://doi.org/10.3389/fpsyt.2023.1188697

Palgi, M., Greco, D., Lindstrom, R., Auvinen, P., & Heino, T. I. (2012). Gene expression analysis of Drosophila Manf mutants reveals perturbations in membrane traffic and major metabolic changes. *BMC Genomics*, *13*(1), 134. https://doi.org/10.1186/1471-2164-13-134

Palgi, M., Lindstrom, R., Peranen, J., Piepponen, T. P., Saarma, M., & Heino, T. I. (2009). Evidence that DmMANF is an invertebrate neurotrophic factor supporting dopaminergic neurons. *Proceedings of the National Academy of Sciences*, *106*(7), 2429–2434. https://doi.org/10.1073/pnas.0810996106

Papadopoli, D., Boulay, K., Kazak, L., Pollak, M., Mallette, F. A., Topisirovic, I., & Hulea, L. (2019). Mtor as a central regulator of lifespan and aging. *F1000Research*, *8*. https://doi.org/10.12688/f1000research.17196.1

Parkash, V., Lindholm, P., Peränen, J., Kalkkinen, N., Oksanen, E., Saarma, M., Leppänen, V.-M. M., & Goldman, A. (2009). The structure of the conserved neurotrophic factors MANF and CDNF explains why they are bifunctional. *Protein Engineering, Design and Selection*, *22*(4), 233–241. https://doi.org/10.1093/protein/gzn080

Peled, M., Bar-Lev, T. H., Talalai, E., Aspitz, H. Z., Daniel-Meshulam, I., Bar, J., Kamer, I., Ofek, E., Mor, A., & Onn, A. (2021). Mesencephalic astrocyte-derived neurotrophic factor is secreted from interferon-γ-activated tumor cells through ER calcium depletion. *PLoS ONE*, *16*(4 April), e0250178. https://doi.org/10.1371/journal.pone.0250178

Petrova, P. S., Raibekas, A., Pevsner, J., Vigo, N., Anafi, M., Moore, M. K., Peaire, A. E., Shridhar, V., Smith, D. I., Kelly, J., Durocher, Y., & Commissiong, J. W. (2003). MANF A New Mesencephalic, Astrocyte-Derived Neurotrophic Factor with Selectivity for Dopaminergic Neurons. *Journal of Molecular Neuroscience*, *20*(February), 173–187. https://doi.org/10.1385/JMN

Popova, N. K., Ilchibaeva, T. V., & Naumenko, V. S. (2017). Neurotrophic factors (BDNF and GDNF) and the serotonergic system of the brain. In *Biochemistry (Moscow)* (Vol. 82, Issue 3, pp. 308–317). Maik Nauka Publishing / Springer SBM. https://doi.org/10.1134/S0006297917030099

Prahlad, V., Cornelius, T., & Morimoto, R. I. (2008). Regulation of the cellular heat shock response in Caenorhabditis elegans by thermosensory neurons. *Science*, *320*(5877), 811–814. https://doi.org/10.1126/science.1156093

Quirós, P. M., Prado, M. A., Zamboni, N., D'Amico, D., Williams, R. W., Finley, D., Gygi, S. P., & Auwerx, J. (2017). Multi-omics analysis identifies ATF4 as a key regulator of the mitochondrial stress response in mammals. *Journal of Cell Biology*, *216*(7), 2027–2045. https://doi.org/10.1083/jcb.201702058

Renko, J. M., Bäck, S., Voutilainen, M. H., Piepponen, T. P., Reenilä, I., Saarma, M., & Tuominen, R. K. (2018). Mesencephalic Astrocyte-Derived Neurotrophic Factor (MANF) Elevates Stimulus-Evoked Release of Dopamine in Freely-Moving Rats. *Molecular Neurobiology*, *55*(8), 6755–6768. https://doi.org/10.1007/s12035-018-0872-8

Richman, C., Rashid, S., Prashar, S., Mishra, R., Selvaganapathy, P. R., & Gupta, B. P. (2018). C. elegans MANF Homolog Is Necessary for the Protection of Dopaminergic Neurons and ER Unfolded Protein Response. *Frontiers in Neuroscience*, *12*(AUG), 1–11. https://doi.org/10.3389/fnins.2018.00544

Saftig, P., & Puertollano, R. (2021). How Lysosomes Sense, Integrate, and Cope with Stress. *Trends in Biochemical Sciences*, *46*(2). https://doi.org/10.1016/j.tibs.2020.09.004

Salminen, A., & Kaarniranta, K. (2012). AMP-activated protein kinase (AMPK) controls the aging process via an integrated signaling network. In *Ageing Research Reviews* (Vol. 11, Issue 2, pp. 230–241). Elsevier. https://doi.org/10.1016/j.arr.2011.12.005

Scheckel, C., & Aguzzi, A. (2018). Prions, prionoids and protein misfolding disorders. *Nature Reviews Genetics*, *19*(7), 405–418. https://doi.org/10.1038/s41576-018-0011-4

Schulz, A. M., & Haynes, C. M. (2015). UPRmt-mediated cytoprotection and organismal aging. In *Biochimica et Biophysica Acta - Bioenergetics* (Vol. 1847, Issue 11, pp. 1448–1456). Elsevier B.V. https://doi.org/10.1016/j.bbabio.2015.03.008

Shpilka, T., & Haynes, C. M. (2018). The mitochondrial UPR: Mechanisms, physiological functions and implications in ageing. In *Nature Reviews Molecular Cell Biology* (Vol. 19, Issue 2, pp. 109–120). https://doi.org/10.1038/nrm.2017.110

Smith, L. L., Ryde, I. T., Hartman, J. H., Romersi, R. F., Markovich, Z., & Meyer, J. N. (2019). Strengths and limitations of morphological and behavioral analyses in detecting dopaminergic deficiency in Caenorhabditis elegans. *NeuroToxicology*. https://doi.org/10.1016/j.neuro.2019.07.002

Sousa-Victor, P., Jasper, H., & Neves, J. (2018). Trophic factors in inflammation and regeneration: The role of ManF and CDNF. *Frontiers in Physiology*, *9*(NOV), 1–9. https://doi.org/10.3389/fphys.2018.01629

Sousa-Victor, P., Neves, J., Cedron-Craft, W., Ventura, P. B., Liao, C. Y., Riley, R. R., Soifer, I., van Bruggen, N., Kolumam, G. A., Villeda, S. A., Lamba, D. A., & Jasper, H. (2019). MANF regulates metabolic and immune homeostasis in ageing and protects against liver damage. *Nature Metabolism 2019 1:2*, *1*(2), 276–290. https://doi.org/10.1038/s42255-018-0023-6

Sousa, N. S., Brás, M. F., Antunes, I. B., Lindholm, P., Neves, J., & Sousa-Victor, P. (2023). Aging disrupts MANF-mediated immune modulation during skeletal muscle regeneration. *Nature Aging 2023*, 1–15. https://doi.org/10.1038/s43587-023-00382-5

Statzer, C., Meng, J., Venz, R., Bland, M., Robida-Stubbs, S., Patel, K., Petrovic, D., Emsley, R., Liu, P., Morantte, I., Haynes, C., Mair, W. B., Longchamp, A., Filipovic, M. R., Blackwell, T. K., & Ewald, C. Y. (2022). ATF-4 and hydrogen sulfide signalling mediate longevity in response to inhibition of translation or mTORC1. *Nature Communications 2022 13:1*, *13*(1), 1–15. https://doi.org/10.1038/s41467-022-28599-9

Taylor, R. C., & Dillin, A. (2011). Aging as an event of proteostasis collapse. *Cold Spring Harbor Perspectives in Biology*, *3*(5), 1–17. https://doi.org/10.1101/cshperspect.a004440

Taylor, R. C., & Dillin, A. (2013). XBP-1 Is a cell-nonautonomous regulator of stress resistance and longevity. *Cell*, *153*(7), 1435. https://doi.org/10.1016/j.cell.2013.05.042

Taylor, R. C., & Hetz, C. (2020). Mastering organismal aging through the endoplasmic reticulum proteostasis network. *Aging Cell*, *June*, 1–12. https://doi.org/10.1111/acel.13265

Taylor, S. K. B., Hartman, J. H., & Gupta, B. P. (2024). The neurotrophic factor MANF regulates autophagic flux and lysosome function to promote proteostasis in C. elegans. *BioRxiv*, 1–58. https://doi.org/10.1101/2023.07.31.551399

Taylor, S. K. B., Minhas, M. H., Tong, J., Selvaganapathy, P. R., Mishra, R. K., & Gupta, B. P. (2021). C. elegans electrotaxis behavior is modulated by heat shock response and unfolded protein response signaling pathways. *Scientific Reports*, *11*(1), 1–17. https://doi.org/10.1038/s41598-021-82466-z

Tran, H. C., & Van Aken, O. (2020). Mitochondrial unfolded protein-related responses across kingdoms: similar problems, different regulators. In *Mitochondrion* (Vol. 53, pp. 166–177). Elsevier. https://doi.org/10.1016/j.mito.2020.05.009

Uno, M., & Nishida, E. (2016). Lifespan-regulating genes in c. Elegans. *Npj Aging and Mechanisms of Disease*, *2*(1), 1–8. https://doi.org/10.1038/npjamd.2016.10

van Heemst, D. (2010). Insulin, IGF-1 and longevity. *Aging and Disease*, *1*(2), 147–157.

Vilchez, D., Morantte, I., Liu, Z., Douglas, P. M., Merkwirth, C., Rodrigues, A. P. C., Manning, G., & Dillin, A. (2012). RPN-6 determines C. elegans longevity under proteotoxic stress conditions. *Nature*, *489*(7415), 263–268. https://doi.org/10.1038/nature11315

Voutilainen, M. H., Arumäe, U., Airavaara, M., & Saarma, M. (2015). Therapeutic potential of the endoplasmic reticulum located and secreted CDNF/MANF family of neurotrophic factors in Parkinson's disease. *FEBS Letters*, *589*(24), 3739–3748. https://doi.org/10.1016/j.febslet.2015.09.031

Voutilainen, M. H., Back, S., Porsti, E., Toppinen, L., Lindgren, L., Lindholm, P., Peranen, J., Saarma, M., & Tuominen, R. K. (2009). Mesencephalic Astrocyte-Derived Neurotrophic Factor Is Neurorestorative in Rat Model of Parkinson's Disease. *Journal of Neuroscience*, *29*(30), 9651–9659. https://doi.org/10.1523/jneurosci.0833-09.2009

Walter, P., & Ron, D. (2011). The unfolded protein response: From stress pathway to homeostatic regulation. In *Science* (Vol. 334, Issue 6059, pp. 1081–1086). American Association for the Advancement of Science. https://doi.org/10.1126/science.1209038

Wang, C. H., Jiang, T. C., Qiang, W. M., Zhang, L., Feng, L. J., Shen, Y. J., & Shen, Y. X.

(2018). Activator protein-1 is a novel regulator of mesencephalic astrocyte-derived neurotrophic factor transcription. *Molecular Medicine Reports*, *18*(6), 5765–5774. https://doi.org/10.3892/mmr.2018.9601

Wang, D., Hou, C., Cao, Y., Cheng, Q., Zhang, L., Li, H., Feng, L., & Shen, Y. (2018). XBP1 activation enhances MANF expression via binding to endoplasmic reticulum stress response elements within MANF promoter region in hepatitis B. *The International Journal of Biochemistry & Cell Biology*, *99*, 140–146. https://doi.org/10.1016/j.biocel.2018.04.007

Watterson, A., Arneaud, S. L. B., Wajahat, N., Wall, J. M., Tatge, L., Beheshti, S. T., Mihelakis, M., Cheatwood, N. Y., McClendon, J., Ghorashi, A., Dehghan, I., Corley, C. D., McDonald, J. G., & Douglas, P. M. (2022). Loss of heat shock factor initiates intracellular lipid surveillance by actin destabilization. *Cell Reports*, *41*(3), 111493. https://doi.org/10.1016/j.celrep.2022.111493

Wilson, D. M., Cookson, M. R., Van Den Bosch, L., Zetterberg, H., Holtzman, D. M., & Dewachter, I. (2023). Hallmarks of neurodegenerative diseases. *Cell*, *186*(4), 693–714. https://doi.org/10.1016/j.cell.2022.12.032

Wu, Z., Senchuk, M. M., Dues, D. J., Johnson, B. K., Cooper, J. F., Lew, L., Machiela, E., Schaar, C. E., DeJonge, H., Blackwell, T. K., & Van Raamsdonk, J. M. (2018). Mitochondrial unfolded protein response transcription factor ATFS-1 promotes longevity in a long-lived mitochondrial mutant through activation of stress response pathways. *BMC Biology*, *16:147*(1). https://doi.org/10.1186/s12915-018-0615-3

Xu, H., Jiao, Y., Li, S., Zhu, X., Wang, S., Zhang, Y., Wei, Y., Shen, Y., Wang, W., Shen, Y., & Shao, J. (2023). Hepatocyte-derived MANF mitigates ethanol-induced liver steatosis in mice via enhancing ASS1 activity and activating AMPK pathway. *Acta Pharmacologica Sinica*, *44*(1), 157–168. https://doi.org/10.1038/s41401-022-00920-8

Xu, J., & Taubert, S. (2021). Beyond Proteostasis: Lipid Metabolism as a New Player in ER Homeostasis. *Metabolites*, *11*(1), 1–19. https://doi.org/10.3390/METABO11010052

Xu, S., Di, Z., He, Y., Wang, R., Ma, Y., Sun, R., Li, J., Wang, T., Shen, Y., Fang, S., Feng, L., & Shen, Y. (2019). Mesencephalic astrocyte-derived neurotrophic factor (MANF) protects against Aβ toxicity via attenuating Aβ-induced endoplasmic reticulum stress. *Journal of Neuroinflammation*, *16*(35). https://doi.org/10.1186/s12974-019-1429-0

Xu, Y., & Park, Y. (2018). Application of caenorhabditis elegans for research on endoplasmic reticulum stress. In *Preventive Nutrition and Food Science* (Vol. 23, Issue 4, pp. 275–281). https://doi.org/10.3746/pnf.2018.23.4.275

Yagi, T., Asada, R., Kanekura, K., Eesmaa, A., Lindahl, M., Saarma, M., & Urano, F. (2020). Neuroplastin Modulates Anti-inflammatory Effects of MANF. *IScience*, *23*(12). https://doi.org/10.1016/j.isci.2020.101810

Zhang, Q., Wu, X., Chen, P., Liu, L., Xin, N., Tian, Y., & Dillin, A. (2018). The Mitochondrial Unfolded Protein Response Is Mediated Cell-Non-autonomously by Retromer-Dependent Wnt Signaling. *Cell*, *174*(4), 870-883.e17. https://doi.org/10.1016/j.cell.2018.06.029

Zhang, W. H., Koyuncu, S., & Vilchez, D. (2022). Insights Into the Links Between Proteostasis

and Aging From C. elegans. *Frontiers in Aging*, *3*. https://doi.org/10.3389/fragi.2022.854157

Zhang, Z., Shen, Y., Luo, H., Zhang, F., Jing, L., Wu, Y., Xia, X., Song, Y., Li, W., & Jin, L. (2018). MANF protects dopamine neurons and locomotion defects from a human α-synuclein induced Parkinson's disease model in C. elegans by regulating ER stress and autophagy pathways. *Experimental Neurology*, *308*(June), 59–71. https://doi.org/10.1016/j.expneurol.2018.06.016

6 Appendix

6.1 Appendix A. Analysis of Stress response, autophagy, lysosomal and proteasomal genes under different conditions.

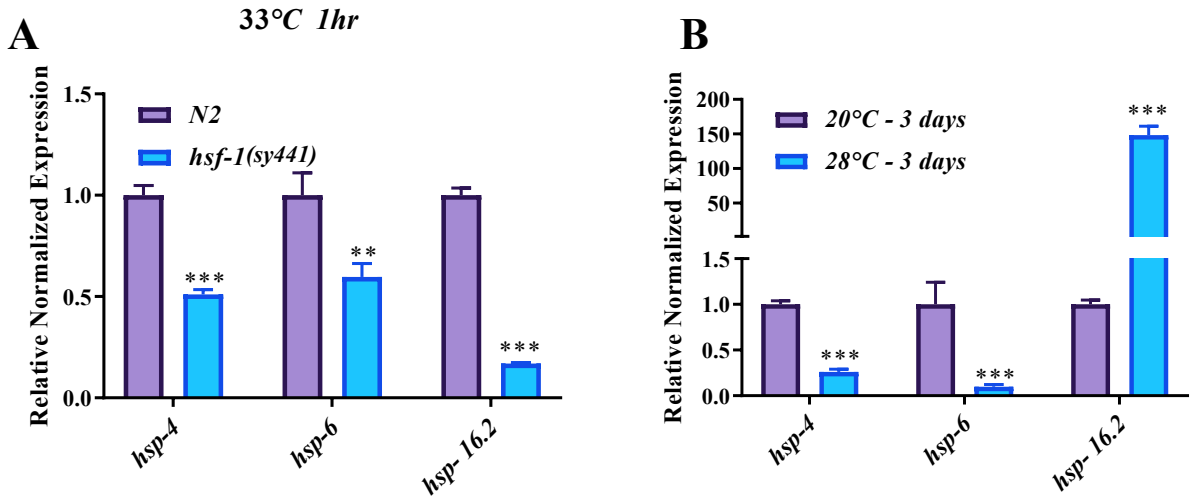

Figure A1. **Analysis of UPR and HSR chaperones following heatshock**. **A)** RT-qPCR analysis of HSP chaperones in N2 and *hsf-1(sy441)* day 1 adults following heat shock at 33°C for 1hr. Animals were unable to mount a heat shock response as *hsp-4(ER-UPR), hsp-6(MT-UPR)* and *hsp-16.2 (HSR)* chaperones were significantly downregulated. **B)** Effect of continuous heat-shock on chaperone expression. Starting at day 1 of adulthood N2 worms were transferred from 20°C and then heat-shocked for 3 days at 28°C. The data shows that continuous heat treatment caused a significant decline in the chaperones of the ER-UPR and MT-UPR but HSR activity continued to be expressed. Results are expressed as mean ± SEM (*p<0.05; **p<0.01; ***p<0.001; ****p<0.0001).

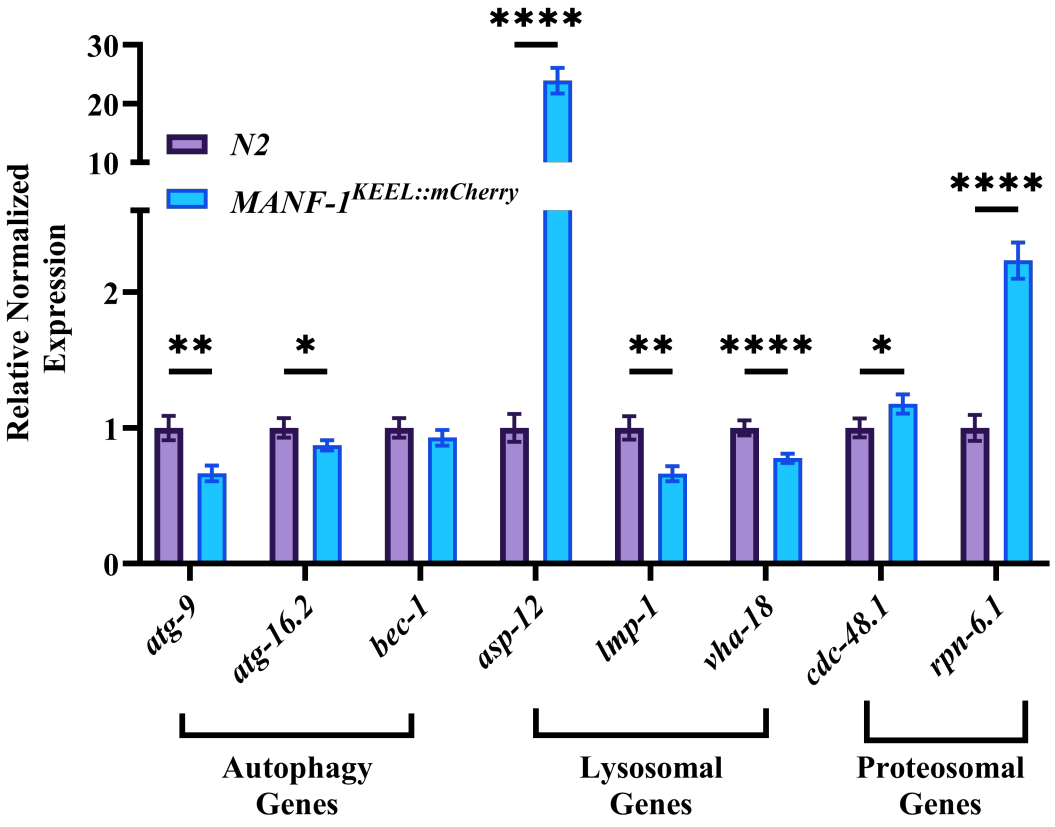

Figure A2. Analysis of autophagy, lysosomal and proteasomal genes in following MANF-1 overexpression. RT-qPCR analysis *MANF-1*$^{KEEL::mCherry}$ day 1 adults showed a significant reduction in genes associated with autophagosome formation. Only *atg-9* and *atg-16.2* are downregulated but *bec-1* remains the same. Overexpression of MANF-1 downregulated lysosome genes, *lmp-1* and *vha-18* which are a lysosomal membrane protein and a V-ATPase that exist on the lysosome membrane. However, the aspartyl protease, *asp-12* is significantly upregulated (~20 fold) and is one of the lysosomal genes identified from the RNAseq. Proteasomal genes were also upregulated following MANF-1 overexpression. Namely, *rpn-6.1* which is an ortholog of human 26S proteasome subunit and *cdc-48.1*, a p97 homolog that shuttles proteins to the proteasome for degradation. Results are expressed as mean ± SEM (*p<0.05; **p<0.01; ***p<0.001; ****p<0.0001).

6.2 Appendix B. Therapeutic effects of TP5, a Cdk5/p25 inhibitor, in in vitro and in vivo models of Parkinson's disease

6.2.1 Preface

This appendix includes the following article published in its original format:

Therapeutic effects of TP5, a Cdk5/p25 inhibitor, in in vitro and in vivo models of Parkinson's disease by Judith Tran, Shane K.B. Taylor, Anika Gupta, Niranjana Amin, Harish Pant, Bhagwati P. Gupta and Ram K. Mishra. *Curr. Res. Neurobiol.* **2**, 100006 (2021)

In this chapter publication we examined the neuroprotective and neurorestorative effects of TP5, a Cdk4/p25 inhibitor using both cell and worm models. We found that TP5 was protective of dopaminergic morphology and locomotion within *C. elegans* and improved cell viability following paraquat exposure. TP5 was demonstrated to block CDK5 activation and be a notable compound in the protection against dopaminergic neurodegeneration, a pathophysiological marker of Parkinson's Disease.

Contributions

Judy Tran performed the *in vitro* experiments, statistical analysis and wrote the manuscript. I assisted Judy in writing, reviewing the initial manuscript draft and responding to reviewers' comments. I conducted the *in vivo* experiments for Figures 5 to 8 in collaboration with Judy Tran and Anika Gupta. Fluorescent images of dopaminergic neurons were taken by me in figures 6 and 7. Niranjana Amin performed the Cdk5 immunoreactivity experiment. All authors were involved in reviewing and editing the manuscript for publication.

6.2.2 Tran *et al.* 2021. Current Research in Neurobiology

Current Research in Neurobiology 2 (2021) 100006

Contents lists available at ScienceDirect

Current Research in Neurobiology

journal homepage: www.editorialmanager.com/crneur/Default.aspx

Therapeutic effects of TP5, a Cdk5/p25 inhibitor, in *in vitro* and *in vivo* models of Parkinson's disease

Judith Tran [a], Shane K.B. Taylor [b], Anika Gupta [b], Niranjana Amin [c], Harish Pant [c], Bhagwati P. Gupta [b], Ram K. Mishra [a,*]

[a] Department of Psychiatry and Behavioural Neurosciences, McMaster University, Hamilton, ON, Canada
[b] Department of Biology, McMaster University, Hamilton, ON, Canada
[c] National Institute of Neurological Disorders and Stroke, National Institutes of Health, Bethesda, MD, USA

ARTICLE INFO

Keywords:
Cdk5/p25
TP5
Paraquat
Parkinson's disease
SH-SY5Y cells
Caenorhabditis elegans
Dopaminergic neurons

ABSTRACT

Parkinson's Disease (PD) is a chronic progressive neurodegenerative disease. Current treatments for PD are symptomatic and only increase striatal dopamine levels. Proactive neuroprotective approaches that slow the progression of PD and maintain appropriate dopamine neuron populations are needed to treat the disease. One suggested mechanism contributing to the pathology of PD involves the binding of cyclin-dependent kinase 5 (Cdk5) to p25, creating a hyperactivated complex to induce cell death. The objective of this study is to investigate the neuroprotective and neurorestorative properties of Truncated Peptide 5 (TP5), a derivative of the p35 activator involved in Cdk5 regulation, via the inhibition of Cdk5/p25 complex function. *SH-SY5Y* cell line and the nematode *Caenorhabditis elegans* were exposed to paraquat (PQ), an oxidative stressor, to induce Parkinsonian phenotypes. TP5 was administered prior to PQ exposure to determine its neuroprotective effects and, in further experiments, after PQ exposure to examine its neurorestorative effects. In the *SH-SY5Y* cell line, TP5 was found to have neuroprotective effects using a cell viability assay and demonstrated neuroprotective and neurorestorative effects in *C. elegans* by examining dopaminergic neurons and dopamine-dependent behaviour. TP5 decreased elevated Cdk5 activation in worms that were exposed to PQ. TP5's inhibition of Cdk5/p25 hyperactivity led to the protection of dopamine neurons in these PD models. This suggests that TP5 can act as a potential therapeutic drug towards PD.

1. Introduction

Parkinson's disease (PD) is a chronic progressive neurodegenerative disease that affects approximately 41 people out of 100 000 over the age of 40, and 1900 people out of 100 000 over 80, making PD the second most common neurodegenerative disease after Alzheimer's disease (AD) (Cacabelos, 2017). This demonstrates the need for a therapeutic treatment as there are currently no available treatments that can slow the progression or prevent the pathology of this neurodegenerative disease. Existing treatments, such as dopamine agonists, levodopa, and monoamine oxidase type B inhibitors, focus on alleviating symptoms by increasing levels of striatal dopamine or stimulating dopamine receptors, which only provide temporary relief and can possibly lead to adverse effects (Cacabelos, 2017; Ellis and Fell, 2017; Miyazaki and Asanuma, 2008). A disease modifying drug that can affect the underlying pathophysiology of Parkinson's Disease is required to alleviate the symptoms from worsening without adverse effects.

Truncated Peptide 5 (TP5), a novel synthetic peptide, has shown to be disease modifying in other studies of neurodegeneration (Zheng et al., 2010). This synthetic peptide contains an 11 amino acid sequence derived from the transactivator of transcription (TAT) protein that is conjugated at the C-terminus. The TAT protein not only penetrates plasma membranes but facilitates the passage of the blood brain barrier as well. TP5 has led to promising results as it was tested initially in AD models, specifically the prevention of increased tau hyperphosphorylation and cell apoptosis in cortical neurons treated with β-amyloid, a marker of AD (Zheng et al., 2010). When mice with AD pathology were pretreated with TP5, cellular dysfunctions, such as neuroinflammation and increased oxidative stress, were also inhibited (Shukla et al., 2013). In addition, behavioural tests demonstrated that

* Corresponding author.
E-mail addresses: tranj27@mcmaster.ca (J. Tran), taylos49@mcmaster.ca (S.K.B. Taylor), anikausa22@gmail.com (A. Gupta), aminn@ninds.nih.gov (N. Amin), panth@ninds.nih.gov (H. Pant), guptab@mcmaster.ca (B.P. Gupta), mishrar@mcmaster.ca (R.K. Mishra).

https://doi.org/10.1016/j.crneur.2021.100006
Received 3 October 2020; Received in revised form 3 February 2021; Accepted 23 February 2021

mice with AD pathology had improvement in working memory. TP5 has also led to neuroprotective effects in mesencephalic primary cultures and in mice treated with 1-methyl-4-phenyl-1,2,3,6-tetrahydropyridine (MPTP) to generate PD's pathology (Binukumar et al., 2015). Although the MPTP model has been widely used in the PD field, its findings cannot be generally applied to other forms of PD due to the idiopathic nature of this disease. Therefore, different models are necessary to determine the underlying pathology and validate the effectiveness of therapeutic treatments for PD.

We chose 1,1′-dimethyl- 4,4′-bipyridium (PQ) as our toxin-induced model of PD due to its clinical and biochemical phenotypes that were characteristic to PD. The exposure of this herbicide has been attributed to the symptoms of idiopathic PD (Nandipati and Litvan, 2016). PQ's main cellular toxicity mechanism consists of mitochondrial dysfunction and increased oxidative stress (Dinis-Oliveira et al., 2006). Studies have demonstrated that mice exposed to PQ develop reduced motor activity due to a loss of dopaminergic neurons (Brooks et al., 1999; Fernagut et al., 2007). PQ has also been found to induce alpha-synuclein aggregation by specifically accelerating the fibril formation rate *in vitro* and *in vivo* (Manning-Bog et al., 2002). The clinical and pathological characteristics of PD exhibited in these models validate the use of PQ to study PD in a laboratory setting. A pathological characteristic of PD, present in many neurodegenerative diseases, is an aberrant cyclin-dependent kinase 5 (Cdk5) activity that remains to be investigated in PQ models of PD.

Cyclin-dependent kinase 5 (Cdk5) is a proline directed serine/threonine kinase that is activated when bound to its regulatory partners, such as p35 or p39; this complex is essential for the proper regulation of the central nervous system (Lopes and Agostinho, 2011). However, when multiple neurotoxic signals are present, such as increased oxidative stress or mitochondrial dysfunction, a Ca^{2+} influx sensor, calpain, cleaves p35 into p25 and p10. High levels of Cdk5/p25 lead to pathological consequences, resulting in neurodegenerative diseases (Wilkaniec et al., 2016). Post-mortem brain tissues of PD patients displayed elevated levels of calpain-related proteolytic formation of p25 as well as an increase in the p25/p35 immunoreactivity ratio (Alvira et al., 2008); thus, signifying the importance of Cdk5/p25 to give rise to further consequences such as Lewy body (LB) formation and dopaminergic degeneration (Avraham et al., 2007; Smith et al., 2003). Regulation of this pathway has been suggested to prevent these detrimental consequences. TP5, derived from the activator p35, has a stronger binding affinity towards Cdk5 than p25, allowing TP5 to be an effective inhibitor against the hyperactivated Cdk5/p25 complex.

In this study, we have investigated the effects of TP5 using *in vitro* and *in vivo* PQ-induced models of PD. We examined if TP5 can act as a Cdk5/p25 inhibitor against PQ that induces Parkinsonian-like properties. The *SH-SY5Y* catecholaminergic neuroblastoma cell line was selected as an *in vitro* model. The cell line was originally derived from *SK-H-SH* cells, that were taken from a bone marrow biopsy of a metastatic neuroblastoma patient (Biedler et al., 1978). This *in vitro* model is representative of PD when differentiated with all-trans retinoic acid, leading to high expression of genes that control dopamine synthesis and degradation, and dopamine transporter thereby confirming that this is an adequate model to mimic dopaminergic neurons. (Korecka et al., 2013). The nematode, *Caenorhabditis elegans,* was chosen as an *in vivo* model due to few dopaminergic neurons and the ease by which neurons can be visualized in live animals. Furthermore, *C. elegans* shows high genetic and neurobiological conservation with humans and pre-clinical models of PD (Ma et al., 2018). The *dat-1p::YFP* transgenic strain chosen in this study has been used in several other studies to confirm dopaminergic degeneration (for example see the review by Maulik et al., 2017). Additionally, this strain was used in a previous study by our group to investigate dopaminergic neurodegeneration in various toxin-treated animals (Salam et al., 2013). Overall, both models have allowed us to determine the pathology of PD and further validate the effectiveness of TP5 as a drug. This report is the first to demonstrate the effect of PQ on Cdk5/p25 activity and that TP5 inhibits the Cdk5/p25 complex function in the pathology of Parkinson's Disease.

2. Materials and methods

2.1. Cell culture conditions

SH-SY5Y cells were obtained from American type culture collection (ATCC) and maintained in Dulbecco's Modified Eagle Medium: Nutrient Mixture F-12 (DMEM:F12), supplemented with heat-inactivated fetal bovine serum (FBS) (10%v/v), L-glutamine (1%v/v), and pencillin-strepomycin (1%v/v) at 37 °C in 5% $C0_2$.

2.2. Drug treatments

Cells were seeded at a density of 1.5×10^5 cells/ml in a 96 well plate and the experimental timeline is shown in Fig. 1. The following day, cultures were differentiated with all-trans retinoic acid (10 μM) and FBS (1%v/v). On the sixth day, cultures were treated with TP5, dissolved in ddH_20, at 12.5 μM for 12 h. Then cultures were treated with PQ at 250 μM, dissolved in differentiation media, for 48 h. Cell viability assay was performed after treatment. Scrambled TP5, which consisted of the same amino acids in TP5 but organized in a different sequence, was used as a negative control. TP5 peptide and scrambled TP5 peptide were synthesized by GenScript (Piscataway, NJ).

2.3. Cell viability assay

Cell viability was determined using the 3-(4,5-Dimethylthiazol-2-yl)-2,5-Diphenyltetrazolium Bromide (MTT) assay. 20 μl of MTT powder, dissolved in differentiation media, was added into each well and incubated at 37 °C for 3–4 h. MTT is metabolically converted into formazan, a precipitate, by the mitochondrial dehydrogenases of living cells. The solution was replaced with dimethyl sulfoxide (DMSO) to dissolve the precipitate and absorbance was measured at 570 nm with a microplate reader (Spectromax).

2.4. Strain and culture conditions

C. elegans worms were cultured on standard Nematode Growth Medium (NGM) agar containing plates with *Escherichia coli* strain OP50 as a food source (Brenner, 1974). The strain used in the study was *DY328 unc-119; bhEx120[unc-119(+) + pGLC72(Cel-dat-1 5′UTR::YFP)].* The *dat-1p::YFP* plasmid pGLC72 was made by amplifying a 710 bp fragment of *dat-1* 5′ genomic region using primers GL563 (5′ AGGAAGCTTCCAGTTTTCACTAAAACGACCTCATACACTTCTC-3′) and GL564 (5′-ATGGGTACCGGCACCAACTGCATGGCTAAAAATTGTTGAG -3′). The resulting PCR product was digested with *Hind*III and *Kpn*I and subcloned into pPD 136.64 (Fire lab vector, www.addgene.com). pGLC72 was injected into *unc-119(ed4)* animals to generate stable transgenic lines. Age-synchronized cultures were obtained by treating the strain with sodium hypochlorite and sodium hydroxide (3:2 ratio of NaOCl:NaOH). The animals were maintained at 20 °C. Day 1 adult worms were used for drug treatments as detailed below.

2.5. Drug treatments

Experimental timelines of the neuroprotective and neurorestorative conditions can be seen in Fig. 2. For the neuroprotective experiment, Day 1 age synchronized adult worms were treated with 10 μM of TP5 then placed into an agar plate containing 250 μM of PQ for 48 h. There were two different techniques of administering TP5: 1) worms were suspended in 500 μL of TP5 (10 μM) inside an Eppendorf tube and placed in a rotator for 1 h; 2) picolitres of TP5 (10 μM) were microinjected into the anterior body cavity of the worm close to the terminal pharyngeal bulb but away from the region where dopaminergic neurons are located. Different routes of administration for TP5 were tested to determine which route was most effective and non-lethal for worms. After exposure to PQ for 48 h, worms were tested for dopamine-dependent locomotor behaviour,

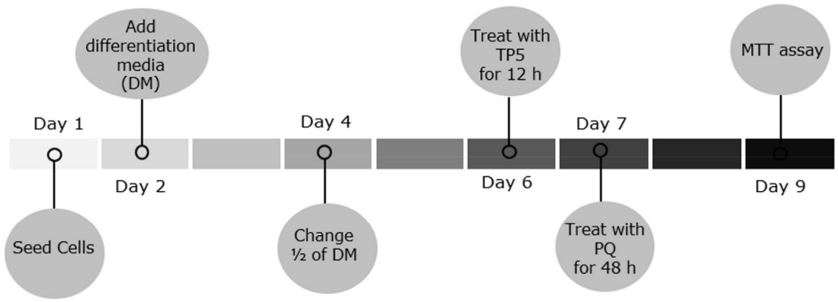

Fig. 1. Timeline of experimental procedure for *SH-SY5Y* cells.

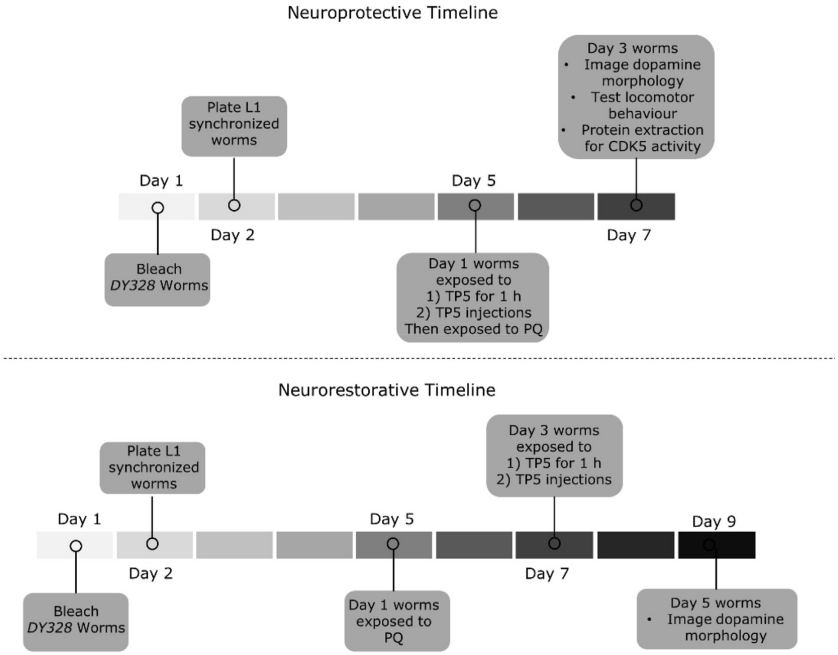

Fig. 2. Timeline of experimental procedure for *C. elegans*. Neuroprotective (top) and neurorestorative conditions (bottom).

imaged for neurodegeneration, and harvested for Cdk5 kinase activity. PQ exposed worms were treated with PQ from Day 1 to Day 3, then tested for dopamine-dependent locomotor behaviour, imaged for neurodegeneration, and harvested. Two negative controls were made: worms were given ddH_20 or scrambled TP5 before exposure to PQ.

For the neurorestorative experiment, Day 1 age synchronized adult worms were placed on an agar plate containing 250 μM of PQ for 48 h. Two days later (Day 3), adult worms were exposed to 1 mM of TP5. There were two different techniques of administering TP5: 1) worms were suspended in 500 μL of TP5 (1 mM) inside an Eppendorf tube and placed in a rotator for 1 h; 2) picolitres of TP5 (1 mM) were microinjected into the anterior body cavity of the worm close to the terminal pharyngeal bulb but away from the region where dopaminergic neurons are located. Different routes of administration for TP5 were tested to determine which route was most effective and non-lethal for worms. After TP5 treatment, worms were transferred to a standard NGM agar plate to recover for two days. Day 5 worms were imaged for neurodegeneration. PQ exposed worms were treated with PQ from Day 1 to Day 3, then transferred onto a standard seeded agar plate for two days to be tested for neurodegeneration. Two negative controls were made: worms were given ddH_20 or scrambled TP5 after exposure to PQ.

2.6. Dopamine dependent locomotion assay

Assay plates were prepared as described (Sawin et al., 2000). The treatments groups in the neuroprotective experiment (Fig. 2, top) were examined using this assay. One condition consisted of seeded plates of *Escherichia coli* HB101 as a food source and another (control) without HB101. Young adults were washed off of NGM agar culture plates and placed in the center of HB101 plates, one worm at a time. After 5 min of recovery, sinusoidal body bends were counted for 20 s in three different trials. Control experiments were carried out in a similar way on plates

devoid of bacteria. In all conditions, body bends were counted blindly in each treatment group.

2.7. Microscopy

Nematodes were mounted on 2% agar pad with a glass coverslip, anesthetized using 30 mM sodium azide. GFP fluorescence was visualized using a Zeiss Observer Z1 microscope equipped with an Apotome 2 and X-Cite R 120LED fluorescence illuminator.

2.8. Dopaminergic neurodegeneration

The detailed methods of scoring neurodegeneration have been described, with modifications, in (Richman et al., 2018; Taylor et al., 2021). Briefly, neuronal phenotype was visually scored by counting cell bodies of dopaminergic neurons and observing dendritic morphologies under a Zeiss Observer Z1 microscope. Typically, wild-type animals have three pairs of dopaminergic neurons with smooth dendritic/axonal projections visible in the head region. Defects in neurons result in fewer cell bodies and/or dendritic projections showing abnormal phenotypes including blebbing, punctate pattern, deformed shape, faint appearance, and complete absence. Multiple batches of animals were scored on different days and from different culture plates to ensure that results were consistent and unbiased.

Animals having defects either in cell bodies or projections were considered abnormal. Neurons were scored in day 1, 3 and 5 old adult animals. Our neuronal scoring has taken both these factors into consideration (Yin et al., 2014).

2.9. Protein extraction

Approximately 100 worms from each condition in Fig. 2 (top) were harvested for protein extraction. Initially, worms were washed with phosphate-buffered saline (PBS) three times then resuspended with 400 μL of M-per lysis buffer (Thermo Fisher), along with protease and phosphatase inhibitors. Next, worms were sonicated to create a lysate and then centrifuged to create a supernatant.

2.10. Immunoprecipitation and kinase assays

Kinase assays were performed as described previously, with modification (Binukumar et al., 2014). Briefly, Cdk5 was immunoprecipitated with polyclonal C8 antibody for 2 h at 4 °C and protein A–Sepharose beads were used to isolate immunoglobulin. Immunoprecipitates were washed three times with lysis buffer and once with 1X kinase buffer. 1X kinase buffer contained 5 mM MOPS, pH 7.4, 2.5 mM β-glycerophosphate, 1 mM EGTA, 0.4 mM EDTA, and 5 mM $MgCl_2$. Samples were added to the reaction mix containing kinase buffer, 50 μM ATP, 20 μg of histone H1, and 0.1 mCi of [^{32}P]ATP containing 0.1 mm DTT and 1X Halt protease and phosphatase inhibitor (Thermo Fisher) and incubated at 30 °C for 1 h. Reactions were stopped by adding Laemmli sample loading buffer, and samples were electrophoresed on 12% SDS–PAGE gels. Histone bands were visualized by Coomassie blue staining and gels were autoradiographed and were scanned on a PhosphorImager. Radioactive band density was analyzed using ImageJ.

2.11. Statistical analysis

Statistical analyses were performed using GraphPad Prism 7. Groups were analyzed by using the One-way Analysis of Variance (ANOVA) Test with Tukey Multiple Comparisons Test. Outliers were removed using a Grubbs outlier test calculator where indicated. All bars are considered to be standard error of the mean (SEM) unless indicated. P values smaller than 0.05 are considered statistically significant.

3. Results

3.1. TP5 protects differentiated SH-SY5Y cells against PQ cell induced toxicity

Studies that have examined PQ as a potential PD model have performed a variety of cell viability assays to determine PQ's toxicity (Yang and Tiffany-Castiglioni, 2005). Using the MTT assay, a widely used tool to determine cell viability *in vitro* (Peng et al., 2004), PQ caused a significant decrease in cell viability at 48 h in a concentration-dependent manner ($p < 0.001$) (Fig. 3). We chose to use 250 μM of PQ in subsequent *in vitro* experiments to evaluate neuroprotection of TP5 in differentiated neuroblastoma cells.

Although TP5 has been tested in mesencephalic primary cultures and mice models (Binukumar and Pant, 2016), we wanted to ensure that there were no toxicity effects with TP5 in this differentiated neuronal culture. We found 12.5 μM to be the optimal concentration of TP5's therapeutic effect and to have no toxicity (Fig. S1). Next, we decided to treat neuronal cultures with TP5 before exposure to PQ. This sequential order was to investigate whether TP5's mechanism of action will protect against PQ induced cell death. TP5, in combination with PQ, were found to have a significantly increased cell viability compared to cells exposed to PQ alone ($p < 0.05$) (Fig. 4A). Scrambled TP5, a negative control, was tested against PQ to confirm that the amino acid sequence of TP5 was indeed essential for this neuroprotective effect. As expected, scrambled TP5, in combination with PQ, had no significant differences against cells exposed to PQ alone (Fig. 4B). This result confirms that the specific sequence of TP5 and the resultant binding to Cdk5 can protect differentiated *SH-SY5Y* cells against PQ.

3.2. TP5 protects dopamine function of Caenorhabditis elegans against PQ

The dopaminergic system of *C. elegans* is essential for responding to environmental stimuli, specifically bacteria as their source of food. This is an adaptive mechanism that allows worms to increase their time spent in the presence of bacteria. It has been shown that upon encountering bacteria, worms exhibit a slower movement. This behaviour, termed

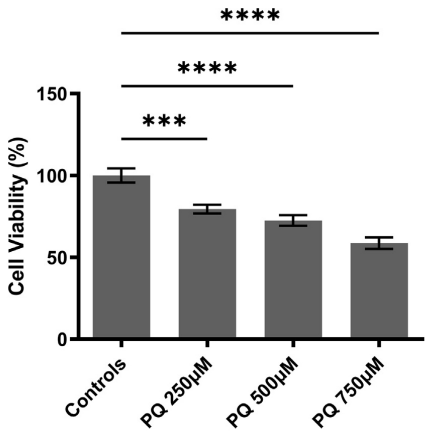

Fig. 3. Paraquat induces concentration dependent cell toxicity in differentiated human neuroblastoma cells. *SH-SY5Y* cells were treated with increasing concentrations of PQ for 48 h then subjected to MTT assays. Cell viability is demonstrated as the percentage of healthy living cells that are normalized to controls. Results are expressed as mean ± SEM and pooled from two independent experiments, with each experiment having at least five different triplicate wells per condition. Data were analyzed using one-way ANOVA with Dunnett's post hoc tests (****$p < 0.0001$; ***$p < 0.001$).

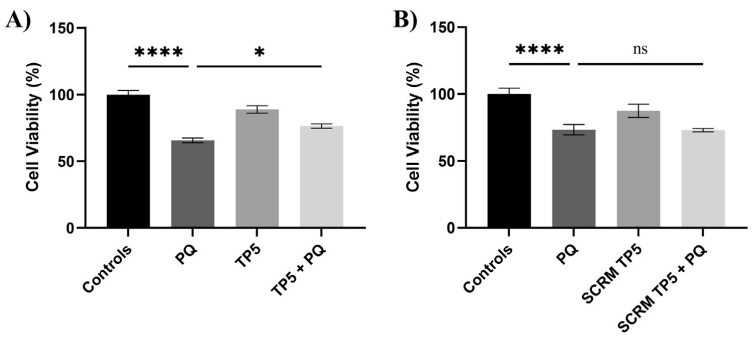

Fig. 4. TP5 inhibits PQ-induced cellular toxicity in differentiated human neuroblastoma cells. *SH-SY5Y* cells were pretreated with A) TP5 (12.5 μM) or B) scrambled TP5 (12.5 μM) for 12 h then further co-treated with PQ (250 μM) for 48 h. The cultures were then subjected to MTT assays. Cell viability is demonstrated as the percentage of healthy living cells that are normalized to controls. Results are expressed as mean ± SEM and pooled from two independent experiments, each experiment having at least seven different triplicate wells per condition. Data were analyzed using one-way ANOVA with Tukey's post hoc tests (****$p < 0.0001$; **$p < 0.01$; *$p < 0.05$). A) There is a significant difference between the PQ exposed group compared to the TP5 group treated with PQ (*$p < 0.05$). B) There are no significant differences between the PQ exposed group compared to the scrambled TP5 treated with PQ ($p > 0.999$).

'basal slowing response,' allows animals to maximize their feeding time (Sawin et al., 2000). Ablation of dopaminergic neurons abolishes the basal slowing response. This method has been used in other studies to demonstrate how toxins, such as lead, affect dopamine dependent behaviour (Akinyemi et al., 2019; Maulik et al., 2017). We investigated the neuroprotective effect of TP5 in worms following PQ-induced dopaminergic neurodegeneration by investigating *C. elegans'* locomotor activity using the basal slowing response assay.

First, we confirmed if PQ can impair dopaminergic functioning in *C. elegans*. Day 1 adult worms were exposed to 250 μM of PQ for 48 h until they reached Day 3 of adulthood. While this treatment did not affect the locomotor activity in the absence of food, animals exhibited a significantly decreased movement response when exposed to food ($p < 0.001$) (Fig. 5).

To determine if TP5 can protect dopaminergic function in *C. elegans'* behaviour against PQ, we pretreated Day 1 adults with TP5 (10 μM) or scrambled TP5 (10 μM) for 1 h in the liquid environment and then transferred them to 250 μM of PQ for 48 h. The results showed that scrambled TP5 treatment caused no difference between non-PQ and PQ exposed groups. However, worms treated with TP5 followed by PQ exposure had a significant increase in their locomotor activity compared to two types of control groups consisting of PQ exposed animals, one of which were not treated with TP5 ($p < 0.001$) and the other were treated with scrambled TP5 ($p < 0.05$) (Fig. 5). Specifically, we found that TP5 treatment had a protective effect against PQ exposure such that the basal slowing response of animals was comparable to wild-type untreated controls, suggesting that TP5 protects against PQ-induced dopaminergic toxicity.

3.3. TP5 protects and restores dopaminergic neurons in C. elegans exposed to PQ

Although we have confirmed that TP5 protects the adaptive mechanism of worms against PQ through dopaminergic function, it is essential to validate whether the morphology of the dopaminergic neurons is also protected. This was done by investigating the cell bodies and trajectories of dopaminergic neurons in live animals using a *dat-1p::YFP* (dopamine transporter) transgenic strain (Fig. 6A–D).

Worms exposed to PQ solely, as well as those pre-treated with scrambled TP5 in liquid before PQ exposure, exhibited neuronal defects indicated by the asterisks in Fig. 6B and C, respectively, suggesting neurodegeneration. By contrast, controls (i.e., no treatment group) and pre-treatment with liquid TP5 followed by PQ exposure, respectively, exhibited little to no neuronal defects in Fig. 6A and D. The quantification of neuronal phenotypes in Day 3 animals showed that TP5 had a significant neuroprotective effect (Controls vs PQ-alone control: $p < 0.0001$,

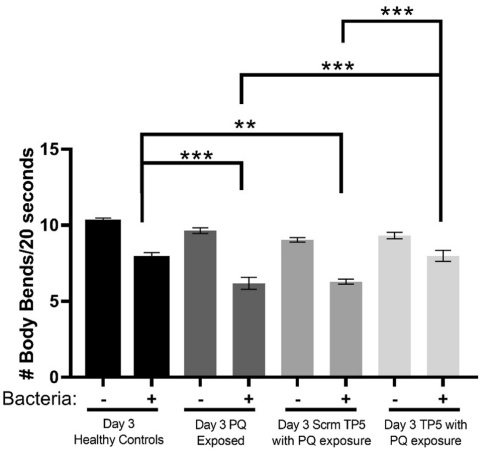

Fig. 5. TP5 protects dopamine dependent locomotor of *DY328* *C.* elegans against PQ. Four groups of well-fed *DY328* worms were transferred to plates with (+) or without (−) bacteria and the locomotion of each worm was recorded. Groups (starting from left to right) consisted of 1) Day 3 control worms; 2) Day 3 worms that were exposed to PQ for 48 h prior; 3) Day 3 worms that were previously treated with scrambled TP5 (10 μM) for 1 h then exposed to PQ for 48 h; 4) Day 3 worms that were previously treated with TP5 (10 μM) for 1 h then exposed to PQ for 48 h. Each worm was recorded for 20 s for an average of three trials. The number of body bends are demonstrated as the locomotor activity of the worms for 20 s. Results are expressed as mean ± SEM and pooled from five independent experiments, each experiment having at least ten worms per condition. Data were analyzed using one-way ANOVA with Tukey's post hoc tests (***$p < 0.001$; **$p < 0.01$).

Controls vs scrambled TP5 + PQ: $p < 0.001$, TP5 vs PQ-alone control: $p < 0.001$, TP5 vs scrambled TP5 + PQ: $p < 0.01$) (Fig. 6E). We repeated this experiment using the injection protocol (see Methods) to determine if the trends were consistent. TP5 injected worms, which were later exposed to PQ, demonstrated significantly decreased neurodegeneration compared to control groups (PQ only $p < 0.001$, injected ddH_20 $p < 0.01$) (Fig. S2). In summary, both methods demonstrate that TP5 can protect the morphology of dopaminergic neurons against PQ toxicity.

Our results have so far revealed that TP5 can protect secondary cell lines *in vitro* as well as the morphology and function of dopaminergic neurons *in vivo* against PQ. Next, we wanted to examine if TP5 has the

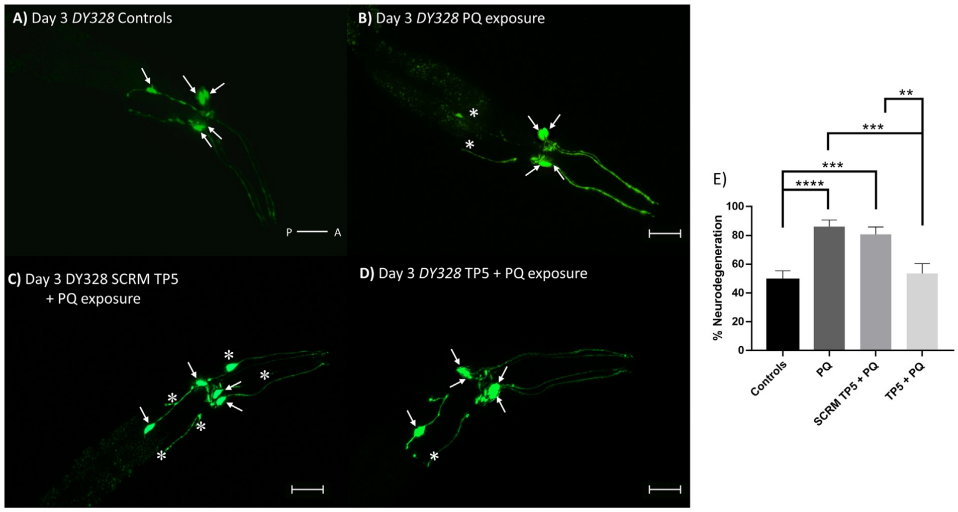

Fig. 6. TP5 provides neuroprotection against PQ in *DY328* worms. Confocal images of dopaminergic neurons in Day 3 *DY328* adults of control **(A)**, PQ exposed **(B)**, pretreated scrambled TP5 then PQ exposure **(C),** and pretreated with TP5 then PQ exposure **(D)** worms. Arrows indicate neuronal cell bodies of the CEPs and ADEs and asterisks represent any abnormalities in the neuron. Scale bar = 50 μM. **E)** Quantification of dopaminergic neuronal defects from groups A to D. Results are expressed as mean ± SEM and pooled from four different batches, each batch had at least 15 worms per condition. Data were analyzed using one-way ANOVA with Tukey's post hoc tests (****$p < 0.0001$; ***$p < 0.001$; **$p < 0.01$).

potential for neuronal restoration. This was done to determine if TP5 can be used in clinical settings to protect dopaminergic neurons. To this end, we made a neurorestorative model to analyze dopaminergic morphology (Fig. 2, bottom). Worms exposed to PQ solely, as well as those post-treated with scrambled TP5 in a liquid environment following PQ, exhibited neuronal defects indicated by the asterisks in Fig. 7B and C, respectively, suggesting neurodegeneration. Controls (i.e., no treatment group) and those post-treated with TP5 following PQ exhibited no neuronal defects (Fig. 7A and D). The quantification of neuronal morphology in Day 5 adults demonstrated that TP5 has significant

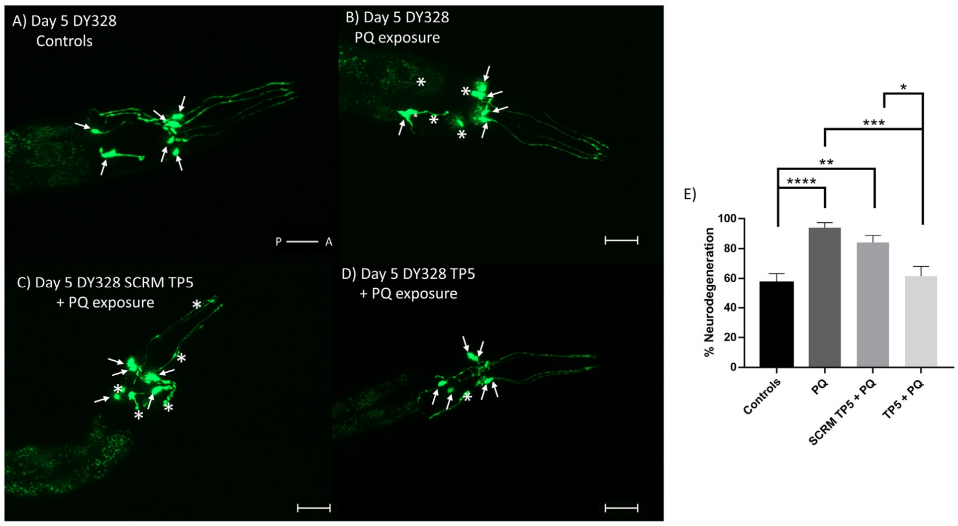

Fig. 7. TP5 induces neurorestoration against PQ in *DY328* worms. Confocal images of dopaminergic neurons in Day 5 *DY328* adults of control **(A)**, PQ exposed **(B)**, pretreated with PQ then exposed to scrambled TP5 (1 mM) for 1 h **(C),** and pretreated with PQ then exposed to TP5 (1 mM) for 1 h **(D)** worms. Arrows indicate neuronal cell bodies of the CEPs and ADEs and asterisks represent any abnormalities in neurons. Scale bar = 50 μM. **E)** Quantification of dopaminergic neuronal defects from groups A to D. Results are expressed as mean ± SEM and are pooled from four different batches, each batch had at least 15 worms per condition. Data were analyzed using one-way ANOVA with Tukey's post hoc tests (****$p < 0.0001$; ***$p < 0.001$; **$p < 0.01$; *$p < 0.05$).

neurorestorative properties (Fig. 7E) (Controls vs PQ-alone control: $p < 0.0001$, Controls vs PQ + post-scrambled TP5: $p < 0.01$, PQ + post TP5 vs PQ-alone control: $p < 0.001$, PQ + post-TP5 vs PQ + post-scrambled TP5: $p < 0.05$). We repeated this experiment by injecting TP5 or ddH_20 to determine if the trends were similar. Surprisingly, worms injected with TP5 did not show a significant decrease in neurodegeneration compared to those exposed to both PQ and ddH_20 ($p = 0.0604$) (Fig. S3). We think that this might be due a combination of PQ exposure and injection-induced stress. PQ toxicity results in the vulnerability of animals, so the addition of injections may cause the worms to become more distressed, which is supported by a higher proportion of deaths in batches that were performed. In summary, our liquid exposure data demonstrates that 1 h TP5 exposure is an effective method for restoring the morphology of dopaminergic neuron damage caused by PQ.

3.4. TP5 blocks Cdk5/p25 activity in C. elegans following exposure to PQ

Research has shown that blocking the cleavage of p35 to p25 has a neuroprotective effect on dopaminergic neurons and causes improved locomotor activity in a PD mice model (Smith et al., 2003). Therefore, after confirming TP5's neuroprotective effects against PQ using cellular and behavioural assays, the mechanism of this effect needs to be validated by observing Cdk5/p25 levels through the hyperactive pathway by using the immunoprecipitation and kinase assay that has been established with TP5 (Binukumar et al., 2014, 2015). This is also the first study that examines the direct relationship of PQ elevating Cdk5/p25 levels. Although TP5 has been shown to inhibit this hyperactivation in an MPTP mice model (Binukumar et al., 2015), we wanted to confirm TP5's mechanism of action since the peptide has shown to be both neuroprotective and neurorestorative in PQ exposed worms. *C. elegans* in the neuroprotective timeline in Fig. 2 (top) were treated and subjected to the kinase assay. Fig. 8 demonstrates that PQ caused a significant increase in Cdk5/p25 levels compared to controls ($p < 0.001$). As expected, TP5 exposure in combination with PQ was found to significantly decrease the levels of Cdk5/p25 compared to worms exposed to PQ alone ($p < 0.001$). These results implicate TP5 having a protective effect on cellular and behavioural processes due to its ability to directly inhibit the elevated levels of Cdk5/p25 caused by PQ.

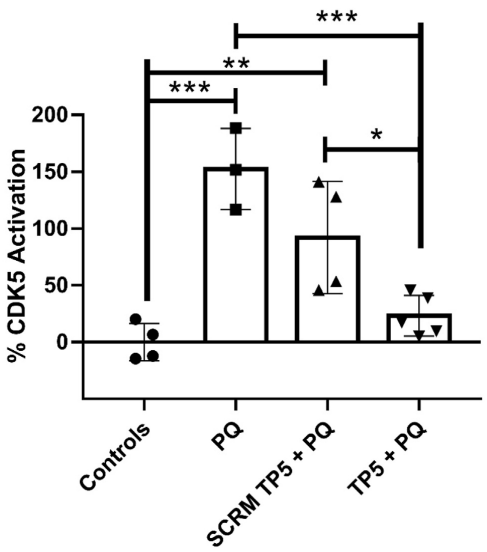

Fig. 8. TP5 blocks elevated Cdk5/p25 levels exhibited by PQ. Conditions are demonstrated in Fig. 2 (top) and Fig. 6A–D. Cdk5 activation is demonstrated as percentage of Cdk5 activation normalized to controls. Results are expressed as mean ± SD and are pooled from four different batches, each batch had at least 100 worms per condition. One outlier was removed from the PQ group. Data were analyzed using one-way ANOVA with Tukey's post hoc tests (***$p < 0.001$; **$p < 0.01$; *$p < 0.05$).

4. Discussion

Parkinson's Disease is hard to detect in early stages; even more so, it cannot be cured once diagnosed and there are currently no disease modifying treatments that exist. Current treatments, such as levodopa, only help patients temporarily. Long-term usage of levodopa can lead to motor and non-motor fluctuations and dyskinesia, which was demonstrated in over 80% of patients using levodopa for over 10 years (Ellis and Fell, 2017). In addition, since many patients can develop PD through familial or idiopathic causes, it is difficult to treat all patients in the same manner. This implicates the importance of toxin-induced models to investigate the pathophysiology of PD.

Many different toxins, such as MPTP, 6-hydroxydopamine (6-OHDA), and rotenone, have been used to model PD (Bové and Perier, 2012). MPTP induces some features that are characteristic of PD, such as impaired dopaminergic function; however, post-mortem samples of individuals exposed to this toxin did not show Lewy bodies, revealing an incomplete representation of the disease (Langston et al., 1999). 6-OHDA and rotenone also led to inconsistencies in PD hallmarks (Bové and Perier, 2012; Drolet et al., 2009). Thus, MPTP and other toxins demonstrate a wide variety of idiopathic cases of PD. Studies by Manning-Bog et al. (2002) and Langston et al. (1999) demonstrated that PQ led to dopaminergic cell death and increased aggregation of alpha-synuclein, the classical hallmarks of PD, further validating why this toxin was used in this study. Furthermore, the toxicity mechanism of PQ also suggests that PQ induces the hyperactivation of Cdk5/p25 mechanism. The Cdk5/p25 pathway is of great interest since this pathway diverges into further downstream effects that can exacerbate the pathology and symptomology.

Our study has shown that TP5 is an effective peptide against *in vitro* and *in vivo* PQ-induced PD-like symptoms and pathology. This is the first study that demonstrates both neuroprotective effects and neurorestorative effects in a PD model, further confirming TP5 as a potential therapeutic drug towards PD. Also, we have shown the therapeutic effects of TP5 in different models of PD, namely *SH-SY5Y* human neuroblastoma cultures and *C. elegans* that are commonly used to investigate the effects of toxins and drugs for neurodegenerative diseases.

Differentiated *SH-SY5Y* human neuroblastoma cultures are an effective model to study morphological, biochemical, and cytotoxic parameters related to PD. Many toxins have been tested in this cell line for PD research due to its dopaminergic properties, including high expression of genes that regulate processes such as dopamine synthesis and degradation (Korecka et al., 2013). PQ has been used in this cell line to examine its cellular mechanism (Yang and Tiffany-Castiglioni, 2008). The presence of PQ decreasing mitochondrial complex I activity and inducing apoptotic markers caspase 9 and 3 coincide with our decreased cell viability results *in vitro*. Specifically, TP5 effectively inhibited PQ's toxic effect suggesting that TP5 is able to protect the *SH-SY5Y* cells by interfering with PQ-induced processes that cause cell death.

Although cell cultures are a great tool to study biochemical and cytotoxic parameters, they can only tell one part of the story. Most cell cultures have a monolayer structure that represents a very simple microenvironment and does not permit observation of the overall behaviour of an organism. *C. elegans*, with a well-defined nervous system with 302 neurons, eight of which are dopaminergic, represents a good model to study PD *in vivo* (Chase and Koelle, 2007). Furthermore, *C. elegans* possesses conserved genes involved in dopamine synthesis, transport, and signaling. As dopaminergic neurons are susceptible to PQ, we can examine dopamine-dependent behaviour such as movement in the presence of food. The transparent body of the worm also makes it

possible to visually examine dopaminergic neurons in live animals for the effect of TP5 on neuroprotection and neurorestoration.

The behavioural research of Sawin et al. (2000) showed that dopaminergic neurons mediate the response towards environmental cues, which allows animals to slow down and spend longer time in the presence of food. However, the locomotion speed is higher in the absence of dopaminergic signaling. Interestingly, we observed that worms exposed to PQ had decreased speed. This might be due to differences in protocols. While Sawin et al. (2000) selectively ablated dopaminergic neurons, PQ treatment in our case does not completely remove the entire set of the neurons. Additionally, PQ may have other effects on dopaminergic signaling. For example, it was demonstrated that increased oxidative stress and mitochondrial dysfunction, induced by PQ, can interfere with locomotion (Wu et al., 2018; Taylor et al., 2021); therefore, worms exposed to PQ exhibit reduced velocity and body bends, which are consistent with our results. The main takeaway from published studies and those described in this paper, is that TP5 is able to protect against impaired dopamine-dependent behaviour.

In addition to behavioural experiments, we also used a YFP-tagged reporter for *in vivo* examination of neurons. It was shown earlier that PQ causes dose-dependent degeneration of dopaminergic neurons (González-Hunt et al., 2014). Similar detrimental effects have also been reported for other toxins, such as 6-OHDA (Nass and Blakely, 2003). We have demonstrated that TP5 protects the neurons against PQ exposure. Additionally, our work shows that there is clinical potential for TP5 treatment based on the neurorestoration of dopaminergic morphology against PQ.

Studies have confirmed the primary toxicity mechanism of PQ; however, the direct correlation of PQ leading to the hyperactivation of Cdk5/p25 levels has not been demonstrated (Yang and Tiffany-Castiglioni, 2005). In PQ's induced cell toxicity, increased oxidative stress and mitochondrial dysfunction will lead to the presence of cell death signals, such as caspase 9 and 3 markers (Yang and Tiffany-Castiglioni, 2008). Neuronal death is induced by triggering apoptosis through increased activation of calpain with caspase 9 and 3, which led to the abnormal activation of Cdk5/p25 (Cagnon and Braissant, 2008). Our results are consistent with these findings and demonstrate that PQ elevates abnormal Cdk5/p25 levels in *C. elegans* likely through activated caspases and calpain. Furthermore, our data validate the use of PQ to generate a PD model as this toxin expresses the hallmarks of PD (Brooks et al., 1999; Fernagut et al., 2007, & Manning-Bog et al., 2002). Finally, we have shown that TP5 can inhibit the increase in Cdk5/p25 levels due to PQ exposure, which coincides with the research of Binukumar et al. (2015). Binukumar et al. (2015) examined the expression of Cdk5, p35 and p25 in Western blots and concluded that Cdk5 and p25 levels were elevated following treatment of MPTP, which has a similar toxicity mechanism to PQ. The addition of TP5 decreased p25 expressio, confirming that TP5 selectively inhibits the activity of Cdk5/p25 without affecting Cdk5/p35 as there was no change in p35 when TP5 was introduced *in vivo* and *in vitro* (Binukumar et al., 2014). Thus, we conclude that TP5 can target the aberrant activation Cdk5/p25 in our PD model, validating the neuroprotective effects of TP5 at the cellular and behavioural level.

The pathophysiological markers of PD, i.e., dopaminergic neuron degeneration and Cdk5/p25 level, were inhibited by TP5. Overall, we have demonstrated the therapeutic potential of TP5 against Parkinsonian-like symptoms, through the protection of dopaminergic neurons and inhibition of elevated Cdk5/p25 levels. Further experiments should investigate other hallmarks of PD to validate the potential of TP5 as a treatment or neuroprotective agent towards PD.

Author roles

J. Tran designed the *in vitro* experimental design with R. Mishra and H. Pant and *in vivo* experimental design with B. Gupta, S. Taylor, and A. Gupta. J. Tran conducted the *in vitro* experiments. J. Tran, S. Taylor and A. Gupta conducted the *in vivo* experiments consisting of the behavioural work and imaging. B. Gupta performed the microinjections. N. Amin performed the Cdk5 immunoreactivity. J. Tran completed all statistical analyses and wrote the manuscript. All authors were involved in reviewing and editing the manuscript.

Funding

This research was supported by Canadian Institute of Health Research grant #126004 to Ram Mishra and Natural Sciences and Engineering Research Council (NSERC) Discovery grants to Ram Mishra and Bhagwati Gupta.

Declaration of competing interest

The authors declare that they have no known competing financial interests or personal relationships that could have appeared to influence the work reported in this paper.

Appendix A. Peer Review Overview and Supplementary data

A Peer Review Overview and (sometimes) Supplementary data associated with this article can be found, in the online version, at https://doi.org/10.1016/j.crneur.2021.100006.

References

Akinyemi, A.J., Miah, M.R., Ijomone, O.M., Tsatsakis, A., Soares, F., Tinkov, A.A., Skalny, A.V., Venkataramani, V., Aschner, M., 2019. Lead (Pb) exposure induces dopaminergic neurotoxicity in Caenorhabditis elegans: involvement of the dopamine transporter. Toxicology reports 6, 833–840. https://doi.org/10.1016/j.toxrep.2019.08.001.

Alvira, D., Ferrer, I., Gutierrez-Cuesta, J., Garcia-Castro, B., Pallàs, M., Camins, A., 2008. Activation of the calpain/cdk5/p25 pathway in the girus cinguli in Parkinson's disease. Park. Relat. Disord. 14 (4), 309–313. https://doi.org/10.1016/J.PARKRELDIS.2007.09.005.

Avraham, E., Rott, R., Liani, E., Szargel, R., Engelender, S., 2007. Phosphorylation of Parkin by the cyclin-dependent kinase 5 at the linker region modulates its ubiquitin-ligase activity and aggregation. J. Biol. Chem. 282 (17), 12842–12850. https://doi.org/10.1074/jbc.M608243200.

Biedler, J.L., Roffler-Tarlov, S., Schachner, M., Freedman, L.S., 1978. Multiple neurotransmitter synthesis by human neuroblastoma cell lines and clones. Cancer Res. 38 (11 Pt 1), 3751–3757.

Binukumar, B.K., Pant, H.C., 2016. TFP5/TP5 peptide provides neuroprotection in the MPTP model of Parkinson's disease. Neural Regen. Res 11 (5), 698–701. https://doi.org/10.4103/1673-5374.182681.

Binukumar, B.K., Shukla, V., Amin, N.D., Grant, P., Bhaskar, M., Skuntz, S., Pant, H.C., 2015. Peptide TFP5/TP5 derived from Cdk5 activator P35 provides neuroprotection in the MPTP model of Parkinson's disease. Mol. Biol. Cell 26 (24), 4478–4491. https://doi.org/10.1091/mbc.E15-06-0415.

Binukumar, B.K., Zheng, Y.L., Shukla, V., Amin, N.D., Grant, P., Pant, H.C., 2014. TFP5, a peptide derived from p35, a Cdk5 neuronal activator, rescues cortical neurons from glucose toxicity. J Alzheimers Dis 39 (4), 899–909. https://doi.org/10.3233/JAD-131784.

Bové, J., Perier, C., 2012. Neurotoxin-based models of Parkinson's disease. Neuroscience 211, 51–76. https://doi.org/10.1016/j.neuroscience.2011.10.057.

Brenner, S., 1974. The genetics of Caenorhabditis elegans. Genetics 77, 71–94. https://doi.org/10.1002/cbic.200300625.

Brooks, A.I., Chadwick, C.A., Gelbard, H.A., Cory-Slechta, D.A., Federoff, H.J., 1999. Paraquat elicited neurobehavioral syndrome caused by dopaminergic neuron loss. Brain Res. 823 (1–2), 1–10. https://doi.org/10.1016/S0006-8993(98)01192-5.

Cacabelos, R., 2017. Parkinson's disease: from pathogenesis to pharmacogenomics. Int. J. Mol. Sci. 18 (3), 551. https://doi.org/10.3390/ijms18030551.

Cagnon, L., Braissant, O., 2008. Role of caspases, calpain and cdk5 in ammonia-induced cell death in developing brain cells. Neurobiol. Dis. 32 (2), 281–292. https://doi.org/10.1016/j.nbd.2008.07.012.

Chase, D.L., Koelle, M.R., 2007. Biogenic amine neurotransmitters in C. elegans. *Worm* : the online review of C. elegans biology 1–15. https://doi.org/10.1895/wormbook.1.132.1.

Dinis-Oliveira, R.J., Remião, F., Carmo, H., Duarte, J.A., Navarro, A.S., Bastos, M.L., Carvalho, F., 2006. Paraquat exposure as an etiological factor of Parkinson's disease. Neurotoxicology 27 (6), 1110–1122. https://doi.org/10.1016/j.neuro.2006.05.012.

Drolet, R.E., Cannon, J.R., Montero, L., Greenamyre, J.T., 2009. Chronic rotenone exposure reproduces Parkinson's disease gastrointestinal neuropathology. Neurobiol. Dis. 36 (1), 96–102. https://doi.org/10.1016/j.nbd.2009.06.017.

Ellis, J.M., Fell, M.J., 2017. Current approaches to the treatment of Parkinson's Disease. Bioorg. Med. Chem. Lett 27 (18), 4247–4255. https://doi.org/10.1016/j.bmcl.2017.07.075.

Fernagut, P.O., Hutson, C.B., Fleming, S.M., Tetreaut, N.A., Salcedo, J., Masliah, E., Chesselet, M.F., 2007. Behavioral and histopathological consequences of paraquat intoxication in mice: effects of α-synuclein over-expression. Synapse 61 (12), 991–1001. https://doi.org/10.1002/syn.20456.

González-Hunt, C.P., Leung, M.C., Bodhicharla, R.K., McKeever, M.G., Arrant, A.E., Margillo, K.M., Ryde, I.T., Cyr, D.D., Kosmaczewski, S.G., Hammarlund, M., Meyer, J.N., 2014. Exposure to mitochondrial genotoxins and dopaminergic neurodegeneration in Caenorhabditis elegans. PloS One 9 (12). https://doi.org/10.1371/journal.pone.0114459 e114459.

Korecka, J.A., van Kesteren, R.E., Blaas, E., Spitzer, S.O., Kamstra, J.H., Smit, A.B., Bossers, K., 2013. Phenotypic characterization of retinoic acid differentiated SH-SY5Y cells by transcriptional profiling. PloS One 8 (5). https://doi.org/10.1371/journal.pone.0063862.

Langston, J.W., Forno, L.S., Tetrud, J., Reeves, A.G., Kaplan, J.A., Karluk, D., 1999. Evidence of active nerve cell degeneration in the substantia nigra of humans years after 1-methyl-4-phenyl-1,2,3,6-tetrahydropyridine exposure. Ann. Neurol. 46 (4), 598–605. https://doi.org/10.1002/1531-8249(199910)46:4<598::AID-ANA7>3.0.CO;2-F.

Lopes, J.P., Agostinho, P., 2011. Cdk5: multitasking between physiological and pathological conditions. Prog. Neurobiol. 94 (1), 49–63. https://doi.org/10.1016/j.pneurobio.2011.03.006.

Ma, L., Zhao, Y., Chen, Y., Cheng, B., Peng, A., Huang, K., 2018. Caenorhabditis elegans as a model system for target identification and drug screening against neurodegenerative diseases. Eur. J. Pharmacol. 819, 169–180. https://doi.org/10.1016/j.ejphar.2017.11.051.

Manning-Bog, A.B., McCormack, A.L., Li, J., Uversky, V.N., Fink, A.L., Di Monte, D.A., 2002. The herbicide paraquat causes up-regulation and aggregation of alpha-synuclein in mice: paraquat and alpha-synuclein. J. Biol. Chem. 277 (3), 1641–1644. https://doi.org/10.1074/jbc.C100560200.

Maulik, M., Mitra, S., Bult-Ito, A., Taylor, B.E., Vayndorf, E.M., 2017. Behavioral phenotyping and pathological indicators of Parkinson's disease in C. elegans models. Front. Genet. 8, 77. https://doi.org/10.3389/fgene.2017.00077.

Miyazaki, I., Asanuma, M., 2008. Dopaminergic neuron-specific oxidative stress caused by dopamine itself. Acta Med. Okayama 62 (3), 141–150. https://doi.org/10.18926/AMO/30942.

Nandipati, S., Litvan, I., 2016. Environmental exposures and Parkinson's disease. Int. J. Environ. Res. Publ. Health 13 (9), 881. https://doi.org/10.3390/ijerph13090881.

Nass, R., Blakely, R.D., 2003. The Caenorhabditis elegans dopaminergic system: opportunities for insights into dopamine transport and neurodegeneration. Annu. Rev. Pharmacol. 43 (1), 521–544. https://doi.org/10.1146/annurev.pharmtox.43.100901.135934.

Peng, J., Mao, X.O., Stevenson, F.F., Hsu, M., Andersen, J.K., 2004. The herbicide paraquat induces dopaminergic nigral apoptosis through sustained activation of the JNK pathway. J. Biol. Chem. 279 (31), 32626–32632. https://doi.org/10.1074/jbc.M404596200.

Richman, C., Rashid, S., Prashar, S., Mishra, R., Selvaganapathy, P.R., Gupta, B.P., 2018. C. elegans MANF homolog is necessary for the protection of dopaminergic neurons and ER unfolded protein response. Front. Neurosci. 12, 544. https://doi.org/10.3389/fnins.2018.00544.

Salam, S., Ansari, A., Amon, S., Rezai, P., Selvaganapathy, P.R., Mishra, R.K., Gupta, B.P., 2013. A microfluidic phenotype analysis system reveals function of sensory and dopaminergic neuron signaling in C. elegans electrostatic swimming behavior. Worm 2 (2). https://doi.org/10.4161/worm.24558 e24558.

Sawin, E.R., Ranganathan, R., Horvitz, H.R., 2000. C. elegans locomotory rate is modulated by the environment through a dopaminergic pathway and by experience through a serotonergic pathway. Neuron 26 (3), 619–631. https://doi.org/10.1016/S0896-6273(00)81199-X.

Shukla, V., Zheng, Y.L., Mishra, S.K., Amin, N.D., Steiner, J., Grant, P., Pant, H.C., 2013. A truncated peptide from p35, a Cdk5 activator, prevents Alzheimer's disease phenotypes in model mice. Faseb. J. 27 (1), 174–186. https://doi.org/10.1096/fj.12-217497.

Smith, P.D., Crocker, S.J., Jackson-Lewis, V., Jordan-Sciutto, K.L., Hayley, S., Mount, M.P., Park, D.S., 2003. Cyclin-dependent kinase 5 is a mediator of dopaminergic neuron loss in a mouse model of Parkinson's disease. Proc. Natl. Acad. Sci. Unit. States Am. 100 (23), 13650–13655. https://doi.org/10.1073/pnas.2232515100.

Taylor, S.K.B., Minhas, H.M., Tong, J., Selvaganapathy, P.R., Mishra, R.K., Gupta, B.P., 2021. *C. elegans* electrotaxis behavior is modulated by heat shock response and unfolded protein response signaling pathways. Sci. Rep. 11 (3115) https://doi.org/10.1038/s41598-021-82466-z.

Wilkaniec, A., Czapski, G.A., Adamczyk, A., 2016. Cdk5 at crossroads of protein oligomerization in neurodegenerative diseases: facts and hypotheses. J. Neurochem. 136 (2), 222–233. https://doi.org/10.1111/jnc.13365.

Wu, S., Lei, L., Song, Y., Liu, M., Lu, S., Lou, D., He, D., 2018. Mutation of hop-1 and pink-1 attenuates vulnerability of neurotoxicity in C. elegans: the role of mitochondria-associated membrane proteins in Parkinsonism. Exp. Neurol. 309, 67–78. https://doi.org/10.1016/j.expneurol.2018.07.018.

Yang, W., Tiffany-Castiglioni, E., 2005. The bipyridyl herbicide paraquat produces oxidative stress-mediated toxicity in human neuroblastoma SH-SY5Y cells: relevance to the dopaminergic pathogenesis. J. Toxicol. Environ. Health Part A 68 (22), 1939–1961. https://doi.org/10.1080/15287390500226987.

Yang, W., Tiffany-Castiglioni, E., 2008. Paraquat-induced apoptosis in human neuroblastoma SH-SY5Y cells: involvement of p53 and mitochondria. J. Toxicol. Environ. Health Part A 71 (4), 289–299. https://doi.org/10.1080/15287390701738467.

Yin, J.A., Liu, X.J., Yuan, J., Jiang, J., Cai, S.Q., 2014. Longevity manipulations differentially affect serotonin/dopamine level and behavioral deterioration in aging Caenorhabditis elegans. J. Neurosci. 34 (11), 3947–3958. https://doi.org/10.1523/JNEUROSCI.4013-13.2014.

Zheng, Y.L., Amin, N.D., Hu, Y.F., Rudrabhatla, P., Shukla, V., Kanungo, J., Pant, H.C., 2010. A 24-residue peptide (p5), derived from p35, the Cdk5 neuronal activator, specifically inhibits Cdk5-p25 hyperactivity and tau hyperphosphorylation. J. Biol. Chem. 285 (44), 34202–34212. https://doi.org/10.1074/jbc.M110.134643.

6.3 Appendix C. Investigation into the regulation of the Stress response by *pry-1, picd-1 and kin-9.*

6.3.1 Preface

This chapter includes the following unpublished work and two articles in their original published and submitted format:

1) The regulation of MANF-1 by PRY-1/AXIN to maintain proteostasis within animals. by Shane K. B. Taylor
2) Cabin1 domain-containing gene *picd-1* interacts with *pry-1/Axin* to regulate multiple processes in *Caenorhabditis elegans* by Avijit Mallick, Shane K. B. Taylor, Sakshi Mehta & Bhagwati P. Gupta. Scientific Reports. **12**, 1–18 (2022). https://doi.org/10.1038/s41598-022-15873-5
3) The FGFR4 Homolog KIN-9 Regulates Lifespan and Stress Responses in *Caenorhabditis elegans* by Avijit Mallick, Leo Xu, Sakshi Mehta, Shane K. B. Taylor, Hannah Hosein and Bhagwati P. Gupta. Frontiers in Aging. (2022). DOI: 10.3389/fragi.2022.866861

In this appendix I examined the relation between *pry-1* and genes which are known to be involved in activating the stress response. In the first section of Appendix B, we find that MANF-1 overexpression is able to protect against neurodegeneration and lifespan defects observed in *pry-1* mutant animals. In section 2 of Appendix B we discovered a novel gene picd-1 which regulates a suite of pry-1 mediated phenotypes, in particular the stress response and lifespan. We find that both pry-1 and picd-1 cause CRTC-1 nuclear localization which regulates longevity in a calcineurin-dependent manner. In section 3 of Appendix B we investigate the Fibroblast Growth Factor Receptor homolog kin-9, and found it is essential in ER-UPR maintenance and is potentially downstream of *pry-1* in mediating longevity.

Contributions

Towards article **1)** above I, Shane Taylor performed all experiments and wrote the summary and discussion of them.

Towards article **2)** above I, Shane Taylor performed experiments and analyzed Figures 8A-C, 9G-H, 10B and 10D. Avijit Mallick and Sakshi performed all other experiments. Avijit created the figures and the initial manuscript. I, Avijit and Dr. Gupta revised the entire manuscript for submission and addressed reviewer comments for publication.

Towards article **3)** above I performed experiments towards Figure 3D and E. All other authors performed the experiments and analyzed the other sets of data. Avijit and Dr. Gupta wrote the manuscript. I edited and aided in reviewer responses for publication.

6.3.2 Taylor and Gupta. The interaction between MANF-1 and PRY-1

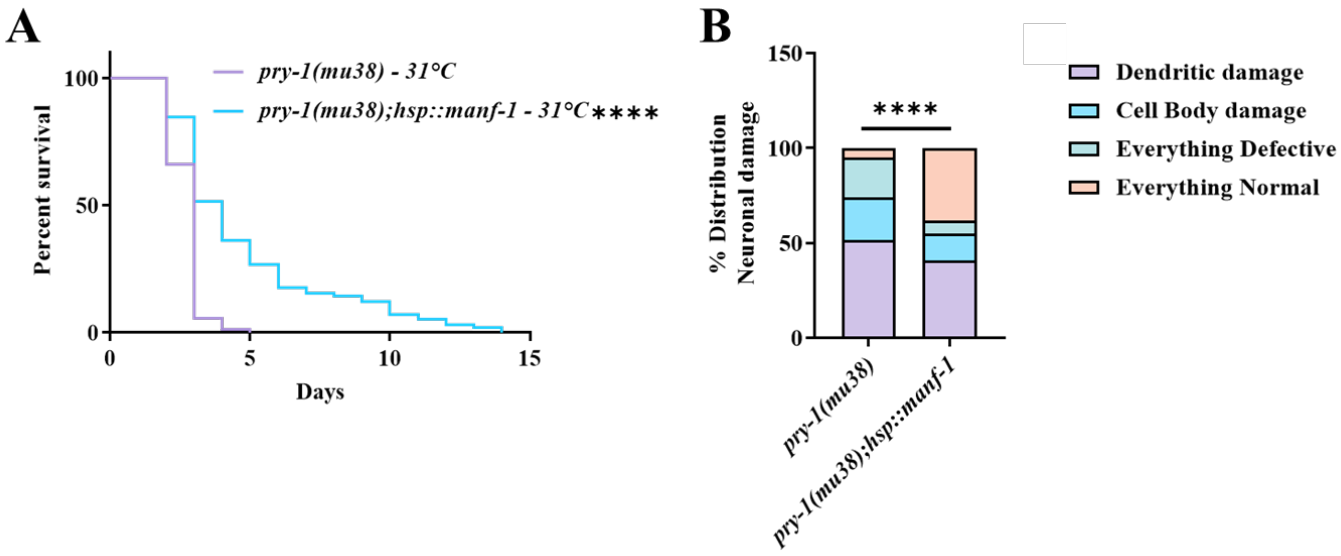

Figure C1. MANF overexpression rescues lifespan and neuronal defect in *pry-1(mu38)* animals. A**)** The lifespan analysis of overexpression of *manf-1* in *pry-1(mu38)* mutants following heat shock at 31°C. This heat treatment was done from the fourth larval stage and on day 1 of adulthood. There was a significant difference in lifespan between *pry-1(mu38)* at 31°C (mean 2.905 ± 0.136) compared with *pry-1(mu38);hsp::manf-1* at 31°C (mean 4.146 ± 0.345). *manf-1* overexpression was able to extend *pry-1* mutant lifespan. **B)** Neuronal analysis of *pry-1(mu38)* day 1 adults with *manf-1* overexpression. Animals had the same heat treatment as in **A**. *pry-1* mutants Animals had significantly improved neuronal health following *manf-1* increased expression. **A-B**: n = 3 batches of pooled worms (>50 in total). Results are expressed as mean ± SEM. **A:** lifespan analysis was done using the log-rank (Kaplan-Meier) method. **B:** was analyzed using Chi square test (*p<0.05;**p<0.01;*** p<0.001;****p<0.0001)

6.3.3 Mallick et al. 2022. Scientific Reports

www.nature.com/scientificreports

scientific reports

Check for updates

OPEN

Cabin1 domain-containing gene *picd-1* interacts with *pry-1/Axin* to regulate multiple processes in *Caenorhabditis elegans*

Avijit Mallick, Shane K. B. Taylor, Sakshi Mehta & Bhagwati P. Gupta✉

The Axin family of scaffolding proteins control diverse processes, such as facilitating the interactions between cellular components and providing specificity to signaling pathways. While several Axin family members have been discovered in metazoans and shown to play crucial roles, their mechanism of action are not well understood. The *Caenorhabditis elegans* Axin homolog, *pry-1*, is a powerful tool for identifying interacting genes and downstream effectors that function in a conserved manner to regulate Axin-mediated signaling. Our lab and others have established *pry-1*'s essential role in developmental processes that affect the reproductive system, seam cells, and a posterior P lineage cell, P11.p. Additionally, *pry-1* is crucial for lipid metabolism, stress responses, and aging. In this study, we expanded on our previous work on *pry-1* by reporting a novel interacting gene named *picd-1* (*pry-1*-interacting and Cabin1 domain-containing). PICD-1 protein shares sequence conservation with CABIN1, a component of the HUCA complex. Our findings have revealed that PICD-1 is involved in several *pry-1*-mediated processes, including stress response and lifespan maintenance. *picd-1*'s expression overlapped with that of *pry-1* in multiple tissues throughout the lifespan. Furthermore, PRY-1 and PICD-1 inhibited CREB-regulated transcriptional coactivator homolog CRTC-1, which promotes longevity in a calcineurin-dependent manner. Overall, our study has demonstrated that *picd-1* is necessary for mediating *pry-1* function and provides the basis to investigate whether Cabin-1 domain-containing protein plays a similar role in Axin signaling in other systems.

Signaling pathways enable cells to communicate with each other and their environment. Because of their essential role in cells, these pathway components are tightly regulated via interaction with a host of cellular factors. The Axin family is a group of scaffolding proteins that bring together different proteins to facilitate their interactions and regulate their activity[1]. There are two Axin homologs in mammals: Axin1 and Axin2. Axin was initially discovered as a negative regulator of the WNT-mediated signaling cascade. However, subsequent studies revealed a much broader role of these proteins in other pathways, including JNK, AMPK, and TGFβ[1–4]. Axin regulates several processes, including organogenesis, anterior–posterior axis formation, neuronal development, and metabolic homeostasis. Further, loss of Axin function causes lethality, neuroectodermal defects, abnormal body axis patterning, and reduced adipogenesis[1]. However, the mechanism by which Axin regulates different biological processes and mediates specific interactions is not well understood.

In the nematode *C. elegans*, the Axin homolog PRY-1 controls processes such as embryogenesis, neuronal differentiation, vulval development, P11.p cell fate, and seam cell development[1,5–7]. The WNT-dependent function of PRY-1 in vulval cells involves its interactions with several other proteins to form a destruction complex that results in the phosphorylation and degradation of BAR-1 (β-Catenin)[5]. However, little is known about the factors that interact with PRY-1 in WNT-independent processes. A comprehensive understanding of *pry-1* function will require identification of its interacting proteins and downstream effectors. To this end, we previously performed a transcriptome profiling of *pry-1* that revealed novel interacting partners and genetic network of *pry-1* that regulate post-developmental events[6,8]. Specifically, we showed that PRY-1 is crucial for lipid metabolism, stress response, and lifespan maintenance, where it interacts with WNT-independent signaling pathway components[4,8–11]. These include SBP-1/SREBP and vitellogenin involved in fatty acid synthesis and lipid storage, AAK-2/AMPK in the muscle that non-autonomously activates DAF-16/FOXO in the intestine and delays aging[8,10], and the components of the endoplasmic reticulum unfolded protein response (ER-UPR) pathway.

Department of Biology, McMaster University, 1280 Main Street West, Hamilton, ON L8S 4K1, Canada. ✉email: guptab@mcmaster.ca

	VPC induction (% induced)							Over-induced VPCs and P12.pa			Pvl and Muv		
Genotype	**P3p**	**P4p**	**P5p**	**P6p**	**P7p**	**P8p**	**N**	**% Over induced**	**% P12pa***	**N**	**% Pvl**	**%Muv**	**N**
N2	0	0	100	100	100	0	20	0	0	20	0	0	20
pry-1(gk3682)	27.3	4.5	100	100	86.4	4.5	22	36.4	72.7 (< 0.01)	22	65.7 (< 0.001)	31.3 (< 0.001)	40
pry-1(mu38)	18.2	0	100	100	81.8	9.1	22	27.2	81.8 (< 0.01)	22	59.6 (< 0.001)	34.2 (< 0.001)	50
picd-1(gk3701)	0	0	100	100	100	0	20	0	0 (n.s.)	20	5 (< 0.05)	0 (n.s.)	40
picd-1(bh40)	0	0	100	100	100	0	20	0	0 (n.s.)	20	16.7 (< 0.01)	0 (n.s.)	40
pry-1(gk3681); picd-1(gk3701)	21.7	8.7	100	100	87	13	23	39.1	74 (n.s.)	23	76.8 (< 0.01)	22 (< 0.01)	40
pry-1(mu38)	18.2	0	100	100	81.8	9.1	22	27.2	81.8	22	59.6	34.2	50
pry-1(mu38); picd-1(bh40)	12.5	12.5	100	100	92	12.5	24	25	100 (n.s.)	24	80 (< 0.01)	20 (< 0.01)	40

Table 1. Analysis of VPC induction, P12.pa cell fate, Pvl, and Muv penetrance in different strains. Each data consists of two independent replicates. Statistical analyses were done using one way-ANOVA. p values are indicated in brackets. n.s., not significant. While *pry-1* and *picd-1* mutants were compared to N2 control, *pry-1; picd-1* double mutants were compared to respective *pry-1* alleles. *Extra P12.pa cell in the place of P11.p. *N* number of animals examined.

Additionally, in a separate study, we reported genes regulated by *pry-1* during stress response and lifespan maintenance that include *cpz-1* (proteolysis), *cdk-1* (cell cycle), *rnr-1* (DNA replication), *his-7* (gene expression), and *ard-1* (mitochondrial oxidation/reduction)[7].

This paper reports a novel downstream effector of *pry-1* signaling called *picd-1* that is critical for regulating multiple developmental and post-developmental processes. PICD-1 shares a domain with the mammalian calcineurin-binding protein 1 (CABIN1), a component of the histone H3.3 chaperone complex HUCA[12]. cabin1 negatively regulates calcineurin signaling, which in turn affects various cellular functions, including stress response and lifespan[13–16]. We show that PICD-1 negatively regulates CREB-regulated transcriptional coactivator (CRTC) homolog, CRTC-1, which promotes longevity mediated by calcineurin signaling[17]. Consistent with the *pry-1*'s role in promoting *picd-1* expression, *pry-1* mutants exhibit nuclear localization of CRTC-1, suggesting that PICD-1 is involved in PRY-1-mediated CRTC-1 regulation. These results demonstrate the critical role of PICD-1 in *C. elegans* and prompt future studies to investigate the involvement of Cabin1 and calcineurin signaling in Axin-mediated processes in eukaryotes.

Results

picd-1* encodes a CABIN1 domain-containing protein.** A CRISPR-based screening was carried out earlier to isolate alleles of *pry-1*[6] (see "Methods"). In that screen we also discovered a mutation (*gk3701)* in an unrelated gene *F56E10.1* (WBGene00018975), now named *picd-1* (p****ry-1* **i**nteracting and **C**abin1 **d**omain-containing, see "Methods"). The *pry-1(gk3681); picd-1(gk3701)* double mutant exhibited a significant increase in the protruding-vulva (Pvl) phenotype (77%, compared to 66% in *pry-1* mutants alone) and pronounced protrusions that frequently burst in the vulva (Table 1, Fig. 1A,B, Video S1). It should be noted that *gk3681* is identical to another *pry-1* mutation, *gk3682,* and both mutant strains were recovered in the same CRISPR screen (see "Methods" and Figure S1). Sequence analysis of *picd-1* identified orthologs in other nematode species (Fig. 1C), all of which contain a domain similar to the histone transcription regulator 3 (Hir3)/calcineurin-binding protein (CABIN1) family members (IPR033053, https://www.ebi.ac.uk/interpro/) (Fig. 1C,D). The alignments of PICD-1 with human CABIN1 (isoform a) showed 26% (729/2853) identity and 38% (1080/2853) similarity (EMBOSS stretcher pairwise alignment tool; https://www.ebi.ac.uk/Tools/psa/). Similar sequence conservation was observed in the case of mouse CABIN1 (Fig. 1C). Studies have shown that human CABIN1 is part of the histone H3.3 chaperone complex HUCA (HIRA/UBN1/CABIN1/ASF1a), involved in nucleosome assembly. Similarly, Gene Ontology (GO) analysis (http://www.wormbase.org) revealed that *picd-1* is associated with the biological process "DNA replication-independent nucleosome assembly" (GO:0006336) and the cellular component "nucleus" (GO:0005634). Thus, *picd-1* is likely to encode a nuclear protein that functions in chromatin assembly and regulation of gene expression. Furthermore, in silico analysis revealed that PICD-1 contains 49 amino acid residues predicted to bind DNA (http://biomine.cs.vcu.edu/servers/DRNApred/#References)[18](Table S1).

Mutations in *picd-1* do not affect vulval induction but cause morphogenetic defects. In addition to using the *gk3701* strain to examine mutant phenotypes, we generated a new allele, *bh40*, which has multiple in-frame stop codons in exon 1 (see "Methods" and Fig. 2A,B). qPCR analysis showed that *bh40* and *gk3701* greatly reduced *picd-1* transcript levels (Fig. 2C). Interestingly, while the Pvl phenotype of *pry-1(mu38)* was enhanced by both the alleles (Fig. 1A,B), neither had an obvious impact on the penetrance of the multivulva (Muv) phenotype in *pry-1(mu38)* animals. In fact, the double mutants showed a slightly less Muv phenotype compared to *pry-1(mu38)* alone (Table 1, Fig. 1B), which may be due to changes in morphogenetic processes as vulval precursor induction is not affected by any of the *picd-1* mutations (Fig. 2D, Table 1). Similar phenotypes were observed following *picd-1* RNAi (Figure S2). In agreement with this, *picd-1(bh40),* but not *picd-1(gk3701),* exhibited abnormal vulval invagination (Fig. 3A) and the vulval morphology phenotype of *pry-1(mu38); picd-*

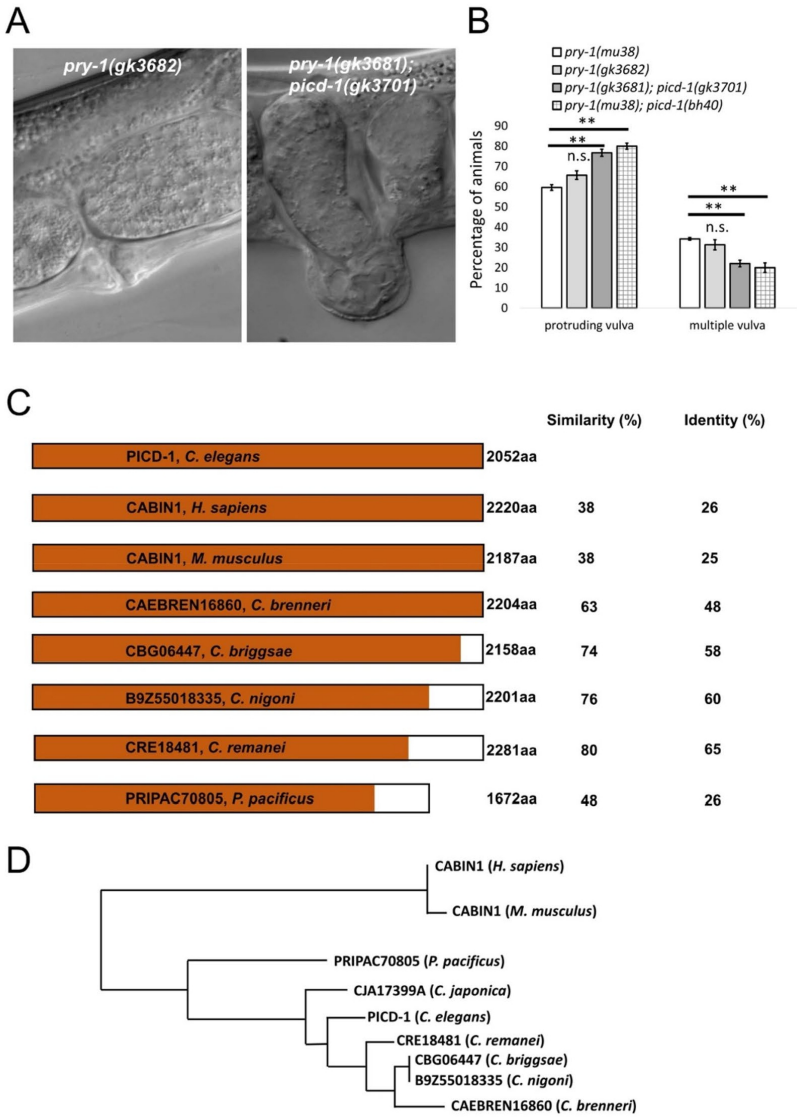

Figure 1. Phenotype of *picd-1* mutants and sequence similarity of PICD-1 with CABIN1 proteins. (**A**) Representative images of Pvl phenotype in *pry-1(gk3682)* and *pry-1(gk3681); picd-1(gk3701)* animals. (**B**) *picd-1* mutation enhances Pvl phenotype of *pry-1* mutants. Data represent a cumulative of two replicates (n = 99 for *pry-1(mu38)*, 160 for *pry-1(mu38); picd-1(bh40)*, 118 for *pry-1(gk3682)* and 156 for *pry-1(gk3682); picd-1(gk3701)*) and error bars represent the standard deviation (Also see Table 1 and Fig. 3). Statistical analyses for panel (**B**) were done compared to *pry-1* mutants alone using one-way ANOVA with Dunnett's post hoc test and significant differences are indicated by stars (*): ** ($p < 0.01$). n.s., not significant. (**C**) Sequence comparison of *C. elegans* PICD-1 with mammalian CABIN1 and nematode homologs. Orange colors indicate regions of the proteins where alignments were identified by NCBI BLAST along with similarity and identity scores. Non-colored regions are those without sequence similarity. (**D**) Sequence alignment dendrogram generated by LIRMM (http://www.phylogeny.fr/simple_phylogeny.cgi) using default parameters.

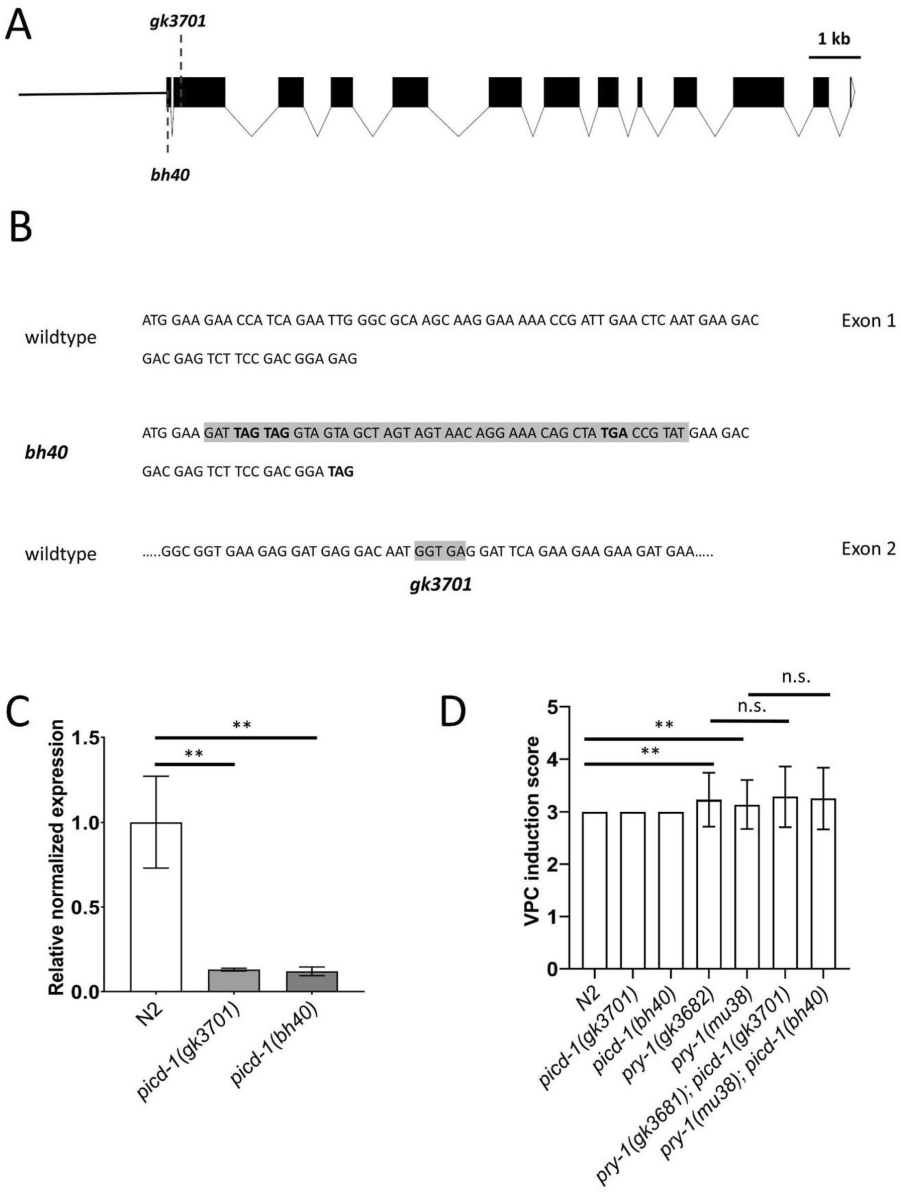

Figure 2. Analysis of *picd-1* alleles and their effect on *pry-1* mutant Pvl phenotype. (**A**) Schematic diagram of the *picd-1* open reading frame. The approximate locations of *bh40* and *gk3701* mutations have been indicated. (**B**) Sequences for *bh40* and *gk3701* mutations are shown in gray color. and stop codons are shown in bold (also see "Methods"). (**C**) Expression levels of *picd-1* in *pry-1(gk3682)* and *pry-1(mu38)* mutants at the L1 stage compared to wild-type. Data represent the means of two replicates and error bars represent the standard error of means. *p* values were calculated using Bio-Rad software (one-way ANOVA). (**D**) Bar graph showing VPC induction score in *picd-1* and *pry-1* mutants alone, and *pry-1; picd-1* double mutants compared to N2. Data represent the means of two replicates. The error bars show the standard deviation (n = 22). Statistical analyses were done using one-way ANOVA with Dunnett's post hoc test. In panels (**C,D**), significant differences are indicated by stars (*): ** ($p < 0.01$). n.s., not significant.

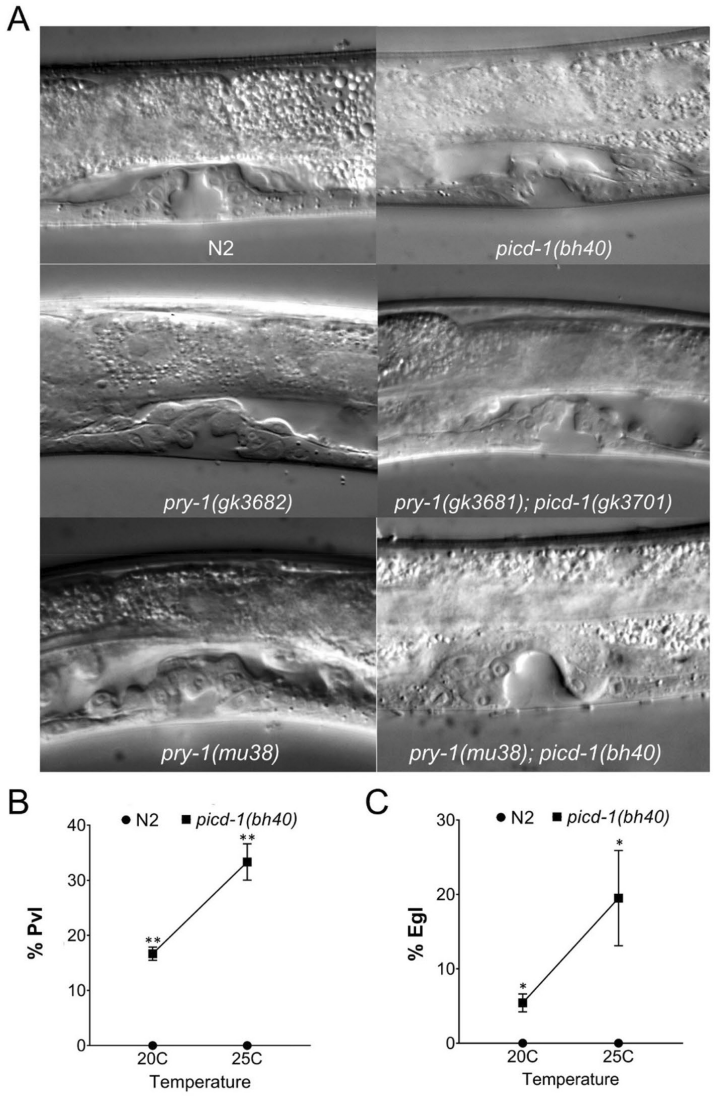

Figure 3. *picd-1* regulates vulval morphology. (**A**) Representative vulval images of wild-type, and *picd-1* and *pry-1* mutants at the mid-L4 stage. *picd-1(bh40)* animals exhibited abnormal vulva morphology (20.8 ± 5.8%, $p < 0.01$, n = 35) compared to N2 animals. Scale bar is 50 µm. (**B**) Line graph showing the percentage of control and *picd-1(bh40)* mutants showing Pvl phenotype at 20 °C and 25 °C compared to wild-type controls (Also see Table 1). (**C**) Line graph showing the percentage of control and *picd-1(bh40)* animals with Egl phenotype at 20 °C and 25 °C. (**B**, **C**) Data represent a cumulative of two replicates (n = 64 for *picd-1(bh40)* and 58 for N2) and error bars represent the standard deviation. Statistical analyses were done using an unpaired t-test and significant differences are indicated by stars (*): * ($p < 0.05$), ** ($p < 0.01$).

1(bh40) double mutant was more severe compared to *pry-1(mu38)* alone. Furthermore, adult *picd-1* mutants were weakly Pvl (Fig. 3B and Table 1).

Phenotypic analysis of both *picd-1* mutant strains did not reveal any obvious defects in movement, feeding, and other characteristics. However, careful examination showed that this gene is involved in the development

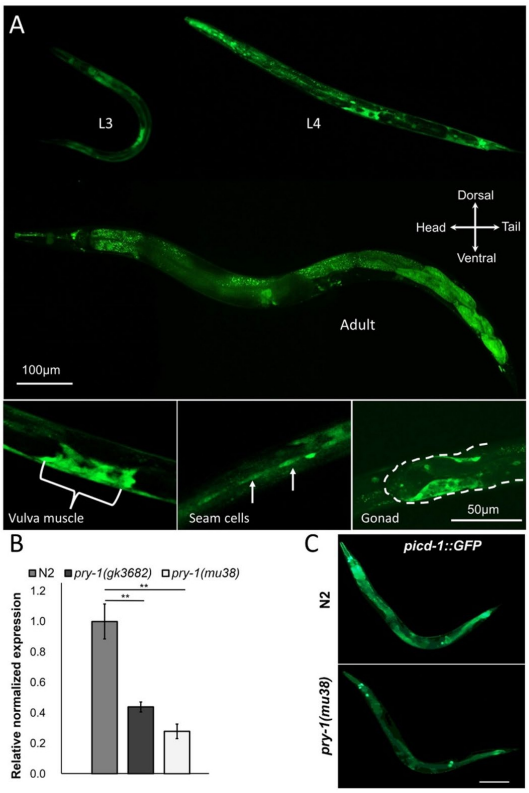

Figure 4. Expression analysis of *picd-1*. (**A**) Representative images of animals expressing *picd-1::GFP* in larvae and adults. Tissues that show fluorescence include pharynx, gonad, hypodermis, intestine, vulva, body wall muscles, and some in the tail region. Scale bars are shown. (**B**) Expression levels of *picd-1* in *pry-1* mutants. Data represent the means of two replicates and error bars represent the standard error of means. *p* values were calculated using Bio-Rad software (one-way ANOVA). In panel (**B**) significant differences are indicated by stars (*): ** ($p < 0.01$). (**C**) Representative images of N2 and *pry-1(mu38)* adults showing *picd-1::GFP* expression. Scale bar is 100 µm.

of the egg-laying system. The *picd-1(bh40)* worms were weakly egg-laying defective (Egl) (Fig. 3C, Video S2), and their Egl and Pvl phenotypes were enhanced at 25 °C (Fig. 3B,C). No Egl phenotype was observed in the *picd-1(gk3701)* strain. While more experiments are needed to determine the molecular basis of phenotypic differences between the two alleles, the data collectively demonstrate that *picd-1* is required for the development of the reproductive system.

***picd-1* is expressed in multiple tissues.** To gain further insights into the function of *picd-1*, we created a stable line carrying a *picd-1::GFP* transcriptional reporter. The analysis of transgenic animals revealed GFP fluorescence in developing tissues and organs, such as the pharynx, intestine, body wall muscles, hypodermis (seam cells), gonads, and vulva (Fig. 4A). This expression pattern resembled that of *pry-1*, which was recently described by our group[10]. As *picd-1::GFP* animals entered adulthood, fluorescence was localized to the intestine and certain head neurons (Fig. 4A), which persisted throughout the life of the animals. A broad range of *picd-1* expression was also supported by previously published RNA-sequencing and microarray studies[19,20]. Overall, our expression analysis suggests that *picd-1* functions in multiple tissues and may play a role in *pry-1*-mediated developmental and post -developmental processes.

Since *picd-1::GFP* is expressed in similar tissues as *pry-1,* and *picd-1* mutation enhanced the *pry-1* Pvl phenotype, we examined whether *pry-1* affects *picd-1* expression. The results of qPCR and *picd-1::GFP* fluorescence showed that *picd-1* is downregulated in *pry-1* mutants (Fig. 4B,C). The GFP levels were generally reduced throughout the animal (Fig. 4C). These results suggest that *picd-1* expression is dependent on *pry-1*.

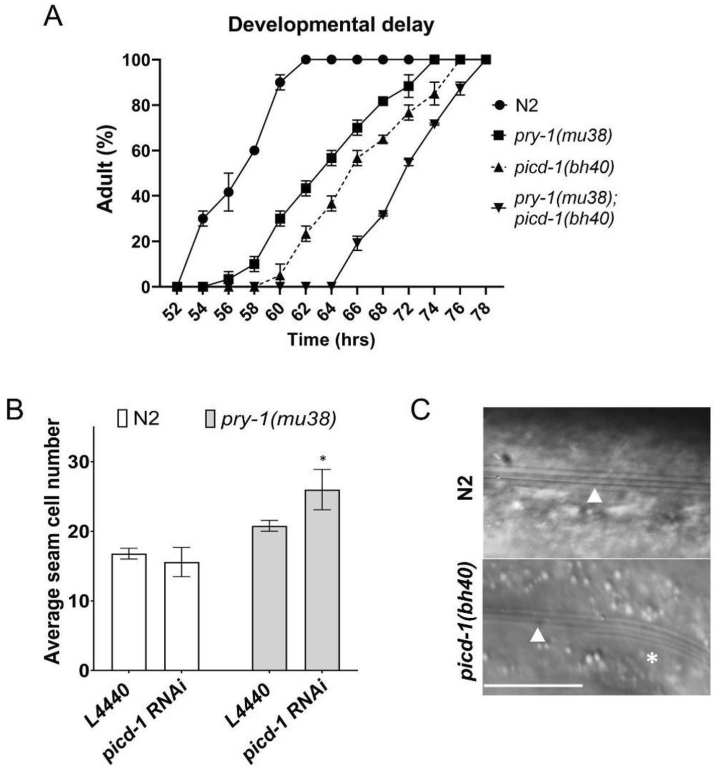

Figure 5. *picd-1* regulates developmental timing, seam cell division and alae formation. (**A**) *picd-1* mutants exacerbate the developmental delay of *pry-1* mutants. The data shows the average time taken by *picd-1(bh40), pry-1(mu38)* and *pry-1(mu38); picd-1(bh40)* double mutants to reach adulthood compared to wild-type animals. The number of animals for two replicates are: n = 60 for N2, *pry-1(mu38),* and *picd-1(bh40)*; and 95 for *pry-1(mu38); picd-1(bh40)*) The error bars represent the standard deviation. (**B**) Bar graph showing the average number of seam cells (two replicates, n = 30) in the wild-type and *pry-1(mu38)* animals following control (L4440) and *picd-1* RNAi. The error bars represent the standard deviation. (**C**) Representative images showing alae (white arrowheads) in wild-type N2 and *picd-1(bh40)* animals. Normal alae are marked with an arrowhead and an extra alae in the *picd-1* mutant is indicated by a star (*) (41.88 ± 0.22%, n = 43, $p < 0.0001$). Statistical analyses were done using multiple unpaired t-test and recorded in Table S2. In panel B, star (*) indicates $p < 0.05$. Scale bar in panel (**C**) is 25 µm.

***picd-1* mutations worsen the phenotypes of *pry-1* mutants.** Next, we investigated the involvement of *picd-1* in other *pry-1*-mediated developmental and post-developmental processes. *picd-1* mutants grew slowly and took longer to reach adulthood than the wild-type and *pry-1(mu38)* animals (Fig. 5A, Table S2). Furthermore, the growth defect in the *pry-1; picd-1* double mutant was significantly worse than in the single mutants (Fig. 5A, Table S2). Among other phenotypes, mutations in *picd-1* enhanced seam cell defects of *pry-1(mu38)* animals (Fig. 5B) that are caused by changes in asymmetric cell division at the L2 stage[6,21]. Moreover, both *picd-1* and *pry-1* mutants exhibited defects in alae, which are structures formed by differentiated seam cells[6] (Fig. 5C). Interestingly, the P lineage defect in *pry-1* mutants that involves P11.p and P12.pa cells was enhanced in *pry-1(mu38); picd-1(bh40)* but not in *pry-1(gk3681); picd-1(gk3701)* animals (Table 1, also see "Methods").

In addition, we observed several other developmental abnormalities in the *picd-1* mutant animals. The analysis of brood size revealed defects in *picd-1(bh40)* but not in *picd-1(gk3701)* animals (Fig. 6A,B). Although the *bh40* allele did not affect embryonic viability, it drastically reduced the brood count and enhanced the embryonic lethality of *pry-1* mutants ($p < 0.001$) (Fig. 6A–C). Further analysis revealed that *pry-1(gk3681); picd-1(gk3701)* and *pry-1(mu38); picd-1(bh40)* double mutants had abnormal oocytes and gonads, respectively (Fig. 7A,B). More specifically, 46 ± 6% (n = 45, $p < 0.01$) of *pry-1(mu38); picd-1(bh40)* animals lacked oocytes in the posterior gonad arm (Figs. 7B). No such phenotype was observed in either of the single mutants.

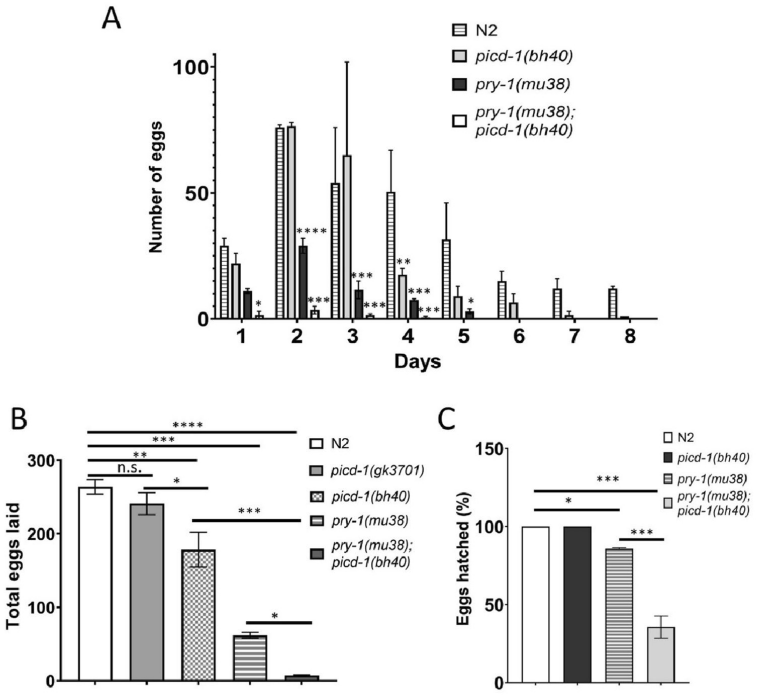

Figure 6. *picd-1* regulates brood size and embryonic viability. Bar graphs showing eggs laid on each day (**A**), totals number of eggs (**B**), and percentage of the hatched eggs (**C**) by N2 and single and double mutant animals. Data represent a cumulative of two replicates (total n = 10 for each genotype shown in panels (**A**) and (**B**); and n = 500 for N2, 120 for *pry-1(mu38)* and 14 for *pry-1(mu38); picd-1(bh40)* double mutants shown in panel (**C**) and error bars represent the standard deviation. (**A**) Statistical analyses were done using two-way ANOVA with Tukey's multiple comparison test and recorded in Table S2. (**B,C**) Statistical analyses were done using one-way ANOVA with Dunnett's multiple comparison test and significant differences are indicated by stars (*): * ($p < 0.05$), ** ($p < 0.01$), *** ($p < 0.001$), and **** ($p < 0.0001$). n.s., not significant.

***picd-1* mutants are sensitive to stress and exhibit a short lifespan.** We previously reported that *pry-1* plays a role in stress response maintenance[7,10]. The analysis of heat shock chaperones—*hsp-4* (ER-UPR), *hsp-6* (MT-UPR), and *hsp-16.2* (cytosolic heat shock response, HSR)—showed that all three were upregulated in *pry-1* mutant animals (Fig. 8A). Similar experiments in *picd-1* mutants showed increased expression of *hsp-4, hsp-16.2*, and the oxidative stress response gene *sod-3* (Fig. 8B). Consistent with these results, both *pry-1* and *picd-1* mutants showed electrotaxis defects (Fig. 8C and "Methods"), a phenotype observed in animals with abnormalities in stress sensitivity and UPR[22].

To further elucidate the stress sensitivity of animals lacking *picd-1* function, we examined the survivability of the animals following chemical treatments. Both *gk3701* and *bh40* alleles were sensitive to paraquat and tunicamycin, although the effect was more pronounced following paraquat exposure (Fig. 8D,E). We also tested paraquat sensitivity of *pry-1(mu38); picd-1(bh40)* double mutants and found no difference compared to *pry-1(mu38)* alone (Fig. 8F), which could be explained by the significantly reduced expression of *picd-1* in *pry-1* mutants.

As increased stress sensitivity can affect the lifespan of an animal, and *pry-1* mutants are short-lived, we analyzed whether *picd-1* plays a role in aging. Neither *picd-1*(*gk3701*) nor *picd-1*(RNAi) enhanced the lifespan defects of animals lacking *pry-1* function (Fig. 9A,B, Table 2). Considering that *pry-1* mutant animals have a significantly reduced expression of *picd-1* than the wild-type animals, it is conceivable that further reduction in *picd-1* cannot exacerbate the short-lived phenotype. Alternatively, it is plausible that *picd-1* is not involved in lifespan maintenance. To explore this further, we examined the lifespan of *picd-1* mutant and RNAi-treated animals in the absence of other mutations. Both *gk3701* and *bh40* alleles reduced the lifespan of the animals. *picd-1(bh40)* worms had a significantly reduced lifespan at both 20 °C and 25 °C, and *picd-1(gk3701)* exhibited a similar phenotype at 25 °C (Fig. 9C,D, Table 2). These results were also supported by the RNAi experiments. The analysis of age-associated biomarkers revealed a progressive age-associated decline in both body bending and

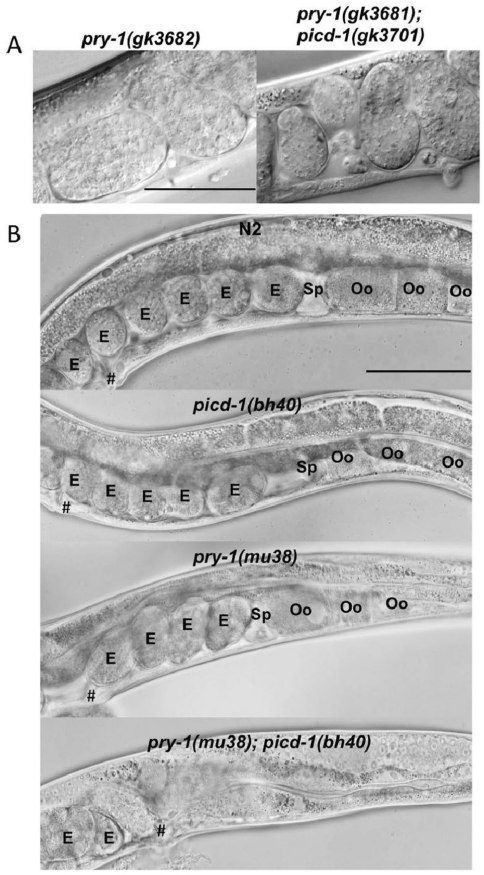

Figure 7. *picd-1* interacts with *pry-1* to regulate oocyte development. (**A**) *pry-1; picd-1* double mutants show abnormal oocytes. Scale bar is 25 µm. (**B**) Posterior gonad arms of wildtype, *picd-1(bh40), pry-1(mu38)* and *pry-1(mu38); picd-1(bh40)* adults. *pry-1(mu38); picd-1(bh40)* animals frequently lack oocytes (46 ± 6%, n = 45, $p < 0.01$) in the posterior gonad arm when compared to N2 and *pry-1(mu38)*. Statistical analysis was done using an unpaired t-test. The spermatheca (Sp), embryos (E), and oocytes (Oo) are marked. Vulva opening is marked (#). Anterior is on the left. Scale bar is 100 mm.

pharyngeal pumping rates (Fig. 9E,F). Overall, the data suggest that while *picd-1* does not enhance the phenotype of *pry-1* mutants, the gene plays an essential role in maintaining the usual lifespan of animals.

We have previously shown that in addition to affecting lifespan, *pry-1* regulates lipid metabolism[8,11]. This result prompted us to analyze whether *picd-1* affects lipid levels and the expression of genes involved in fatty acid synthesis. The analysis of Δ9 desaturases showed that while *fat-5* and *fat-7* were downregulated, *fat-6* was unaffected (Fig. 9G). Among the three transcription factors regulating the expression of Δ9 desaturases, *nhr-80* (NHR family) was downregulated, but *sbp-1* (SREBP1 homolog) was upregulated (Fig. 9G)[23]. We also quantified lipids by Oil Red O staining but saw no change in *picd-1* mutants (Fig. 9H), possibly due to functional redundancies within the *fat*[24,25] and *nhr* family of genes[23]. Hence, we conclude that *picd-1* is necessary for the expression of a subset of lipid synthesis genes but is not crucial for regulating lipid levels.

Loss of *picd-1* and *pry-1* promotes CRTC-1 nuclear localization. Research has shown that calcineurin (a calcium-activated phosphatase) signaling promotes nuclear localization of CRTC-1, leading to a reduction in the lifespan of *C. elegans*[17]. Given that human cabin1 negatively regulates calcineurin signaling[13,26], we investigated whether *picd-1* could affect the subcellular localization of CRTC-1::RFP. The RNAi knockdown of *picd-1* caused CRTC-1 to be nuclear localized, consistent with the short lifespan of *picd-1* mutants (Figs. 9C,D,

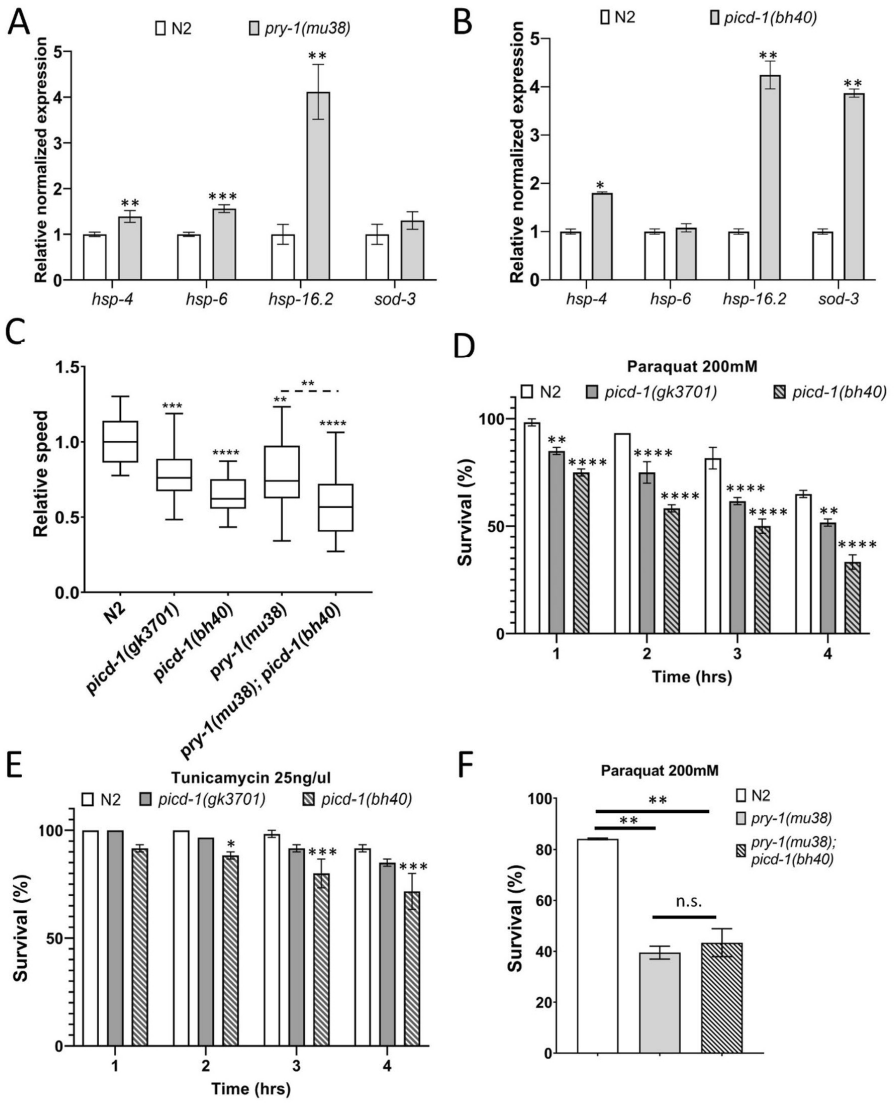

Figure 8. *picd-1* mutants are stress sensitive. (**A**, **B**) Expression levels of *hsp-4, hsp-6, hsp-16.2*, and *sod-3* in *picd-1(bh40)* and *pry-1(mu38)* young adults. Data represent the means of three replicates and error bars represent the standard error of means. *p* values were calculated using Bio-Rad software (t-test). (**C**) Box and whisker plots represent normalized electrotaxis speeds of *picd-1(gk3701)*, *picd-1(bh40)*, *pry-1(mu38)* and *pry-1(mu38); picd-1(bh40)* mutants (n = 20). Measurements show 25 to 75th percentiles of data, central horizontal lines represent medians, and vertical lines extend to 10th and 90th percentiles**.** (**D**) Bar graphs represent percentage survival following 200 mM paraquat exposure for 4 h (n = 90). (**E**) Bar graphs represent percentage survival of animals following 25 ng/µl tunicamycin exposure for 4 h. (**F**) Bar graphs represent percentage survival of animals following 200 mM paraquat exposure for 2 h (n = 120 for N2, 150 for *pry-1(mu38)* and 169 for *pry-1(mu38); picd-1(bh40)*). For panels (**C**–**F**), data are the cumulative of two replicates and error bars represent the standard deviation. (**C**, **F**) Statistical analyses were done using one-way ANOVA with Dunnett's multiple comparison test. (**D**, **E**) Statistical analyses were done using two-way ANOVA with Tukey's multiple comparison test. In all cases significant differences are indicated by stars (*): * ($p < 0.05$), ** ($p < 0.01$), *** ($p < 0.001$), **** ($p < 0.0001$). Refer to Table S2 for detailed statistical analyses.

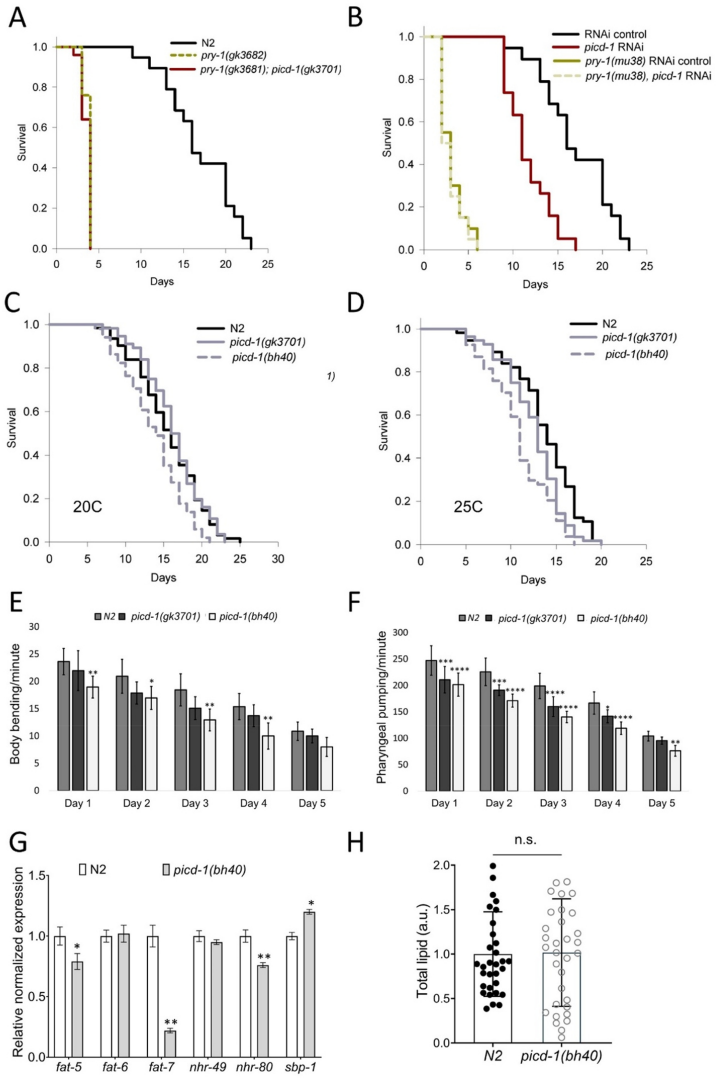

Figure 9. *picd-1* mutation reduces lifespan and causes age-associated deterioration. (**A**) *picd-1* mutation does not affect the lifespan of *pry-1* mutants. (**B**) *picd-1* RNAi reduces the lifespan of control animals but not that of *pry-1* mutants. (**C,D**) Lifespan of *picd-1(gk3701)* and *picd-1(bh40)* mutants at 20 °C and 25 °C. See "Materials and methods" section and Table 2 for lifespan data and statistical analyses. (**E,F**) Bar graphs showing the rates of body bending and pharyngeal pumping of *picd-1* mutants compared to wild-type over a period of 5 days. Data represent a cumulative of two replicates (n = 10 animals) and error bars represent the standard deviation. Statistical analyses were done using two-way ANOVA with Tukey's multiple comparison test. See Table S2 for detailed statistical analyses. (**G**) Expression analysis of *fat-5*, *fat-6*, *fat-7*, *nhr-49*, *nhr-80* and *sbp-1* genes in the *picd-1(bh40)* mutants compared to wild-type. Data represent the means of two replicates and error bars represent the standard error of means. *p* values were calculated using Bio-Rad software (one-way ANOVA). (**H**) Quantification of total lipid using Oil Red O in the wild-type and *picd-1(bh40)* animals. Data represent a cumulative of two replicates (n > 30 animals) and error bars represent the standard deviation. Statistical analysis was done using an unpaired t-test. In all cases, significant differences are indicated by stars (*): * ($p < 0.05$), ** ($p < 0.01$), *** ($p < 0.001$), and **** ($p < 0.0001$).

Genotype	Treatment	Mean lifespan (days)	Median lifespan (days)	Maximum lifespan (days)	N	*p* value
N2	–	16.9 ± 0.9	16	23	56	–
pry-1(gk3681)	–	3.1 ± 0.2	3	5	86	< 0.0001
pry-1(gk3682)	–	3.7 ± 0.1	4	4	45	< 0.0001
pry-1(gk3681); picd-1(gk3701)	–	3.6 ± 0.1	4	4	50	< 0.0001
picd-1(gk3701)	–	15.3 ± 0.5	16	21	44	n.s
picd-1(bh40)	–	13.7 ± 0.5	14	21	51	< 0.001
N2	*Empty vector*	16.6 ± 0.9	16	21	75	–
	picd-1 RNAi	11.6 ± 0.6	18	22	58	< 0.001
	crtc-1 RNAi	20.4 ± 0.9	22	26	63	< 0.01
pry-1(mu38)	*empty vector*	3.1 ± 0.3	3	6	79	–
	picd-1 RNAi	2.9 ± 0.3	2	6	80	n.s
	crtc-1 RNAi	5.1 ± 0.4	6	8	48	< 0.001
pry-1(gk3682)	*empty vector*	4.1 ± 0.3	4	6	52	–
	crtc-1 RNAi	7.1 ± 0.7	7	10	64	< 0.001
N2	25 °C	13.4 ± 0.5	14	20	56	–
picd-1(gk3701)	25 °C	11.9 ± 0.5	12	16	48	< 0.001
picd-1(bh40)	25 °C	10.9 ± 0.4	11	17	54	< 0.001

Table 2. Lifespan analysis of animals. Each lifespan assay was carried out in two or more batches (see Methods). Statistical analyses were done by comparing mutants with N2 control and RNAi treated animals with empty vector control. Comparisons of *pry-1(gk3681); picd-1(gk3701)* with *pry-1(gk3682)* and *picd-1(gk3701)* with *picd-1(bh40)* showed no significant differences. N, number of animals examined, n.s., not significant.

10A,B). Moreover, CRTC-1 responsive genes, *dod-24* and *asp-12*[27], were upregulated in the *picd-1(bh40)* mutants (Fig. 10C).

As *pry-1* is necessary for *picd-1* expression, we examined its effect on the CRTC-1::RFP and found that the fluorescence was nuclear-localized and *dod-24* and *asp-12* were upregulated in *pry-1* mutants (Fig. 10D–F). To further understand the mechanism of PRY-1-PICD-1-mediated CRTC-1 localization, we examined the involvement of the Wnt canonical pathway component BAR-1/β-catenin. The *bar-1* RNAi did not affect CRTC-1::RFP nuclear localization in *pry-1* mutants (Fig. 10G,H), suggesting that PRY-1 may function in a WNT-independent manner to regulate CRTC-1. This conclusion agrees with our previous findings that *pry-1*-mediated lifespan maintenance does not depend on *bar-1*[10]. Next, we examined the involvement of CRTC-1 in PRY-1-mediated lifespan and stress response and found that *crtc-1* RNAi performed during the adult stage significantly rescued the short lifespan and stress sensitivity defects of *pry-1* mutants (Fig. 10I,J and Table 2). Hence, we propose that PRY-1 inhibits CRTC-1-dependent transcriptional response to delay age-associated processes.

Given that calcineurin and CRTC-1 mediated lifespan regulation involves the *C. elegans* CREB transcription factor homolog 1 (CRH-1), we wanted to know whether PRY-1 and CRH-1 regulate a common set of target genes. Consistent with our hypothesis, we found a significant overlap in differentially expressed genes between *pry-1* and *crh-1* mutant transcriptomes (406 common genes, R.F 2.5, $p < 5.108e{-}78$)[8,27]. Furthermore, the number of overlapping sets of genes regulated in an opposite manner between *pry-1* and *crh-1* mutants were also significant (Figure S3 and Table S3) and were enriched with GO biological processes such as response to stress (18), metabolic processes (18), and cellular processes (40) (FDR < 0.05). In conclusion, these data demonstrate a novel functional relationship between PRY-1 and CRTC-1 in *C. elegans*.

Discussion

In this study, we identified a new gene, *picd-1*, in *C. elegans* that interacts with *pry-1* and regulates several larval and adult processes. *picd-1* is predicted to encode a nuclear protein containing a conserved Cabin1 domain, which belongs to the HUCA complex in humans[12]. The HUCA complex is implicated in diverse chromatin regulatory events, where it preferentially deposits a histone variant H3.3. This leads to transcriptional activation by nucleosome destabilization or transcriptional repression through heterochromatinization[28]. cabin1 is expressed in all human tissues and localized to the nucleoplasm and cytoplasm[29,30]. Studies in other systems have also uncovered homologous proteins of CABIN1. For example, the yeast *Saccharomyces cerevisiae* contains Hir1p and Hir2p (both HIRA orthologs) and Hir3, Hpc2, and Asf1p, orthologs of CABIN1, UBN1, and ASF1a, respectively[28].

Our study provides the first genetic evidence of a Cabin1 domain-containing protein regulating biological processes in *C. elegans*. Other complex components in worms include HIRA-1 (HIRA homolog), ASFL-1, and UNC-85 (both ASF1a homologs)[31–33]. However, it remains to be seen if any of these proteins interact with PRY-1. Mutations in *picd-1* led to multiple defects such as Pvl, Egl, small brood size, developmental delay, stress sensitivity, and short lifespan. While there are differences in phenotypic severity between two *picd-1* alleles, it is important to emphasize that the loss of *picd-1* function enhanced various phenotypes of the *pry-1* mutant. For

example, *pry-1; picd-1* double mutant showed a Pvl phenotype and exhibited P11.p cell fate changes. In addition, *picd-1* RNAi enhanced seam cell defects in the *pry-1* mutants. Interestingly, mutations in *picd-1* did not enhance vulval precursor cell induction or Muv phenotype in *pry-1* mutants. One possible model to explain genetic interactions between *pry-1* and *picd-1* is that *pry-1* functions via both *picd-1* dependent and independent pathways, and *picd-1* is regulated by multiple factors.

We analyzed the role of *picd-1* in *pry-1*-mediated non-developmental events, such as egg-laying, embryonic survivability, aging, stress response, and lipid metabolism. Loss of *picd-1* function worsened the embryonic lethality of *pry-1* mutants. Moreover, *pry-1; picd-1* double mutant had a very small brood size due to defects in the gonad arms. These findings suggest that *pry-1* and *picd-1* interact to regulate embryonic viability and fertility in animals. Similar phenotypes are observed in the mutants of other HIRA complex components. Knockdown of *hira-1* leads to embryonic lethality, *asfl-1* or *unc-85* single mutants have low brood size, and *asfl-1; unc-85* double mutant is sterile[32–34]. Together, these data show that *pry-1* and *picd-1* interact to regulate embryonic viability and fertility in animals. It remains to be seen whether PRY-1 and PICD-1 interact with other HIRA complex components to mediate their function.

Furthermore, we found that *picd-1* is required for normal stress response maintenance. *picd-1* mutants showed enhanced sensitivity to paraquat and tunicamycin. The mutant animals also exhibited increased levels of UPR markers. Both *picd-1* and *pry-1* mutants significantly increased *hsp-16.2,* and *hsp-4*, suggesting that these genes function together to regulate ER-UPR and HSR. However, more work is needed to determine whether these two genes uniquely affect MT-UPR and oxidative stress and their biological significance.

Mutants that show sensitivity to stress typically have a short lifespan[35–37]. Similar to *pry-1* mutants, *picd-1(bh40)* animals are short-lived and exhibit defects in age-related physiological markers. This result is consistent with the fact that both genes function together to regulate stress response and aging. However, there are functional differences between the two genes. For example, we found that lipid levels were greatly reduced in *pry-1* but not in *picd-1* mutants. The *nhr-80* and *fat-7* levels were reduced in *picd-1* mutant animals, consistent with the known role of *nhr-80* in regulating *fat-7* expression[24]. However, while *picd-1* is needed for the expression of *fat-5*, *fat-7* and *nhr-80*, a lack of its function does not compromise lipid levels in animals. These results are consistent with the above model of *picd-1* participating in a subset of *pry-1*-mediated processes. However, the extent to which the two genes interact and the precise nature of their interactions is unknown.

A possible mechanism of *picd-1* function in lifespan maintenance may involve calcineurin. AMPK and calcineurin modulation of CRTCs are conserved in mammals and *C. elegans*[17,38–41]. In *C. elegans*, AAK-2 and calcineurin regulate CRTC-1 post-translationally in an opposing manner, where activated AAK-2 causes nuclear exclusion of CRTC-1 and extends lifespan. Such a phenotype was also observed after deactivating calcineurin[17]. Our data showed that loss of *picd-1* function resulted in the nuclear localization of CRTC-1 and activated the CRTC-1 target genes. These findings, together with the fact that mammalian cabin1 inhibits calcineurin-mediated signaling[13,26,42], allows us to hypothesize that PICD-1 regulates CRTC-1 via downregulation of calcineurin in *C. elegans*. According to this, loss of *picd-1*/cabin-1 is expected to increase calcineurin signaling, which may explain the shorter lifespan of *picd-1* mutants. Further experiments are needed to investigate the extent to which the regulatory relationship between cabin1 and calcineurin is conserved in *C. elegans*.

As *picd-1* is downregulated in *pry-1* mutants, and both genes are needed for the proper subcellular localization of CRTC-1 and its downstream targets, we speculate that PRY-1 and PICD-1 use CRTC-1 to regulate stress response and lifespan of animals. While there is no evidence for the interaction between mammalian Axin and CRTCs, studies have shown that CREB, which associates with CRTCs, is inhibited by Axin-GSK3β signaling[43,44]. Our work provides the first evidence of genetic interactions between *pry-1*, *picd-1*, and *crtc-1* in *C. elegans*, which has uncovered a novel crosstalk between Axin and calcineurin signaling. However, several questions remain unanswered. For instance, the components of *pry-1* signaling affecting CRTC-1 nuclear localization are unknown. In preliminary experiments, *tax-6* RNAi (calcineurin catalytic subunit) did not affect the *pry-1* phenotype; however, more experiments are needed to completely ascertain its requirements. Additionally, whether *picd-1* is regulated by *pry-1* in a WNT-dependent manner or it is co-regulated by *pry-1* and *aak-2*[4,10] independently of WNT needs thorough investigation. Moreover, it is unknown whether other HUCA complex components interact with PICD-1 to mediate PRY-1's role during stress response and lifespan, as well as whether PRY-1 and PICD-1 co-regulate a common set of targets during these processes. Further work is needed to investigate these questions and to gain a deeper understanding of the conserved mechanisms involved in Axin-CABIN1 signaling in eukaryotes.

Materials and methods

Worm strains. Cultures were maintained at 20 °C on standard nematode growth media (NGM) plates seeded with OP50 *E. coli* bacteria. The strains used in this study are listed below.

N2 (wild-type).
DY220 *pry-1(mu38).*
VC3710 *pry-1(gk3682).*
VC3709 *pry-1(gk3681); picd-1(gk3701).*
DY725 *pry-1(mu38); picd-1(bh40).*
DY678 *bhEx287[pGLC150(picd-1::GFP) + myo-3::wCherry].*
DY750 *bhEx301[pGLC150(picd-1::GFP) + pGLC 72(dat-1::YFP)].*
DY752 *pry-1(mu38); bhEx301[pGLC150(picd-1::GFP) + pGLC 72(dat-1::YFP)].*
DY698 and DY753 *picd-1(bh40).*
DY694 *picd-1(gk3701).*
DY747 *pry-1(gk3681).*

Figure 10. Reduced or loss of *picd-1* function affects CRTC-1 localization and CRTC-1 transcriptional response. (**A**) *picd-1*, but not L4440 control, RNAi causes nuclear accumulation of CRTC-1::RFP fluorescence. (**B**) Quantification of nuclear localization in (**A**). (**C**) qPCR analysis of *dod-24* and *asp-12* in *picd-1(bh40)* animals shows increased expression. (**D–F**) Similar experiments performed in *pry-1* mutants. For panels (**C**) and (**F**), data represent the means of two replicates and error bars represent the standard error of means. (**G**) CRTC-1::RFP localization analysis in N2 and *pry-1(gk3682)* mutants following L4440 control RNAi, *bar-1* and *crtc-1* RNAi treatments. Nuclear fluorescence is absent in the case of *crtc-1* RNAi. (H) Quantification of nuclear localization in (**G**). (**B**,**E**,**G**) Data represent the means of three replicates and error bars represent the standard deviation. At least n > 50 animals were examined in each assay. (**I**) Lifespan of wild type and *pry-1* mutant animals following L4440 control and *crtc-1* RNAi (also see Table 2). (**J**) Bar graphs represent percentage survival of animals following 100 mM paraquat exposure for 2 h. Data represent a cumulative of two replicates (n > 60 animals) and error bars represent the standard deviation. For panels (**B**,**E**,**G**,**J**), statistical analyses were done using an unpaired t-test. Data for panels (**C**) and (**F**) were analyzed using Bio-Rad software (t-test). In all cases, significant differences are indicated by stars (*): * ($p < 0.05$), ** ($p < 0.01$), and **** ($p < 0.0001$). n.s., not significant.

RG733 *wIs78[scm::GFP + ajm-1::GFP].*
AGD418 *uthIs205[crtc-1::CRTC-1::RFP::unc-54 3' UTR + rol-6(su1006)].*
DY740 *pry-1(gk3682); uthIs205[crtc-1::CRTC-1::RFP + rol-6(su1006)].*

Mutant alleles and transgenic strains. The *gk3701* mutation was discovered in a CRISPR screen that was carried out in Moerman lab to obtain alleles of *pry-1* and several other genes of interest[6,45,46]. Since the original *picd-1* mutant strain also contained *pry-1(gk3681)*, it was deconstructed to establish separate strains of *picd-1(gk3701)* (outcrossed 3x) and *pry-1(gk3681)* (outcrossed 2x). The presence of CRISPR mutations was confirmed by PCR and sequencing. Molecular changes in *pry-1(gk3682)* were described earlier by our group[6]. Both *gk3682* and *gk3681* carry a CRISPR GFP cassette[45] We sequenced *gk3681* as part of this study and found that the allele is identical to *gk3682* (Table S4). In agreement with this, *pry-1(gk3681)* animals are phenotypically similar to *pry-1(gk3682)* (Figure S1 and Table 2).

The *picd-1(gk3701)* does not contain a CRISPR GFP cassette. Instead, it carries a 5 bp sequence (GGTGA) deletion in the second exon of the gene (flanking 25 nucleotides: GTGAAGAGGATGAGGACAATGGTGA and GGATTCAGAAGAAGAAGATGAAGAA) that causes multiple premature in-frame stop codons.

The other *picd-1* allele *(bh40)* was generated in a separate CRISPR screen using a published protocol[47]. Here, we replaced the 84 bp in the first exon by a synthetic sequence containing stop codons in different reading frames. See primers in Table S4. *bh40* animals were outcrossed 2 × and examined for various phenotypes. Another 2 × outcross of the strain was subsequently carried out (total 4x), which showed similar defects (Table S5).

To generate the *picd-1p::GFP* transgenic animals (DY678), pGLC150 was injected in N2 background along with *myo-3::wCherry* or *dat-1::YFP* marker. pGLC150 was constructed by cloning a 3,885 bp PCR-amplified fragment (using the primers GL1372 and GL1373), spanning the promoter region and a portion of the first exon of the *picd-1* gene, into the vector pPD95.81 using the restriction sites SalI and KpnI.

Molecular biology. RNA was extracted from synchronized L3 and day-1 adult animals. Protocols for RNA extraction, cDNA synthesis and qPCR were described earlier[7]. Briefly, total RNA was extracted using Trizol (Thermo Fisher, USA). The RNA was used to prepare cDNA and, subsequently, perform qPCR using the SensiFast cDNA synthesis kit (Bioline, USA), and SYBR green mix (Bio-Rad, Canada), respectively. Primers are listed in Table S4.

RNAi. RNAi mediated gene silencing was performed using a protocol previously published by our laboratory[48]. Plates were seeded with *E. coli* HT115 expressing either dsRNA specific to candidate genes or empty vector (L4440). Gravid hermaphrodites were treated with a mild bleach solution (3:2 ratio of commercial bleach and 4 N NaOH) and eggs were plated. Animals were subjected to RNAi treatment from egg stage unless otherwise stated. Phenotypes were examined at the young adult stage.

Fluorescent and DIC microscopy. Animals were paralyzed in 10 mM Sodium Azide and mounted on glass slides containing 2% agar pads and covered with glass coverslips. Images were captured using a Zeiss Apotome microscope and Zeiss ZEN software. For acquiring live videos of gonad, animals were suspended in M9 without Sodium Azide. Videos were captured by a high-speed camera fitted on a Leica MZ-FLIII fluorescent stereomicroscope[49].

Seam cells were identified using *scm::GFP* and *ajm-1::GFP* markers, The nuclei of these cells were counted, and adult lateral alae were scored using Nomarski differential interference contrast and epifluorescence optics. Images were acquired using a Hamamatsu Camera mounted on a Nikon Eclipse 80i upright Nomarski fluorescence microscope and NIS Element software (Nikon, USA).

Vulval induction and P cells. Vulval induction and P11.p and P12.p phenotypes were examined in mounted L4 stage animals using a Nomarski microscope. VPCs were considered induced if they gave rise to progeny. Wild-type (N2) animals have three induced VPCs, one each for P5.p, P6.p, and P7.p. Mutants with more than three induced VPCs were termed as 'over-induced'. Muv and Pvl phenotypes were scored in adults.

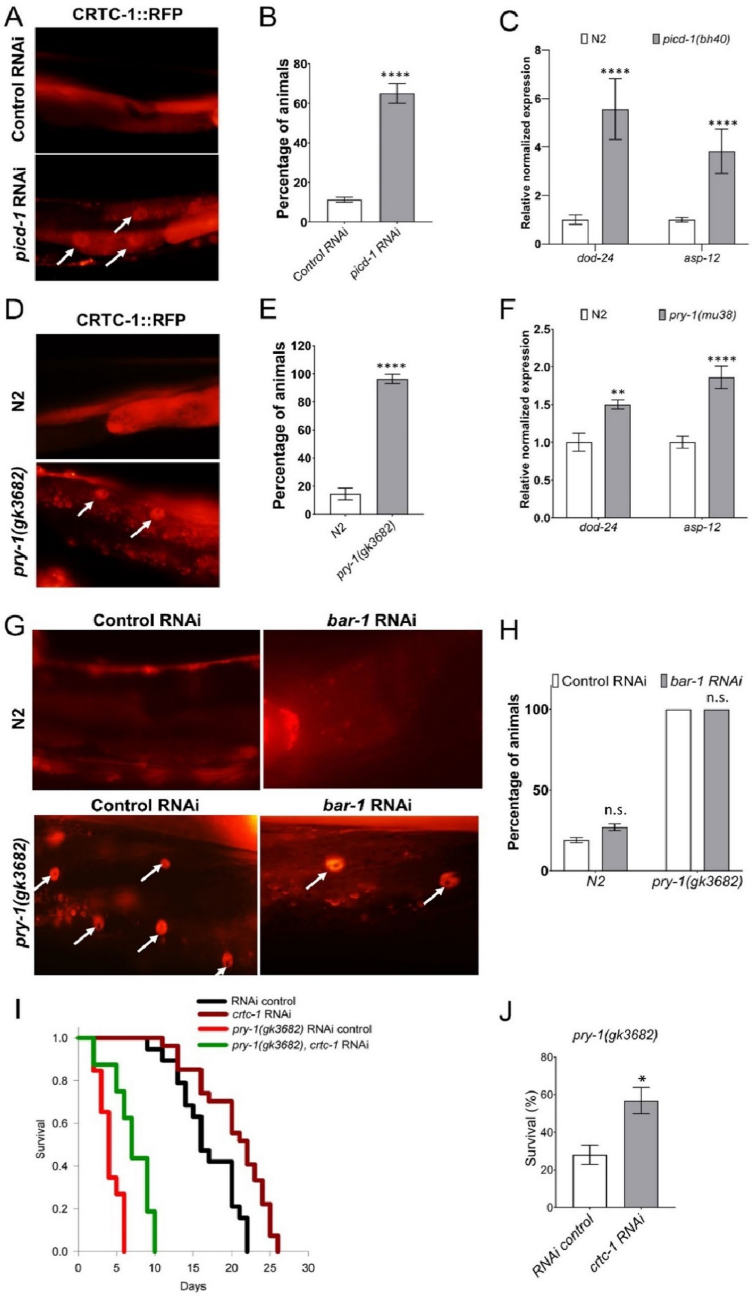
A
CRTC-1::RFP
Control RNAi
picd-1 RNAi
B
Percentage of animals
Control RNAi
picd-1 RNAi
C
N2
picd-1(bh40)
Relative normalized expression
dod-24
asp-12
D
CRTC-1::RFP
N2
pry-1(gk3682)
E
Percentage of animals
N2
pry-1(gk3682)
F
N2
pry-1(mu38)
Relative normalized expression
dod-24
asp-12
G
Control RNAi
bar-1 RNAi
N2
pry-1(gk3682)
H
Control RNAi
bar-1 RNAi
n.s.
Percentage of animals
N2
pry-1(gk3682)
I
RNAi control
crtc-1 RNAi
pry-1(gk3682) RNAi control
pry-1(gk3682), crtc-1 RNAi
Survival
Days
J
pry-1(gk3682)
Survival (%)
RNAi control
crtc-1 RNAi

Vulval morphogenesis is described previously[50]. At the L4 stage VPC progeny undergo a series of changes that involve invagination of vulva progeny and selective cell fusion to give rise to a characteristic morphology of the vulva. Defects in morphogenetic processes can lead to an abnormal shape of the vulva.

P11.p and P12.pa cells can be readily distinguished under a Nomarski microscope based on their nuclear size and morphology[51–53]. In *pry-1* mutants, two P12.pa-like cells are observed and P11.p is missing.

Aging-related analysis. Lifespan experiments of RNAi-treated animals were carried out using a previously described protocol[10]. Synchronized eggs were allowed to grow on NGM OP50 seeded plates till the late L4 larval stage after which they were transferred to RNAi bacteria seeded plates to perform adult stage-specific knockdown. Cultures were screened daily for dead animals and surviving adults were transferred every other day till the progeny production ceased. Censoring was done for animals that had either escaped, burrowed into the medium, showed a bursting at the vulva, or had progeny hatching inside the uterus[54].

Body bending per 1 min and pharyngeal pumping per 30 s were analyzed in young adults over a period of four days[7]. For this, individual hermaphrodites were placed on OP50 plates and examined under a dissecting microscope. Pharyngeal pumping was assessed by observing the number of pharyngeal contractions. For body bending, animals were stimulated by tapping once on the tail by a platinum wire. Each full sinusoidal motion was counted as one body bend. Only animals that moved actively within 1 min were included in the analysis.

Stress assay and electrotaxis. Oxidative and endoplasmic reticulum mediated stress experiments were performed using 200 mM paraquat (unless specified) (Thermo Fisher Scientific, USA) and 25 ng/µl tunicamycin (Sigma-Aldrich, Canada) respectively. Animals were incubated for 1 h, 2 h, 3 h and 4 h, following a previous published protocol[6]. The final working concentrations were made in M9. At least 30 animals of each strain were tested in replicates. Means and standard deviations were determined from experiments performed in duplicate. Animals were considered dead if they did not respond to a platinum wire touch and showed no thrashing or swimming movement in M9. Moreover, dead animals usually had an uncurled and straight body shape in comparison to the normal sinusoidal shape of worms.

The electrotaxis assay protocol has been described previously[55]. Briefly, synchronized worms were introduced into a microfluidic channel and subjected to an electric field of 3 V/cm. Locomotory data was extracted from recorded videos using custom MATLAB-based worm tracking software. Electrotaxis speed data was plotted using box plots.

Oil Red O staining. Neutral lipid staining was done on synchronized day-1 adults using Oil Red O dye (Thermo Fisher Scientific, USA) following a published protocol[11]. Quantifications were performed using ImageJ software as described earlier[56].

Statistical analyses. SigmaPlot 11 was used to plot lifespan data that provided detailed statistical analysis on survival curves. The curves were estimated using the Kaplan–Meier test and differences among groups were assessed using the log-rank test. qPCR data analysis was done using software (Maestro 3.1) that controls the Bio-Rad CFX qPCR machine. The software performs built-statistical analyses of t-test and one-way ANOVA. For all other assays, data from repeat experiments were pooled and analyzed together, and statistical analyses were done using GraphPad Prism 9. p values less than 0.05 were considered statistically significant. Data for all the Figure panels are reported in Table S5.

Data availability

All data generated or analysed during this study are included in this published article (and its Supplementary Information files). Additional details are available from the corresponding author on reasonable request.

Received: 11 February 2022; Accepted: 30 June 2022
Published online: 14 July 2022

References

1. Mallick, A., Taylor, S. K. B., Ranawade, A. & Gupta, B. P. Axin family of scaffolding proteins in development: lessons from C. elegans. *J. Dev. Biol.* **7**, 1–23 (2019).
2. Clevers, H. & Nusse, R. Wnt/β-catenin signaling and disease. *Cell* **149**, 1192–1205 (2012).
3. Luo, W. & Lin, S. C. Axin: A master scaffold for multiple signaling pathways. *Neurosignals* **13**, 99–113 (2004).
4. Mallick, A. & Gupta, B. P. AXIN-AMPK signaling : Implications for healthy aging. *F1000Research* **10**, 1–14 (2022).
5. Sawa, H. & Korswagen, H. C. Wnt signaling in C. elegans *. *WormBook* https://doi.org/10.1895/wormbook.1 (2013).
6. Mallick, A., Ranawade, A. & Gupta, B. P. Role of PRY-1/Axin in heterochronic miRNA-mediated seam cell development. *BMC Dev. Biol.* **19**, 1–12 (2019).
7. Mallick, A. *et al.* Genetic analysis of Caenorhabditis elegans pry-1 / Axin suppressors identifies genes involved in reproductive structure development , stress responses , and aging. *G3 Genes, Genomes, Genet.* **jkab430**, (2021).
8. Ranawade, A., Mallick, A. & Gupta, B. P. PRY-1/Axin signaling regulates lipid metabolism in Caenorhabditis elegans. *PLoS ONE* **13**, e0206540 (2018).
9. Mallick, A. *et al.* The FGFR4 homolog KIN-9 regulates lifespan and stress responses in Caenorhabditis elegans. *Front. Aging* **3**, 1–11 (2022).
10. Mallick, A., Ranawade, A., van den Berg, W. & Gupta, B. P. Axin-mediated regulation of lifespan and muscle health in C. elegans requires AMPK-FOXO Signaling. *Science* **23**, 101843 (2020).
11. Mallick, A. & Gupta, B. P. Vitellogenin-2 acts downstream of PRY-1 / Axin to regulate lipids and lifespan in C. elegans. *Micropublication Biol.* **1**, 19–21 (2020).

12. Rai, T. S. *et al.* Human CABIN1 is a functional member of the human HIRA/UBN1/ASF1a histone H3.3 chaperone complex. *Mol. Cell. Biol.* **31**, 4107–4118 (2011).
13. Sun, L. *et al.* Cabin 1, a negative regulator for calcineurin signaling in T lymphocytes. *Immunity* **8**, 703–711 (1998).
14. Park, Y. J., Yoo, S. A., Kim, M. & Kim, W. U. The role of calcium–calcineurin–NFAT signaling pathway in health and autoimmune diseases. *Front. Immunol.* **11**, 1–14 (2020).
15. Park, H. S., Lee, S. C., Cardenas, M. E. & Heitman, J. Calcium-calmodulin-calcineurin signaling: A globally conserved virulence cascade in eukaryotic microbial pathogens. *Cell Host Microbe* **26**, 453–462 (2019).
16. Bandyopadhyay, J., Lee, J. & Lee, J. Calcineurin, a calcium/calmodulin-dependent protein phosphatase, is involved in movement, fertility, egg laying, and growth in Caenorhabditis elegans. *Mol. Biol. Cell* **13**, 3281–3293 (2002).
17. Mair, W. *et al.* Lifespan extension induced by AMPK and calcineurin is mediated by CRTC-1 and CREB. *Nature* **470**, 404–408 (2011).
18. Yan, J. & Kurgan, L. DRNApred, fast sequence-based method that accurately predicts and discriminates DNA-and RNA-binding residues. *Nucleic Acids Res.* **45**, 1–16 (2017).
19. Grün, D. *et al.* Conservation of mRNA and protein expression during development of C.elegans. *Cell Rep.* **6**, 565–577 (2014).
20. Golden, T. R., Hubbard, A., Dando, C., Herren, M. A. & Melov, S. Age-related behaviors have distinct transcriptional profiles in Caenorhabditis elegans. *Aging Cell* **7**, 850–865 (2008).
21. Gleason, J. E. & Eisenmann, D. M. Wnt signaling controls the stem cell-like asymmetric division of the epithelial seam cells during C elegans larval development. *Dev. Biol.* **348**, 58–66 (2010).
22. Taylor, S. K. B. *et al.* C elegans electrotaxis behavior is modulated by heat shock response and unfolded protein response signaling pathways. *Sci. Rep.* **11**, 1–17 (2021).
23. Watts, J. L. & Ristow, M. Lipid and carbohydrate metabolism in Caenorhabditis elegans. *Genetics* **207**, 413–446 (2017).
24. Brock, T. J., Browse, J. & Watts, J. L. Genetic regulation of unsaturated fatty acid composition in C elegans. *PLoS Genet.* **2**, 0997–1005 (2006).
25. Brock, T. J., Browse, J. & Watts, J. L. Fatty acid desaturation and the regulation of adiposity in Caenorhabditis elegans. *Genetics* **176**, 865–875 (2007).
26. Lai, M. M., Burnett, P. E., Wolosker, H., Blackshaw, S. & Snyder, S. H. Cain, a novel physiologic protein inhibitor of calcineurin. *J. Biol. Chem.* **273**, 18325–18331 (1998).
27. Burkewitz, K. *et al.* Neuronal CRTC-1 governs systemic mitochondrial metabolism and lifespan via a catecholamine signal. *Cell* **160**, 842–855 (2015).
28. Szenker, E., Ray-Gallet, D. & Almouzni, G. The double face of the histone variant H3.3. *Cell Res.* **21**, 421–434 (2011).
29. Thul, P. J. *et al.* A subcellular map of the human proteome. *Science* **356**, 2 (2017).
30. Uhlén, M. *et al.* Tissue-based map of the human proteome. *Science* **347**, 2 (2015).
31. Burkhart, K. B., Sando, S. R., Corrionero, A. & Horvitz, H. R. H3.3 nucleosome assembly mutants display a late-onset maternal effect. *Curr. Biol.* **30**, 2343–2352 (2020).
32. Grigsby, I. F., Rutledge, E. M., Morton, C. A. & Finger, F. P. Functional redundancy of two C. elegans homologs of the histone chaperone Asf1 in germline DNA replication. *Dev. Biol.* **329**, 64–79 (2009).
33. Grigsby, I. F. & Finger, F. P. UNC-85, a C. elegans homolog of the histone chaperone Asf1, functions in post-embryonic neuroblast replication. *Dev. Biol.* **319**, 100–109 (2008).
34. Piano, F. *et al.* Gene clustering based on RNAi phenotypes of ovary-enriched genes in C elegans. *Curr. Biol.* **12**, 1959–1964 (2002).
35. Morton, E. A. & Lamitina, T. Caenorhabditis elegans HSF-1 is an essential nuclear protein that forms stress granule-like structures following heat shock. *Aging Cell* **12**, 112–120 (2013).
36. Taylor, R. C. & Dillin, A. XBP-1 Is a cell-nonautonomous regulator of stress resistance and longevity. *Cell* **153**, 1435 (2013).
37. Libina, N., Berman, J. R. & Kenyon, C. Tissue-specific activities of C elegans DAF-16 in the regulation of lifespan tissues play an important role in establishing the ani-mal's rate of aging. First, the C elegans genome con-tains more than 35 insulin-like genes expressed in a. *Cell* **115**, 489–502 (2003).
38. Screaton, R. A. *et al.* The CREB coactivator TORC2 functions as a calcium- and cAMP-sensitive coincidence detector. *Cell* **119**, 61–74 (2004).
39. Koo, S. H. *et al.* The CREB coactivator TORC2 is a key regulator of fasting glucose metabolism. *Nature* **437**, 1109–1114 (2005).
40. Komiya, T. *et al.* Enhanced activity of the CREB co-activator Crtc1 in LKB1 null lung cancer. *Oncogene* **29**, 1672–1680 (2010).
41. Wang, Y., Vera, L., Fischer, W. H. & Montminy, M. The CREB coactivator CRTC2 links hepatic ER stress and fasting gluconeogenesis. *Nature* **460**, 534–537 (2009).
42. Jang, H., Cho, E. J. & Youn, H. D. A new calcineurin inhibition domain in Cabin1. *Biochem. Biophys. Res. Commun.* **359**, 129–135 (2007).
43. Gavagan, M., Fagnan, E., Speltz, E. B. & Zalatan, J. G. The scaffold protein axin promotes signaling specificity within the Wnt pathway by suppressing competing kinase reactions. *Cell Syst.* **10**, 515-525.e5 (2020).
44. Fiol, C. J., Wang, A., Roeske, R. W. & Roach, P. J. Ordered multisite protein phosphorylation. Analysis of glycogen synthase kinase 3 action using model peptide substrates. *J. Biol. Chem.* **265**, 6061–6065 (1990).
45. Chamberlin, H. M. *et al.* Evolution of transcriptional repressors impacts caenorhabditis vulval development. *Mol. Biol. Evol.* **37**, 1350–1361 (2020).
46. Richman, C. *et al.* C. elegans MANF homolog is necessary for the protection of dopaminergic neurons and ER unfolded protein response. *Front. Neurosci.* **12**, 1–11 (2018).
47. Vicencio, J., Martínez-Fernández, C., Serrat, X. & Cerón, J. Efficient generation of endogenous fluorescent reporters by nested CRISPR in caenorhabditis elegans. *Genetics* **211**, 1143–1154 (2019).
48. Seetharaman, A., Cumbo, P., Bojanala, N. & Gupta, B. P. Conserved mechanism of Wnt signaling function in the specification of vulval precursor fates in C. elegans and C. briggsae. *Dev. Biol.* **346**, 128–139 (2010).
49. Chalich, Y., Mallick, A., Gupta, B. & Jamal Deen, M. Development of a low-cost, user-customizable, high-speed camera. *PLoS ONE* **15**, 1–21 (2020).
50. Mok, D. Z. L., Sternberg, P. W. & Inoue, T. Morphologically defined sub-stages of C. Elegans vulval development in the fourth larval stage. *BMC Dev. Biol.* **15**, 1–8 (2015).
51. Eisenmann, D. M. & Kim, S. K. Protruding vulva mutants identify novel loci and wnt signalling factors that function during Caenorhabditis elegans vulva development. *Genetics* **156**, 1097–1116 (2000).
52. Walston, T. *et al.* mig-5/Dsh controls cell fate determination and cell migration in C. elegans. *Dev. Biol.* **298**, 485–497 (2006).
53. Jiang, L. I. & Sternberg, P. W. Interactions of EGF, Wnt and HOM-C genes specify the P12 neuroectoblast fate in C. elegans. *Development* **125**, 2337–2347 (1998).
54. Amrit, F. R. G., Ratnappan, R., Keith, S. A. & Ghazi, A. T. C. elegans lifespan assay toolkit. *Methods* **68**, 465–475 (2014).
55. Tong, J., Rezai, P., Salam, S., Selvaganapathy, P. R. & Gupta, B. P. Microfluidic-based electrotaxis for on-demand quantitative analysis of Caenorhabditis elegans' locomotion. *J. Vis. Exp.* https://doi.org/10.3791/50226 (2013).
56. Soukas, A. A., Kane, E. A., Carr, C. E., Melo, J. A. & Ruvkun, G. Rictor/TORC2 regulates fat metabolism, feeding, growth, and life span in Caenorhabditis elegans. *Genes Dev.* https://doi.org/10.1101/gad.1775409.2004 (2009).

Acknowledgements

We are indebted to Moerman lab for generating both *pry-1(gk3681)* and *picd-1(gk3701)* strains. We also thank Drs. Andrew Dillin (University of California, Berkeley) and Brent Derry (University of Toronto) for providing the CRTC-1::RFP strain and *crtc-1* RNAi plasmid, respectively. Hannan Minhas assisted with electrotaxis experiments and Wouter van den Berg with the screening of *picd-1* CRISPR allele *bh40*. This work was supported by the NSERC Discovery grant to Bhagwati Gupta and NSERC CGS-D scholarship to Avijit Mallick. Some of the strains were obtained from the *Caenorhabditis* Genetics Center (CGC), which is funded by the NIH Office of Research Infrastructure Programs (P40 OD010440).

Author contributions

A.M. initially characterized the *picd-1* mutants and generated many reagents for the study. A.M., S.M. and S.K.B.T. carried out the experiments. A.M., S.K.B.T., and B.G. analyzed the data. A.M. wrote the first draft of the manuscript and, subsequently, A.M. and S.K.B.T. worked together to revise it. All authors reviewed the final version. B.G. supervised the study.

Competing interests

The authors declare no competing interests.

Additional information

Supplementary Information The online version contains supplementary material available at https://doi.org/10.1038/s41598-022-15873-5.

Correspondence and requests for materials should be addressed to B.P.G.

Reprints and permissions information is available at www.nature.com/reprints.

Publisher's note Springer Nature remains neutral with regard to jurisdictional claims in published maps and institutional affiliations.

6.3.4 Mallick *et al*. 2022. Frontiers in aging

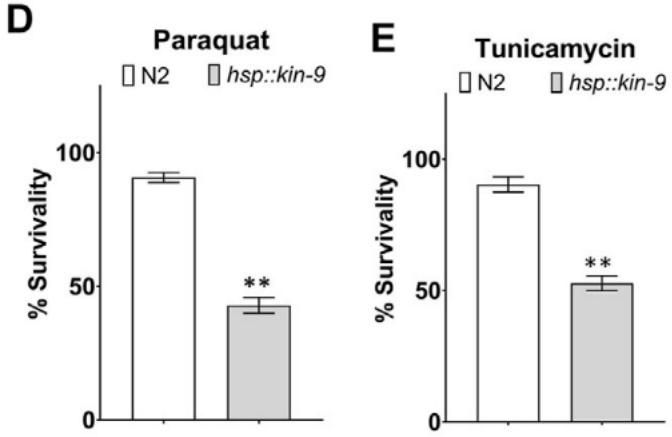

Figure C2. Sensitivity of *hsp::kin-9* animals to paraquat and tunicamycin. **D & E**) Bar graph showing the survivability of *hsp::kin-9* adults compared to N2 following paraquat (200 mM) and tunicamycin (25 ng/ µL) exposure for 2hrs. (D&E) Data represent the mean of two to three replicates (n > 50 animals in each replicate) and error bars represent the SEM. Statistical analyses were done using unpaired t-tests with Welch correction (*p<0.05;**p<0.01;*** p<0.001;****p<0.0001). Figure Adapted from Mallick *et al.* (2022).

6.4 Appendix D. Chronic Metal Exposure impacts the electrotaxis behavior and Heat Shock Response in *Caenorhabditis elegans*

6.4.1 Preface

This appendix includes the following unpublished article in its original format:

Chronic Metal Exposure impacts the electrotaxis behavior and Heat Shock Response in *Caenorhabditis elegans by* Shane K. B. Taylor, Muhammad H. Minhas, Justin Tong, P. Ravi Selvaganapathy, Ram K. Mishra, and Bhagwati P. Gupta

In this appendix we discuss how various metal salts impact the movement of animals represented as defects in dopaminergic neurons, body bends and body oscillations. Furthermore, we show that the severity of certain metals is mediated by *hsf-1* in *C. elegans*. This works emphasizes the detriment that chronic exposure of metals can have on a species. Additionally, it provides insight into the role of the HSR in the response against chemical toxicity.

Contributions

I revised the manuscript, created the figures and analyzed the data. I performed experiments for figure 2B, Figure 4, Figure 5A. Hannan and Justin performed all other experiments. I and Dr. Gupta revised the current manuscript.

6.4.2 Taylor, S. K. B. *et al.* 2024. To be submitted.

Chronic Metal Exposure impacts the electrotaxis behavior and Heat Shock Response in *Caenorhabditis elegans*

Shane K. B. Taylor[1], Muhammad H. Minhas[1], Justin Tong[1], P. Ravi Selvaganapathy[2], Ram K. Mishra[3], and Bhagwati P. Gupta[1]

[1]Department of Biology, McMaster University, Hamilton, ON

[2]Department of Mechanical Engineering, McMaster University, Hamilton, ON

[3]Department of Psychiatry and Behavioural Neurosciences, McMaster University, Hamilton, ON

Short title: Metal salts induce electrotactic swimming defects in *C. elegans*

Corresponding author: guptab@mcmaster.ca

Key words: *C. elegans*, microfluidics, electrotaxis, bioindicator, metals

ABSTRACT

We examined the effects of chronic exposure to various environmental toxicants on the nematode *C. elegans*' electrotactic behavior using a specially designed microfluidic channel device. The results provide the first evidence that electrotactic swimming behavior is particularly susceptible to knockdown by metal salts. We found that Ag, Hg, Cu, Pb and Mn caused speed deficits in animals. Prolonged, metal exposure also significantly reduced the speed of animals. We also observed that *hsf-1* mutants are insensitive to metal salts and that the heat shock response is activated following metal exposure. In conclusion, our work demonstrates that the electrotactic swimming behavior of *C. elegans* is susceptible to metal exposure which may involve the HSR. The speed and sensitivity of the microfluidic assay makes it a promising non-invasive approach to detect environmental toxicants and examine their effects on locomotory behavior in multicellular eukaryotes.

INTRODUCTION

Heavy metals are known to have detrimental health effects. Metal exposure can occur from anywhere in the environment, food source and general day to day life. Organisms have developed multiple ways to clear these toxic substances from their system that include reducing metal uptake, expelling the metal from the system, or activating stress response systems. While mammalian models such as mice and rats can be used to study metal toxicity in laboratory settings however these systems are complex, slow growing, expensive to maintain, and require sophisticated equipment to manipulate them. Cell cultures can also be used however they are good for *in vitro* studies and cannot mimic the response observed in whole animal models (Hunt, 2017). In these regards, the nematode (worm) *Caenorhabditis elegans* is an excellent system because it offers many advantages such as the ease of cultivation, short life cycle, inexpensive to maintain and manipulate, relatively simple nervous system, and requiring no ethical approvals.

C. elegans are sensitive to most toxicants of interest, including metal salts, and have been used for toxicity studies (Hunt, 2017). The sensitivity of worms to a diverse range of toxicants renders it useful for assessing toxicity at environmentally relevant concentration (Akinyemi et al., 2019; Ju et al., 2013; Wu et al., 2012). The present study describes deleterious effects of chronic exposure to a range of heavy metals, namely Hg, MeHg, Ag, Cu, Fe, Pb, Mn, Ni, and Cd, on *C. elegans* using a novel movement assay.

Hg and its compounds are notorious for their extreme toxicity and the targets of Hg are quite diverse, including the respiratory and gastrointestinal tracts. A large fraction of the Hg that enters aquatic ecosystems undergoes methylation to assume its organic form MeHg, which represents a major concern (Forsyth et al., 2004; Hong et al., 2012). Hg is most infamous for its neurotoxic properties: even acute exposures can induce an assortment of cognitive, personality, sensory, and motor abnormalities, possibly culminating in coma and death (Clarkson & Magos, 2006).

Three of the metals tested, Cu, Fe, and Mn, are essential trace metals that are involved in vital enzymatic reactions. The deficiency of any of these or their high exposures can result in detrimental health effects (Wazir & Ghobrial, 2017), including neurological and behavioral

abnormalities (V. Kumar et al., 2015; Ndayisaba et al., 2019). Cellular studies have reported oxidative stress and mitochondrial dysfunction due to Mn toxicity (Raj et al., 2021). Experiments in mice have found that bioaccumulation of Mn affects GST and AChE activity, lipids and proteins. Similar to Cu and Mn, Fe also plays important roles in healthy organisms; yet acute Fe overload can cause iron poisoning (Chen et al., 2013; Ruszkiewicz et al., 2018)

Of the remaining four metals (Ag, Ni, Pb, and Cd), Ag is known to be toxic to humans and many other taxa. Ag is a known skin and eye irritant, and its prolonged exposure causes discoloration of the skin and eyes known as argyria and argyrosis, respectively (Drake & Hazelwood, 2005; Hadrup et al., 2018). Other studies on Ag toxicity have reported developmental deformities in zebrafish, neurotoxicity in mice, and mitochondrial damage to human cells (AshaRani et al., 2009; Bar-Ilan et al., 2009; Gonzalez-Carter et al., 2017; Rahman et al., 2009). Ni, too, while fairly ubiquitous in industrial and consumer products, is associated with toxicity at large doses or with chronic exposure. Chronic exposures to Ni affect skin such as causing itching or rashes, respiratory defect, and some forms of cancers affecting lung and other tissues (Genchi et al., 2020). Experiments in mice have shown that Ni causes acute lung inflammation (Mo et al., 2019), although skin and cancerous phenotypes were not observed. Pb is a pervasive environmental neurotoxicant; it is particularly toxic to developmental brains, causing long-term detrimental effects on learning, memory and behavior in children (Neal and Guilarte, 2010). Pb poisoning also results in symptoms such as neuromuscular weakness., anemia, delirium, convulsions, and death (Jaishankar et al., 2014). Studies have shown that high Pb exposures in mice can lead to altered movement, exploratory responses, and hyperactivity (Jaishankar et al., 2014; Silbergeld & Goldberg, 1974). And, finally, Cd is a known carcinogen that has been associated with mutagenic responses (Jaishankar et al., 2014). Cellular and molecular studies have report that Cd exposures affect expression of genes involved in cell cycle, apoptosis, oxidative stress and inflammation (Kim et al., 2017). Studies on Cd exposures have also reported cirrhosis, kidney dysfunction, and defects in the skeletal system (Jaishankar et al., 2014).

A number of test endpoints such as movement, viability, brood size, and lifespan are used for toxicity analyses with *C. elegans* (Chen et al., 2013; Tang et al., 2019; D. Wang & Xing, 2008). Additionally, transgenic and fluorescent microscopy techniques have been employed to visualize metal-induced damage (Chen et al., 2013).

Locomotory behavior of *C. elegans* is a simple yet highly reliable indicator of toxicity, with slow and abnormally uncoordinated movement being associated with nervous system defects (Hart, 2006). Our group has developed a microfluidic-based locomotion assay (termed 'electrotaxis') that measures the electrosensory response of animals. Microfluidic electrotaxis provides an environment where the animal reliably chooses to swim toward the negative electrode in the presence of a direct current (DC) electric field (Rezai et al., 2010). Electrotaxis assay provides a powerful, on-demand, and quantitative measurement of movement behavior, which can be combined with other common endpoints such as brood size, growth, and lifespan to enable a better understanding of the harmful impact of toxicants on multicellular eukaryotes. The present study describes the first use of the electrotaxis assay to evaluate the deleterious effects of chronic exposure to heavy metals on *C. elegans* movement.

Our results show that among the metal salts tested, Ag, Hg, Cu, Mn, and Pb induced significant electrotaxis abnormalities in *C. elegans*. Three of these (Cu, Ag, and Hg) were analyzed further using our exposure paradigm and were found to cause growth and physiological defects in animals.

The remaining three metals (Ni, Fe, and Cd) showed no obvious electrotaxis phenotype even after exposing animals for an extended period. We observed a significant correlation between electrotaxis defect and dopaminergic neurodegeneration in animals, which is consistent with previous findings of dopamine signaling being involved in mediating electrotaxis behavior (Salam et al., 2013). We carried out additional experiments to further investigate the basis of electrotaxis defects. The analysis of cytosolic unfolded protein response (UPR) for a subset of metals (Pb, Cd, and Mn) did not show a correlation between metal toxicity, stress response, and electrotaxis, suggesting differences in how metals affect behavior. Finally, we determined the post-exposure effect of two of the metals (Pb and Mn) and found that animals continued to exhibit abnormal electrotaxis. Overall, these findings provide the first evidence for metal toxicants causing electrotaxis defects in *C. elegans*. Our sensitive assay serves as an additional tool to understand different mechanisms involved in metal toxicity and allows investigations of environmental impact of metals in living systems.

RESULTS

Chronic exposures to some metal salts cause defects in electrotaxis

To evaluate the toxic effects of metal exposure on the electrotaxis behavior of worms, we introduced Day 1 adult *C. elegans* grown on media plates containing metal toxicants into the microchannel device and measured their electrotaxis speed. Initially, worms were exposed to three different metals, Ag, Hg, and Cu. Previous studies have reported LC50 values for these chemicals (Du & Wang, 2009; Ruszkiewicz et al., 2018; Shen et al., 2009). Based on this, we chose 5 µM as a starting concentration for electrotaxis assays. While Ag and Hg caused reduced electrotaxis speed, Cu had no such effect (**Figure 1A**). Two additional doses, 50 µM and 150 µM, were also tested. For Ag and Hg, both doses were highly toxic thereby precluding electrotaxis assays, whereas Cu once again showed no adverse effect at the eye level (**Figure 1A**, see Methods). It took a much higher level of Cu, i.e., 500 µM, to elicit an electrotaxis defect (**Figure 1A**). Consistent with these results, examination of other biological endpoints, namely brood size, body length, and lifespan also supported detrimental effects of metals on animals (**Supplementary Figure 1**) and are in line with previous findings (Roh et al., 2009). Specifically, Ag and Cu inhibited reproduction, however Hg caused no visible change. Body length was not affected by Ag and Hg, but Cu exposure led to a small but statistically significant reduction. All metals had harmful effects on the lifespan of animals.

An organic Hg salt was also tested. As mentioned above, the methyl form of Hg (MeHg) is particularly toxic to humans and causes nervous system abnormalities and birth defects (Hong et al., 2012). *C. elegans* are highly sensitive to MeHg since even a short acute exposure leads to lethality and defects in development, reproduction and locomotion (Helmcke & Aschner, 2010; McElwee & Freedman, 2011). Of the four different concentrations tested (2 µM, 4.5 µM, 9 µM, 18 µM), the lowest dose (2 µM) was the only one suitable for electrotaxis assays as it did not appear to harm the animals at the plate level although progeny counts were significantly reduced (data not shown). Exposed animals showed major reduction in electrotaxis (**Figure 1B, Supplementary data x**). Overall, the results show that the electrotaxis phenotype of *C. elegans* is highly sensitive to low, chronic doses of Ag, Hg, Cu, and MeHg. Additionally, movement defects correlate well with other phenotypes observed.

To determine if electrotaxis abnormalities were due to metals being taken up by animals in our exposure paradigm, we used the ICP-MS technique. The analysis revealed that metal contents were significantly higher inside worms than what was recovered from agar media. While Ag, Hg, and Cu accumulated at 8-fold, 4-fold, and 4-fold, respectively, MeHg accumulation was 33-fold (**Figure 1C, Supplemental Figure 2**). These data show that metal toxicants, particularly MeHg, increase at high levels inside animals' bodies when present in their external environment. The results demonstrate an efficient uptake of metals in our method.

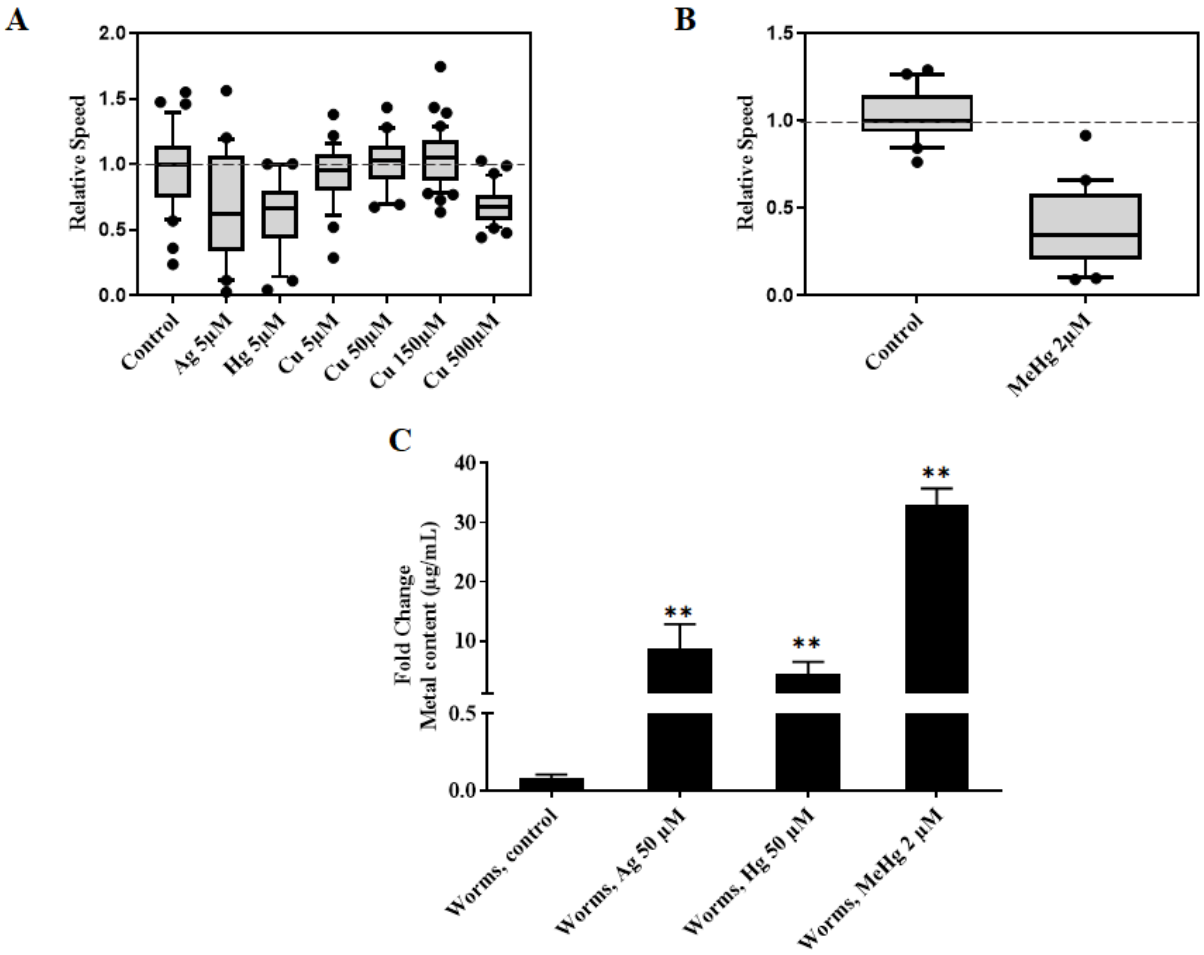

Figure 1. Electrotaxis of animals chronically exposed to Ag, Hg or Cu. Boxes represent measurements from 25th to 75th percentiles, central horizontal lines represent medians, vertical lines extend to 10th and 90th percentiles, and dots represent outliers. **A)** Defects manifesting as slower swimming speeds appear in animals grown on plates containing 5 μM Ag ($P < 0.01$) or 5 μM Hg ($P < 0.01$). Cu-induced electrotaxis speed defects do not appear with plates containing 5 μM ($P > 0.05$), 50 μM ($P > 0.05$) or 150 μM ($P > 0.05$) but do appear at 500 μM ($P < 0.01$). **B)** Defects manifesting as slower swimming speeds appear in animals grown on plates containing 2 μM MeHg ($P < 0.01$). **C)** Metal content in *C. elegans* following 69 h metal salt exposure. Elemental content was measured as a function of total sample volume. Metal content in worms is significantly higher

than in control following treatment with Ag 50 µM ~5.4 µg/mL, Hg 50 µM ~10.0 µg/mL, or MeHg 2 µM ~0.4 µg Hg/mL. Data is pooled from independent replicates (n > 30 animals). Statistical analysis for panel **A** and **C** was done using a one-way ANOVA with Dunnett's post hoc test. Student's unpaired t-test was used for panel **B**. Significant data points are marked by the following: *p<0.05; **p<0.01; ***p<0.001; ****p<0.0001.

Having demonstrated the effect of three metals (Ag, Hg, and Cu) on electrotaxis, we tested an additional set of five metals, Cd-50µM, Fe-150µM, Ni-150µM, Mn-150µM and Pb-150µM. The concentrations of all of these used in our experiments were well below published LC50(Du & Wang, 2009; Ruszkiewicz et al., 2018; Shen et al., 2009). Plate-level observations showed that animals were healthy and exhibited responses similar to wild-type animals (see Methods and **Supplementary table 1**). Analysis of the electrotaxis responses showed that Mn and Pb were the only two metals that caused defects (**Figure 2A**). Interestingly, while Mn reduced the speed, Pb exposure resulted in a hyperactive response (**Figure 2A**). The remaining metals (Ni, Fe and Cd) did not cause any change in electrotaxis response of exposed animals.

We also analyzed body oscillations, which is another parameter of movement (Hart, 2006; D. Wang & Xing, 2008), to see if these correlated with speed defects. The data showed that except for 500 µM Cu, which resulted in slower oscillations, the responses of all metals are comparable to wild type controls (**Figure 2A and Supplementary Figure 2**). A lack of correlation with electrotaxis speed leads us to conclude that changes in the electrotaxis speed are likely not affected by the movement pattern of animals, although minor effects cannot be ruled out. Overall, our findings show that the electrotaxis response of animals is sensitive to chronic exposures of Ag, Cu, Hg, MeHg, Mn and Pb.

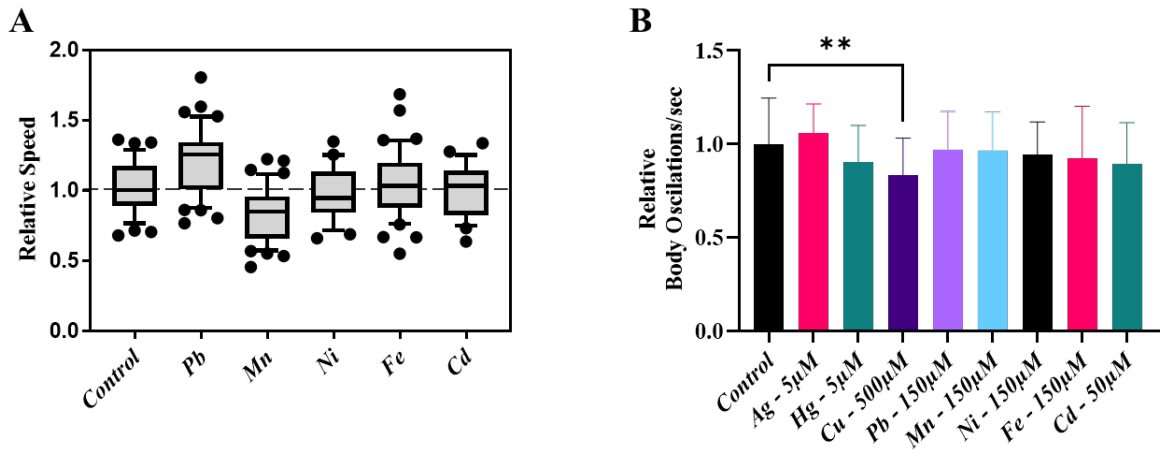

Figure 2. Analysis of movement defects in animals exposed to a set of heavy metals. Refer to Figure 1 for a description of the box plot. (**A**) Electrotaxis of animals chronically exposed to Pb, Mn, Cd, Ni, Fe and Cd. Both Cu and Mn caused a slower speed ($p < 0.001$), Pb results in an increased speed ($p < 0.001$). The other metals Ni, Fe, and Cd did not alter the speed of the animals. (**B**) The body oscillations of chronically exposed animals in the microfluidic channel calculated using the MATLab software. Cu had significantly more body oscillations within the channel compared to control. The other metals did affect the body oscillations. Data is pooled from independent replicates of 3 (n=15 to 45 animals). Statistical analysis for panel A and B was done using a one-way ANOVA with Dunnett's post hoc test. *$p<0.05$; **$p<0.01$; ***$p<0.001$; ****$p<0.0001$.

Prolonged exposure to metals can cause electrotaxis defect

We reasoned that a lack of phenotype for some metals may be due to insufficient exposure. To investigate this further, we exposed *C. elegans* to Ni (150µM), Fe (150µM) and Cd (50µM) for a longer duration. In addition, a low dosage of Cu (150µM) was also tested that had no effect on electrotaxis. Animals were exposed till day-3 adulthood (day-1 adults plus 48 hrs). Results revealed that while Cu caused a reduction in speed, other metals had no detrimental effect (**Figure 3**). At the plate level, Cd-exposed worms were slightly slow growing, but adults appeared normal. The other three metals (Cu, Ni, and Fe) caused no visible abnormality on the plate. We conclude that the electrotaxis responses of animals is sensitive to chronic treatments of Cu.

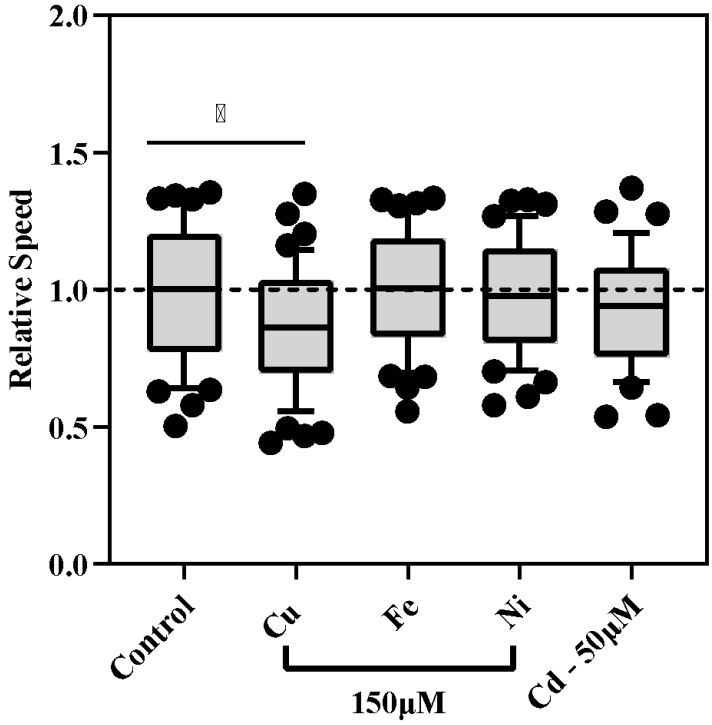

Figure 3: Electrotaxis speed of animals exposed to four different metal salts until day 3 of adulthood (150 µM Cu, 150 µM Fe, 150 µM Ni, and 50 µM Cd). Only Cu-exposed animals exhibited a significantly reduced speed (p= 0.0275). The other heavy metals Fe, Ni and Cd did not alter the electrotaxis speed of the animals (p= 0.9902,0.9999,0.6746 respectively). Data is pooled from independent replicates (n > 30 animals). Statistical analysis for panel A and B was done using a one-way ANOVA with Dunnett's post hoc test. *p<0.05; **p<0.01; ***p<0.001; ****p<0.0001.

Effects of metal exposures on cytosolic stress response and DAergic neurons

Since dopamine signaling is in part involved in mediating electrotaxis behavior (Salam et al., 2013), we reasoned that metals in our assay may affect neuronal phenotypes. This reasoning is consistent with other studies showing that heavy metals have an impact on the health of dopaminergic neurons and affect the dopamine signaling pathway (Benedetto et al., 2010; Jaishankar et al., 2014).

DAergic neurons were examined using a *dat-1p::YFP* marker. In wild-type animals, the DA transporter *dat-1* is expressed in four pairs of CEP and one pair of ADE neurons, which allows easy identification of cell bodies and their projections (**Figure 4A**). Upon quantification, we found that Ag and Hg caused damage in more than half of the worms examined, Cu affected roughly 40% of the population (**Figure 4A & B**). The phenotypes included loss of cell bodies, and faint and punctate projections. Of the remaining metals, Mn, Pb, and Cd affected roughly one-third of

animals, with phenotypes mainly confined to neuronal projections. Ni and Fe did not exhibit any significant neuronal defects (affecting roughly one-fifth of the population tested).

Since three of the metals, Fe, Ni and Cd, did not affect electrotaxis but Cd has a mild effect on dopamine neurons, we chose these metal exposures to perform a basal slowing response (BSR) assay. Animals having defects in DAergic neurons, such as *bas-1* mutant (DOPA decarboxylase), have an abnormal BSR (Sawin et al., 2000) (**Figure 4C**). We found that none of the three metals affected the responses of animals (**Figure 4C**), a finding that is consistent with their electrotaxis phenotypes. It was interesting to note that while Cd did have a low penetrant effect on DAergic neurons, the changes were inconsistent with behavioral responses of exposed worms. We conclude that metals cause variable damage to DAergic neurons. More work is needed to determine the precise relationship between neuronal phenotype, electrotaxis, and BSR in metal-exposed *C. elegans*.

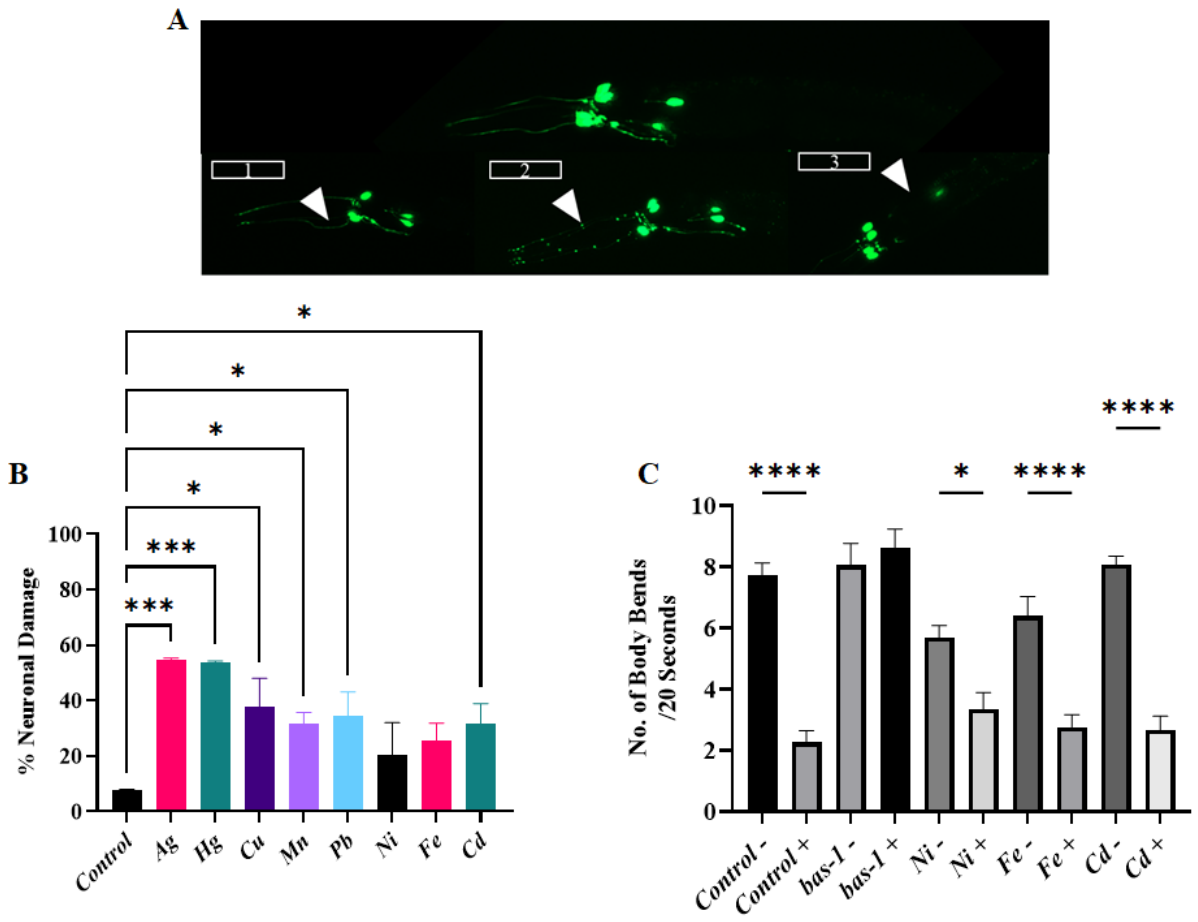

Figure 4. Neurodegenerative phenotypes of young adult *dat-1p::YFP* transgenic animals resulting from chronic exposure to metal salts. **A)** Representative images of neuronal defects observed in animals. Dopaminergic neurons and processes are healthy in untreated *dat-1p::YFP* control animals. Sub-panels show the defects that arise in metal-exposed dat-1p::YFP animals including 1. abnormal CEP dendrite morphology, 2. punctate patterns in CEP dendrites and ectopic neurite growth, and 3. loss of CEP neurons and dendrite segments. **B)** The percentage distribution of *dat-1p::YFP* animals with normal fluorescent neurons following metal exposure. **C)** The Basal slowing response of Day 3 adults following metal Exposure. Well-fed animals exposed to metals were transferred to plates (+) with and (-) without bacteria. As a control both wildtype *N2* and *bas-1* animals were used. *N2* had a normal BSR and as expected *bas-1* animals had a defective BSR, demonstrating the effectiveness of this assay in our hands. Data is expressed as +/- SEM and pooled from individual replicates (n=16 animals) per group. Statistical analysis for panel **B** and **C** was done using a one-way ANOVA with Dunnett's post hoc test. *p<0.05; **p<0.01; ***p<0.001; ****p<0.0001.

Previous work from our lab has shown that chemicals which alter the electrotaxis behavior can affect the stress responses of animals. Additionally, toxic metals are known to compromise unfolded protein response (UPR) pathways such as the cytosolic heat shock response (HSR) which is known to work with metallothionein in clearing metals leading to reduced cellular stress and proteotoxicity (Liu & Thiele, 1996; Martinez-Finley & Aschner, 2011; Uenishi et al., 2006). To investigate the role of HSR in metal-induced response, we first examined the effect of three metals, namely Mn and Pb, both of which affect electrotaxis but in an opposite way, and Cd that causes no electrotaxis phenotype but is reported to activate the HSR marker *hsp-16.2*(S. Wang et al., 2020). Our qPCR analysis showed that while Mn and Cd increased *hsp-16.2* transcript levels, Pb had no significant effect (**Figure 5A**). Interestingly, there was no increase in *hsf-1* levels, a transcription factor that plays a major role in regulating expression of heat shock chaperons including *hsp-16.2*. It is conceivable that *hsf-1* affects *hsp-16.2* levels by acting post-transcriptionally or additional heat shock proteins may be involved. Moreover, electrotaxis defects in *hsf-1* mutants (Taylor et al., 2021), were not further enhanced by Mn, Pb and Cd (**Figure 5B**). Overall, these data show that changes in the cytosolic stress response do not correlate with metal induced electrotaxis defects, suggesting that other factors are likely to play a role in mediating metal toxicity.

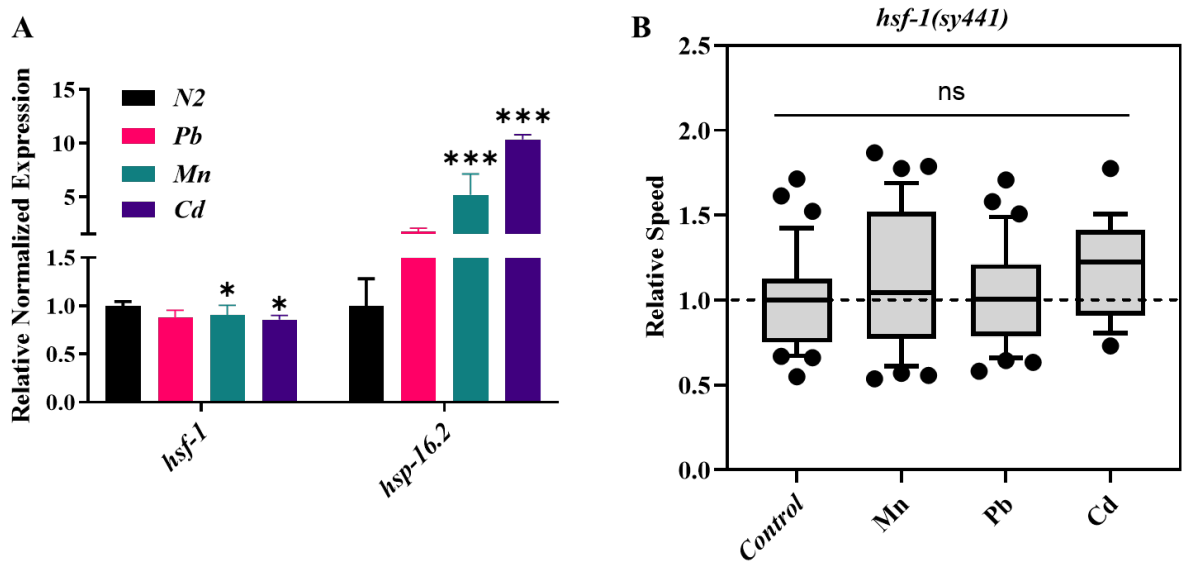

Figure 5: Effect of selected heavy metals of the cytosolic stress response. **A)** RT-qPCR analysis of Mn and Cd exposed worms showing increased expression of *hsf-1* (p=0.03 and 0.006) and *hsp-16.2* (p<0.001). However, Pb exposure did not significantly alter the *hsf-1 (*p=0.13494) or *hsp-16.2* (p=0.578049) expression. Statistical analysis for panel A was done using a one-way ANOVA with Tukey's post hoc test. **B)** *hsf-1(sy441)* animals were exposed to Pb, Mn, and Cd. No significant difference between any conditions. *p<0.05; **p<0.01; ***p<0.001; ****p<0.0001.

Post-exposure recovery does not revert electrotaxis defect

Studies have shown that acute exposure to toxic chemicals can have a lasting effect on animals (Benedetto et al., 2010). We therefore wondered if our exposure paradigm would elicit a similar persisting detrimental effect on the electrotaxis behaviour of animals. To this end, two metal salts were tested, namely Pb and Mn. Both cause electrotaxis defects. However, responses were opposite, i.e., Pb induced a hyperactive response characterized by faster speed whereas Mn caused animals to move slowly. Animals were exposed to metals until day 1 adulthood followed by recovery for four days. They were then tested on day 5. Surprisingly, both Pb and Mn led to a slower electrotaxis speed (**Figure 6)**. We conclude that exposure to these two metals causes irreversible damage to *C. elegans.*

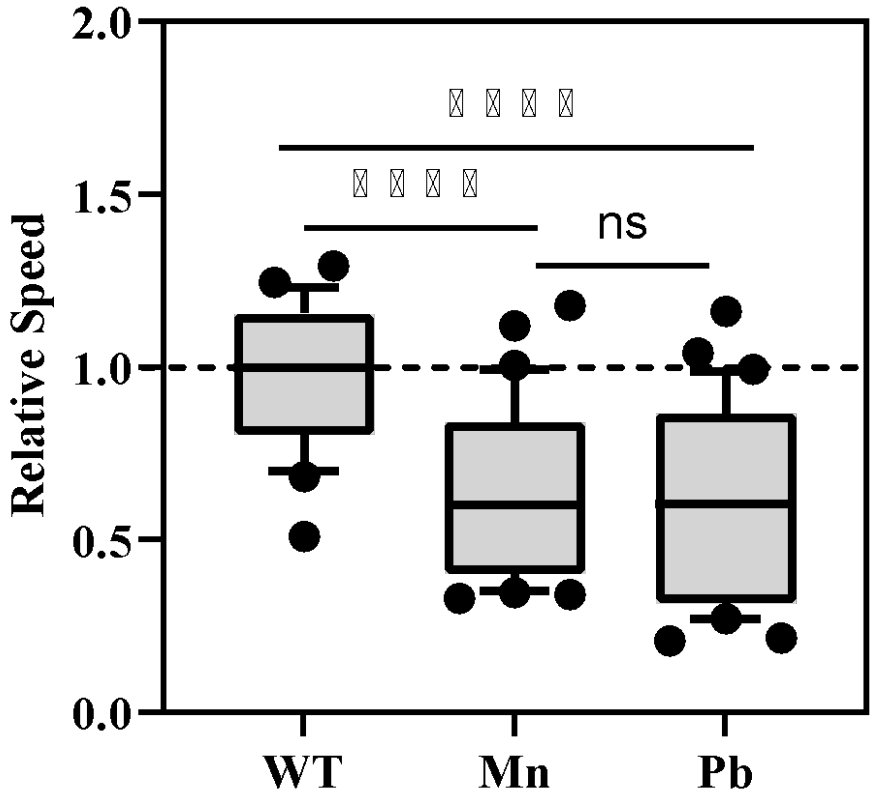

Figure 6. Electrotaxis speed of metal-treated animals following post exposure recovery. Animals were treated with Pb and Mn salts throughout development till day 1 adulthood and allowed to grow on normal, metal-free plates for an additional four days. Following recovery both Mn and Pb significantly reduced the speed of animals. Data pooled from individual replicates (n=20 to 34 animals) per group. Statistical analysis was done using a one-way ANOVA with Dunnett's post hoc test. *p<0.05; **p<0.01; ***p<0.001; ****p<0.0001.

DISCUSSION

We have characterized the electrotactic movement of *C. elegans* following exposures to commonly found heavy metals and demonstrate their toxic effects on *C. elegans*' electrotactic response. Many of the chemicals used in our study such as Hg, MeHg, Fe, Cd, and Ni were reported previously to cause defects in standard plate and liquid assays(Bovio et al., 2021; Colonnello et al., 2020; De Almeida Fagundez et al., 2015; Ijomone et al., 2020; Klang et al., 2014; R. Kumar et al., 2015; Morton & Lamitina, 2013; Moyson et al., 2019; Tang et al., 2019; D. Wang & Xing, 2008). However, the absence of a constant stimulus in these assays meant that quantifying behavioral responses of animals presented difficulties. This is because *C. elegans* arbitrarily exhibit pauses, reorientations, omega turns, and backward locomotion, creating complex patterns abundant in background noise (Vidal-Gadea et al., 2012). To overcome these challenges, we used a microfluidic channel device that incorporates mild electric fields and linear path into the assay, resulting in a tightly controlled stimulation which produces directional locomotion, thereby providing a sensitive way to quantify movement of animals (Rezai et al., 2010; Tong et al., 2013).

The electrotaxis data reported here shows that depending on the concentration and exposure duration, metal salts can be toxic to animals. The defects caused by metals can be attributed to their capacity to bioaccumulate. In support of this, we found that metals bioaccumulate to varying levels in exposed animals that correlated with the severity of their electrotaxis phenotypes. Cu is a physiological mineral, there are endogenous mechanisms in place to regulate its homeostasis, including metallochaperones like CUTC-1(Calafato et al., 2008). The relatively lower potency of Cu as a toxicant in electrotaxis assay may be due to its role in normal biological function as an essential component of cytochrome c oxidase, superoxide dismutase, and other conserved enzymes (Halfdanarson et al., 2008). However, high concentrations of Cu (150 µM and higher) are toxic to *C. elegans* as demonstrated in our study and previous findings (Vidal-Gadea et al., 2012). Consistent with this, chronic excesses of Cu in humans due to regular ingestion or by Cu retention (i.e. Wilson's disease) are linked to brain and liver damage (Ala et al., 2007).

Unlike Cu, Ag and Hg exposures caused electrotaxis defects at much lower concentrations suggesting higher sensitivity of biological processes to these two chemicals. As mentioned in the introduction Ag and Hg are toxic to organisms, causing a variety of defects in development, behavior, and organ function (Chen et al., 2013; Hunt, 2017). MeHg is known to molecularly mimic methionine and enter cells via the large amino acid transporter, LAT1(Helmcke & Aschner, 2010), which promotes its accrual. This might explain in part why we observed over 10-fold higher accumulation of metal in case of MeHgCl exposure compared to other metal salt treatments. Consistent with previous findings all three metal salts are harmful to *C. elegans* as they cause defects in development, behavior, reproduction, and lifespan (Hunt et al., 2014; D. Y. Wang & Yang, 2007). Behavioral defects included head thrashing, body bending and the number of forward turns following Ag, Cu, Hg exposure (D. Wang & Xing, 2008). Our electrotaxis results show reduced speed following exposure to Ag, Cu, Hg. The data are not only consistent with movement phenotypes observed in previous studies but further demonstrate that worms are sensitive to Ag and Hg at much lower dose.

Among other metals, we observed defects following exposures to Mn and Pb. These metals have many harmful effects in mammalian systems that are described in the introduction. Studies in C. elegans have also reported a range of toxic effects. For example, exposures to L1 worms cause defects in survival, body length, brood size, movement and dopaminergic neurons (Akinyemi et

al., 2019; Benedetto et al., 2010; Tang et al., 2019). While the electrotaxis speed was lower in Mn-exposed worms, Pb caused a faster speed. One potential mechanism by which these metals affect electrotaxis is due to altered stress response signaling since chronic stress affects electrotaxis (Taylor et al., 2021). Both Mn and Pb affect ROS and chaperon expression in different exposure conditions (Ali et al., 1995; Avila et al., 2016; Flora et al., 2012; Kitada et al., 2020; Martinez-Finley et al., 2013; Shao et al., 2019; Shinkai et al., 2010). The precise reason for Pb-induced response is unclear however it is worth mentioning that Pb is known to cause hyperactivity in animals (Ramírez Ortega et al., 2021; Silbergeld & Goldberg, 1974). Whether the faster electrotaxis speed represents a hyperactive response in worms remains to be investigated. The remaining three metal salts (Ni, Fe and Cd) did not cause a statistically significant difference in the electrotaxis speed. Additionally, the animals appeared to develop normally and exhibited typical behavior on culture plates. It remains to be seen if other aspects of electrotaxis, such as amplitude of body bends and turning are affected. In this regard, it is worth mentioning that the frequency of body oscillations of exposed animals showed a lack of correlation with electrotaxis speed.

Unlike *C. elegans*, these metals are known to have toxic effects in other systems as described above. It is conceivable that subjecting worms to more severe toxic conditions may lead to electrotaxis defects. However, we found that animals subjected to an additional 48 hrs of exposure to Fe, Ni, and Cd showed a normal response. By contrast, a lower dose of Cu, i.e., 150 uM, did cause electrotaxis defects upon prolonged exposure. These results suggest different sensitivities to different metals. While we did not examine electrotaxis phenotypes at doses higher than 150 uM, published studies have reported a variety of defects when animals were acutely exposed to high doses that involved viability, neuronal function and other processes (Colonnello et al., 2020; Hu et al., 2008; Tang et al., 2019; D. Wang & Xing, 2008). It is worth emphasizing that these studies had no fixed animal stages and uniform exposure paradigm, making direct comparisons difficult (Anderson et al., 2004; Benedetto et al., 2010; Ruszkiewicz et al., 2018). Clearly, additional experiments are needed to consolidate results of a variety of metal exposure paradigms in *C. elegans*(Bovio et al., 2021; Chen et al., 2013; Colonnello et al., 2020; De Almeida Fagundez et al., 2015; Ijomone et al., 2020; Klang et al., 2014; R. Kumar et al., 2015; Morton & Lamitina, 2013; Moyson et al., 2019; Tang et al., 2019; D. Wang & Xing, 2008).Studies have also reported gene expression changes following exposures of worms to metals. For example, Hg and MeHg altered stress response genes expression (McElwee & Freedman, 2011). Genes involved in the resistance to Cd toxicity were shown to be associated with metabolic enzymes and proteolysis categories (Cui et al., 2007). In another study, a cocktail of Zn, Cu and Cd metals caused increased expression of an array of genes mediating heat shock response, oxidative stress, metal stress, development, and innate immunity and apoptosis (R. Kumar et al., 2015).

While our experiments did not reveal a common trend in *hsp-16.2* and *hsf-1* expression, one possibility may be that these metals affect stress response signaling by acting post-transcriptionally. In agreement with this, Mn and Pb exposures to *hsf-1* mutants caused no change in their electrotaxis speed. More experiments are needed to investigate the role of chaperons and stress response signaling following heavy metal exposures.

We showed earlier that animals exhibiting electrotaxis defects also exhibit degeneration of DAergic neurons (Salam et al., 2013; Taylor et al., 2021). Furthermore, both these phenotypes are

impacted by stress-inducing conditions (Taylor et al., 2021). This led us to examine DAergic neurons in metal-exposed animals. Based on their toxic effects metals can be placed into three groups. Ag and Hg caused neuronal damage in more than 50% of animals, followed by Cu, Pb, Mn, and Cd affecting roughly 30-40%. Less than a quarter of animals showed defects when exposed to Ni and Fe. Further experiments showed that Cd, Ni, and Fe had no effect on dopamine-induced movement (Sawin et al., 2000).

Previous studies provide support to our data showing neurotoxic effects of these metals in *C. elegans* (Du & Wang, 2009; Gonzalez-Carter et al., 2017; Hunt, 2017; Ke et al., 2021; Ruszkiewicz et al., 2018). More work is needed to understand the mechanism by which these metals affect neurons. One possibility may be enhanced aggregation of misfolded proteins since Cu was found to cause an increase in the paralysis of muscle-expressing amyloid beta transgenic worms (Chen et al., 2013). In some cases, metals may directly affect DA signaling, e.g., Pb exposure was found to interfere with *dat-1* (dopamine transporter) expression resulting in DAergic neuronal dysfunction (Akinyemi et al., 2019). Overall, these data show that while metals cause harm to both neurons and electrotaxis responses of worms, the phenotypes do not always coexist. More experiments are needed to determine whether a lack of correlation is due to differing sensitivities of DAergic neurons to metals and the extent to which neuronal changes contribute to electrotaxis defects. Additionally, since amphid neurons have been shown to be necessary for sensing the electric field (Gabel et al., 2007) it will be necessary to examine their sensitivities to metal salts.

As we continued to analyze the toxic effects of metals, we investigated if the effects can be mitigated after animals were removed from the toxic environment. This is because of the mechanisms to clear the metal from the system (Martinez-Finley & Aschner, 2011). To this end, we allowed exposed worms to recover for four days, which is roughly one-fifth of their lifespan. This was done in the case of Mn and Pb, two metals that cause electrotaxis defects. We found that not only did the animals continue to show abnormal movements, but the Pb-exposed population unexpectedly showed a reduced speed. More work is needed to determine the precise reason for such a phenotype and whether there was irreversible damage to certain tissues and processes.

In summary, this work reports the various levels of toxicity exhibited by metals using a novel microfluidic-based assay. Our data show that some but not all metals have detrimental effects on worms, highlighting the complexity of the response. Furthermore, locomotory behavior, which requires the integration of processes at multiple levels, is highly susceptible to chemical insults such as toxic metal exposure. Finally, the data demonstrate that electrotaxis is a sensitive and quantitative method to investigate mechanisms by which metals induce damage in multicellular eukaryotes.

MATERIALS AND METHODS

Strains and culturing

Worms were grown and maintained at 20°C on LB-agar and Modified Youngren's Only Bactopeptone (MYOB)-agar plates containing *Escherichia coli* OP50 culture using previously described methods (Brenner, 1974). All experiments used age-synchronous populations obtained by bleach treatment. Strains used are N2, *hsf-1(sy441), DY353: bhEx138[pGLC72(Cel-dat-1p::YFP)], MT7988 bas-1(ad446)*

Chemicals and treatments

We used the plate-based exposure paradigm which provides efficient bioavailability of chemicals (Vidal-Gadea et al., 2012). All chemicals were obtained from Sigma-Aldrich (St. Louis, MO, USA). All toxicants were first prepared as 200x solutions in 100% DMSO, then diluted 10x with water. 500 µL of the resultant 20x LB agar finally resulting in 1x concentrations of toxicant and 0.5% DMSO.

We chose appropriate concentrations as the highest concentrations of each compound at which chronic exposure would have low to no plate-level phenotypes such as lethality, larval arrest or significant developmental delay. A complete listing of all concentrations tested in this way is shown in the **Supplementary Table 1**.

Two of the metal salts, $AgNO_3$ and $HgCl_2$ were tested at three different concentrations (5 µM, 50 µM, and 150 µM)). MeHgCl, an organometallic form of Hg, is highly toxic and was used at 2 µM. Cu was tested at a wider range of concentrations (5 µM, 50 µM, 150 µM, and 500 µM), none of which caused an obvious defect at the plate level.

In subsequent electrotaxis assays involving five other metals (Cd, Fe, Ni, Pb, and Mn), we started out with 150um concentration of each metal. In our plate level analysis, the animals had a similar growth rate, brood size and movement to control with a few exceptions (Supplementary Table x). Cadmium and Iron cause some delayed growth including arrested L1 larvae. Higher concentrations of both of these chemicals and Nickel were detrimental as animals showed L1 stage arrest. The movement tracks and brood size of the worms on day 1 adulthood were also very similar to untreated controls.

Two of the metals, Fe and Cd, were also tested at other concentrations. Animals exposed to 300 uM of FeSO4 showed obvious defects on plates (i.e., growth arrest), which precluded any further analysis. Cd was less toxic at 100 uM but still caused severe growth arrest. However, animals exposed to 50 uM Cd showed a mild growth defect at the plate level but otherwise appeared normal during adulthood, thereby allowing us to test their electrotaxis responses.

We first observed *hsf-1* animals at a plate level and found that those exposed to Cd had animals arrested at L1 but some were still able to reach adulthood. In the case of Pb exposure, animals were developmentally delayed by a few hours and Mn did not have an effect on the animals overall. All together the animals looked visually healthy and had normal movement tracks on the plate.

Electrotaxis assay

Microfluidic channels were fabricated as previously described (Rezai et al., 2010). Nematodes were grown under exposure conditions starting from the L1 larval or egg stage. Upon becoming young adults, nematodes were washed off their culture plates, cleaned, and suspended in M9 buffer. Animals were then aspirated into the channel using the syringe pump. Individual animals were isolated by adjusting the tubes' relative height to hydrostatically manipulate the flow of M9 through the channel. Both tubes were then laid flat at the same elevation to eliminate pressure-induced flow. Next, a 3 V/cm DC electric field was applied, and the animal's resultant behavior recorded by camera. Locomotory data was later extracted from recorded videos either manually using NIH ImageJ (*http://rsbweb.nih.gov/ij/*) or automatically with custom MATLAB-based tracking software. Toxicant-exposed animals were grown for 69 h at 20°C before scoring. At least three batches of 10 animals each were scored for each condition. Speed data was normalized to the median of the control.

Brood size, growth and lifespan assays

Reproductive capacity of toxicant-exposed animals was determined by counting the hatched progeny of isolated hermaphrodites.

Five L4-stage larvae were picked onto fresh spiked MYOB plates and incubated for an additional 96 h at 20°C for maturation and egg-laying; afterwards, the number of offspring was estimated by suspending the population in M9 and counting the animals in aliquots of the suspension.

In the cases of 50 and 150 μM Ag and Hg, nematodes were grown for 2 weeks instead of 6 days to account for these animals' slower growth, and progeny were counted and removed from plates daily. The resultant progeny on two batches of four plates per test condition were quantified in this way.

Body length of metal-exposed nematodes was determined after 69 h of growth at 20°C on toxicant-spiked MYOB plates containing food. Measurements were made from photographs of animals anesthetized through placement in a 15-μL drop of 30 mM NaN_3 in M9, which lay on a solidified pad of 4% agar on a glass slide. Photographs were taken and analyzed with a Hamamatsu ORCA-AG camera on a Nikon Eclipse 80i Nomarski microscope, using NIS-Elements BR software version 3.0 (www.nis-elements.com). At least two batches of 10 animals each were measured for each test condition.

For lifespan assays two batches of 20 age synchronous L1 larvae per condition were transferred into four fresh spiked MYOB plates (five animals per plate) and grown at 20°C. Viability of animals was checked each day under a stereomicroscope. If immobile, animals were checked for viability by tapping the plate and gently touching their bodies with a platinum pick. Nematodes were transferred to fresh spiked MYOB plates after 120 h, 168 h, and 216 h to prevent contamination of parent animals by offspring.

Determination of metal content

Approximately 10,000 age-synchronous L1 larvae per condition were transferred into fresh spiked MYOB plates and grown at 20°C for 69 h, at the conclusion of which both live and dead animals were collected and washed twice with deionized water. Two biological replicates were prepared for each exposure. Untreated worms were used as controls. The pelleted pool of worms was frozen at -80°C for further processing at Actlabs (Ancaster, ON, Canada). Each sample was weighed into a 50-mL centrifuge tube followed by the addition of 2 mL of concentrated HNO_3. Centrifuge tubes were placed in a boiling water bath for 1 h to digest samples. The fully digested content in each tube was then diluted to 50 mL with water and analyzed by inductively coupled plasma-mass spectrometry (ICP-MS) using QOP Hydrogeo Rev. 6.6. In addition to testing worms, we also measured metal concentrations in the exposure media.

The elemental contents of Ag, Hg, and MeHg were measured as a test case to determine the effectiveness of our agar plate-based exposure paradigm. The results revealed that while Hg was recovered with somewhat lower efficiency (71% for $HgCl_2$, and 37% for MeHgCl), possibly due to speciation and precipitation, Ag was fully recoverable.

Neuronal phenotype analyses

Fluorescence microscopy and quantification. Animals were mounted on 2% agar pad containing glass slides. Before placing the cover slip, they were anesthetized using 30 mM NaN3. GFP fluorescence was visualized using a Zeiss Observer Z1 microscope equipped with an Apotome 2 and X-Cite R 120LED fluorescence illuminator. The *dat-1p::YFP* strain was used to visualize CEP and ADE dopaminergic neurons. Protocol was adapted from (Taylor et al., 2021). The percentage of animals with defects was plotted.

Basal Slowing Response Assay

The protocol was adapted from (Sawin et al., 2000). Body Bend was measured for 20 secs 3 times per worm. 200uL of bacteria was plated to seed half of the plate. Worms were transferred to the area without food and then allowed to crawl to the side of the plate with food. Day 3 adult animals were used. Experiment was repeated in two independent trials(replicates) using 8 animals per trial for each metal.

Post - exposure recovery

Test two chemicals (Pb and Mn) – Animals were grown in the presence of metal salts from egg stage till day-1 adulthood. On day 1 animals were washed thoroughly and move to normal OP50 culture plates. They were transferred every other day until day 5 adulthood.

Data analysis

Graphpad Prism 9 was used to perform statistical analysis. Electrotaxis speed data was plotted in box plots and compared with the non-parametric Mann-Whitney test. Lifespan data was assessed with the Kaplan-Meier method and compared with the log-rank test. All other data was analyzed with Student's *t*-test. For all assays, data from all repeats were pooled and analyzed together.

ACKNOWLEDGEMENTS

We thank Anne Xia (undergraduate thesis student) and Dr. Pouya Rezai (York University, Canada) for discussions and assistance with experiments. Some strains were provided by the CGC, which is funded by NIH Office of Research Infrastructure Programs (P40 OD010440). We are grateful to Drs. Chris Wood and James McNulty (both at McMaster University, Canada) for providing some of the chemicals. This work was supported by grants from the Ontario Ministry of Research and Innovation (awarded to BPG) and the Collaborative Health Research Project, co-funded by the Natural Sciences and Engineering Research Council of Canada and the Canadian Institutes of Health Research (awarded to PRS, BPG and RKM).

REFERENCES

Akinyemi, A. J., Miah, M. R., Ijomone, O. M., Tsatsakis, A., Soares, F. A. A., Tinkov, A. A., Skalny, A. V., Venkataramani, V., & Aschner, M. (2019). Lead (Pb) exposure induces dopaminergic neurotoxicity in Caenorhabditis elegans: Involvement of the dopamine transporter. *Toxicology Reports*, *6*, 833–840. https://doi.org/10.1016/j.toxrep.2019.08.001

Ala, A., Walker, A. P., Ashkan, K., Dooley, J. S., & Schilsky, M. L. (2007). Wilson's disease. *The Lancet*, *369*(9559), 397–408. https://doi.org/10.1016/S0140-6736(07)60196-2

Ali, S. F., Duhart, H. M., Newport, G. D., Lipe, G. W., & Slikker, W. (1995). Manganese-induced reactive oxygen species: Comparison between Mn+2 and Mn+3. *Neurodegeneration*, *4*(3), 329–334. https://doi.org/10.1016/1055-8330(95)90023-3

Anderson, G. L., Cole, R. D., & Williams, P. L. (2004). Assessing behavioral toxicity with Caenorhabditis elegans. *Environmental Toxicology and Chemistry*, *23*(5), 1235–1240. https://doi.org/10.1897/03-264

AshaRani, P., Hande, M. P., & Valiyaveettil, S. (2009). Anti-proliferative activity of silver nanoparticles. *BMC Cell Biology*, *10*(1), 65. https://doi.org/10.1186/1471-2121-10-65

Avila, D. S., Benedetto, A., Au, C., Bornhorst, J., & Aschner, M. (2016). Involvement of heat shock proteins on Mn-induced toxicity in Caenorhabditis elegans. *BMC Pharmacology and Toxicology*, *17*(1), 1–9. https://doi.org/10.1186/S40360-016-0097-2/FIGURES/5

Bar-Ilan, O., Albrecht, R. M., Fako, V. E., & Furgeson, D. Y. (2009). Toxicity Assessments of Multisized Gold and Silver Nanoparticles in Zebrafish Embryos. *Small*, *5*(16), 1897–1910. https://doi.org/10.1002/smll.200801716

Benedetto, A., Au, C., Avila, D. S., Milatovic, D., & Aschner, M. (2010). Extracellular Dopamine Potentiates Mn-Induced Oxidative Stress, Lifespan Reduction, and Dopaminergic Neurodegeneration in a BLI-3–Dependent Manner in Caenorhabditis elegans. *PLoS Genetics*, *6*(8), e1001084. https://doi.org/10.1371/journal.pgen.1001084

Bovio, F., Sciandrone, B., Urani, C., Fusi, P., Forcella, M., & Regonesi, M. E. (2021). Superoxide dismutase 1 (SOD1) and cadmium: A three models approach to the comprehension of its neurotoxic effects. *NeuroToxicology*, *84*, 125–135. https://doi.org/10.1016/J.NEURO.2021.03.007

Brenner, S. (1974). The Genetics of Caenorhabditis elegans. *Genetics*, *77*, 71–94.

Calafato, S., Swain, S., Hughes, S., Kille, P., & Stürzenbaum, S. R. (2008). Knock down of Caenorhabditis elegans cutc-1 Exacerbates the Sensitivity Toward High Levels of Copper. *Toxicological Sciences*, *106*(2), 384–391. https://doi.org/10.1093/toxsci/kfn180

Chen, P., Martinez-Finley, E. J., Bornhorst, J., Chakraborty, S., & Aschner, M. (2013). Metal-induced neurodegeneration in C. elegans. In *Frontiers in Aging Neuroscience* (Vol. 5, Issue MAY). Frontiers Media SA. https://doi.org/10.3389/fnagi.2013.00018

Clarkson, T. W., & Magos, L. (2006). The Toxicology of Mercury and Its Chemical Compounds. *Critical Reviews in Toxicology*, *36*(8), 609–662. https://doi.org/10.1080/10408440600845619

Colonnello, A., Aguilera-Portillo, G., Rubio-López, L. C., Robles-Bañuelos, B., Rangel-López, E., Cortez-Núñez, S., Evaristo-Priego, Y., Silva-Palacios, A., Galván-Arzate, S., García-Contreras, R., Túnez, I., Chen, P., Aschner, M., & Santamaría, A. (2020). Comparing the Neuroprotective Effects of Caffeic Acid in Rat Cortical Slices and Caenorhabditis elegans: Involvement of Nrf2 and SKN-1 Signaling Pathways. *Neurotoxicity Research*, *37*(2), 326–337. https://doi.org/10.1007/S12640-019-00133-8/FIGURES/7

Cui, Y., McBride, S. J., Boyd, W. A., Alper, S., & Freedman, J. H. (2007). Toxicogenomic analysis of caenorhabditis elegans reveals novel genes and pathways involved in the resistance to cadmium toxicity. *Genome Biology*, *8*(6), R122. https://doi.org/10.1186/gb-2007-8-6-r122

De Almeida Fagundez, D., Câmara, D. F., Salgueiro, W. G., Noremberg, S., Luiz Puntel, R., Piccoli, J. E., Garcia, S. C., Da Rocha, J. B. T., Aschner, M., & Ávila, D. S. (2015). Behavioral and dopaminergic damage induced by acute iron toxicity in Caenorhabditis elegans. *Toxicology Research*, *4*(4), 878–884. https://doi.org/10.1039/C4TX00120F

Drake, P. L., & Hazelwood, K. J. (2005). Exposure-Related Health Effects of Silver and Silver Compounds: A Review. *The Annals of Occupational Hygiene*, *49*(7), 575–585. https://doi.org/10.1093/ANNHYG/MEI019

Du, M., & Wang, D. (2009). The neurotoxic effects of heavy metal exposure on GABAergic nervous system in nematode Caenorhabditis elegans. *Environmental Toxicology and Pharmacology*, *27*(3), 314–320. https://doi.org/10.1016/j.etap.2008.11.011

Flora, G., Gupta, D., & Tiwari, A. (2012). Toxicity of lead: A review with recent updates. *Interdisciplinary Toxicology*, *5*(2), 47. https://doi.org/10.2478/V10102-012-0009-2

Forsyth, D. S., Casey, V., Dabeka, R. W., & McKenzie, A. (2004). Methylmercury levels in predatory fish species marketed in Canada. *Food Additives and Contaminants*, *21*(9), 849–856. https://doi.org/10.1080/02652030400004259

Gabel, C. V., Gabel, H., Pavlichin, D., Kao, A., Clark, D. A., & Samuel, A. D. T. (2007). Neural Circuits Mediate Electrosensory Behavior in Caenorhabditis elegans. *Journal of Neuroscience*, *27*(28), 7586–7596. https://doi.org/10.1523/JNEUROSCI.0775-07.2007

Genchi, G., Carocci, A., Lauria, G., Sinicropi, M. S., & Catalano, A. (2020). Nickel: Human Health and Environmental Toxicology. *International Journal of Environmental Research and Public Health*, *17*(3). https://doi.org/10.3390/IJERPH17030679

Gonzalez-Carter, D. A., Leo, B. F., Ruenraroengsak, P., Chen, S., Goode, A. E., Theodorou, I. G., Chung, K. F., Carzaniga, R., Shaffer, M. S. P., Dexter, D. T., Ryan, M. P., & Porter, A. E. (2017). Silver nanoparticles reduce brain inflammation and related neurotoxicity through induction of H2S-synthesizing enzymes. *Scientific Reports*, *7*. https://doi.org/10.1038/SREP42871

Hadrup, N., Sharma, A. K., & Loeschner, K. (2018). Toxicity of silver ions, metallic silver, and silver nanoparticle materials after in vivo dermal and mucosal surface exposure: A review. *Regulatory Toxicology and Pharmacology*, *98*, 257–267. https://doi.org/10.1016/J.YRTPH.2018.08.007

Halfdanarson, T. R., Kumar, N., Li, C., Phyliky, R. L., & Hogan, W. J. (2008). Hematological manifestations of copper deficiency: a retrospective review. *European Journal of Haematology*, *80*(6), 523–531. https://doi.org/10.1111/j.1600-0609.2008.01050.x

Hart, A. (2006). Behavior of the C. elegans. *WormBook*, 1–67. https://doi.org/10.1895/wormbook.1.87.1

Helmcke, K. J., & Aschner, M. (2010). Hormetic effect of methylmercury on Caenorhabditis elegans. *Toxicology and Applied Pharmacology*, *248*(2), 156–164. https://doi.org/10.1016/j.taap.2010.07.023

Hong, Y.-S., Kim, Y.-M., & Lee, K.-E. (2012). Methylmercury Exposure and Health Effects. *Journal of Preventive Medicine & Public Health*, *45*(6), 353–363. https://doi.org/10.3961/jpmph.2012.45.6.353

Hu, Y. O., Wang, Y., Ye, B. P., & Wang, D. Y. (2008). Phenotypic and Behavioral Defects Induced by Iron Exposure Can Be Transferred to Progeny in Caenorhabditis elegans. *Biomedical and Environmental Sciences*, *21*(6), 467–473. https://doi.org/10.1016/S0895-3988(09)60004-0

Hunt, P. R. (2017). The C. elegans model in toxicity testing. In *Journal of Applied Toxicology* (Vol. 37, Issue 1, pp. 50–59). https://doi.org/10.1002/jat.3357

Hunt, P. R., Keltner, Z., Gao, X., Oldenburg, S. J., Bushana, P., Olejnik, N., & Sprando, R. L. (2014). Bioactivity of nanosilver in Caenorhabditis elegans: Effects of size, coat, and shape. *Toxicology Reports*, *1*, 923–944. https://doi.org/10.1016/J.TOXREP.2014.10.020

Ijomone, O. M., Miah, M. R., Akingbade, G. T., Bucinca, H., & Aschner, M. (2020). Nickel-Induced Developmental Neurotoxicity in C. elegans Includes Cholinergic, Dopaminergic and GABAergic Degeneration, Altered Behaviour, and Increased SKN-1 Activity. *Neurotoxicity Research*, *37*(4), 1018–1028. https://doi.org/10.1007/s12640-020-00175-3

Jaishankar, M., Tseten, T., Anbalagan, N., Mathew, B. B., & Beeregowda, K. N. (2014). Toxicity, mechanism and health effects of some heavy metals. *Interdisciplinary Toxicology*, *7*(2), 60. https://doi.org/10.2478/INTOX-2014-0009

Ju, J., Ruan, Q., Li, X., Liu, R., Li, Y., Pu, Y., Yin, L., & Wang, D. (2013). Neurotoxicological evaluation of microcystin-LR exposure at environmental relevant concentrations on nematode

Caenorhabditis elegans. *Environmental Science and Pollution Research*, *20*(3), 1823–1830. https://doi.org/10.1007/s11356-012-1151-2

Ke, T., Prince, L. M., Bowman, A. B., & Aschner, M. (2021). Latent alterations in swimming behavior by developmental methylmercury exposure are modulated by the homolog of tyrosine hydroxylase in Caenorhabditis elegans. *Neurotoxicology and Teratology*, *85*, 106963. https://doi.org/10.1016/j.ntt.2021.106963

Kim, J., Song, H., Heo, H. R., Kim, J. W., Kim, H. R., Hong, Y., Yang, S. R., Han, S. S., Lee, S. J., Kim, W. J., & Hong, S. H. (2017). Cadmium-induced ER stress and inflammation are mediated through C/EBP–DDIT3 signaling in human bronchial epithelial cells. *Experimental & Molecular Medicine 2017 49:9*, *49*(9), e372–e372. https://doi.org/10.1038/emm.2017.125

Kitada, M., Xu, J., Ogura, Y., Monno, I., & Koya, D. (2020). Manganese superoxide dismutase dysfunction and the pathogenesis of kidney disease. *Frontiers in Physiology*, *11*, 1–16. https://doi.org/10.3389/FPHYS.2020.00755/BIBTEX

Klang, I. M., Schilling, B., Sorensen, D. J., Sahu, A. K., Kapahi, P., Andersen, J. K., Swoboda, P., Killilea, D. W., Gibson, B. W., & Lithgow, G. J. (2014). Iron promotes protein insolubility and aging in *C. elegans*. *Aging*, *6*(11), 975–988. https://doi.org/10.18632/AGING.100689

Kumar, R., Pradhan, A., Khan, F. A., Lindström, P., Ragnvaldsson, D., Ivarsson, P., Olsson, P. E., & Jass, J. (2015). Comparative analysis of stress induced gene expression in caenorhabditis elegans following exposure to environmental and lab reconstituted complex metal mixture. *PLoS ONE*, *10*(7). https://doi.org/10.1371/journal.pone.0132896

Kumar, V., Kalita, J., Misra, U. K., & Bora, H. K. (2015). A study of dose response and organ susceptibility of copper toxicity in a rat model. *Journal of Trace Elements in Medicine and Biology*, *29*, 269–274. https://doi.org/10.1016/J.JTEMB.2014.06.004

Liu, X. D., & Thiele, D. J. (1996). Oxidative stress induces heat shock factor phosphorylation and HSF-dependent activation of yeast metallothionein gene transcription. *Genes and Development*, *10*(5), 592–603. https://doi.org/10.1101/gad.10.5.592

Martinez-Finley, E. J., & Aschner, M. (2011). Revelations from the nematode caenorhabditis elegans on the complex interplay of metal toxicological mechanisms. *Journal of Toxicology*, *2011*. https://doi.org/10.1155/2011/895236

Martinez-Finley, E. J., Gavin, C. E., Aschner, M., & Gunter, T. E. (2013). Manganese Neurotoxicity and the Role of Reactive Oxygen Species. *Free Radical Biology & Medicine*, *62*, 65. https://doi.org/10.1016/J.FREERADBIOMED.2013.01.032

McElwee, M. K., & Freedman, J. H. (2011). Comparative toxicology of mercurials in Caenorhabditis elegans. *Environmental Toxicology and Chemistry*, *30*(9), 2135–2141. https://doi.org/10.1002/etc.603

Mo, Y., Jiang, M., Zhang, Y., Wan, R., Li, J., Zhong, C. J., Li, H., Tang, S., & Zhang, Q. (2019). Comparative mouse lung injury by nickel nanoparticles with differential surface modification. *Journal of Nanobiotechnology*, *17*(1), 1–18. https://doi.org/10.1186/s12951-018-0436-0

Morton, E. A., & Lamitina, T. (2013). Caenorhabditis elegans HSF-1 is an essential nuclear protein that forms stress granule-like structures following heat shock. *Aging Cell*, *12*(1), 112–120.

Moyson, S., Town, R. M., Vissenberg, K., & Blust, R. (2019). The effect of metal mixture composition on toxicity to C. elegans at individual and population levels. *PLOS ONE*, *14*(6), e0218929. https://doi.org/10.1371/JOURNAL.PONE.0218929

Ndayisaba, A., Kaindlstorfer, C., & Wenning, G. K. (2019). Iron in neurodegeneration - Cause or consequence? In *Frontiers in Neuroscience* (Vol. 13). Frontiers Media SA. https://doi.org/10.3389/fnins.2019.00180

Rahman, M. F., Wang, J., Patterson, T. A., Saini, U. T., Robinson, B. L., Newport, G. D., Murdock, R. C., Schlager, J. J., Hussain, S. M., & Ali, S. F. (2009). Expression of genes related to oxidative stress in the mouse brain after exposure to silver-25 nanoparticles☆. *Toxicology Letters*, *187*(1), 15–21. https://doi.org/10.1016/j.toxlet.2009.01.020

Raj, V., Nair, A., & Thekkuveettil, A. (2021). Manganese exposure during early larval stages of C. elegans causes learning disability in the adult stage. *Biochemical and Biophysical Research Communications*, *568*, 89–94. https://doi.org/10.1016/J.BBRC.2021.06.073

Ramírez Ortega, D., González Esquivel, D. F., Blanco Ayala, T., Pineda, B., Gómez Manzo, S., Marcial Quino, J., Carrillo Mora, P., & Pérez de la Cruz, V. (2021). Cognitive Impairment Induced by Lead Exposure during Lifespan: Mechanisms of Lead Neurotoxicity. *Toxics 2021, Vol. 9, Page 23*, *9*(2), 23. https://doi.org/10.3390/TOXICS9020023

Rezai, P., Siddiqui, A., Selvaganapathy, P. R., & Gupta, B. P. (2010). Electrotaxis of Caenorhabditis elegans in a microfluidic environment. *Lab on a Chip*, *10*(2), 220–226. https://doi.org/10.1039/b917486a

Roh, J., Sim, S. J., Yi, J., Park, K., Chung, K. H., Ryu, D., & Choi, J. (2009). Ecotoxicity of Silver Nanoparticles on the Soil Nematode Caenorhabditis elegans Using Functional Ecotoxicogenomics. *Environmental Science & Technology*, *43*(10), 3933–3940. https://doi.org/10.1021/es803477u

Ruszkiewicz, J. A., Pinkas, A., Miah, M. R., Weitz, R. L., Lawes, M. J. J. A., Akinyemi, A. J., Ijomone, O. M., & Aschner, M. (2018). C. elegans as a model in developmental neurotoxicology. *Toxicology and Applied Pharmacology*, *354*, 126. https://doi.org/10.1016/J.TAAP.2018.03.016

Salam, S., Ansari, A., Amon, S., Rezai, P., Selvaganapathy, P. R., Mishra, R. K., & Gupta, B. P. (2013). A microfluidic phenotype analysis system reveals function of sensory and dopaminergic neuron signaling in C. elegans electrotactic swimming behavior. *Worm*, *2*(2), e24558. https://doi.org/10.4161/worm.24558

Sawin, E. R., Ranganathan, R., & Horvitz, H. R. (2000). C. elegans locomotory rate is modulated by the environment through a dopaminergic pathway and by experience through a serotonergic pathway. *Neuron*, *26*(3), 619–631. https://doi.org/10.1016/S0896-6273(00)81199-X

Shao, W., Li, M., Teng, Z., Qiu, B., Huo, Y., & Zhang, K. (2019). Effects of Pb(II) and Cr(VI) Stress on Phosphate-Solubilizing Bacteria (Bacillus sp. Strain MRP-3): Oxidative Stress and

Bioaccumulation Potential. *International Journal of Environmental Research and Public Health*, *16*(12). https://doi.org/10.3390/IJERPH16122172

Shen, L., Xiao, J., Ye, H., & Wang, D. (2009). Toxicity evaluation in nematode Caenorhabditis elegans after chronic metal exposure. *Environmental Toxicology and Pharmacology*, *28*(1), 125–132. https://doi.org/10.1016/j.etap.2009.03.009

Shinkai, Y., Yamamoto, C., & Kaji, T. (2010). Lead Induces the Expression of Endoplasmic Reticulum Chaperones GRP78 and GRP94 in Vascular Endothelial Cells via the JNK-AP-1 Pathway. *Toxicological Sciences*, *114*(2), 378–386. https://doi.org/10.1093/TOXSCI/KFQ008

Silbergeld, E. K., & Goldberg, A. M. (1974). Hyperactivity: A Lead-Induced Behavior Disorder. *Environmental Health Perspectives*, *7*, 227. https://doi.org/10.1289/EHP.747227

Tang, B., Tong, P., Xue, K. S., Williams, P. L., Wang, J. S., & Tang, L. (2019). High-throughput assessment of toxic effects of metal mixtures of cadmium(Cd), lead(Pb), and manganese(Mn) in nematode Caenorhabditis elegans. *Chemosphere*, *234*, 232–241. https://doi.org/10.1016/j.chemosphere.2019.05.271

Taylor, S. K. B., Minhas, M. H., Tong, J., Selvaganapathy, P. R., Mishra, R. K., & Gupta, B. P. (2021). C. elegans electrotaxis behavior is modulated by heat shock response and unfolded protein response signaling pathways. *Scientific Reports*, *11*(1), 1–17. https://doi.org/10.1038/s41598-021-82466-z

Tong, J., Rezai, P., Salam, S., Selvaganapathy, P. R., & Gupta, B. P. (2013). Microfluidic-based electrotaxis for on-demand quantitative analysis of Caenorhabditis elegans' locomotion. *Journal of Visualized Experiments : JoVE*, *75*, 50226. https://doi.org/10.3791/50226

Uenishi, R., Gong, P., Suzuki, K., & Koizumi, S. (2006). Cross talk of heat shock and heavy metal regulatory pathways. *Biochemical and Biophysical Research Communications*, *341*(4), 1072–1077. https://doi.org/10.1016/J.BBRC.2006.01.066

Vidal-Gadea, A. G., Davis, S., Becker, L., & Pierce-Shimomura, J. T. (2012). Coordination of behavioral hierarchies during environmental transitions in Caenorhabditis elegans. *Worm*, *1*(1), 5. https://doi.org/10.4161/WORM.19148

Wang, D., & Xing, X. (2008). Assessment of locomotion behavioral defects induced by acute toxicity from heavy metal exposure in nematode Caenorhabditis elegans. *Journal of Environmental Sciences*, *20*(9), 1132–1137. https://doi.org/10.1016/S1001-0742(08)62160-9

Wang, D. Y., & Yang, P. (2007). Silver Exposure Causes Transferable Defects of Phenotypes and Behaviors in Nematode Caenorhabditis elegans. *Environmental Bioindicators*, *2*(2), 89–98. https://doi.org/10.1080/15555270701457695

Wang, S., You, M., Wang, C., Zhang, Y., Fan, C., & Yan, S. (2020). Heat shock pretreatment induced cadmium resistance in the nematode Caenorhabditis elegans is depend on transcription factors DAF-16 and HSF-1. *Environmental Pollution*, *261*, 114081. https://doi.org/10.1016/j.envpol.2020.114081

Wazir, S. M., & Ghobrial, I. (2017). Copper deficiency, a new triad: anemia, leucopenia, and myeloneuropathy. *Journal of Community Hospital Internal Medicine Perspectives*, *7*(4), 265–268. https://doi.org/10.1080/20009666.2017.1351289

Wu, Q., Qu, Y., Li, X., & Wang, D. (2012). Chromium exhibits adverse effects at environmental relevant concentrations in chronic toxicity assay system of nematode Caenorhabditis elegans. *Chemosphere*, *87*(11), 1281–1287. https://doi.org/10.1016/j.chemosphere.2012.01.035

SUPPLMENTARY MATERIALS

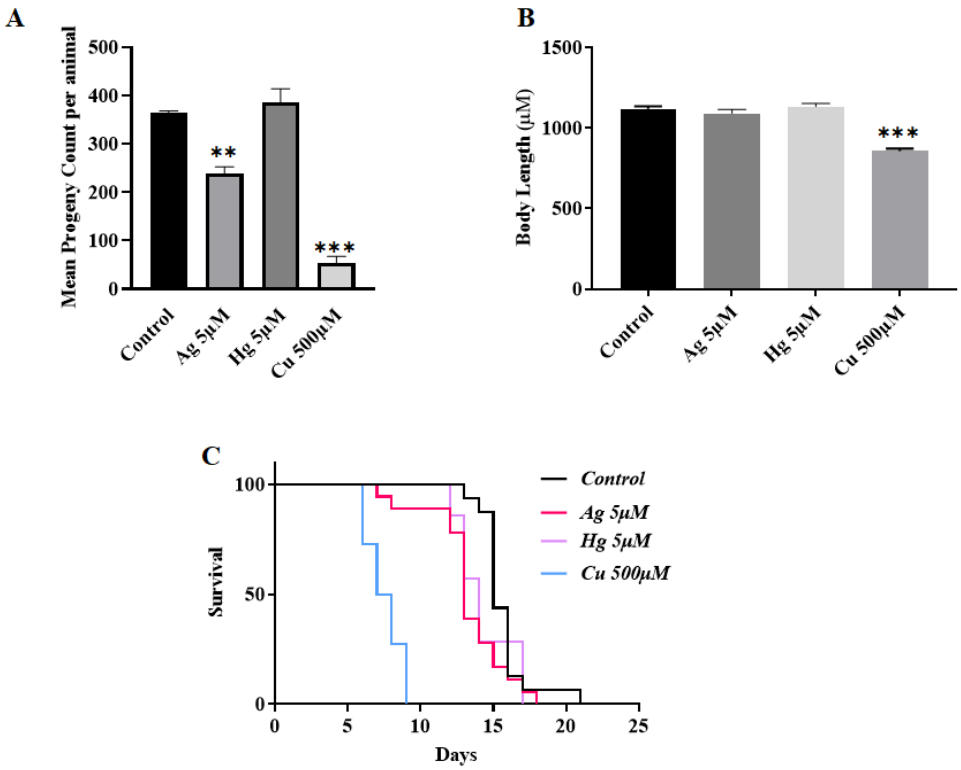

Supplementary Figure 1. Influence of chronic Ag, Hg, and Cu exposures on reproduction, body length and lifespan. **A)** reproductive capacity of *C. elegans*. At 5 µM Ag caused 36% reduction in brood size, however 5 µM Hg had no effect. Increasing the concentration by 10 fold, i.e. 50 µM, both Ag and Hg caused 99% and 87% reduced brood size, respectively. **B)** Body length was also reduced following exposure to Ag and Hg. Ag 50 µM: 39% length reduction, Ag 150 µM: 56% reduction, Hg 50 µM: 62% reduction, Hg 150 µM: 77% reduction. **C)** Influence of chronic metal exposure on lifespan. 5 µM Ag and Hg had no obvious effect on the lifespan. Cu 500 µM significantly reduced the lifespan of animals. Data is pooled from independent replicates (n > 30 animals). Statistical analysis for panel A and B was done using a one-way ANOVA with Dunnett's post hoc test. The lifespan data for C were plotted as survival curves which were estimated using the Kaplan- Meier test followed by the log-rank test for group differences. *p<0.05; **p<0.01; ***p<0.001; ****p<0.0001.

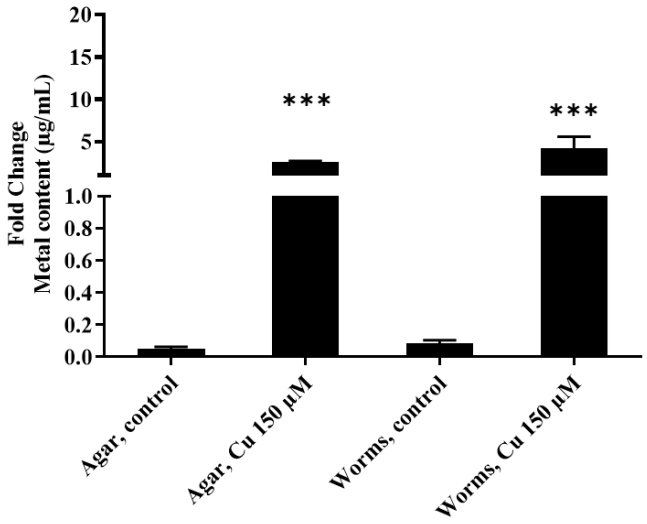

Supplementary Figure 2. Metal content in *C. elegans* following 69h Cu exposure. Elemental content was measured as a function of total sample volume. Metal content in worms is significantly higher than in control following treatment with Cu 150 µM. Student's unpaired t-test was used. *p<0.05; **p<0.01; ***p<0.001; ****p<0.0001.

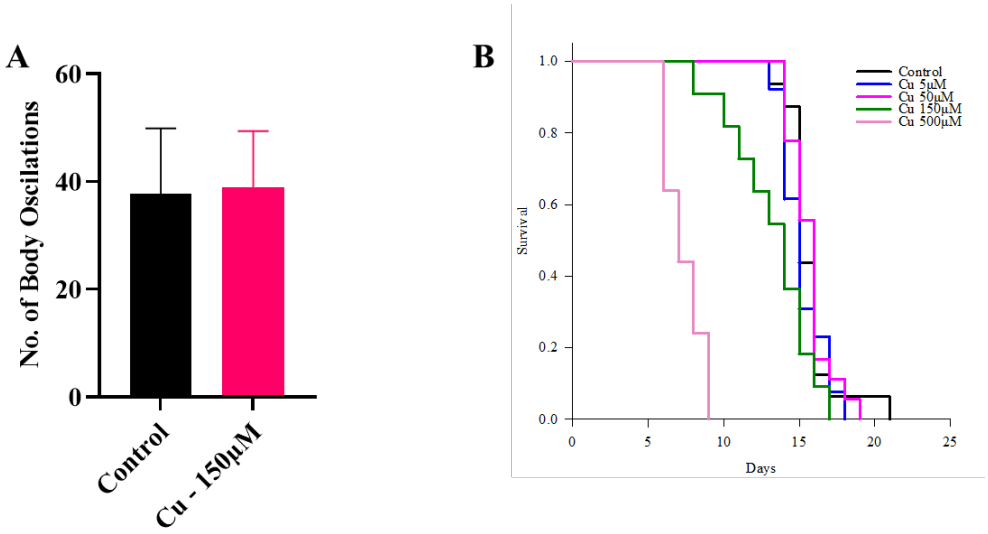

Supplementary Figure 2. Influence of chronic Cu exposures on body oscillation calculated using the MATLab software. Cu at 150µM had no significant changes in body oscillations.

Supplementary Table 1. Plate level responses of animals exposed to different concentrations of metal salts. The phenotypes included slower growth rate, arrest during L1 larval stage (including lethality), and visual morphological observations i.e. if they looked healthy and were moving normally on the plate. Animals were scored as normal (no difference from untreated controls), intermediate (mild phenotype, affecting few animals), and defective (abnormal response that is clearly visible, affecting most or all animals). The dash in the table means that animals couldn't be analyze as they arrested.

	L1 Arrest	Developmental Growth Rate	Visual Observations
Ni 150 uM	Intermediate	Normal	Normal
Pb - 150uM	Normal	Normal	Normal
Mn 150uM	Normal	Normal	Normal
Fe 150uM	Intermediate	Normal	Normal
Fe 300 uM	Defective	-	Intermediate
Cd 50uM	Intermediate	Intermediate	Normal
Cd 100 uM	defective	defective	intermediate
Cd 150uM	Defective	-	-
Cu 150uM	Normal	Normal	Normal
Cu 500uM	Normal	Normal	Normal

6.5 Appendix E. Review Article: Axin Family of Scaffolding Proteins in Development: Lessons from *C. elegans*

6.5.1 Preface

This appendix includes the following unpublished article in its original format:

Axin family of scaffolding protein in development: Lesson from *C. elegans*", by Avijit Mallick, Shane Taylor, Ayush Ranawade, and Bhagwati P. Gupta. Journal of Developmental Biology (2019). DOI: 10.3390/jdb7040020).

In this appendix, we discussed the major role of AXIN/PRY-1 in various processes and other animal models with a specific focus on *C. elegans.* We presented a possible interaction with MANF-1 and PRY-1 in this published paper. This review provided an up to date understanding of Axin in various systems.

Contributions

I provided preliminary data for Figures 5C-D and edited the initial manuscript draft for submission. Avijit, Ayush and Dr. Gupta, wrote and revised the manuscript for submission.

6.5.2 Mallick *et al*. (2019). Journal of Developmental Biology

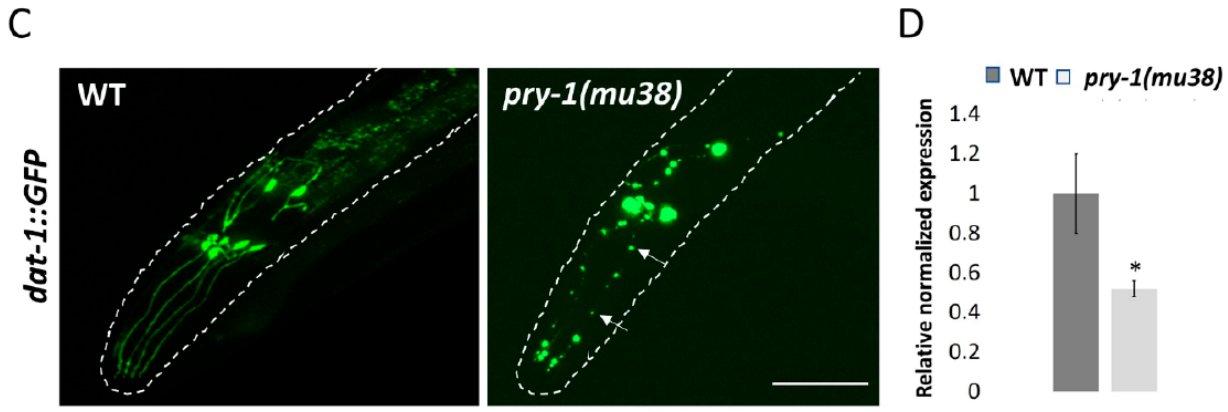

Figure E1. PRY-1 regulates neuronal development in C. elegans. (**C**) *pry-1* mutants exhibit defects in dopaminergic neurons (marked with *dat-1p::GFP*). The cell bodies are frequently missing or appear abnormal and dendrites show punctate-like patterns (arrows) (scale bar= 50µm). (**D**) qPCR experiment shows that *manf-1* is significantly downregulated in *pry-1* mutant adults (* $p < 0.05$, two batches). Figure Adapted from Mallick *et al.* (2019).